TRB

TRANSPORTATION RESEARCH RECORD

Journal of the Transportation Research Board, No. 2158

Environment 2010

TRANSPORTATION RESEARCH BOARD
OF THE NATIONAL ACADEMIES

TRANSPORTATION RESEARCH BOARD
OF THE NATIONAL ACADEMIES

TRANSPORTATION RESEARCH RECORDS, which are published throughout the year, consist of collections of papers on specific transportation modes and subject areas. Each Record is classified according to the subscriber category or categories covered by the papers published in that volume. The views expressed in papers published in the Transportation Research Record series are those of the authors and do not necessarily reflect the views of the peer review committee(s), the Transportation Research Board, the National Research Council, or the sponsors of TRB activities. The Transportation Research Board does not endorse products or manufacturers; trade and manufacturers' names may appear in a Record paper only if they are considered essential.

PEER REVIEW OF PAPERS: All papers published in the Transportation Research Record series have been reviewed and accepted for publication through the Transportation Research Board's peer review process established according to procedures approved by the Governing Board of the National Research Council. Papers are refereed by the TRB standing committees identified on page ii of each Record. Reviewers are selected from among committee members and other outside experts. The Transportation Research Board requires a minimum of three reviews; a decision is based on reviewer comments and resultant author revision. For details about the peer review process, see the information on the inside back cover.

THE TRANSPORTATION RESEARCH RECORD PUBLICATION BOARD, comprising a cross section of transportation disciplines and with equal representation from the academic and practitioner communities, assures that the quality of the *Transportation Research Record: Journal of the Transportation Research Board* and the TRB paper peer review process is consistent with that of a peer-reviewed scientific journal. Members from the academic community make decisions on granting tenure; all academic and practitioner members have authored papers published in peer-reviewed journals and all have participated in the TRB peer review process.

TRANSPORTATION RESEARCH BOARD PUBLICATIONS may be ordered directly from the TRB Business Office, through the Internet at www.TRB.org, or by annual subscription through organizational or individual affiliation with TRB. Affiliates and library subscribers are eligible for substantial discounts. For further information, contact the Transportation Research Board Business Office, 500 Fifth Street, NW, Washington, DC 20001 (telephone 202-334-3213; fax 202-334-2519; or e-mail TRBsales@nas.edu).

TRANSPORTATION RESEARCH RECORD PAPERS ONLINE: The TRR Journal Online website provides electronic access to the full text of papers that have been published in the Transportation Research Record series since 1996. The site is updated as new Record papers become available. To search abstracts and to find subscription and pricing information, go to www.TRB.org/TRROnline.

TRANSPORTATION RESEARCH BOARD 2010 EXECUTIVE COMMITTEE*

Chair: Michael R. Morris, Director of Transportation, North Central Texas Council of Governments, Arlington
Vice Chair: Neil J. Pedersen, Administrator, Maryland State Highway Administration, Baltimore
Executive Director: Robert E. Skinner, Jr., Transportation Research Board

J. Barry Barker, Executive Director, Transit Authority of River City, Louisville, Kentucky
Allen D. Biehler, Secretary, Pennsylvania Department of Transportation, Harrisburg
Larry L. Brown, Sr., Executive Director, Mississippi Department of Transportation, Jackson
Deborah H. Butler, Executive Vice President, Planning, and CIO, Norfolk Southern Corporation, Norfolk, Virginia
William A. V. Clark, Professor, Department of Geography, University of California, Los Angeles
Eugene A. Conti, Jr., Secretary of Transportation, North Carolina Department of Transportation, Raleigh
Nicholas J. Garber, Henry L. Kinnier Professor, Department of Civil Engineering, and Director, Center for Transportation Studies, University of Virginia, Charlottesville
Jeffrey W. Hamiel, Executive Director, Metropolitan Airports Commission, Minneapolis, Minnesota
Paula J. Hammond, Secretary, Washington State Department of Transportation, Olympia
Edward A. (Ned) Helme, President, Center for Clean Air Policy, Washington, D.C.
Adib K. Kanafani, Cahill Professor of Civil Engineering, University of California, Berkeley (Past Chair, 2009)
Susan Martinovich, Director, Nevada Department of Transportation, Carson City
Debra L. Miller, Secretary, Kansas Department of Transportation, Topeka (Past Chair, 2008)
Sandra Rosenbloom, Professor of Planning, University of Arizona, Tucson
Tracy L. Rosser, Vice President, Corporate Traffic, Wal-Mart Stores, Inc., Mandeville, Louisiana
Steven T. Scalzo, Chief Operating Officer, Marine Resources Group, Seattle, Washington
Henry G. (Gerry) Schwartz, Jr., Chairman (retired), Jacobs/Sverdrup Civil, Inc., St. Louis, Missouri
Beverly A. Scott, General Manager and Chief Executive Officer, Metropolitan Atlanta Rapid Transit Authority, Atlanta, Georgia
David Seltzer, Principal, Mercator Advisors LLC, Philadelphia, Pennsylvania
Daniel Sperling, Professor of Civil Engineering and Environmental Science and Policy; Director, Institute of Transportation Studies; and Interim Director, Energy Efficiency Center, University of California, Davis
Kirk T. Steudle, Director, Michigan Department of Transportation, Lansing
Douglas W. Stotlar, President and Chief Executive Officer, Con-Way, Inc., Ann Arbor, Michigan
C. Michael Walton, Ernest H. Cockrell Centennial Chair in Engineering, University of Texas, Austin (Past Chair, 1991)

Peter H. Appel, Administrator, Research and Innovative Technology Administration, U.S. Department of Transportation (ex officio)
J. Randolph Babbitt, Administrator, Federal Aviation Administration, U.S. Department of Transportation (ex officio)
Rebecca M. Brewster, President and COO, American Transportation Research Institute, Smyrna, Georgia (ex officio)
George Bugliarello, President Emeritus and University Professor, Polytechnic Institute of New York University, Brooklyn; Foreign Secretary, National Academy of Engineering, Washington, D.C. (ex officio)
Anne S. Ferro, Administrator, Federal Motor Carrier Safety Administration, U.S. Department of Transportation (ex officio)
LeRoy Gishi, Chief, Division of Transportation, Bureau of Indian Affairs, U.S. Department of the Interior, Washington, D.C. (ex officio)
Edward R. Hamberger, President and CEO, Association of American Railroads, Washington, D.C. (ex officio)
John C. Horsley, Executive Director, American Association of State Highway and Transportation Officials, Washington, D.C. (ex officio)
David T. Matsuda, Deputy Administrator, Maritime Administration, U.S. Department of Transportation (ex officio)
Victor M. Mendez, Administrator, Federal Highway Administration, U.S. Department of Transportation (ex officio)
William W. Millar, President, American Public Transportation Association, Washington, D.C. (ex officio) (Past Chair, 1992)
Robert J. Papp (Adm., U.S. Coast Guard), Commandant, U.S. Coast Guard, U.S. Department of Homeland Security (ex officio)
Cynthia L. Quarterman, Administrator, Pipeline and Hazardous Materials Safety Administration, U.S. Department of Transportation (ex officio)
Peter M. Rogoff, Administrator, Federal Transit Administration, U.S. Department of Transportation (ex officio)
David L. Strickland, Administrator, National Highway Traffic Safety Administration, U.S. Department of Transportation (ex officio)
Joseph C. Szabo, Administrator, Federal Railroad Administration, U.S. Department of Transportation (ex officio)
Polly Trottenberg, Assistant Secretary for Transportation Policy, U.S. Department of Transportation (ex officio)
Robert L. Van Antwerp (Lt. General, U.S. Army), Chief of Engineers and Commanding General, U.S. Army Corps of Engineers, Washington, D.C. (ex officio)

* Membership as of August 2010.

TRB

TRANSPORTATION RESEARCH RECORD

Journal of the Transportation Research Board, No. 2158

Environment 2010

A Peer-Reviewed Publication

TRANSPORTATION RESEARCH BOARD
OF THE NATIONAL ACADEMIES

Washington, D.C.
2010

www.TRB.org

Transportation Research Record 2158
ISSN 0361-1981
ISBN 978-0-309-14284-7

Subscriber Categories
Highways; public transportation; environment; pavements; vehicles and equipment; materials; planning and forecasting

Printed in the United States of America

TRANSPORTATION RESEARCH RECORD PUBLICATION BOARD
C. Michael Walton, PhD, PE, Ernest H. Cockrell Centennial Chair in Engineering and Professor of Civil Engineering, University of Texas, Austin (Cochair)
Mary Lynn Tischer, PhD, Director, Office of Transportation Policy Studies, Federal Highway Administration, Washington, D.C. (Cochair)
Daniel Brand, SB, SM, PE, Consultant, Lyme, New Hampshire
Mary R. Brooks, BOT, MBA, PhD, William A. Black Chair of Commerce, Dalhousie University, Halifax, Nova Scotia, Canada
Charles E. Howard, Jr., MCRP, Director, Transportation Planning, Puget Sound Regional Council, Seattle, Washington
Thomas J. Kazmierowski, PEng, Manager, Materials Engineering and Research Office, Ontario Ministry of Transportation, Toronto, Canada
Michael D. Meyer, PhD, PE, Frederick R. Dickerson Professor, School of Civil and Environmental Engineering, Georgia Institute of Technology, Atlanta
Sandra Rosenbloom, MA, PhD, Professor of Planning, University of Arizona, Tucson
Kumares C. Sinha, PhD, PE, Olson Distinguished Professor, School of Civil Engineering, Purdue University, West Lafayette, Indiana
L. David Suits, MSCE, Executive Director, North American Geosynthetics Society, Albany, New York

Peer Review of Transportation Research Record 2158

PLANNING AND ENVIRONMENT GROUP
Katherine F. Turnbull, Texas Transportation Institute (Chair)

Environment and Energy Section
Kathleen H. Quinn, Federal Highway Administration (Chair)

Environmental Analysis in Transportation Committee
Charles Stoll, San Diego Association of Governments (Chair), Jennifer Johnson, HNTB Corporation (Secretary), Kathleen S. Ames, Doug Booher, Earl Downey Brill, Jr., Craig T. Casper, Joe Crossett, Carol D. Cutshall, Ronald S. DeNadai, Buddy D. Desai, Jeremiah P. Dumas, Christopher G. Gesing, David Grachen, Jeff S. Heilman, Kenneth J. Hess, Kris A. Hoellen, Tamara Hollowell, Charles Hostovsky, Ileana S. Ivanciu, Robert L. Jacobsen, Susan L. Killen, Wayne W. Kober, Mark S. Kross, Lynn Patrick Malbrough, Byron J. O'Quinn, Martin A. Palmer, Richard L. Record, Shari M. Schaftlein, Joseph S. Shalkowski, Carissa Schively Slotterback, Douglas L. Smith, Patricia C. Trombly, Colleen E. Vaughn, Thomas L. Weck

Transportation and Air Quality Committee
Robert M. O'Loughlin, Federal Highway Administration (Chair), Jeffrey P. Ang-Olson, Richard Baldauf, Brian S. Bochner, Kanok Boriboonsomsin, Harold Mallory Brazil, Tracy Clymer, Antonio Comi, Douglas S. Eisinger, Julia A. Gamas, Huaizhu Oliver Gao, Joddie Gray, Stephen Peter Greaves, Shauna L. Hallmark, Cecilia Ho, Christopher Klaus, Michael J. Krimmer, Jie Lin, Robert B. Noland, Robin J. North, Scott A. Peterson, Alison K. Pollack, Christopher L. Saricks, Philip M. Sheehy, Lynn J. Soporowski, David Robert Souten, John M. E. Storey, John H. Suhrbier, Nagendra Rao Velaga, Mohan M. Venigalla, Mia Waters, Lei Yu

Ecology and Transportation Committee
Thomas E. Linkous, Westerville, Ohio (Chair), Bethaney L. Bacher-Gresock, Hans G. J. Bekker, Alison M. Berry, Marcia A. Bowen, William L. Branch, Joseph A. Burns, Lars H. Carlson, Michelle S. Cohen, Patricia Cramer, Carol D. Cutshall, Peter J. Dodds, Bridget M. Donaldson, Robert L. Goo, Mary E. Gray, Susan Hagood, Marcel P. Huijser, Sandra L. Jacobson, Patrick Jeffers, Keith K. Knapp, Alexander F. Levy, James B. Martin, Debra A. Nelson, Douglas L. Smith, Paul J. Wagner, Patricia A. White, Brian Yanchik, Dale A. Youngkin

Transportation-Related Noise and Vibration Committee
Judith L. Rochat, Research and Innovative Technology Administration (Chair), Grant S. Anderson, Hans Bendtsen, Mariano Berrios, Chris Blaney, Michael Blumenthal, William Bowlby, Paul L. Burge, Karel L. Cubick, Ahmed A. El-Aassar, Mark A. Ferroni, Areg Gharabegian, Raquel Girvin, Rudolf W. Hendriks, Lloyd A. Herman, John R. Jaeckel, H. Wayne Jones, Kevin J. Keller, Harvey S. Knauer, Erwin R. Kohler, Winfield M. Lindeman, Christopher W. Menge, Michael S. Mulbarger, James Tuman Nelson, Geoffrey Pratt, Shankar Rajaram, Robert Otto Rasmussen, James A. Reyff, Bruce C. Rymer, Ulf S. I. Sandberg, Hugh Saurenman, Timothy V. Sexton, Natalia Sizov, Michael A. Staiano, Eric Stusnick, Jay A. Waldschmidt, Roger Wayson, Jeffrey A. Zapfe

Waste Management and Resource Efficiency in Transportation Committee
Edward D. Wallingford, Virginia Department of Transportation (Chair), Diane M. Anderson, WRScompass (Secretary), Jennie Armstrong, Brendon D. J. Bailey, Rodney Todd Concienne, Steven Eget, Kevin H. Gardner, Steven Gobelman, Faisal Hameed, James D. Heeren, Thomas G. Lewis, Kerry John McManus, Steven J. Miller, Milkas Scholz, David Emil Soltis, Robert E. Tatman, Nicole L. Villamizar

Peer review is indicated by a footnote at the end of each paper. The organizational units, officers, and members are as of December 31, 2009.

Transportation Research Board Staff
Christine Gerencher, Senior Program Officer for Aviation and Environment
Freda R. Morgan, Senior Program Associate
Mary Kissi, Senior Program Associate

Publications Office
Betsy Winship, Editor; Mary E. Cadette, Production Editor; Kristin C. Sawyer, Proofreader; Claudia Sauls, Manuscript Preparer

Ann E. Petty, Managing Editor; Juanita Green, Production Manager; Phyllis Barber, Publishing Administrator; Jennifer J. Weeks, Manuscript Preparation Manager

THE NATIONAL ACADEMIES

Advisers to the Nation on Science, Engineering, and Medicine

The **National Academy of Sciences** is a private, nonprofit, self-perpetuating society of distinguished scholars engaged in scientific and engineering research, dedicated to the furtherance of science and technology and to their use for the general welfare. On the authority of the charter granted to it by the Congress in 1863, the Academy has a mandate that requires it to advise the federal government on scientific and technical matters. Dr. Ralph J. Cicerone is president of the National Academy of Sciences.

The **National Academy of Engineering** was established in 1964, under the charter of the National Academy of Sciences, as a parallel organization of outstanding engineers. It is autonomous in its administration and in the selection of its members, sharing with the National Academy of Sciences the responsibility for advising the federal government. The National Academy of Engineering also sponsors engineering programs aimed at meeting national needs, encourages education and research, and recognizes the superior achievements of engineers. Dr. Charles M. Vest is president of the National Academy of Engineering.

The **Institute of Medicine** was established in 1970 by the National Academy of Sciences to secure the services of eminent members of appropriate professions in the examination of policy matters pertaining to the health of the public. The Institute acts under the responsibility given to the National Academy of Sciences by its congressional charter to be an adviser to the federal government and, on its own initiative, to identify issues of medical care, research, and education. Dr. Harvey V. Fineberg is president of the Institute of Medicine.

The **National Research Council** was organized by the National Academy of Sciences in 1916 to associate the broad community of science and technology with the Academy's purposes of furthering knowledge and advising the federal government. Functioning in accordance with general policies determined by the Academy, the Council has become the principal operating agency of both the National Academy of Sciences and the National Academy of Engineering in providing services to the government, the public, and the scientific and engineering communities. The Council is administered jointly by both the Academies and the Institute of Medicine. Dr. Ralph J. Cicerone and Dr. Charles M. Vest are chair and vice chair, respectively, of the National Research Council.

The **Transportation Research Board** is one of six major divisions of the National Research Council. The mission of the Transportation Research Board is to provide leadership in transportation innovation and progress through research and information exchange, conducted within a setting that is objective, interdisciplinary, and multimodal. The Board's varied activities annually engage about 7,000 engineers, scientists, and other transportation researchers and practitioners from the public and private sectors and academia, all of whom contribute their expertise in the public interest. The program is supported by state transportation departments, federal agencies including the component administrations of the U.S. Department of Transportation, and other organizations and individuals interested in the development of transportation. **www.TRB.org**

www.national-academies.org

TRB SPONSORS*

Transportation Departments of the 50 States, Puerto Rico, and the District of Columbia

Federal Government
U.S. Department of Transportation
- Federal Aviation Administration
- Federal Highway Administration
- Federal Motor Carrier Safety Administration
- Federal Railroad Administration
- Federal Transit Administration
- National Highway Traffic Safety Administration
- Research and Innovative Technology Administration

Bureau of Indian Affairs
Science and Technology Directorate, U.S. Department of Homeland Security
U.S. Army Corps of Engineers
U.S. Coast Guard

Nongovernmental Organizations
American Association of State Highway and Transportation Officials
American Public Transportation Association
American Transportation Research Institute
Association of American Railroads

---

*As of August 2010.

TRANSPORTATION RESEARCH RECORD

Journal of the Transportation Research Board, No. 2158

Contents

Foreword vii

Environmental Analysis in Transportation: Washington State's Ecological Application of Collaborative Approach to Identify a Preferred Alternative and Mitigation Strategy for I-90 Snoqualmie Pass East Project 1
Jason Smith and Amanda Sullivan

Regionwide Cumulative Effects Analysis of Long-Range Transportation Plans 10
Chris Paulsen, Patrick J. Crist, Gwen Kittel, and Ian Varley

Estimating Diesel Vehicle Emission Factors at Constant and High Speeds for Short Road Segments 19
Hyung-Wook Choi and H. Christopher Frey

Effects of Transportation and Land Use Policies on Air Quality: A Case Study in Austin, Texas 28
Elena C. McDonald-Buller, Alba Webb, Kara M. Kockelman, and Bin (Brenda) Zhou

Bus Technology Meta-Analysis 36
Hilda Martínez, Jorge Macias Mora, and Alper Unal

Analysis of Real-World Lead Vehicle Operation for Modal Emissions and Traffic Simulation Models 44
Eric Jackson and Lisa Aultman-Hall

Using Portable Emission Measurement Systems for Transportation Emissions Studies: Comparison with Laboratory Methods 54
Huan Liu, Matthew Barth, George Scora, Nicole Davis, and James Lents

TAMNROM-3D: Three-Dimensional Eulerian Model to Simulate Air Quality near Highways 61
Sri Harsha Kota, Qi Ying, and Yunlong Zhang

Comprehensive Field Study of Fuel Use and Emissions of Nonroad Diesel Construction Equipment 69
H. Christopher Frey, William Rasdorf, and Phil Lewis

Mobile Source Air Toxic Emissions: Sensitivity to Traffic Volume, Fleet Composition, and Average Speed 77
Alexandra Timoshek, Douglas Eisinger, Song Bai, and Deb Niemeier

Particle Number and Size Distribution of Emissions During Light-Duty Vehicle Cold Start: Data from the Total Onboard Tailpipe Emissions Measurement System 86
Mitchell K. Robinson, Karen M. Sentoff, and Britt A. Holmén

Second-by-Second Characterization of Cold-Start Gas-Phase and Air Toxic Emissions from a Light-Duty Vehicle 95
Karen M. Sentoff, Mitchell K. Robinson, and Britt A. Holmén

Estimating In-Vehicle Concentration of and Exposure to Fine Particulate Matter: Near-Roadway Ambient Air Quality and Variability in Vehicle Operation 105
Xiaozhen Liu, H. Christopher Frey, and Ye Cao

Ecology and Transportation: I-90 Snoqualmie Pass East Project's Design Engineering Challenges of Integrating Transportation Needs with Landscape-Level Connectivity and Transportation Corridor-Crossing Objectives in Washington State 113
Randy Giles, Scott Golbek, Amanda Sullivan, and Jerry Wood

California–Denmark Study on Acoustic Aging of Road Pavements 122
Hans Bendtsen, Erin Kohler, Qing Lu, and Bruce Rymer

Acoustic Radiation from Pavement Joint Grooves Between Concrete Slabs 129
Paul R. Donavan

Quantitative Assessment of Environmental and Economic Benefits of Recycled Materials in Highway Construction 138
Jin Cheol Lee, Tuncer B. Edil, James M. Tinjum, and Craig H. Benson

Environmental and Sustainability Impact Assessment of Infrastructure in the United Kingdom 143
Richard Willetts, Jim Burdon, Jacqui Glass, and Matthew Frost

Foreword

The 2010 series of the *Transportation Research Record: Journal of the Transportation Research Board* consists of approximately 900 papers selected from 3,700 submissions after rigorous peer review. The peer review for each paper published in this volume was coordinated by the committee acknowledged at the end of the text; members of the reviewing committees for the papers in this volume are listed on page ii.

Additional information about the *Transportation Research Record: Journal of the Transportation Research Board* series and the peer review process appears on the inside back cover. TRB appreciates the interest shown by authors in offering their papers, and the Board looks forward to future submissions.

Note: Many of the photographs, figures, and tables in this volume have been converted from color to grayscale for printing. The electronic files of the papers, posted on the web at **www.TRB.org/TRROnline**, retain the color versions of photographs, figures, and tables as originally submitted for publication.

Measurement Conversion Factors

To convert from the unit in the first column to the unit in the second column, multiply by the factor in the third column.

Customary Unit	*SI Unit*	*Factor*
Length		
inches	millimeters	25.4
inches	centimeters	2.54
feet	meters	0.305
yards	meters	0.914
miles	kilometers	1.61
Area		
square inches	square millimeters	645.1
square feet	square meters	0.093
square yards	square meters	0.836
acres	hectares	0.405
square miles	square kilometers	2.59
Volume		
gallons	liters	3.785
cubic feet	cubic meters	0.028
cubic yards	cubic meters	0.765
Mass		
ounces	grams	28.35
pounds	kilograms	0.454
short tons	megagrams	0.907
Illumination		
footcandles	lux	10.76
footlamberts	candelas per square meter	3.426
Force and Pressure or Stress		
poundforce	newtons	4.45
poundforce per square inch	kilopascals	6.89
Temperature		
To convert Fahrenheit temperature (°F) to Celsius temperature (°C), use the following formula: °C = (°F – 32)/1.8		

SI Unit	*Customary Unit*	*Factor*
Length		
millimeters	inches	0.039
centimeters	inches	0.394
meters	feet	3.281
meters	yards	1.094
kilometers	miles	0.621
Area		
square millimeters	square inches	0.00155
square meters	square feet	10.764
square meters	square yards	1.196
hectares	acres	2.471
square kilometers	square miles	0.386
Volume		
liters	gallons	0.264
cubic meters	cubic feet	35.314
cubic meters	cubic yards	1.308
Mass		
grams	ounces	0.035
kilograms	pounds	2.205
megagrams	short tons	1.102
Illumination		
lux	footcandles	0.093
candelas per square meter	footlamberts	0.292
Force and Pressure or Stress		
newtons	poundforce	0.225
kilopascals	poundforce per square inch	0.145
Temperature		
To convert Celsius temperature (°C) to Fahrenheit temperature (°F), use the following formula: °F = (°C × 1.8) + 32		

Abbreviations Used Without Definitions

AASHO	American Association of State Highway Officials
AASHTO	American Association of State Highway and Transportation Officials
ACRP	Airport Cooperative Research Program
APTA	American Public Transportation Association
ASCE	American Society of Civil Engineers
ASTM	American Society for Testing and Materials (known by abbreviation only)
FAA	Federal Aviation Administration
FHWA	Federal Highway Administration
FMCSA	Federal Motor Carrier Safety Administration
FRA	Federal Railroad Administration
FTA	Federal Transit Administration
IEEE	Institute of Electrical and Electronics Engineers
ISO	International Organization for Standardization
ITE	Institute of Transportation Engineers
NASA	National Aeronautics and Space Administration
NCHRP	National Cooperative Highway Research Program
NHTSA	National Highway Traffic Safety Administration
RITA	Research and Innovative Technology Administration
SAE	Society of Automotive Engineers
SHRP	Strategic Highway Research Program
TCRP	Transit Cooperative Research Program
TRB	Transportation Research Board

Environmental Analysis in Transportation

Washington State's Ecological Application of Collaborative Approach to Identify a Preferred Alternative and Mitigation Strategy for I-90 Snoqualmie Pass East Project

Jason Smith and Amanda Sullivan

Since 1999, the I-90 Snoqualmie Pass East Project (I-90 project) of the Washington State Department of Transportation (WSDOT) team has worked with dozens of government agencies and nongovernmental groups to develop a range of potential solutions to meet project needs and mitigate the project's potential adverse impacts on the Central Cascades' ecosystem and the state's economy. WSDOT created a multiagency interdisciplinary team (IDT) as an advisory body to recommend a preferred alternative that incorporated relevant science and the concerns of agency stakeholders. The project's original IDT included eight primary and advisory agencies and was later expanded to include 12 participating agencies. The IDT went on to form the mitigation development team (MDT), a technical advisory subcommittee consisting of hydrologists and biologists from different agencies, to identify locations and develop performance criteria for investments in ecological connectivity. In addition to the IDT and the MDT, formal technical committees were formed to assist in planning and permitting challenges for final designs on wetlands mitigation, wildlife monitoring, and stormwater. WSDOT has also established innovative partnerships with university researchers and conservation groups to help establish citizen awareness, wildlife monitoring, and targeted habitat acquisitions. Relationships with transportation-based organizations and businesses were formed to gain insight into the requirements of highway users. WSDOT's innovative approach to developing partnerships to understand and meet landscape-scale, watershed-based objectives on the I-90 project provides a scalable model for the integration of context-sensitive solutions for future WSDOT and other state departments of transportation projects.

In 1999, FHWA, in collaboration with the Washington State Department of Transportation (WSDOT), published a Notice of Intent to scope a 15-mi section of Interstate 90 between the community of Hyak and the town of Easton for an environmental impact study. Initially, this evaluation focused on reducing winter closures of the Interstate, but the aim quickly expanded to include other needs, including reducing the risk of rock and debris falling on the roadway from unstable slopes, fixing structural deficiencies, providing for increases in traffic volumes, and connecting habitat across I-90 for fish and wildlife.

During the public scoping process, which began in 2000, complex issues arose for designing and constructing this project. Land ownership and management objectives along the corridor were changing, and the project was being scoped without taking these factors into consideration. To address the issue, WSDOT adopted the ecological approach. This ecosystem approach helped guide WSDOT and its partners in developing a long-term vision for the I-90 corridor and mitigating the effects of the infrastructure project.

In 2000, an interagency interdisciplinary team (IDT) was formed, and preliminary engineering and environmental analysis began. Through the IDT, WSDOT accomplished ecological project goals by applying a landscape-level, watershed-based mitigation strategy. This mitigation strategy allowed WSDOT and its partners to consider multiple ecological needs in the project design, including connecting habitat, streams, and groundwater across I-90 at various connectivity emphasis areas (CEAs), or ecological linkages. (CEAs are mostly located at existing bridge and culvert locations and include water crossings as part of the design strategy.)

When the Transportation Partnership Account finance package was passed in 2005 by the Washington State Legislature, WSDOT received funding to ramp up the design effort, finish National Environmental Policy Act (NEPA) compliance, and prepare construction documents for the first 5 mi of the project area from Hyak to the Keechelus Dam vicinity (*1*). WSDOT published the "I-90 Snoqualmie Pass East Project Draft Environmental Impact Statement" (draft EIS) for public review and comment in summer 2005. The landscape-level, watershed-based approach helped WSDOT secure the necessary agency and citizen approval for the draft EIS. Over the next 2 years, WSDOT continued using existing partnerships and formed new teams, including specialized technical committees, to identify a preferred design alternative for the I-90 project. These collaborative efforts culminated with the release of the final EIS in August 2008 that identified WSDOT's preferred design alternative for the I-90 project. In October 2008, FHWA issued its record of decision, selecting the preferred alternative for construction.

Through the I-90 project, WSDOT will ensure the continued availability of I-90 as a primary statewide corridor by improving the safety and reliability of a 15-mi stretch of the interstate east of Snoqualmie Pass. WSDOT will reduce avalanche risks to the traveling public, minimize road closures required for avalanche control work, and reduce the risk of rock and debris falling onto the interstate from unstable slopes. WSDOT will also fix structural deficiencies, provide for the recent and predicted increases in traffic volume, and

J. Smith, WSDOT South Central Region, 3190 160th Avenue, SE, Bellevue, WA 98008. A. Sullivan, I-90 Project Communications, 1710 South 24th Avenue, Suite 100, Yakima, WA 98902. Corresponding author: A. Sullivan, Sulliva@consultant.wsdot.wa.gov.

Transportation Research Record: Journal of the Transportation Research Board, No. 2158, Transportation Research Board of the National Academies, Washington, D.C., 2010, pp. 1–9.
DOI: 10.3141/2158-01

work to reduce wildlife–vehicle collisions by reconnecting habitat across I-90 for improved mobility of fish and wildlife. Plans for the project include widening the existing four-lane interstate to six lanes, replacing deteriorated concrete pavement, straightening sharp roadway curves, stabilizing unstable rock slopes, building new bridges and culverts (including the construction of wildlife under- and overcrossings), and building a new, more efficient snowshed (a concrete shed covering the roadway to provide permanent protection from avalanches and other falling debris to travelers passing through Snoqualmie Pass).

Construction of the first phase of the project from Hyak to Keechelus Dam consists of 5 project miles broken into multiple construction contracts. WSDOT started work on the first construction contract in July 2009 by building a long-term detour bridge (which will be in place for up to 3 years) and excavating materials from Keechelus Lake, an irrigation reservoir, to mitigate for project impacts to reservoir storage during future construction activities. In November 2009, WSDOT advertised the second contract to begin replacing the old lanes and adding a new lane in each direction, rebuilding bridges, and extending chain-up and -off areas along the first 3 mi of the project. This contract is expected to begin construction in 2010. In fall 2010, WSDOT will advertise the third contract to continue adding a lane in each direction, replace the snowshed, address unstable slopes, build new bridges, and construct new chain-up and -off areas for the next 2 project miles. This contract is scheduled to begin construction in 2011. Several smaller contracts are planned to start after 2011. These contracts will consist of specialty work, including stormwater retrofit, wetland and roadside mitigation, and the installation of wildlife fencing.

The first 5 mi of the I-90 project from Hyak to Keechelus Dam is funded at $595 million. The remaining portion of the project (10 mi) from Keechelus Dam to Easton remains unfunded.

UNDERSTANDING THE I-90 PROJECT CORRIDOR

To better understand WSDOT's use of partnerships and how a preferred alternative was identified, it is necessary to first discuss the I-90 project's geographic landscape. I-90 spans 300 mi in Washington State from the Port of Seattle to the Idaho state line, and then continues east across the United States to Boston, Massachusetts. I-90 is the major east–west transportation corridor across Washington and is vital to the state's economy (*2*). The I-90 project improves a 15-mi portion of I-90, beginning on the eastern side of Snoqualmie Pass at milepost 55.1, just east of the Hyak Interchange, where the existing highway narrows from six lanes to four lanes. The project end point is at milepost 70.3 at the West Easton Interchange, where the terrain becomes flatter and the highway is straighter. This 15-mi stretch of I-90 is in Kittitas County, Washington, and passes through the Okanogan-Wenatchee National Forest (see Figure 1).

I-90 is a critical link connecting Puget Sound's large population and business centers with the farmlands, diverse industries, and extensive recreational areas of eastern Washington. The uninterrupted movement of people, freight, and business over Snoqualmie Pass is essential to quality of life and the economic vitality of Washington State (*2*).

The I-90 project presents many unique environmental and design challenges because of its location along a high mountain pass in the Central Cascades. The general topography is one of mountainous peaks and valleys. For the first 6 mi of the project area, I-90 runs along a narrow corridor between the shores of Keechelus Lake, a deep-water agricultural reservoir of glacial origin, and steep mountain slopes (see Figure 1). These steep mountain slopes contain volcanic bedrock at varying depths that are subject to deep fissures and stress cracks with weakened slip planes, which, when combined with high annual precipitation and freeze–thaw conditions, makes them suscep-

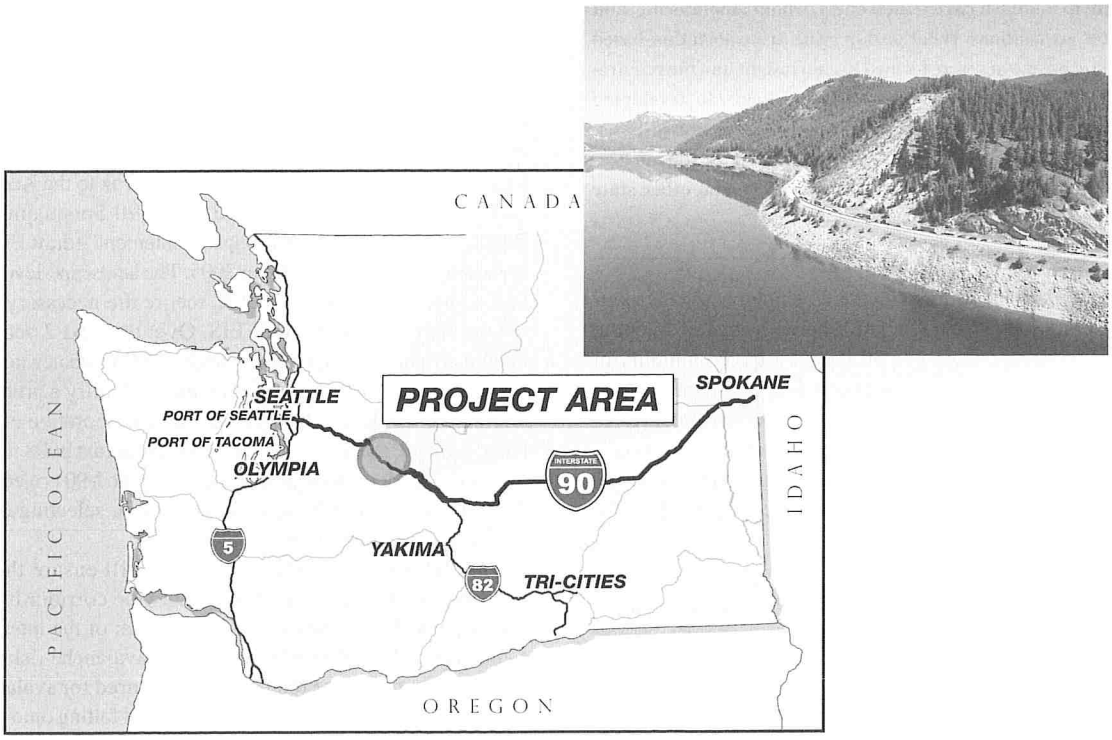

FIGURE 1 Washington State map showing Interstate 90, the I-90 project location, and typical topography.

tible to landslides, debris flow, and avalanche. Geotechnical studies indicate that certain portions of the project area contain stable rock and favorable sediment, while other areas contain soft frangible rock and liquefiable soil conditions. These conditions, combined with short construction windows and a planned annual winter shutdown, require a unique set of plans for designing bridges, improving ground conditions for foundations, and stabilizing rock slope cuts before and during construction.

The I-90 project area (15 mi) is built on national forest land. The large areas of protected state, federal, and conservation land north and south of I-90 support a broad range of habitats and a diverse array of plants and wildlife. Endangered species and focal species in the area include the northern spotted owl, bull trout, and migrating ungulates. Since the late 1990s, the area has been managed according to the Snoqualmie Pass Adaptive Management Area Plan. This plan requires protection of old-growth habitat, removal of portions of existing U.S. Forest Service (USFS) roads, and management of recreation to facilitate species movement. In recent years, through the acquisition of private land, there have been substantial private and public land conservation efforts to protect old-growth forest, provide larger contiguous blocks of forested habitat, and facilitate habitat connectivity across the I-90 corridor. The Cascades Conservation Partnership, the Mountains-to-Sound Greenway Trust, the U.S. Fish and Wildlife Service (USFWS), and USFS have invested more than $100 million in these efforts during the past 5 years. These land purchases, along with the I-90 land exchange, have added 75,000 acres (approximately 117 mi^2) of land to the national forest system adjacent to and within the I-90 project area. The land management by USFS and conservation groups has given WSDOT confidence that ecological connectivity investments will be protected in perpetuity.

Even with conservation efforts, I-90's presence limits wildlife movement and forms a physical barrier between upstream and downstream terrestrial and aquatic environments. Existing culverts and narrow bridges limit aquatic species movement and, in many cases, the highway embankment has filled in habitat that once made up channels, floodplains, and associated wetlands. Adequate connections between habitats and hydrologic features on either side of I-90 are necessary for the continued health of the project area's diverse ecosystems.

IDENTIFYING PROJECT PARTNERS WITH A VESTED INTEREST

The I-90 project's complex engineering and environmental design issues led WSDOT to look outside of the agency for partners with a vested interest in solving challenges and focusing on a landscape-level, watershed-based design and mitigation strategy. In 2000, WSDOT formed the IDT to provide effective and efficient interagency advice to the I-90 project team, develop a project purpose and need statement, help meet NEPA and State Environmental Policy Act guidance during the environmental analysis phase, and move quickly through the permitting actions.

WSDOT and FHWA were the lead agencies on the IDT. The original IDT consisted of eight agency members: five voting members and three advisory members. By 2005, the IDT was expanded to include 12 agencies, including WSDOT and FHWA. Partnership agencies included USFS, U.S. Bureau of Reclamation, USFWS, U.S. Army Corps of Engineers, U.S. Environmental Protection Agency (EPA), National Marine Fishery Service, Washington Department of Fish and Wildlife (WDFW), Washington Department of Ecology (Ecology), Washington State Parks, and Kittitas County.

WSDOT and FHWA often required multiple participants in the IDT. In addition to WSDOT, each nonlead agency provided one primary and one or more alternate representatives to participate in monthly or bimonthly IDT meetings. IDT meetings allowed WSDOT and the IDT to talk openly about project descriptions based on information learned from recent field work. Frequent agenda topics included the existing and proposed project conditions, the project's impacts and benefit opportunities, risks and management strategies, a value engineering study, cost evaluation validation process (*3*), analysis of ecological connectivity information and design features, and review of design engineering data such as geotechnical, structural investigations, alignment data, advanced stormwater design, and avalanche modeling (*4*). Between meetings, IDT members worked proactively to identify and assist in developing management strategies for project risks associated with engineering design and environmental impacts. IDT members conducted, coordinated, and group-reviewed the project's designs and permit application materials and arranged physical and virtual field reviews focusing on water resources and watershed context. The IDT's contributions to the I-90 project were tracked using a series of commitment tracking databases and geographic information system modeling. These data management technologies were used to support the collaborative approach and assist in information sharing.

With guidance from the IDT, WSDOT and FHWA developed the purpose and need for the I-90 project. It was determined that the I-90 project, regardless of the build alternative, must

- Reduce the risk of avalanche to the traveling public and reduce the frequency and duration of road closures required for avalanche control work,
- Reduce the risk of rock and debris falling onto the roadway from unstable slopes,
- Fix structural deficiencies by replacing damaged pavement,
- Provide for the growth-related increases in traffic volume, and
- Connect habitat across I-90 for fish and wildlife (*5*); this ecological commitment as part of a project purpose and need statement was a first for WSDOT.

To identify a preferred alternative and complete the final EIS, WSDOT and the IDT had to resolve issues with integrating ecological connectivity objectives with other project objectives. Specifically, WSDOT and the IDT needed to identify solutions to issues regarding the location of crossing structures, wetlands mitigation, wildlife monitoring, and stormwater treatment best management practices (BMPs). Therefore, specialized teams were created to make project recommendations to WSDOT and the IDT.

The first specialized team that WSDOT and the IDT formed was the mitigation development team (MDT) to provide technical support regarding ecological connectivity and the development of an environmental design and mitigation strategy. The MDT worked closely with the project team to prepare and publish the MDT recommendation package (*6*).

ESTABLISHING THE MITIGATION DEVELOPMENT TEAM

To integrate ecological connectivity into the project design, the IDT convened a multiagency team of biologists and hydrologists to form the MDT. Partnership agencies included WSDOT, USFS, USFWS, and WDFW.

The MDT was tasked to make recommendations that responded to the following central question: "Given what we know about wildlife movement, habitat fragmentation, and ecological connectivity needs, and framing this knowledge within the context of a limited design/construction budget, where are the locations within the project area that provide the highest benefit-to-cost ratio and long-term solutions to the issue of ecological connectivity?" (*6*)

The MDT's first order of business was to review the existing scientific information and site-specific technical report data developed by WSDOT, USFS, and other agencies during the 1990s to determine the existing ecological conditions within the project area. Among other topics, the MDT considered high-mobility species, low-mobility species, roadkill data, fish passage, landscape permeability, existing habitat conditions, aquatic habitat connectivity, and hydrologic function. At the projectwide scale, the MDT identified three generalized north–south linkage zones: the Gold Creek Valley, Keechelus Lake to Amabalis Mountain, and the Easton Hill area. Within these zones, they also identified 14 CEAs across the project area. Each CEA provided an opportunity to improve connectivity for a unique assemblage of species. CEAs ranged in complexity from single stream crossings to multiple stream crossings with associated wetlands and areas of diffuse surface flow, to upland areas that are important movement routes for wildlife (see Figure 2) (*6*).

The I-90 project design team collaborated with the MDT to develop alternative conceptual designs for the highway at each CEA. The design team also developed some designs independently so that a range of alternatives could be evaluated. The IDT requested that the MDT evaluate the likely performance of the different design options to determine which would meet ecological connectivity objectives.

After evaluating design options and developing specific performance standards and CEA-specific connectivity objectives, the MDT found that crossing structures would be more effective for some species if they contained habitat, rather than simply being physical connections for opposite sides of the highway. For instance, lower-mobility animals would feel more secure using a crossing structure containing hiding cover. Different animals show different preferences for crossing structures, whether the structures are small, medium, or large (*6*).

The MDT also noted that projectwide wildlife connectivity objectives were likely to be met and would profoundly improve ecological connectivity relative to the existing condition by (*a*) combining design options at CEAs that meet CEA-specific objectives, (*b*) installing small or medium crossing structures at upland sites, and (*c*) implementing recommended performance standards outside of CEAs. The MDT also recommended that a combination of structure types (i.e., overcrossing and undercrossing) be considered to serve a large variety of species. They recommended additional small or medium (drainage-type culverts or box culverts) crossings at intervals of approximately every 820 ft throughout the corridor to further support the linkage of upland habitats and the movement of smaller animals. From a hydrologic perspective, projectwide connectivity needs are predominantly met by design options that meet objectives within CEAs (*6*). These recommendations were presented to the IDT, who integrated them into the overall recommendations for the preferred alternative and forwarded them to FHWA and WSDOT decision makers. After these recommendations were adopted by the decision makers, the I-90 project design team used these recommendations to move conceptual design to final design plans at each CEA.

While working with the MDT, WSDOT identified further challenging areas where the I-90 project design team could use the help of interagency collaboration. These areas included responding to the challenges associated with wildlife monitoring, stormwater treatment, and wetland mitigation. Therefore, technical committees were created to provide direction on WSDOT designs. The Wetlands Mitigation Technical Committee was created to assess wetlands and other jurisdictional waters within the project area and analyze the project's mitigation designs. The Wildlife Monitoring Technical Committee was established to oversee and review information gathered from preconstruction, and later postconstruction, wildlife monitoring efforts. The Stormwater Technical Committee (STC) was created to help WSDOT develop solutions to stormwater and hydraulic challenges.

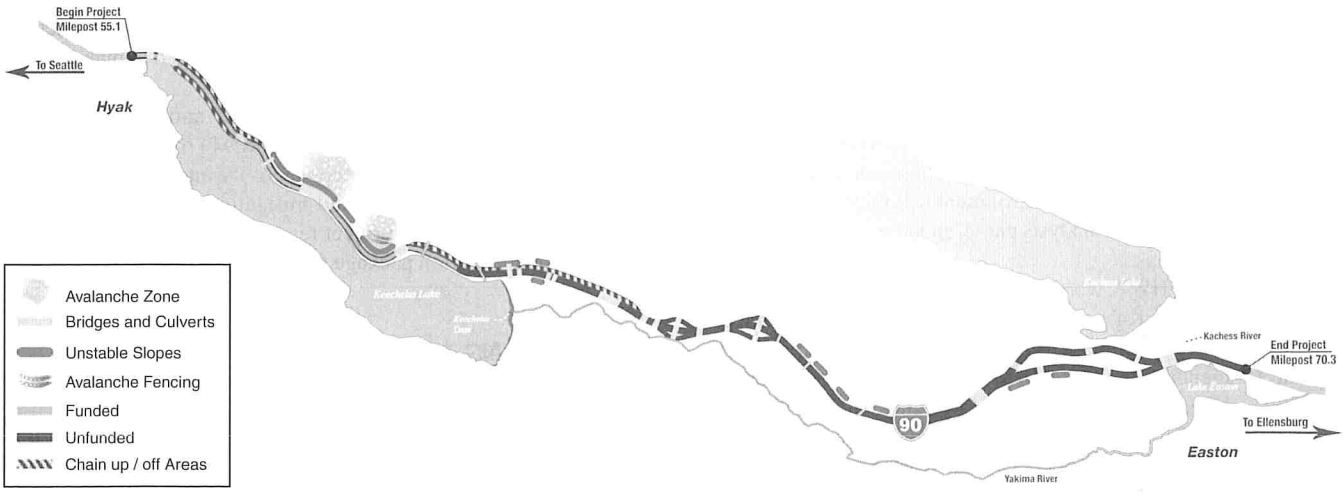

FIGURE 2 Map showing identified CEAs and the bridges and culverts (in yellow) that will be placed at each CEA to improve connectivity.

ESTABLISHING A WETLANDS MITIGATION TECHNICAL COMMITTEE

The Wetland Mitigation Technical Committee consisted of interagency personnel with expertise in wetland, hydrology, horticulture, and related scientific fields (see Figure 3). The committee was established to advise WSDOT design and environmental teams on challenges facing the specific wetland mitigation designs related to meeting wetland replacement requirements. The wetlands team reviewed preliminary designs, provided guidance and support for habitat acquisitions, and worked with other agencies to help resolve conflicts associated with the unique mitigation proposed on the project.

Mitigation for the I-90 project focuses on improvements to CEAs and consists of mitigation underneath and adjacent to bridge and culvert structures, identification and connection of habitat types and aquatic features, and preservation and restoration that is consistent with project and partnership objectives.

DEVELOPING A WILDLIFE MONITORING PROGRAM

Ecological connectivity objectives, specifically wildlife connectivity, focus on improving motorists' safety by reducing wildlife–vehicle collisions and improving the ecological permeability of the highway for fish and wildlife. In order to understand how WSDOT's investments perform over time, and to incorporate lessons learned into future phases of design and construction, baseline and postconstruction wildlife monitoring programs were needed. Because of the broad landscape context of road systems, ecological connectivity objectives, and surrounding land management agencies, wildlife monitoring and assessment needed to address the broader landscape, ecological processes, and restoration of important linkages for a multiple-species ecosystem. Implementing a wildlife monitoring plan of this spatial and ecological scale was beyond WSDOT's capacity, however. Therefore, WSDOT, other agencies, and interested groups came together to launch a multitiered monitoring program.

WSDOT first formed a Wildlife Monitoring Technical Committee to assist with developing a wildlife monitoring program and help with solving problems associated with the implementation of a program. The committee provided a venue where experts in wildlife biology and road ecology could develop guidance on how to perform baseline and postconstruction wildlife monitoring for WSDOT (*7*). Members of the committee included WSDOT, USFS, USFWS, EPA, WDFW, Central Washington University (CWU), and Western Transportation Institute (WTI) at Montana State University.

WSDOT contracted with WTI to help develop the multitiered Wildlife Monitoring Plan. Under the plan, WTI would provide services during the preconstruction monitoring as the lead role in coordinating research efforts with all active committee participants, support the development of new partnerships, and help identify and seek funding for joint efforts.

To assess the many aspects of meeting ecological connectivity objectives on the I-90 project, the I-90 Wildlife Monitoring Plan focuses on a two-tiered approach to wildlife monitoring. Tier 1 evaluates basic transportation management questions regarding the performance of crossing structures and fencing (such as changes in wildlife–vehicle collisions and use of new crossing structures). Tier 2 builds on the results of Tier 1 to address more complex questions about the effects of the project on wildlife populations (such as genetic and demographic structure, viability, and dispersal) (*8*).

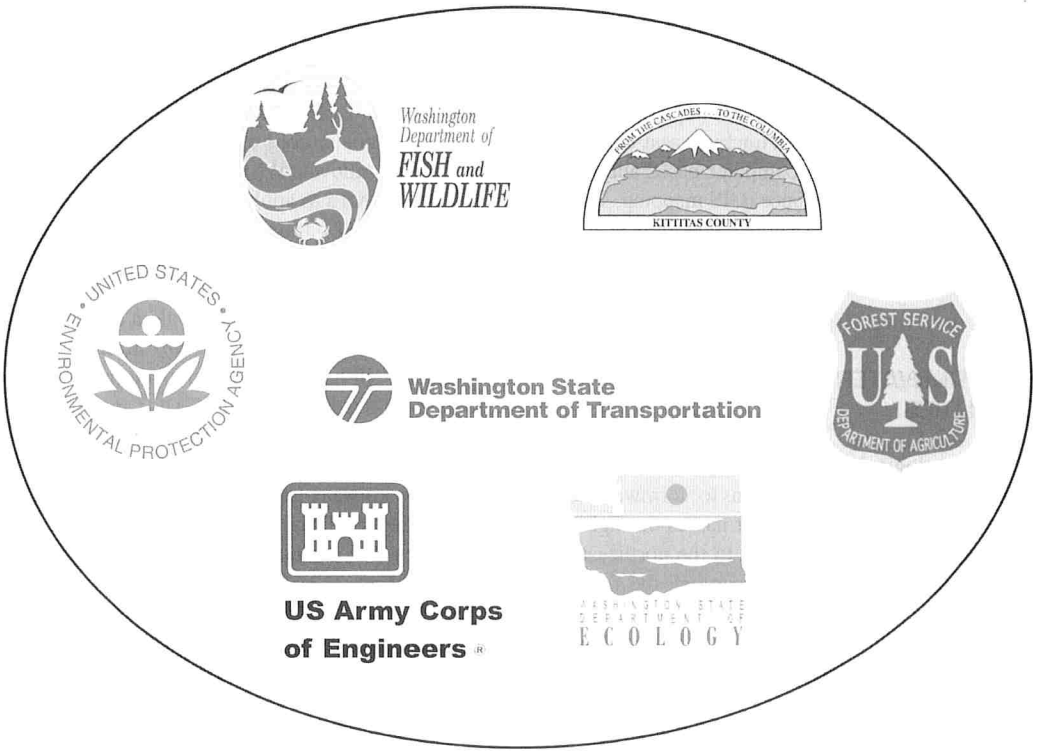
Washington Department of FISH and WILDLIFE
FROM THE CASCADES TO THE COLUMBIA
KITTITAS COUNTY
UNITED STATES ENVIRONMENTAL PROTECTION AGENCY
Washington State Department of Transportation
FOREST SERVICE
US
DEPARTMENT OF AGRICULTURE
US Army Corps of Engineers
WASHINGTON STATE DEPARTMENT OF ECOLOGY

FIGURE 3 Wetlands Mitigation Technical Committee member agencies.

Wildlife monitoring focuses on a select group of species (focal species) and occurs on multiple spatial scales, over time. Both high- and low-mobility focal species are used based on the assumption that they will provide an indication of the generalized response to a given stimulus by a larger assemblage of species. Ecological attributes are used to determine which species serve as the best indicators of change.

Tier 1 objectives include evaluating the locations and rate of wildlife–vehicle collisions, assessing the use and effectiveness of wildlife crossing structures—both existing and planned, characterizing the locations and rate of at-grade highway crossings by wildlife, estimating species occurrence and distribution in the project area, assessing the effectiveness of fencing, and appraising the effectiveness of jump-outs (*8*).

WSDOT and its partners have been conducting both CEA-specific and projectwide monitoring for Tier 1 activities to identify baseline conditions since 2008. Methods being used to meet Tier 1 objectives include assessing wildlife use of existing culverts and underpasses via remote cameras, documenting crossing rates via snow tracking, evaluating the distribution of various target species via noninvasive survey methods and live-capture, and documenting wildlife–vehicle collisions. In addition, specific projects to monitor low-mobility species, such as fish, amphibians, and pikas, have been initiated in partnership with CWU. Early monitoring results have documented how species are moving through the corridor, and genetic samples collected from various target species will be used for assessment of highway permeability both pre- and postconstruction.

Postconstruction Tier 2 monitoring activities, research, and objectives will focus on landscape and population-level connectivity and complement Tier 1 monitoring by providing a more comprehensive understanding of how the project connectivity measures perform at a larger scale. Tier 2 monitoring efforts are somewhat unique to the I-90 project, because few other Tier 2 monitoring efforts have been instituted in the county. Tier 2 efforts will allow WSDOT and its partners to evaluate wildlife usage and performance of the various crossing structures to determine their effectiveness. Research methods will include pre- and postpopulation level benefits (hair collection, scat-detection dogs), pre- and postregional species occurrence (remote cameras, hair collection, tracking, scat-detection dogs), postpopulation viability analysis (computer-based analysis), and pre- and postextent of human disturbance (GIS mapping, spatial stats, trail and traffic counters). Tier 2 research will require a continued collaboration and partnering between WSDOT and other entities in order to be successful (*8*).

INTEGRATING STORMWATER TREATMENT FACILITIES

In addition to integrating ecological connectivity objectives, WSDOT had to specifically look into and develop solutions to stormwater and hydraulic challenges. The I-90 project corridor passes through the Wenatchee National Forest and runs adjacent to the northeastern shore of Keechelus Lake for the first 6 mi, then parallels the Yakima River for the remaining 9 mi. The project crosses five tributaries to Keechelus Lake and nine significant tributaries to the Yakima River, including the Kachess River. The project also crosses or is adjacent to numerous wetlands (*9*).

The nature of the surrounding alpine environment, climatic extremes, and the need to protect water quality made the selection, design, and mitigation process for stormwater management systems challenging. Additionally, portions of the project are located on steep slopes (rock cliffs) where the construction of stormwater BMPs would be very difficult and require extensive structural support. Other typical freeway BMPs are infeasible because portions of the project are located in narrow corridors where cliffs are on one side of the freeway and a lake or river is on the other side, with no room for a median. And while not exactly a physical constraint, snow management and snow hydrology play a large role in how space is utilized and what BMPs are most suitable, with open areas in the median or adjacent to the freeway likely doubling as both snow storage areas as well as stormwater BMP locations (*9*).

The project team relied on additional expertise outside of the current team by establishing a multiagency STC to review stormwater design and permitting issues; evaluate analysis and preliminary engineering approaches developed by WSDOT; and recommend appropriate, effective, and efficient mitigation methods to the design team. STC members included WSDOT, USFS, Ecology, and consultant staff. These members have permitting approval roles or are partner agencies with a strong interest in helping solve stormwater problems.

The general objectives of the STC were to review WSDOT stormwater analysis and recommendations and provide feedback, help identify areas where stormwater management will be particularly challenging (unconstrained, partially constrained, and fully constrained areas), and help formulate and evaluate innovative stormwater solutions and mitigation alternatives (*9*). The STC was also charged with reviewing stormwater technical and permitting issues and directly enhancing the clarity and assurance of project stormwater-related design and approvals (*10*). Other topics for the STC to address included site-specific water quality concerns, cold climate considerations, maintenance of the hydrologic cycle, capital costs, maintenance and operations effort and cost, constraints on BMP types, and optimal versus less than optimal BMP performance (*10*).

While recommended stormwater treatment designs are currently under way, the STC has made recommendations to WSDOT on how to resolve these complex issues. WSDOT and the STC have selected permanent stormwater BMPs to maximize the amount of on-site treatment. WSDOT selected the recommendations that were considered most suitable given stormwater standards, space limitations, ecological goals, cold climate concerns, and other criteria. The STC's work allowed WSDOT to receive approval from Ecology for a range of BMPs to apply to the project area.

The physical setting of the project, however, sometimes makes constructing on-site BMPs infeasible. These areas were identified as "constrained areas." WSDOT intends to mitigate for constrained areas by providing off-site equivalent area treatment, as allowed by WSDOT's 2008 *Highway Runoff Manual* (*11*). Equivalent area treatment will be provided by retrofitting stormwater treatment on suitable off-site freeway and WSDOT maintenance facility locations within the Keechelus Lake drainage basin (*12*). Recent work has focused on developing conceptual WSDOT Hyak Maintenance Facility stormwater treatment retrofit options, including bioinfiltration swales; the use of passive, nonstructural treatment BMPs preceded by settling vaults; and buffer strips along creeks.

COMMUNICATING WITH PROJECT STAKEHOLDERS, PARTNERS, AND THE PUBLIC

Since beginning the public scoping process in 1999, WSDOT has engaged in a continuous process of communication with the public, interest groups, and other stakeholders. WSDOT has shared infor-

mation with these groups in an open and transparent manner, which has made the agency credible and qualified to act in the public's best interest.

In addition to communicating and collaborating with federal, state, tribal, and local agencies on the IDT, MDT, and technical committees, WSDOT formed relationships with transportation-based organizations, associations, and businesses in order to gain insight into the requirements of highway users. This includes relationships with the Ports of Seattle and Tacoma, Washington State Good Roads and Transportation Association, Washington Trucking Association, Freight Mobility Strategic Investment Board, and local importing and exporting freight business. WSDOT also developed partnerships with a variety of agencies, landowners, and citizen groups (such as the Sierra Club and Cascade Land Conservancy) to reduce conflicts that could affect the project (*2*). WSDOT's I-90 project representatives have also attended more than 40 outreach events throughout the year, including community fairs, festivals, farmers' markets, student science fairs, and presentations to various groups.

USING COLLABORATIVE APPROACH FOR IDENTIFYING PREFERRED ALTERNATIVE

FHWA published the Notice of Availability for the draft EIS in the *Federal Register* on June 10, 2005. The draft EIS presented existing environmental conditions along the I-90 project corridor, along with a range of six possible alternatives for WSDOT, FHWA, and the IDT to analyze that would potentially meet the project's purpose and need. The draft EIS analyzed the environmental, social, and economic consequences of each alternative, based on technical reports or memoranda prepared for key environmental disciplines. FHWA and WSDOT distributed 2,071 copies of the draft EIS to tribes, agencies, libraries, and members of the public (*2*).

After publishing the draft EIS, the lead agencies solicited written and oral comments from the public, agencies, and organizations during the 45-day comment period. Public hearings held in Ellensburg, Hyak, and Seattle, in June and July 2005, gave citizens and agencies the opportunity to comment on the draft EIS as well as meet project staff. The lead agencies also maintained a project website that provided the public with the opportunity to provide comments via e-mail.

After reviewing comments received during the draft EIS and gathering final recommendations, WSDOT and the IDT identified the I-90 project preferred alternative by using the collaborative processes mentioned above. The general process for identifying the preferred alternative included the following:

- Presenting on individual issues such as tunneling logistics, structural engineering, and considering the MDT's recommendations related to ecological connectivity;
- Reviewing draft EIS comments;
- Using this information to develop IDT recommendations for the preferred alternative;
- Identifying the preferred alternative based on the lead agencies' (FHWA and WSDOT) concurrence with the IDT's recommendations; and
- Performing additional technical studies and cost estimates to refine the preferred alternative before issuing the Final EIS (*2*).

FHWA and WSDOT published the notice of availability for the final EIS on August 29, 2008. WSDOT circulated over 6,500 copies of the final EIS, mostly in a DVD/CD set. The preferred alternative in the final EIS met the project's purpose and need in the following ways:

- The highway will be expanded from two to three lanes in each direction. This will accommodate projected traffic volumes for the next 25 years.
- The aging, deteriorated highway surface will be replaced with new concrete pavement. This will provide a smoother ride and reduce maintenance costs.
- Where possible, highway curves will be straightened to increase sight distance, drivability, and safety.
- New chain-up areas will be built, providing additional area for trucks and motorists to move out of the travel lanes.
- Low, narrow bridges at two interchanges will be replaced, making truck travel through the interchanges safer and more efficient.
- Avalanche risks and associated closures will be reduced substantially by replacing the existing Lake Keechelus Snowshed Bridge with an expanded six-lane snowshed covering all highway lanes. This will increase safety and reduce road closures for avalanche control work.
- Slopes will be stabilized to reduce rock fall hazards. This will increase safety and reduce road closures due to rock fall.
- Structures for wildlife passage will be built at the 14 major wildlife crossing areas within the project. This will increase safety by reducing collisions between wildlife and vehicles and will connect habitat that is currently separated by the highway. Wildlife passage will be improved by
  - Replacing narrow bridges and culverts with longer, wider bridges and culverts;
  - Adding wildlife exclusion fences and other features to keep wildlife off the highway; and
  - Adding wildlife overcrossings at strategic locations (*2*).

After publishing the notice of availability, a 30-day review period began for the public, agencies, and other relevant reviewers. WSDOT hosted open houses in Ellensburg, Hyak, Bellevue, and online to give citizens and agencies the opportunity to learn about the preferred alternative, as well as to meet project staff. Additionally, to educate the public about the release of the final EIS and open houses, WSDOT mailed over 4,900 postcards to residents living along the I-90 project corridor, sent e-mails to those registered on project mailing lists, posted informational flyers, placed advertisements in 15 newspapers, mailed letters, and conducted 12 media interviews. The FHWA issued a Record of Decision on October 6, 2008, concurring with WSDOT in its choice to construct the preferred alternative.

SUCCESSES AND CHALLENGES OF USING THE COLLABORATIVE APPROACH

Benefits

WSDOT was able to meet I-90 project design and environmental objectives by using the collaborative approach to identifying a preferred alternative. Several key factors contributed to the success of this approach, including the early identification of the project's purpose and need, early information sharing, agency role definition, and expectation management.

Even though it took months to complete, clearly defining the project's purpose and need was the critical first step in forming the foundation needed for collaborative success. The project purpose and

need ensured that the I-90 project design team and partners were working to accomplish common goals and outcomes.

After identifying the purpose and need, WSDOT and its partners agreed that the early sharing of information and open communication were critical to shaping the project and identifying issues to investigate. The project team used the philosophy of "no surprises," and information sharing was targeted toward that goal. The no-surprises goal was achieved by sharing information with project partners that was preliminary in nature. As the information was refined, each partner could contribute and track its progression. Information sharing and open communication were essential in developing a project that incorporated the concerns of agencies and the public into project designs.

Early information sharing also helped WSDOT identify and manage reasonable and unreasonable expectations of partnership agencies and the project team. Expectation management is an essential component to the collaborative approach. WSDOT identified its partners' expectations early on in order to filter through the realistic and unrealistic ones. WSDOT worked with its group of partners to deliver on the realistic expectations and eliminate or modify the unrealistic ones. Expectations are equivalent to the scope of the project and of each partner; therefore, management of expectations is critical to keeping a project on scope, on budget, and on schedule.

Identifying and managing agency expectations leads to establishing agency role definitions. Agency role definitions ensure mutually compatible partnerships. For the I-90 project, it was important that WSDOT's collaborative approach benefit all agencies and organizations involved, so that together they could provide a holistic landscape management plan that considered each agency's mission while meeting project needs and benefiting the natural environment.

The collaborative approach process is scalable. WSDOT's South Central Region manages the I-90 project and has used this partnership approach on other projects before, albeit not to this scale. For the I-90 project, WSDOT budgeted $10 million to $12 million for preliminary project engineering and environmental. Over the course of 8 years, WSDOT conducted hundreds of meetings between 12 agencies and four tribes that resulted in the creation of over 30 discipline reports for the I-90 project. WSDOT believes the collaborative approach builds projects that build communities. For the I-90 project, the support of agency, tribal, and public communities were taken into account, which in turn, allows the project to support Washington State as a whole.

Challenges to the Collaborative Approach

The collaborative approach, although successful, also presents challenges. WSDOT faced many challenges when collaborating on the I-90 project, including issues with timely negotiations, conflicts and strained relationships, drawbacks to early information sharing, and wavering perseverance.

Federal, state, and local agencies, as well as tribes, all have unique cultures, and because of these cultures, negotiations take an incredible amount of time to complete. Every agency is its own bureaucracy, and its business practices must be respected and accommodated. Respecting business practices includes recognizing each agency's sensitivity to certain issues. Conflicts can arise that strain the partnership if these factors are not recognized. WSDOT realizes that it is okay to agree to disagree, as conflicts will occur. Therefore, proactively planning for these conflicts is an important part of interagency management. WSDOT has learned that when a conflict arises, it is best to discuss the conflict, identify resolution options, and decide on a course of action as a group. Additionally, it is important to recognize that personal opinions are part of a conflict, so when a conflict arises, extra effort must be made toward respecting the feelings and emotions of invested partners. Another important method to managing conflict is ensuring that group facilitators and team managers have conflict management and resolution training.

Even though early information sharing was critical to the no-surprises goal, it proved challenging at times. Early information must be presented within the boundaries defined by the project team. When sharing information of a preliminary nature, it is important to clearly explain that the data are in draft form, may not contain certain details, and will require visionary thinking. Since not all individuals are visionary thinkers, early information can oftentimes blur the natural progression of project design, making it difficult for partnership agencies to formulate a response to the data.

Lastly, perseverance to succeed is critical when using the collaborative approach. It is important to have a group of leaders and facilitators who are dedicated to the project and its outcomes, and are willing to persevere through the challenges and inevitable conflict and see it to the end. There are always solutions to problems, despite how bleak the situation appears.

Final Lessons Learned

Over the past 10 years of designing the I-90 project, WSDOT has learned that no matter how clearly roles, expectations, and partnerships are defined, open, honest, and respectful interaction between people drives success. Understanding agency cultures, recognizing and managing conflict, and taking the time to nurture and invest in partnerships are equally important to both the project and the collaborative approach's success.

NEXT STEPS FOR WSDOT AND I-90 PROJECT PARTNERS

Completion of design plans for the second construction contract within the first phase of the I-90 project occurred on November 2, 2009, with construction scheduled to begin spring 2010. Design plans and permitting actions for the third construction contract are scheduled for completion in fall 2010, with construction scheduled for spring 2011. The highway improvements from Hyak to Keechelus Dam will be completed by 2015. Other projects within Phase 1 are still being scheduled for completion thereafter.

Phase 2 of the I-90 project from Keechelus Dam to Easton is currently unfunded. However, WSDOT and project partners are actively trying to secure funding for the contracts comprising this important phase.

WSDOT will continue working with the I-90 project IDT throughout design and construction of Phase 1 and will continue this coordination into future Phase 2. The Stormwater Technical Committee and Wetlands Mitigation Technical Committee will continue to be engaged as designs progress and issues are identified that require technical input from WSDOT's partners.

WSDOT is committed to working with the Wildlife Monitoring Technical Committee to monitor ecological connectivity structures for the Wildlife Monitoring Plan's Tier 1 objectives and support partners in reaching the plan's Tier 2 objectives. WSDOT's role as the lead on this committee will likely diminish as agencies who

manage the land and wildlife resources at the landscape scale move into a lead role.

In summation, WSDOT will continue to collaborate with project partners, stakeholders, and resource agencies to overcome challenges as they arise during construction and in future designs. While the remaining 10 project miles from Keechelus Dam to Easton remain unfunded at this time, WSDOT, along with its project partners, stand ready to deliver.

REFERENCES

1. National Environmental Policy Act. *NEPA Special Report,* GNB ed. 33, March 2009, p. 66.
2. *I-90 Snoqualmie Pass East Project Final Environmental Impact Statement.* FHWA-WA-EIS-05-01-F. Washington State Department of Transportation, Aug. 2008, pp. ES-1–ES-4, ES-7, ES-8, ES-11, 1-1, 1-17, 1-18, 1-20.
3. *Cost Estimate Validation Process.* Washington State Department of Transportation, 2009.
4. *Interdisciplinary Team Boundaries Statement.* Washington State Department of Transportation, 2000, p. 1.
5. *I-90 Snoqualmie Pass East Project Draft Environmental Impact Statement.* FHWA-WA-EIS-05-01-D. Washington State Department of Transportation, June 2005, p. ES-1.
6. *Interstate 90 Snoqualmie Pass East Mitigation Development Team Recommendation Package.* Washington State Department of Transportation, July 2006, pp. ES-7, ES-8, ES-11, 1-5.
7. *Wildlife Monitoring Technical Committee Memo.* Washington State Department of Transportation Interdisciplinary Team, 2007, p. 1.
8. *I-90 Wildlife Monitoring Plan.* Washington State Department of Transportation and Western Transportation Institute, Feb. 2008, pp. viii, ix, 1–8.
9. *Stormwater Treatment and BMP Report.* Washington State Department of Transportation and Otak, Inc., Aug. 2007, pp. 1-2, 2-3, 2-7.
10. *Draft Final Technical Memorandum #3 I-90 Snoqualmie Pass East Stormwater Technical Committee Process and Schedule.* Washington State Department of Transportation and Otak, Inc., Feb. 2007, p. 2.
11. *Highway Runoff Manual.* Washington State Department of Transportation, 2008.
12. *Stormwater Treatment Constrained Areas and Off-Site Mitigation Areas Progress Report.* Washington State Department of Transportation and Otak, Inc., Nov. 2008, p. 3.

The Environmental Analysis in Transportation Committee peer-reviewed this paper.

Regionwide Cumulative Effects Analysis of Long-Range Transportation Plans

Chris Paulsen, Patrick J. Crist, Gwen Kittel, and Ian Varley

This study investigated the feasibility and limitations of a regionwide cumulative effects analysis of long-range transportation plans (LRTPs). The key to meaningful regional cumulative effects assessment and resource conservation planning is determining when a significant impact to any given resource has been reached. This study applied a select set of natural and cultural resource metrics to the 2035 long-range transportation plans of large, medium, and small metropolitan planning organizations (MPOs). A spatial analysis was conducted to calculate the cumulative loss in the distribution of four representative resources from the proposed transportation network and land use changes. The results generated information about the resource spatial distribution and retention requirements for long-term viability. The cumulative effects were measured against quantitative sustainability indicators of high, medium, and low risk; at that time, stakeholders and decision makers could make a determination of the significance of the environmental impacts before the LRTP was complete. Informed decisions can be made about trade-offs; changes can be made to plan alternatives to create more compatible plans, or mitigation of plan effects can be identified. The model used for this study is a flexible but robust model that does not impose an undue burden on a department of transportation or MPO, but it does rely on input from resource agency experts and other stakeholders. Data were readily available in a geographic information system format, and the process appears viable for most MPOs and partners.

The Safe, Accountable, Flexible, Efficient Transportation Equity Act: A Legacy for Users (SAFETEA-LU), enacted in 2005, established requirements that metropolitan transportation plans provide for actions and strategies to protect and enhance the environment. These requirements were intended to promote efficient project management and reduce delays in the project-level environmental review process by providing the opportunity to identify and resolve issues of concern early in the long-range transportation planning process.

Metropolitan planning organizations (MPOs) and departments of transportation (DOTs) must consult with the public, state, tribal, and local land management, environmental, conservation, and historic preservation agencies and compare proposed transportation plans with any available conservation plans, maps, and inventories of natural and historic resources. The long-range transportation plan (LRTP) must include a discussion of potential environmental mitigation activities and locations to carry out those activities, including those activities that may have the greatest potential to restore and maintain the environmental functions affected by the plan. Although there are some similarities to the National Environmental Policy Act (NEPA) environmental analysis, a NEPA analysis of the LRTP is not required. However, when decisions that are made in planning are consistent with NEPA requirements, they can be used to streamline the project-level NEPA analysis (*1*). DOTs and MPOs need the tools to analyze resource data and present quantitative results of cultural and natural resource impacts to stakeholders and decision makers so that meaningful environmental information can inform decision makers of potential significant impacts before the plan is completed.

C. Paulsen, ICF International, 9300 Lee Highway, Fairfax, VA 22031. P. J. Crist, G. Kittel, and I. Varley, NatureServe, Suite 2110, 4001 Discovery Drive, Boulder, CO 80303. Corresponding author: C. Paulsen, cpaulsen@icfi.com.

Transportation Research Record: Journal of the Transportation Research Board, No. 2158, Transportation Research Board of the National Academies, Washington, D.C., 2010, pp. 10–18.
DOI: 10.3141/2158-02

RESEARCH OBJECTIVE

The objective of this study was to develop a framework and toolkit to support regional cumulative effects assessments for LRTPs and to test and evaluate them in three MPOs with different levels of staff capacity. The approach applied natural and cultural resource metrics to the transportation plans, similar to an air quality conformity analysis, to help decision makers determine significant cumulative effects of a transportation network on a given resource within the planning region.

METHODOLOGY

The general cumulative impact assessment workflow model shown in Figure 1 describes the flow of information from source inputs [current and future land use geographic information system (GIS) maps, resource maps, expert knowledge, stakeholder input, etc.] through analytical functions to calculate the cumulative loss in resource distribution or condition. The purpose of creating this workflow was to provide a relatively simple but highly robust and flexible approach to conducting a regional cumulative impact assessment. Cumulative effects are measured against defined indicators, at which point stakeholders and decision makers can make a determination of the significance of the resource impacts. The results can then be used to identify a preferred transportation and land use scenario and potential mitigation strategies.

The workflow is modeled on some of the core concepts of systematic conservation planning (*2*) and the use of spatial decision support tools that automate a great deal of the technical GIS work necessary to carry it out (*3*).

CUMULATIVE IMPACT ASSESSMENT

The general cumulative impact assessment model consists of three submodels (land use scenarios, resource distribution, and impact evaluation) that map or generate scenarios of infrastructure, land use,

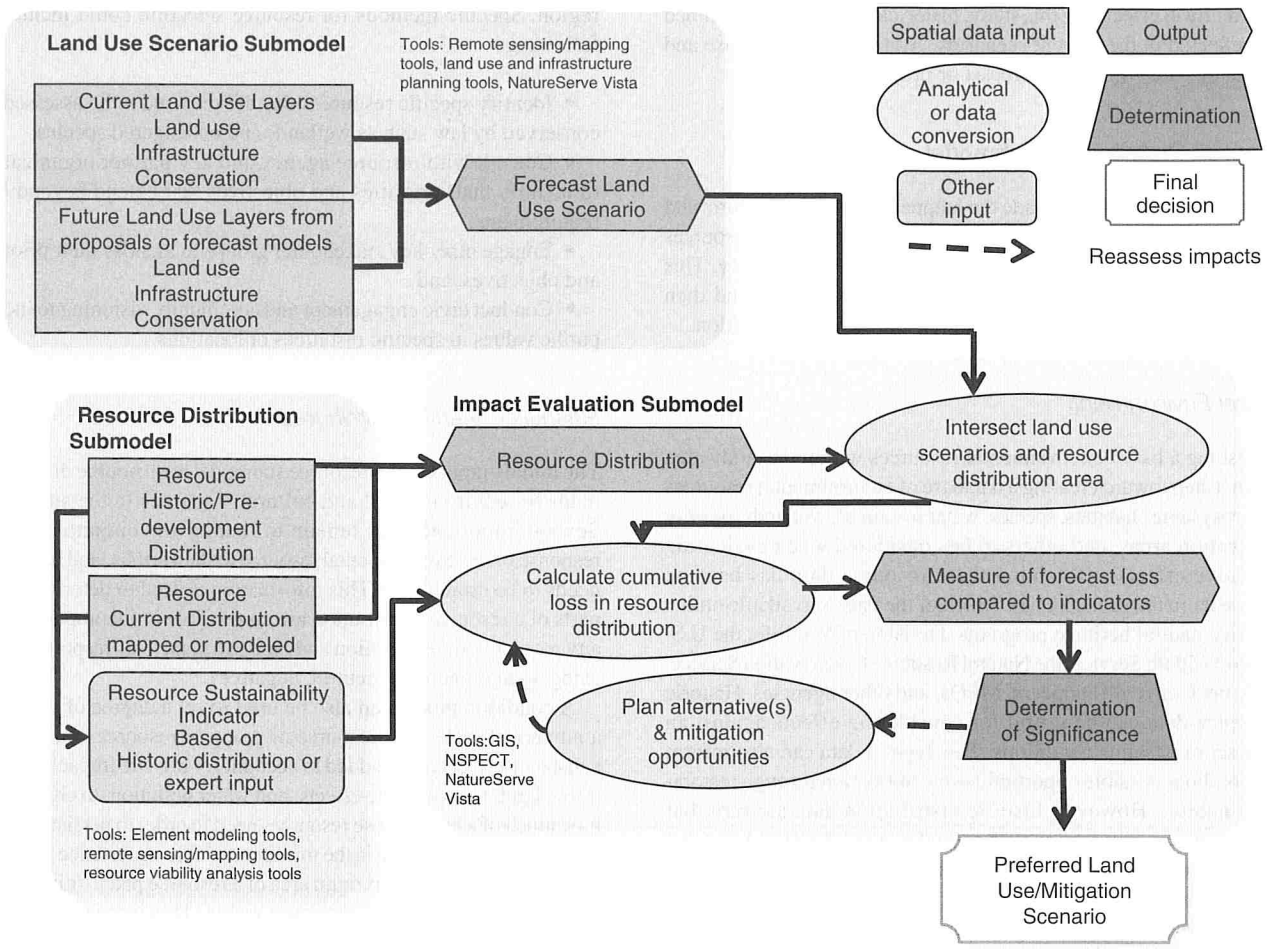
Land Use Scenario Submodel
Tools: Remote sensing/mapping tools, land use and infrastructure planning tools, NatureServe Vista
Current Land Use Layers
Land use
Infrastructure
Conservation
Future Land Use Layers from proposals or forecast models
Land use
Infrastructure
Conservation
Forecast Land Use Scenario
Spatial data input
Output
Analytical or data conversion
Determination
Other input
Final decision
Reassess impacts
Resource Distribution Submodel
Resource Historic/Pre-development Distribution
Resource Current Distribution mapped or modeled
Resource Sustainability Indicator Based on Historic distribution or expert input
Tools: Element modeling tools, remote sensing/mapping tools, resource viability analysis tools
Impact Evaluation Submodel
Resource Distribution
Intersect land use scenarios and resource distribution area
Calculate cumulative loss in resource distribution
Measure of forecast loss compared to indicators
Plan alternative(s) & mitigation opportunities
Determination of Significance
Tools:GIS, NSPECT, NatureServe Vista
Preferred Land Use/Mitigation Scenario

FIGURE 1 General cumulative impact assessment model.

natural and cultural resource distribution, and other factors important for assessing cumulative effects of the LRTP. The following sections describe the inputs and outputs of the workflow model shown in Figure 1.

Land Use Scenario Submodel

A cumulative analysis describes physical factors (land uses, management practices, natural disturbances, etc.) occurring or planned or predicted to occur on the land, in the water, or in the air. Typically, a baseline scenario of current actual factors is constructed and then separate scenarios are constructed that add factors to the baseline to describe allowed factors under current policies, proposed factors, or expected factors under market or ecological and climate trend models. With planned or predicted factors layered on the baseline, cumulative factors are expressed. Long-range transportation or corridor plans are represented as "proposed" scenarios but would be inclusive of current factors and may also include trends (e.g., in urban growth) and other disturbances that would add cumulative effects. During this step, the decision makers would define the spatial and temporal limits of the study area in order to identify appropriate factors as inputs to land use scenario mapping.

Many land use map layers are becoming increasingly available online through state, regional, county, or city GIS clearinghouses. Future land use layers can be extracted from the MPO's 20+-year comprehensive plans or vision assessments. If these data are difficult or impossible to obtain, tools can be used to model future urban growth spatially on the basis of spatial trends or more complex object-based models.

Because the land use scenario factor source maps will come from different organizations or programs, they will use different codes and names to describe similar factors. For this reason, it is imperative to develop a common land use classification to be used in the analyses. These typically already exist for most planning jurisdictions but often contain considerably more detail (e.g., dozens of urban land use types) than are needed for a cumulative effects analysis. As described below, the descriptions of factors will be used by resource experts to determine the response of resources to the factors. Therefore, it is important to have a classification that is informative but as simple as possible. Tips for creating land use classifications include the following:

- Good classifications are simple and intuitive.
- Classification factors should be hierarchical and nest more specific types within more general types.
- Classifications should allow new factors to be incorporated as they are identified or changed depending on expert input.

The outputs of this process are different scenarios. An initial or baseline scenario may simply reflect what land uses and land policies

are currently in effect. For this study, historical land use was assumed to be reflected in the current scenarios. Adding future land use and land policy data will create forecast or proposed scenarios.

Resource Distribution Submodel

The resource submodels include the mapped or modeled historic and current distribution of the natural and human environmental resources present in the planning area and their metrics of sustainability. This section provides an overview of the types of resources and then describes recommendations for resource and indicator selection.

Natural Environment

Establishing a list of environmental resources within the study area is the first step toward creating a database of environmental resources (e.g., ecosystems, habitats, species, water resources, wetlands, priority conservation areas, and others to be considered when evaluating cumulative effects). Obtaining these resource data has become much easier in the past 20 years. Much of the data is available online from state natural heritage programs, Division of Wildlife, the U.S. Fish and Wildlife Service, the Natural Resource Conservation Service, U.S. Army Corps of Engineers, MPOs, and other agencies. Historic occurrence data can be useful for considering effects against an earlier set of baseline conditions. This type of data can also inform planners about possible opportunities for mitigation through restoration of habitat. However, historic distribution data are rare, but imperilment or rarity ratings such as Endangered Species Act status can be used to represent the relative amount of historic loss of resources with such ranks.

Certain resources may be of concern but have limited occurrence data. Predictive distribution maps can be very useful for calculating expected effects on resource distributions and avoiding surprises during project environmental studies that should have been considered during the LRTP process.

Human Environment

The human environment includes such features as historic properties, low-income and minority communities, green infrastructure (parks, greenways, and designated open space), paleontological resources, and other resources valued by the local stakeholders. In recent years cultural resource information has become more accessible online through state and local government GIS data clearinghouses, but data security and privacy issues may make the data for some resources more difficult to obtain (e.g., historic resources). As with similarly secure environmental data, partnerships are important for gaining data access.

In contrast to environmental resources that tend to decline over time, some cultural resources tend to increase in number. For example, properties that are not considered historic today may change in status over the life of the LRTP. However, it is likely that these changes cannot be predicted and the resources may have to be reassessed during project-level analyses.

Selection of Resources

The selection of resources is conducted primarily by considering legal requirements and stakeholder and citizen values in the planning region. Specific methods for resource selection could include the following:

- Identify specific resources that are required to be assessed and conserved by law such as wetlands and endangered species,
- Consult with resource agency and key partner organizations to identify their priorities and objectives that extend beyond legal requirements,
- Engage other key stakeholder groups to identify their priorities and objectives, and
- Conduct civic engagement and community visioning to include public values in specific resources or locations.

Resource Viability Attributes

The initial outputs of the resource submodel are resource distribution maps for environmental and cultural resources in the study area. Several important steps remain to finalize the outputs. First, the response of the environmental resource to the various land use factors needs to be established. This information is used to determine what parts of a resource distribution are compatible or incompatible with any particular transportation and land use plan. This response can be categorical (beneficial, neutral, negative).

A condition model can also be used to set a degree of impact on a numerical scale for a resource or group of resources. In addition, a distance effect can be added to account for off-site impacts, such as noise, light, microclimate effects, and water pollution, to characterize how much of a buffer these resources need in order to persist. Another useful resource attribute is the minimum viable occurrence size. This usually describes the minimum area of a resource patch or interacting group of patches that is considered viable. This information can be obtained from a variety of sources: environmental impact statements, game management plans, individual species studies, historic maps, and most productively through direct resource expert input.

Resource Sustainability Indicators

Recommendations are provided for setting quantitative goals for retaining resources. This is a key part of systematic conservation planning and regional cumulative effects assessment to determine when levels of significance of effects have been reached. Setting goals for resource sustainability serves four useful purposes. First, goals allow an evaluation of how effective a proposed plan will be in retaining resources at levels believed to be necessary to achieve their long-term viability within the region or project area. Second, setting explicit goals enables planners and managers to better understand and account for the trade-offs that often must be made in trying to sustain cultural and natural resources. Most decision makers are routinely placed in such positions by laws and policies that require them to make these sorts of trade-offs. Third, goals will help planners realize how many conservation areas are needed at regional and local scales and may underline how important a particular conservation area may be. Fourth, goals are quantifiable and document a desired vision of future scenarios by stakeholders, the general public, and resource agencies as well as planners.

The primary purpose of setting goals is to estimate the effort that will be necessary to sustain resources well into the future. "Sustain" does not mean keeping resources at minimal levels. How much is really enough? What proportion of a resource needs to be conserved to be maintained into the future? These are among the most difficult

questions for planners, biologists, and resource managers to answer and are some of the most discomforting because there are no definitive answers. The overarching goal or vision is to identify priorities with all stakeholders to meet resource-specific protection goals. Resource experts apply scientific concepts to set sustainability goals but are informed by public values in the form of laws, policy, or stakeholder input.

Guidelines for Setting Resource Retention Goals

The following are some guidelines for setting resource retention goals:

- Use recommendations from literature, recovery plans, and experts.
- Use results from species–area relationships for communities and ecosystems.
- Use history as a guide to the past and future. It is helpful to have some understanding of the historic extent of the resource. If only 30% of historic values remain, then a goal to retain all that is left can be presumed justifiable.
- Use alternative goals to explore potential optional scenarios. Maps of alternate scenarios can be a powerful tool to illustrate future options.
- Set retention goals with safety margins, especially when little is known about a certain resource.

Impact Evaluation Submodel

The process of quantifying and evaluating the cumulative effects is done in the evaluation submodel by comparing resource distributions with future land use scenarios and assessing effects against resource responses and sustainability requirements.

Compare Forecast Resource Loss with Performance Indicators

The model intersects resource distribution maps with scenario maps of cumulative land use factors. Each resulting combination of resources and factors is first assessed for resource response to determine if that area of intersection is compatible with resource sustainability or not. Next, aggregated areas of compatible resources are compared to a minimum required occurrence size input and, if that threshold is met, the area is summed to determine if the overall indicator is met. Results are output in both tabular report form and map graphics as shown in Figure 2. Specific outputs are detailed as follows:

- Scenario performance by resource. Reports resource indicator performance for each evaluated scenario according to percent of indicator achieved and quantity of resource remaining. Resources not meeting the indicator threshold are flagged.
- Scenario conflicts map. Depicts areas of the map containing resources that failed to meet retention goals (indicator threshold) and are incompatible with the scenario factors (e.g., land use) at those locations. Conflict areas are colored in an increasingly darker gradient to indicate the number of resource conflicts at those locations.
- Resource impact maps. Intersecting incompatible factors with resource data will produce maps for each resource illustrating areas where impacts are occurring or could occur given a particular scenario.
- Quantitative indicator reports by resource. The report provides detailed statistical and map outputs for each resource as it performed under each scenario.

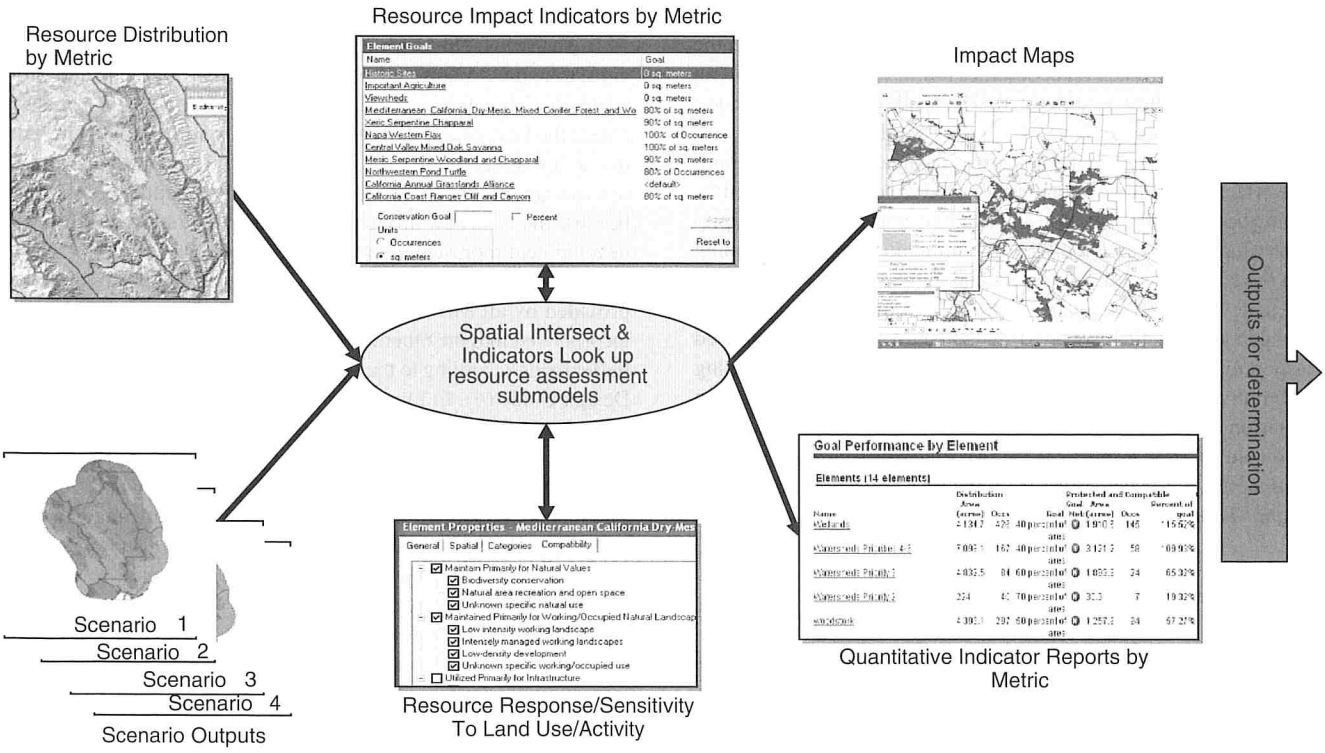

FIGURE 2 Scenario evaluation of cumulative effects.

Determination of Significant Impacts

These evaluations are used by planners, resource subject matter experts (SMEs), and decision makers to determine if impacts are sufficiently significant to reject a plan option or if modifications could be made to create an acceptable plan either through creating new alternative or mitigating impacts.

Plan Alternative Development and Mitigation

After cumulative effects and significance of impacts are understood, this workflow assists MPOs, DOTs, resource experts, and other key stakeholders in developing plan alternatives through avoidance or identification of other specific mitigation needs and opportunities. A modification course suggests that impacts could be avoided by changing the land use and transportation features of conflicting sites to compatible uses and relocating (if necessary) those conflicting uses to locations that would not cause conflicts. An alternative mitigation course suggests that some land use and transportation features cannot be changed or relocated and impacts will be incurred (some of which may be mitigated through minimization via project design, which is not addressed in this workflow). This workflow would address the process of identifying off-site locations and methods to achieve resource retention goals. Equipped with this information, decision makers can then determine the preferred land use and mitigation scenario.

TOOLS

Tools can include software, such as decision support systems, as well as documented methods. This assessment focused on the former though the entire workflow can be considered a documented method. There is no supertool capable of conducting all computerized analyses necessary for regional cumulative impact assessment; therefore, the use of a toolkit approach that combines multiple tools to support an information workflow is suggested. The toolkit used for this study consists of NatureServe Vista (*4*) on the ArcGIS 9.x platform with Spatial Analyst. NatureServe Vista was designed to support cumulative effects assessment and alternatives development followed by ongoing use in implementation and adaptive management. Complementary tools to this core toolkit are CommunityViz (for developing trend models of urban development and iterating with NatureServe Vista to develop land use plans), N-SPECT (estimating and comparing impacts to aquatic resources), and QuantM (fine tuning planned transportation corridors and optimizing alternatives). However, using a different combination of tools could produce similar results. An evaluation of the capability and limitations of a range of tools is included in *NCHRP Report 25-25 (54): Evaluate Colorado's ACEA Methodology as a Mechanism for Cumulative Impacts Assessment in Regional Transportation Plans* (*5*).

RESULTS

Three pilot MPOs in Colorado were used to test and evaluate the workflow and toolkit but focused on the regionwide cumulative effects analysis. The MPOs were selected to represent different levels of capacity defined primarily as the technical capability and number of staff available to conduct the workflow. The three MPOs included the high-capacity Denver metropolitan district, the Denver Regional Council of Governments (DRCOG); the medium-capacity Pikes Peak Area Council of Governments (PPACG) (Colorado Springs and eastern towns of El Paso County); and the lower-capacity Pueblo Area Council of Governments (PACOG).

Current and Future Land Use for Pilot MPOs

At 3,608 mi^2, DRCOG was the largest area examined. Current land use was represented by a map developed in 2008 to conduct a municipal-level analysis. Every parcel in the region is designated one of five development types: urban, semiurban, semirural, rural, and undevelopable (the latter typically representing local, state, or federal lands or areas restricting development due to steep gradient, etc.). DRCOG projected future land use by using the 2035 urban growth boundary assuming all parcels would be converted to urban or undevelopable land use future planned parks, for example.

The PPACG focused on El Paso County with a project area of 2,130 mi^2. This decision was based on availability of data and focused on the effects of new roads and development in the I-25 corridor. PPACG provided current and 2035 land use and transportation layers. The analysis also incorporated a second future scenario for transit-oriented development developed in 2007 for El Paso County.

PACOG consisted of Pueblo County, containing an area of 2,398 mi^2. Data used included present scenarios from various land use layers and the future scenario from the 2035 Long-Range Transportation Plan (which included land use).

Spatial Analysis Workflow

The spatial analyses of the workflow were conducted as follows:

1. Scenarios. This study used the council of governments (COGs) current land use maps and 2035 plans to create baseline and future scenarios. The plans were already produced by the COGs and represent the best guess of urban and transportation expansion. Land use and management data were translated into "standard" land use categories. The 2035 scenarios represent cumulative scenarios because they add new infrastructure and urbanization to the existing development represented in the baseline scenario.
2. Assessment of the road network effects. Road networks were provided by all MPOs for inclusion in the scenarios. These were incorporated into the other land use layers by using the lane width to buffer roads according to the Colorado Department of Transportation Design Guide (*6*). In future scenarios, road networks are expanded through addition of new roads or widening of existing roads to accommodate projected increase in capacity needs. The buffers ranged from 120 ft for a two-lane highway to 300 ft for a six-lane highway. The recommended widths include lanes, shoulders, medians, and side slopes. These distances are more reflective of newer or rural cross-sectional roadways and likely overestimate the width of existing urban roadways.
3. Resource data. Many resources used for this study have been subjected to considerable expert scrutiny and represent cultural and recreational priorities already established at the local or regional level. Resources were divided and categorized into cultural and environmental groups to create separate conservation value summary maps for each group.

4. Documentation of resource responses: Resource responses to factors in the scenarios are combined with spatial analyses to calculate cumulative impacts and map conflict zones. A resource response describes how the resource is expected to fair when the scenario factor (e.g., urbanization) spatially coincides with the resource. The toolkit used in this study supports both categorical responses (e.g., negative, neutral, beneficial) and more detailed and precision models of how scenario factors affect the condition of the resource both on and off site. The simpler categorical response was assigned a negative response for most resources to transportation networks and most urban growth factors. For this demonstration project, these response assignments were based on general "rules-of-thumb" and professional judgment. Resource responses to scenario factors can be fine tuned as necessary and documented as to source and reasoning.

5. Calculation of cumulative effects. Scenario evaluations were run for three different significance and risk levels (high, medium, and low) in order to compare goal attainment and significance of impacts across scenarios and at different indicators of risk.

6. Scenario evaluation map and report products. These were generated for each scenario and indicator risk level. Products included a report and several visualization layers to be used in the decision-making process. The report summarized, in total and by category, the performance of the scenario in terms of the number and percentage of resources that met conservation goals. The report also provided a detailed comparison of individual resources against the scenario: their original distribution and the amount and percentage that was retained in areas with compatible land use, both with and without adequate protection (reliable policies).

7. Evaluation of site-level performance. The Vista Site Explorer tool was used on potential conservation areas (PCAs) to demonstrate the provision of an inventory of scenario factors and resources within the sites. Site reports include the inventory of resources and land use factors within the site, the number and percentage of resource occurrences that are compatible and protected (i.e., areas with compatible land uses along with policy types that will reliably ensure that the actual land uses will be no more intensive than the uses indicated), and the achievement of resource retention goals within the site and across the planning region. The site query also informs whether the site is capable of significantly providing for resource goal achievement if changes are made to land use factors or policy, or both. It also indicates which factors are causing conflicts and the area of each factor.

8. Development of alternatives or mitigating impacts. In addition to data on the PCAs and resources that occur, the Site Explorer tool was employed to demonstrate the process for creating more compatible scenarios. This was done by developing and saving an alternative (e.g., mitigation) scenario specifying more compatible land uses to achieve conservation of the PCA. This provides a critical feedback loop for transportation planners, allowing them to develop alternate scenarios that meet the goals and can be shared with stakeholders and decision makers for further input. This same tool and process can be used alternatively to specify resource conservation off site when relocating the conflicting land use factors is not feasible.

Resource Indicators and Metrics

In an actual LRTP assessment, a range of resources would be included to adequately represent biodiversity, ecosystem services, and cultural resources. For this study, four representative environmental and cultural resource areas of interest—biodiversity, priority conservation areas, environmental justice populations, and green infrastructure—were selected to test the feasibility of conducting the regionwide cumulative effects analysis.

Biodiversity

Biodiversity included native wildlife habitat expressed as ecological systems, wetlands (including riparian areas), individual plant communities (more specific components of broad habitat and ecological systems), and rare and threatened plant, animal, and fish species. This assessment used the ecological systems (natural habitats) and rare or imperiled species that occurred within or in close proximity to the future urban growth and new proposed roads.

- Example indicators for a low-risk plan
  - No loss of any regulated wetland,
  - No loss of nonjurisdictional wetland or riparian habitats,
  - No confinements, encroachment, or constriction of natural floodplains or drainages,
  - No more than 10% of the historic ranges of upland habitats are affected, and
  - 100% of known threatened or endangered species are not affected.
- Example indicators for a medium-risk plan
  - Up to 25% loss of any regulated wetland,
  - Up to 25% loss of nonjurisdictional wetland or riparian habitats,
  - Up to 30% confinement, encroachment, or constriction of natural floodplains or drainages,
  - No more than 30% of the historic ranges of upland habitats are affected, and
  - 80% of known threatened or endangered species are not affected.
- Example indicators for a high-risk plan
  - Up to 50% loss of any regulated wetland,
  - Up to 25% loss of nonjurisdictional wetland or riparian habitats,
  - Up to 50% confinement, encroachment, or constriction of natural floodplains or drainages,
  - No more than 70% of the historic ranges of upland habitats are affected, and
  - 50% of known threatened or endangered species are not affected.

Priority Conservation Areas

Priority conservation areas consisted of mapped areas identified through science-based, collaborative, and reviewed processes but not yet officially designated for conservation. A suite of areas were identified as the most important sites required to protect biodiversity and to maintain healthy functioning ecosystems and species populations in perpetuity. These include ecoregionwide assessments of biodiversity, its current status, and threats identified by the Nature Conservancy (TNC) and other conservation planning agencies. Smaller scale PCAs identified by the Colorado Natural Heritage Program were also included. In the DRCOG area, there were more than 100 PCAs identified by the Heritage Program. In the PPACG area, two PCAs were used, and in the PACOG area, none were employed for the demonstration.

- Example indicators for a low-risk plan
  - No impacts, encroachments, or loss of hydrologic functioning to any of the identified sites and
  - Where required, connectivity and wildlife movement is maintained unimpeded between sites.
- Example indicators for a medium-risk plan
  - Impacts, encroachments, or loss of hydrologic functioning of 20% of the identified sites and
  - Connectivity and wildlife movement is lost between sites by 20% to 40%.
- Example indicators for a high-risk plan
  - Impacts, encroachments, or loss of hydrologic functioning to 80% of the identified sites and
  - Connectivity and wildlife movement is lost between sites by 60% to 80%.

Environmental Justice Populations

Environmental justice populations included the location of low-income, minority, elderly, and other vulnerable neighborhoods.

- Example indicator for a low-risk plan. No fragmentation of low-income or minority communities.
- Example indicator for a medium-risk plan. Intrusion of new road(s) on up to 3% of a low-income or minority community.
- Example indicator for a high-risk plan. Intrusion of new road(s) on greater than 3% of a low-income or minority community.

Green Infrastructure

Green infrastructure (public recreational resources) included established ballparks, picnic areas, soccer fields, bike paths, and other green corridors designed for recreational and public use. This evaluation used currently mapped locations of established parks and bike paths as available for the pilot sites.

- Example indicators for a low-risk plan
  - No impacts or loss to established bike paths and parks and
  - Effects allowable only where unavoidable.
- Example indicators for a medium-risk plan
  - Impacts or loss up to 30% of established bike paths and parks and
  - Effects allowable only where unavoidable.
- Example indicators for a high-risk plan
  - Impacts or loss up to 50% of established bike paths and parks and
  - Effects allowable only where unavoidable.

Figure 3 provides a sample evaluation report. The report quantifies the performance of the scenario for each resource. Resources are reported according to categories and individually. Information includes (reading from left to right): the resource name (linked to more detailed individual resource reports), the resources' current mapped area, the retention goal (indicator) used in the evaluation, a graphic indication of goal achievement (green: goal met; yellow: 90% to 99.9% of goal met; and red: <90% of goal met), amount of area expected to remain for each resource, and the percent of the goal achieved.

In practice and fundamental to this process, the appropriate indicators and retention goals would be identified with MPO, DOT, resource agency, and other stakeholder input during scoping for the LRTP. No public or agency scoping meetings were held for this study and the authors developed example indicators and risk levels based on past experience with similar resource issues. There are many other possible resource metrics and indicators of risk for each resource will vary from one MPO to another.

CONCLUSION

The following sections present the results of this research.

Challenges and Limitations for Different-Size MPOs

Inherent in the requirements of this study was that the approach be tested and evaluated in three MPOs of different size and capacity to determine the capacity limitations of its implementation. The primary burden in carrying out the proposed workflow is on the resource agencies, partner nongovernmental organizations (NGOs), and various SMEs that would be required to develop the key information inputs. The technical requirements are actually quite low as described earlier.

The requirements for implementing the workflow and toolkit are somewhat scalable. That said, the workflow as detailed cannot be accomplished without involvement by resource agencies or NGOs that can provide key resource data and expertise in using resource data and conducting conservation and mitigation planning. Although the larger MPOs are likely to have the capacity and expertise to set up and maintain these partnerships, it will be very challenging for low-capacity MPOs to do the same. In addition, *NCHRP Report 25-25 (32): Linking Environmental Resource and Transportation Planning* (7) cited that transportation organizations recognize the importance of high-quality data, conservation planning expertise, and the resources needed to ensure participation by natural resource agencies in the transportation planning process, but resource agencies often report that they do not have sufficient staff to participate actively in interagency planning.

The lack of capacity by resource agencies can be mitigated somewhat by involvement of science-based NGOs such as TNC, but in the long run, more capacity for resource agencies to routinely engage with transportation planning activities will be required, as has been identified and acknowledged elsewhere. This will require internal capacity building and training in methods and tools.

Suggestions for Implementing the Workflow

This workflow represents an appropriate level of rigor and robustness for conducting regional cumulative impact assessments, identifying mitigation strategies for decision makers, and meeting SAFETEA-LU requirements for integrating planning and environmental considerations. Suggestions for implementing the workflow as described are followed by suggestions for a reduced approach.

- The simplest way for low-capacity MPOs and resource agencies to implement the workflow is to secure the necessary outside assistance to fill gaps in skills and capacity. NGOs and academic partners often have both the skills and motivation to provide such services in addition to many private consulting firms.

Summary

Name	Protected and Compatible Goal Met For	Goal Unmet For	Compatible Goal Met For	Goal Unmet For
element occurrences (4 elements)			2 elements (50%)	2 elements (50%)
ecological systems (8 elements)			7 elements (87.5%)	1 elements (12.5%)
pca (1 elements)			1 elements (100%)	0 elements (0%)
floodplains (1 elements)			0 elements (0%)	1 elements (100%)
environmental justice (2 elements)			1 elements (50%)	1 elements (50%)
green infrastructure (4 elements)			4 elements (100%)	0 elements (0%)

Back to top

Details

element occurrences (4 elements)

Name	Distribution Area (acres)	Occs	Avg Condition	Compatible Goal	Goal Met	Area (acres)	Occs	Avg Condition	Percent of goal
Plains Sharp-Tailed Grouse	71,668	17	NaN	80 percent of area	Y	62,561	17	NaN	109.12%
Mottled Duskywing	220,933	16	NaN	80 percent of area	N	96,922	16	NaN	54.84%
Bell's Twinpod	2,303	9	NaN	80 percent of area	Y	2,010	9	NaN	109.1%
shrwers elfin	250,424	18	NaN	80 percent of area	N	172,793	18	NaN	86.25%

ecological systems (8 elements)

Name	Distribution Area (acres)	Occs	Avg Condition	Compatible Goal	Goal Met	Area (acres)	Occs	Avg Condition	Percent of goal
Foothill and Piedmont Grassland	155,965	10670	NaN	70 percent of area	Y	124,362	7940	NaN	113.91%
Foothill shrubland	39,980	5382	NaN	70 percent of area	Y	33,319	4296	NaN	119.06%
Ponderosa Pine	378,027	10281	NaN	70 percent of area	Y	318,271	8442	NaN	120.28%
Gambels Oak Shrubland	98,044	5593	NaN	70 percent of area	Y	77,589	4454	NaN	113.05%
Shrub-dominated Wetlands	62,563	12322	NaN	70 percent of area	N	38,940	7253	NaN	88.92%
Shortgrass Prairie	88,261	6666	NaN	70 percent of area	Y	69,670	4700	NaN	112.77%
Sand Dune Complex Shrub	2,441	672	NaN	70 percent of area	Y	1,861	508	NaN	108.91%
Sagebrush	1,032	328	NaN	70 percent of area	Y	860	269	NaN	119.05%

pca (1 elements)

Name	Distribution Area (acres)	Occs	Avg Condition	Compatible Goal	Goal Met	Area (acres)	Occs	Avg Condition	Percent of goal
Potential Conservation Areas	232,948	115	NaN	70 percent of area	Y	197,483	113	NaN	121.11%

floodplains (1 elements)

Name	Distribution Area (acres)	Occs	Avg Condition	Compatible Goal	Goal Met	Area (acres)	Occs	Avg Condition	Percent of goal
Floodplains	185,145	1249	NaN	70 percent of area	◡	128,132	1220	NaN	98.87%

environmental justice (2 elements)

Name	Distribution Area (acres)	Occs	Avg Condition	Compatible Goal	Goal Met	Area (acres)	Occs	Avg Condition	Percent of goal
High percent minority areas	85,628	264	NaN	70 percent of area	Y	68,233	264	NaN	113.84%
High percent poverty areas	13,002	85	NaN	70 percent of area	N	6,997	82	NaN	76.88%

green infrastructure (4 elements)

Name	Distribution Area (acres)	Occs	Avg Condition	Compatible Goal	Goal Met	Area (acres)	Occs	Avg Condition	Percent of goal
open space and parks	771,190	4	NaN	70 percent of area	Y	754,825	4	NaN	139.83%
Bike paths	11,488	1	NaN	70 percent of area	Y	9,411.75	1	NaN	117.04%

FIGURE 3 Sample evaluation report.

- There are great efficiencies in streamlining the delivery of resource agency input into the planning process that can overcome what must appear as a torrent of requests for project-level input. Given that wildlife resources, for example, tend to be similar over larger regions than MPOs, the resource SMEs could be tapped once to provide information to numerous planning activities. It would be helpful for natural resource and transportation agencies to identify existing interagency groups and plug planning activities into those existing interagency dialogs. Thus, the ability to consolidate resource agency engagement across MPOs would make the involvement of resource agencies and NGOs in planning much more likely and efficient, thereby addressing many of the needs identified as being critical to a successful planning process.
- Where NGOs have developed conservation priority maps, they are logical partners to provide information to properly assess and apply those maps. Where current priority maps are lacking or inadequate for LRTP purposes, these organizations can act as SMEs to identify resources and retention goals along with additional necessary inputs.

- A single computer or computer lab can be used to conduct all technical work and input of SMEs gathered either through distribution of an input spreadsheet to SMEs or by convening an SME workshop. Thus, this need not be a long burdensome process nor require a large information technology capability to gather and integrate the necessary information.
- In cases where the MPO lacks any capacity to implement the proposed spatial analyses workflow, it is possible to use a significantly scaled back process, which can rely on SME involvement or be automated through a statewide system. The process in its most minimal form would entail overlaying (graphically with hard copies or through GIS) proposed LRTP alternatives with other spatial conservation priority maps for the resources of interest. Areas of potential conflict would be identified and SMEs would identify resources that might be impacted and make an expert judgment about the significance of the impact and options for mitigation. This alternative approach would accomplish the rudimentary need for comparing the LRTP to the resources but falls far short of the recommended framework in terms of ability to quantify cumulative effects and to support a full cycle of LRTP option development, assessment, selection, and implementation.

Data Availability

A regionwide cumulative effects analysis of the LRTP appears tractable for most MPOs and partners in terms of data availability and spatial analyses. For the four representative resource areas considered in this study, data were readily available from the MPOs and resource agencies in a GIS format. For the most part, the availability of the ecological data used in this study is typical nationwide. Cultural resources were represented by data from the MPOs and online census data. The data that MPOs have at hand vary from agency to agency and additional resource data may be scattered among different agencies. Most agencies will readily provide the data, particularly for biological resources.

ACKNOWLEDGMENTS

This paper was prepared by ICF International and NatureServe, and the original work (ICF International 2009) was guided by a task group chaired by Mia Waters of the Washington State Department of Transportation, which included Brad Beckham of the Colorado Department of Transportation, Craig Casper of Pikes Peak Area Council of Governments, Kelly McGourty of Puget Sound Regional Council, Caroline Twenter of East-West Gateway Council of Governments, and Rebecca Lupes of Federal Highway Administration. The project was managed by Nanda Srinivasan.

REFERENCES

1. *AASHTO Practitioner's Handbook 10. Using the Transportation Planning Process to Support the NEPA Process.* Feb. 2008. http://environment.transportation.org/pdf/programs/practitioners_handbook10.pdf. Accessed March 30, 2009.
2. Margules, C. R., and R. L. Pressey. Systematic Conservation Planning. *Nature,* Vol. 405, 2000, pp. 243–253.
3. Sarkar, S., R. Pressey, D. Faith, C. Margules, T. Fuller, D. Stoms, A. Moffett, K. Wilson, K. Williams, P. Williams, and S. Andelman. Biodiversity Conservation Planning Tools: Present Status and Challenge for the Future. *Annual Review of Environment and Resources,* Vol. 31, 2006, pp. 123–159.
4. NatureServe Vista online software available at http://www.natureserve.org/vista.
5. ICF International and NatureServe. *NCHRP Report 25-25 (54): Evaluate Colorado's ACEA Methodology as a Mechanism for Cumulative Impacts Assessment in Regional Transportation Plans.* AASHTO Standing Committee on the Environment, Sept. 2009.
6. Colorado Department of Transportation. *CDOT Design Guide 2005.* http://www.dot.state.co.us/DesignSupport/Design%20Guide%2005/Index.htm. Accessed June 17, 2009.
7. Cambridge Systematics, Inc., and NatureServe. *NCHRP Report 25-25 (32): Linking Environmental Resource and Transportation Planning.* AASHTO Standing Committee on the Environment, Dec. 2008. Available online at: http://onlinepubs.trb.org/onlinepubs/archive/NotesDocs/25-25(32)_FR.pdf.

The Environmental Analysis in Transportation Committee peer-reviewed this paper.

Estimating Diesel Vehicle Emission Factors at Constant and High Speeds for Short Road Segments

Hyung-Wook Choi and H. Christopher Frey

Vehicle emission estimates with high spatial and temporal resolution are needed to estimate near-roadway air quality and human exposure to emissions. The U.S. Environmental Protection Agency's (EPA) MOBILE6 emission factor model is based on test cycles with transient speeds and durations on the order of 10 min. MOBILE6 does not report emission factors for average speeds higher than 65 mph. However, for near-roadway studies, emission factors are needed for short highway segments that represent only a few seconds of vehicle travel time at approximately constant speed and speeds greater than 65 mph. Constant-speed and high-speed correction factors for nitrogen oxides, hydrocarbons, carbon dioxide (CO_2), and carbon monoxide were developed on the basis of 59,286 s of EPA dynamometer emissions data for diesel vehicles from which speed–acceleration modal models were derived. The constant speed correction factor is the ratio of the emission factor at constant speed to the emissions factor during transient cycles with an equivalent average speed. For example, the constant speed correction factor for CO_2 increases from 0.71 to 1 as speed increases from 31 to 78 mph. High-speed correction factors are based on the ratio of emission factors at a constant speed greater than 65 mph to emission factors at a constant speed of 65 mph. For example, at 80 mph, the high-speed correction factor is approximately 1.5 for CO_2. Sensitivity analysis of emission estimates to these correction factors was conducted for speeds of 40 to 80 mph.

Highway diesel vehicles contribute 16% of nitrogen oxides (NO_x) nationally (*1*). During the 1990s, the sales of heavy-duty pickup trucks increased approximately 38% (*2*). Recently, there has been interest in improving the quantification of human exposure to air pollutants near roadways (*3*). Vehicle emissions are needed at high spatial and temporal resolution to estimate near-roadway air quality and human exposures. An exposure scenario of concern is a school or residential area located near a high traffic volume highway.

Near-roadway exposures are associated with relatively short air pollutant transport distances. Therefore, there is a need to characterize emissions and air quality for relatively short segments of highway. Depending on the time of day, travel direction, and traffic volume, vehicle speeds on such segments can be well in excess of posted speed limits. Furthermore, such segments represent only a few seconds of vehicle travel, during which vehicles may be traveling at approximately constant speed, depending on traffic conditions. In contrast, existing emission factor models, such as MOBILE6, are based on test cycles with transient speeds and durations on the order of 10 min. MOBILE6 does not report emission factors for average speeds greater than 65 mph. Therefore, there is a need to develop an emission factor estimation methodology for speeds higher than 65 mph and for constant, rather than transient, speed (*4*). The objective of this paper is to develop such a methodology and demonstrate its use for diesel vehicles.

Department of Civil, Construction, and Environmental Engineering, North Carolina State University, Campus Box 7908, Raleigh, NC 27695-7908. Corresponding author: H. C. Frey, frey@ncsu.edu.

Transportation Research Record: Journal of the Transportation Research Board, No. 2158, Transportation Research Board of the National Academies, Washington, D.C., 2010, pp. 19–27.
DOI: 10.3141/2158-03

METHODOLOGY

To estimate emission factors based on MOBILE6 at speeds greater than 65 mph for short segments of highway, two correction factors were developed. These factors were derived based on speed–acceleration modal models for heavy-duty diesel vehicles (HDDVs), using U.S. Environmental Protection Agency (EPA) second-by-second dynamometer emissions data.

Emission factors for eight driving cycles that have different average speeds were estimated using the speed–acceleration modal models. The constant speed correction factor is based on the ratio of the emission factor of a given pollutant at constant speed to that for an average emission factor of a transient driving cycle with the same average speed. The high-speed correction factor is the ratio of an emission factor at an average speed greater than 65 mph to that at 65 mph.

Speed–Acceleration Modal Emission Rates

Vehicle emissions are sensitive to vehicle speed and acceleration (*5, 6*). Speed–acceleration modes can be used to represent a wide variety of driving cycles, because engine load depends on speed and acceleration (*7, 8*).

To estimate constant and high-speed correction factors, speed–acceleration modal models for NO_x, hydrocarbons (HC), carbon monoxide (CO), and carbon dioxide (CO_2) were developed based on 59,286 s of chassis dynamometer data from the EPA Mobile Source Observation Database (MSOD) for five diesel vehicles (*9*). Data were not available on a second-by-second basis for particulate matter emissions.

These data were selected for several reasons. Second-by-second data are needed to develop a modal emissions model that can be used to estimate emission rates for transient cycles and for constant speed. Chassis dynamometer data are associated with specific values

of speed and acceleration. In contrast, engine dynamometer data are based on engine shaft output in units of brake horsepower hour and do not take into account loads associated with the power train. However, there are few chassis dynamometer data in the MSOD for HDDVs for which second-by-second data are available. Most dynamometer data are reported only as an average over an entire cycle or continuous portions ("bags") of a cycle. There are few heavy-duty chassis dynamometer facilities that are in use and no second-by-second data were available from MSOD from such facilities. Hence, only data from light-duty chassis dynamometers were available.

The five vehicles selected were the largest that could be tested on a light-duty chassis dynamometer. The characteristics of the tested vehicles are given in Table 1. With gross vehicle weight (GVW) of 8,800 to 9,900 lbs, these vehicles are slightly above the threshold of 8,500 lb GVW that defines the category of HDDVs (*10*). Of the available diesel vehicle second-by-second chassis dynamometer data, the most recent available model years were selected.

The purpose of using the data for the five selected vehicles is to develop correction factors on a relative basis. The assumption here is that the relative trends in emissions rates are similar for these vehicles as they are for other HDDVs. As noted in the results section, the relative trends in emission rates versus speed and acceleration were similar for these five vehicles. These trends are likely to be similar to those of other diesel vehicles. Furthermore, the five selected vehicles were used by EPA as the basis for developing the HDDV speed correction factor in MOBILE6. The correction factors developed here are applied to a base emission rate obtained from the MOBILE6 model that is based on a representative fleet average. Thus, the absolute value of the emission factors estimated here is not based on the five vehicles used for developing the correction factors.

For each selected truck, there are 11,272 to 12,354 s of emissions data for several test cycles, including FTP, LA92, US06, ART-CD, FWY-E, FWY-G, FWY-High, and NYCC. These cycles have wide variation in second-by-second speed and acceleration and thus provide a robust basis for inferring correction factors.

To calculate average emission rates for each speed–acceleration mode, 16 speed bins and 5 acceleration bins were created for a total of 80 modes. The speed mode ranged from 0 to 80 mph in 5-mph increments. Acceleration modes are defined as follows:

- High acceleration: acceleration $\geq$ 2 mph/s,
- Low acceleration: 0.5 mph/s $\leq$ acceleration $<$ 2 mph/s,
- Cruise: -0.5 mph/s $<$ acceleration $<$ 0.5 mph/s,
- Low deceleration: $-2 <$ acceleration ≤ -0.5 mph/s, and
- High deceleration: acceleration ≤ -2 mph/s.

TABLE 1 Heavy-Duty Diesel Vehicle Information for Speed–Acceleration Modal Models

Make	Model	Engine Power (HP)	Engine Displacement (L)	Gross Vehicle Weight (lb)
Ford	F250	235	7.3	8,800
Ford	F350 4 × 4	235	7.3	9,900
Ford	F350 4 × 4	235	7.3	9,900
Dodge	Ram 2,500	230	5.9	8,800
Dodge	Ram 2,500 4 × 4	230	5.9	8,800

NOTE: All vehicles are 1999 model year.

This methodology is somewhat different from, but conceptually similar to, that used in EPA's recently released Draft MOVES 2009 model (*11*). The MOVES model uses a modal approach based on vehicle specific power, which is a function of speed, acceleration, and road grade. A speed–acceleration matrix approach can account for road grade effects by adding a correction to the acceleration estimate (*6*).

Driving Cycles

To assess trends in emission factors versus average cycle speed, four EPA driving cycles developed for the MOBILE6 model were selected. These cycles include LOS E, LOS D, LOS A–C, and high-speed, with average speeds of 31, 53, 60, and 63 mph, respectively (*12, 13*). These cycles represent highways with levels of service (LOS) ranging from A to E, plus a slightly higher speed free-flow cycle.

To estimate average emission factors for higher speeds, four additional cycles were selected based on results of real-world emission measurements conducted using a portable emission measurement system in the Research Triangle Park, North Carolina area (*14*). These cycles are denoted as R40, R66, R70, and R78, with average speeds of 40, 66, 70, and 78 mph, respectively, and were measured on interstate highways under varying levels of traffic congestion. One of these cycles overlaps with the speed range of the MOBILE6 cycles, to enable evaluation of the consistency of the trend in average emission factor versus average speed within the range of speeds represented by MOBILE6. The other three cycles enable estimation of average emission rates at speeds higher than those included in MOBILE6. Table 2 provides a description of the EPA facility-specific driving cycles and real-world driving cycles.

As an example, time distributions among the speed–acceleration modes for the LOS E, R40, high-speed, and R70 driving cycles are shown in Figure 1. The most frequent mode for each cycle differs because of driving patterns. For example, for the LOS-E cycle, which has an average cycle speed of 31 mph, the mode for speed range from 20 to 25 mph at cruise occurs most frequently. For the R40 cycle, the most frequent speed mode was from 40 to 45 mph at cruise. For the high-speed cycle, modes for speeds from 55 to 70 at cruise are the most frequent. Since the R70 cycle is a highway cycle with high average speed, the most frequent mode is for speeds from 70 to 75 mph at cruise.

Constant-Speed Correction Factor

When vehicles operate at very high speeds on short segments of interstates, it is hypothesized that they tend to operate at approximately constant speed. A comparison of the real-world link-based driving cycles at high average speed, such as 70 and 78 mph, to those at lower average speed is consistent with this hypothesis, in that there is less variation in second-by-second speed as average speed increases. Because near-roadway air quality studies might be conducted in areas influenced by segments of roadway of only 1,000 ft or less, an assumption of approximately constant vehicle speed may be reasonable.

However, neither MOBILE6 nor the real-world driving cycles represent constant speed for such a short segment of highway. Therefore, a correction factor was developed comparing vehicle operation at a constant speed to vehicle operation at an equivalent average speed for a time-varying driving cycle. As average speed increases, this ratio is expected to approach unity. The vehicle

TABLE 2 Description of Facility-Specific and Real-World Driving Cycles

Driving Cycle	Average Speed (mph)	Maximum Speed (mph)	Maximum Acceleration (mph/s)	Standard Deviation (mph)	Duration (s)	Length (mi)
Freeway, LOS E[a]	31	63	5.3	15.8	456	3.9
R40[b]	40	50	3.7	5.7	250	2.7
Freeway, LOS D[a]	53	71	2.3	9.9	406	6.0
Freeway, LOS A–C[a]	60	73	3.4	5.9	516	8.6
Freeway, high-speed[a]	63	74	2.7	4.5	610	10.7
R66[b]	66	70	1.9	1.7	321	5.9
R70[b]	70	74	2.5	2.7	306	5.9
R78[b]	78	83	2.5	2.4	324	7.0

[a]Environmental Protection Agency's test cycles (*13*).
[b]Real-world driving cycles (*14*).

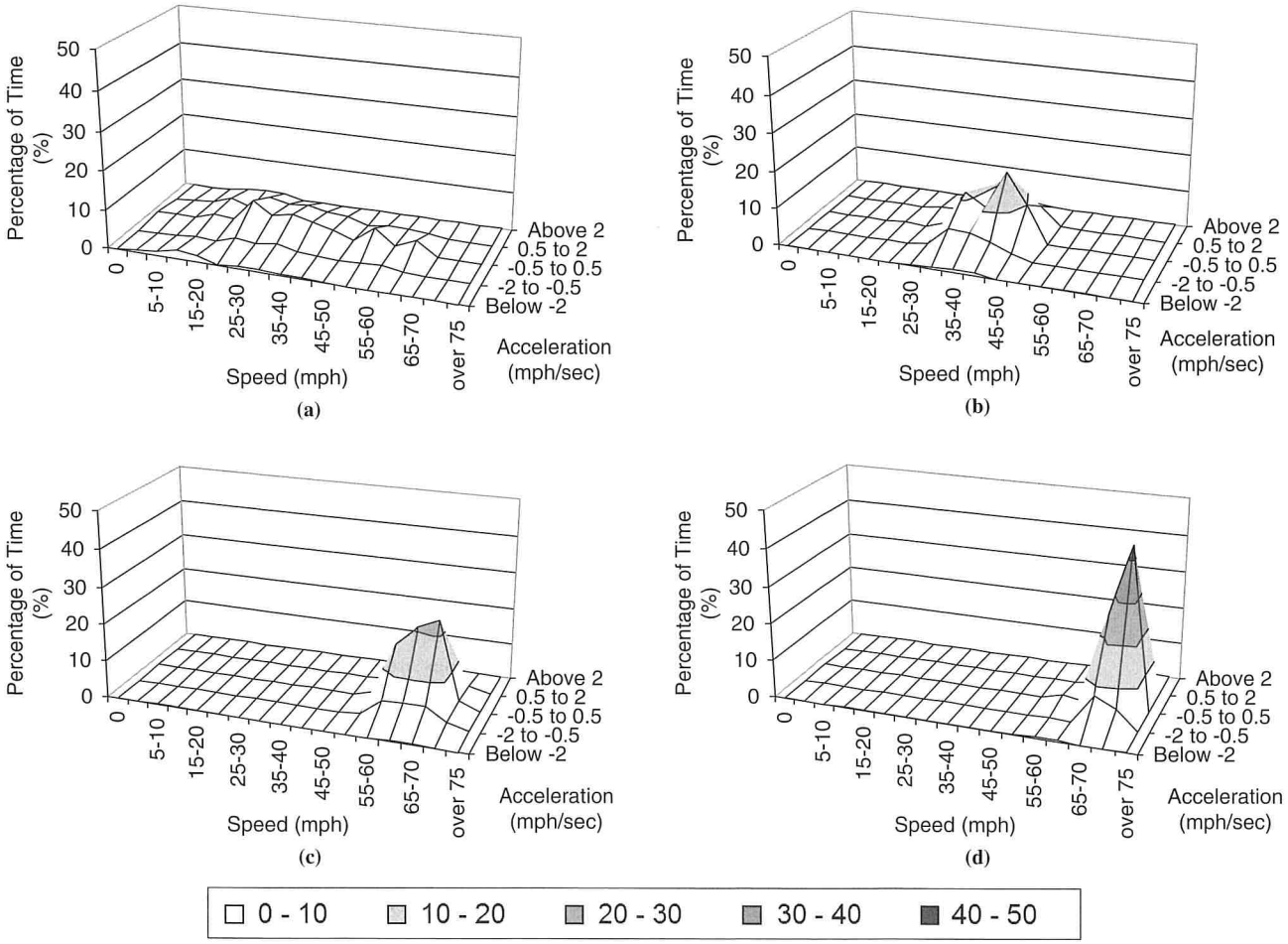

FIGURE 1 Time distribution of speed–acceleration modes for (*a*) LOS E, (*b*) R40, (*c*) high-speed, and (*d*) R70 cycles.

emission rate at constant speed is estimated based on assuming zero acceleration and zero road grade and use of the corresponding speed–acceleration modal average emission rate. The constant-speed correction factor (R_C) is the ratio of an emission factor at constant speed to an average emission factor for a driving cycle with average speed equal to the constant speed:

$$R_{C,s,j} = \frac{EF_{s,j}}{\sum_m EF_{m,j} \times F_m^s} \quad (1)$$

where

$R_{C,s,j}$ = ratio for emission factor (grams per mile) at constant speed s to cycle average emission factor for average speed s for species j (pollutant species: NO_x, HC, CO, and CO_2),
$EF_{s,j}$ = emission factor (grams per mile) of species j based on speed–acceleration modal model at constant speed s (mph) and zero acceleration,
$EF_{m,j}$ = emission factor (grams per mile) of species j and speed–acceleration mode m, and
F_m^s = fraction of time spent in speed–acceleration mode m at driving cycle with average speed s (mph).

High-Speed Correction Factor

The high-speed correction factor (R_H) is the ratio of modal average emission rates for each speed mode at cruise to the modal average emission rate for the cruise mode with a speed range of 60 to 65 mph. Using the speed–acceleration modal model, modal average emission factors were used for each of the 16 speed modes for cruise to estimate emission factors for speeds other than 65 mph. Trends in average emission factors versus modal average speeds for each speed mode were characterized for speed modes ranging from 3 to 80 mph. In order to estimate high-speed correction factors, the trend in mode average emission factor versus median speed for each speed mode was quantified by fitting a regression model, thereby enabling estimation of average emission rates for speeds as high as 78 mph. These trends are normalized to the emission factor estimated at an average speed of 63 mph, corresponding to the speed mode for 60 to 65 mph at cruise.

$$R_{H,s,j}^{63} = \frac{EF_{s,j}}{EF_{63,j}} \quad (2)$$

where

$R_{H,s,j}^{63}$ = ratio of average emission factor at average speed s (mph) for each speed mode to average emission factor for speed mode at average speed of 63 mph for cruise acceleration mode for species j,
$EF_{s,j}$ = emission factor (grams per mile) of species j at average speed s (mph) for cruise based on speed–acceleration modal model, and
$EF_{63,j}$ = emission factor (grams per mile) of species j at average speed of 63 mph, which is midpoint of the speed range from 60 to 65 mph, for cruise based on the speed–acceleration modal model.

When the MOBILE6 input speed is greater than 65 mph, MOBILE6 reports the same emission rates as for 65 mph. Therefore, it is not necessary to correct emission rates for speeds less than 65 mph. For speeds greater than 65 mph, the high-speed correction factor can be used to correct emission factors for speeds higher than 63 mph.

The high-speed correction factor is estimated relative to a datum for a MOBILE6 driving cycle. Although MOBILE6 produces different emission factors for speeds up to 65 mph, the highest average speed among the driving cycles used to develop the model is 63 mph. Therefore, the high-speed correction factor is developed by reference to an average speed of 63 mph. As a first step in developing the speed correction, a regression model was fit to describe variations in the emission factor versus average speed using 63 mph as a datum. The final correction factor was estimated using 65 mph, rather than 63 mph, as a reference point:

$$R_{H,s,j}^{65} = \frac{R_{H,s,j}^{63}}{R_{H,65,j}^{65}} = \frac{\left(\frac{EF_{s,j}}{EF_{63,j}}\right)}{\left(\frac{EF_{65,j}}{EF_{63,j}}\right)} = \frac{\left(EF_{s,j}\right)}{\left(EF_{65,j}\right)} \quad (3)$$

where

$R_{H,s,j}^{63}$ = high-speed correction factor for 63 mph basis; ratio of emission factor at speed i to emission factor at 63 mph for cruise acceleration mode for species j; and
$R_{H,s,j}^{65}$ = high-speed correction factor for 65 mph basis; ratio of emission factor at speed i to emission factor at 65 mph for cruise acceleration mode for species j.

RESULTS AND DISCUSSION

Results are presented in this section for the speed–acceleration modal model, constant-speed correction factor, high-speed correction factor, and a case study of how the two factors are used together to estimate emission factors at constant high speed, such as to support near-roadway air quality studies.

Speed–Acceleration Modal Emission Rates

Figure 2 shows speed–acceleration modal emission rates for diesel vehicle. These are based on pooling the data from the five identified vehicles for which chassis dynamometer data were available on a second-by-second basis for the MOBILE6 speed correction driving cycles. Since the trends of emission factors versus speed–acceleration modes are similar among each of the five vehicles, the average emission rates of five diesel trucks were used for each speed–acceleration mode.

The average emission rates were found to differ significantly between speed–acceleration modes. In general, modal emission rates are significantly higher at high speed and high acceleration than those at low speed and deceleration. NO_x emission rates tend to increase as speed and acceleration increase. For speeds greater than 75 mph, the NO_x emission rate is approximately a factor of 5 greater than that of the speed range from 0 to 5 mph. When high acceleration is compared to high deceleration for NO_x, the emission rates vary by approximately a factor of 1.2 for the speed modes ranging from 0 to 5 mph. As speed increases, NO_x emission rate is more sensitive to increases in acceleration. For example, the NO_x emission rate is a factor of 5 greater for high acceleration than for high deceleration at speeds from 70 to 75 mph.

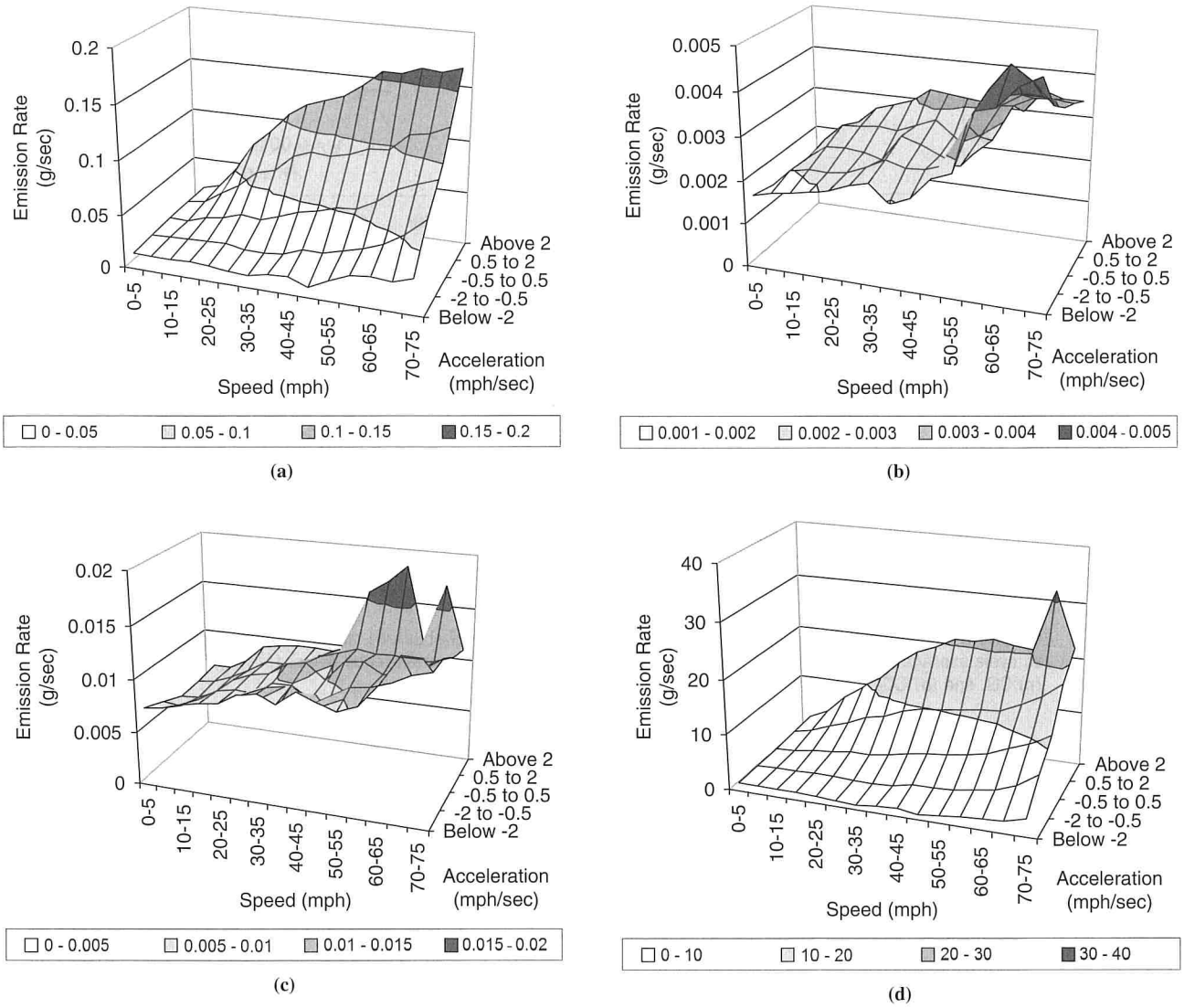

FIGURE 2 Speed–acceleration matrix profiles for average emission rates of (*a*) NO_x, (*b*) HC, (*c*) CO, and (*d*) CO_2, based on 62,419 s of data for five diesel vehicles.

In most cases, the emission rates tend to increase with speed and acceleration. For example, for NO_x emissions, the response surface shown in Figure 2*a* monotonically increases with both speed and acceleration. CO_2 emission rate, which is a surrogate for fuel flow rate, also increases monotonically. The NO_x and CO_2 emissions are very sensitive to differences in speed and acceleration. For example, when comparing extreme modes for the lowest speed and acceleration to the highest speed and acceleration, the NO_x emission rate varies by a factor of 10 and the CO_2 emission factor varies by a factor of 15. The apparent peak in CO_2 emission rate at 68 mph and high acceleration is an artifact of small sample size. This artifact has negligible effect on results because this particular speed–acceleration mode has very little weight in any of the driving cycles used to develop correction factors.

The HC emission factor is relatively less sensitive to variations in speed and acceleration compared to NO_x and CO_2. HC emission rates tend to be more sensitive to air-to-fuel ratio than other pollutants (*15, 16*). Because diesel engines operate with substantial excess air over all engine load ranges, the HC emissions do not vary strongly. For example, comparing the lowest speed and acceleration mode to the highest, the emission rate varies by a factor of only 4.7, much lower than that for NO_x and CO_2. At lower speeds, the HC emission rate is weakly sensitive to acceleration.

The CO emission rate tends to increase monotonically with speed. At low speeds, the CO emission rate has little sensitivity to acceleration. Some of the modal average emission rates for CO are based on very small sample sizes. For example, at high acceleration and average speeds of 48 to 68 mph, the sample sizes are less than 37. Excluding these modes, the CO emission rate varies by a factor of 2.2 when comparing highest to lowest modal emission rates.

Constant-Speed Correction Factor

The results for the constant-speed correction factor (R_C) are shown in Figure 3. In general, as average speed increases, there is less fluctuation in speed on a second-by-second basis. In order to have very

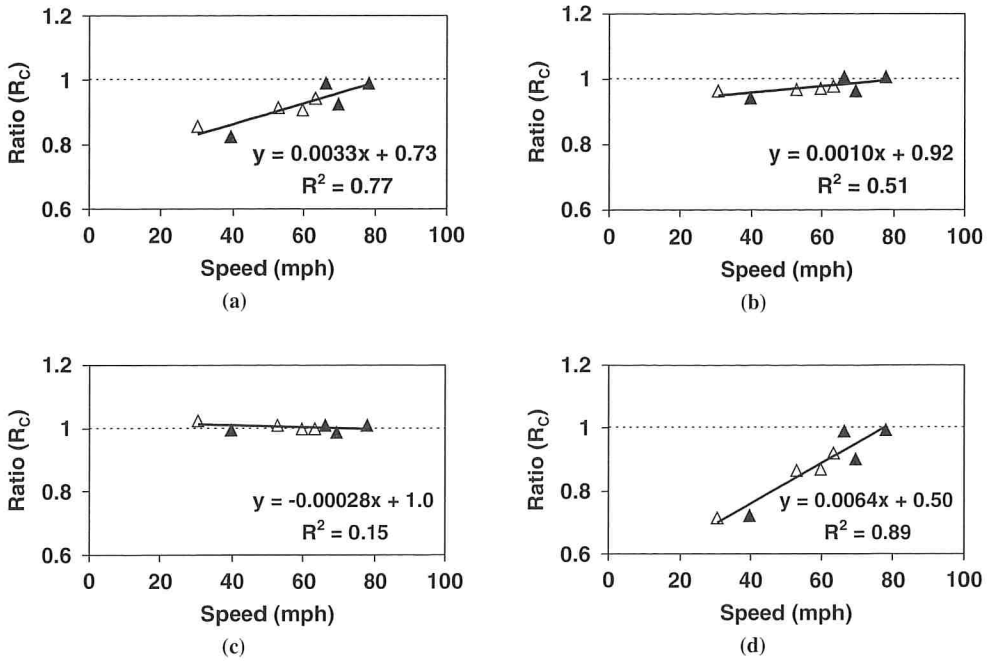

FIGURE 3 Constant-speed correction factors (R_C) based on ratio of constant-speed emission factors to cycle average emission factors for the same driving cycle speed on a distance basis: (*a*) NO_x, (*b*) HC, (*c*) CO, and (*d*) CO_2.

high average speed, such as 78 mph, a vehicle must consistently be traveling at speeds close to this average. However, for a vehicle traveling at 30 mph on an interstate highway, speeds could vary from stop to approximately free-flow speed, depending on traffic conditions. Thus, as expected, the constant-speed correction factor tends to increase with average speed and to asymptotically approach unity, for most pollutants.

For NO_x and HC, the constant-speed correction factors increase with average speed for both pollutants. R_C for NO_x is highly sensitive to speed but weakly sensitive for HC. Furthermore, R_C asymptotically approaches a value of 1. For NO_x, there are emission penalties at low speeds for the fluctuations associated with typical driving cycles compared to constant speed. For example, the NO_x emission factor at a constant speed of 31 mph is more than 14% less than the emission rate for a driving cycle with speed variations that has an average speed of 31 mph. For HC, at 31 mph, the emissions are approximately 4% lower. At 78 mph, the NO_x emission factors at constant speed are similar to those from speed-varying driving cycles with the same average speed.

The results for R_C for CO are unique compared with the other three pollutants. The value of R_C is relatively insensitive to speed. R_C has a value of approximately 1 at all speed ranges. As shown in the speed–acceleration modal emission rates earlier, the CO emission rate is less sensitive to vehicle acceleration than is the case for NO_x and HC.

For CO_2, R_C reaches a value of approximately 1 at speeds of 80 mph. This implies that at such speeds, there is little difference in CO_2 emission rate and fuel economy between driving at constant speed versus driving with typically small fluctuations in speed that are characteristic of these average speeds. However, at lower speeds, such as for 31 to 60 mph, R_C varies from approximately 0.7 to 0.9, indicating that there are benefits to maintaining a constant speed rather than having fluctuations in speed.

High-Speed Correction Factor

The results for the distance-based high-speed correction factor (R_H) at speeds greater than 63 mph are shown in Figure 4 for NO_x, HC, CO, and CO_2, along with data illustrating the trend in emission factors for a wide range of speeds. R_H is estimated using the speed–acceleration-based modal emission models under cruise modes. By definition, R_H is 1 at an average speed of 63 mph. Because the goal here is to develop a model for high speeds, a trend line was fit to the emission ratios using the speed–acceleration mode at 63 mph as a datum and inclusive of cruising modes at modal average speeds of 63 mph and higher.

For NO_x, R_H is not sensitive to high speed. For example, R_H for NO_x is 0.97 at 78 mph. While the NO_x emission rate increases according to the speed–acceleration modal model at cruise as speed increases, NO_x emissions per distance of vehicle travel are approximately constant since the increase of the time-based emission rates is approximately linear with respect to an increase in speed.

For HC, R_H slightly decreases as speed increases at high speed. For example, R_H for HC is 0.87 at 78 mph. For CO, R_H increases as speed increases above 63 mph. For example, for an average speed of 78 mph compared to 63 mph, the average emission rate for CO is approximately 26% higher.

For CO_2, R_H increases from approximately 1 to 1.5 for average speeds from 63 to 78 mph. Since typically over 99% of the carbon in the fuel is converted to CO_2, the results for CO_2 imply that optimal fuel economy is obtained at average speeds of approximately 28 to 58 mph, with degradation of fuel economy at very high speed. Typically, diesel vehicles have relatively low fuel economy above approximately 60 mph (*17*). For low speeds, the CO_2 emission factor decreases as speed increases from 8 to 28 mph and tends to be approximately constant at speeds from 28 to 58 mph.

Overall, the trends in the ratio of emission factors for CO and CO_2 at high speeds are qualitatively consistent with expectations, theory,

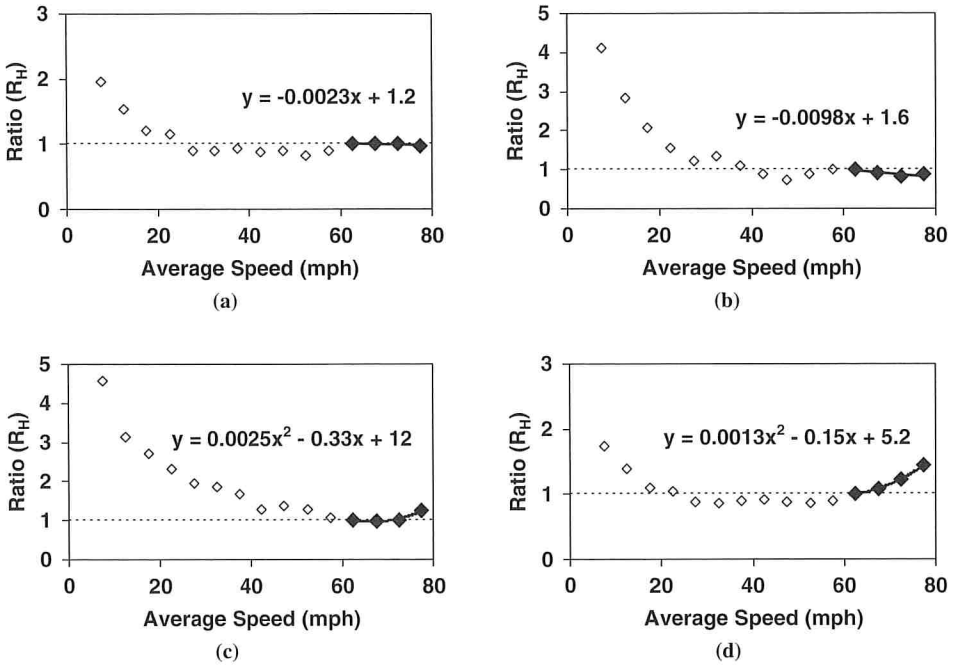

FIGURE 4 High constant-speed correction factors (R_H) for (*a*) NO_x, (*b*) HC, (*c*) CO, and (*d*) CO_2 based on the ratio of distance-based emission factors to emission factors at 63 mph during cruise.

or experience. In other studies, the emission rates of CO and CO_2 are sensitive to vehicle speed at high speeds such as 60 to 80 mph. However, the NO_x and HC emission factors are relatively insensitive to speeds above 63 mph (*18*). Since HC emission rates are associated primarily with the air-to-fuel ratio (*16*), which for diesel engines is based on excess air over all load ranges, HC emissions tend to be less sensitive to speed than other pollutants. Similar to results in Figure 4*a* for NO_x, Weinblatt et al. report that the NO_x emission rate per distance slightly decreases as speed increases above 60 mph (*19*).

Sensitivity Analysis of High-Speed and Constant-Speed Correction Factors

The application of the correction factors for constant speed and high constant speed are illustrated based on a sensitivity analysis. The results of the analysis are shown in Figure 5 for vehicle speeds varying from 40 mph to 80 mph. The base emission factor from MOBILE6 is shown in the figure. This base emission factor is used to estimate a fleet average emission rate and takes into account data for HDDVs of various sizes. The correction factors inferred from the second-by-second chassis dynamometer data are used only to estimate the relative changes in emission rate as quantified using correction factors. MOBILE6 does not predict any change in the emission rate as average speed increases above 65 mph. Therefore, the base emission factors shown for speeds of 70 and 80 mph are the same for each pollutant.

The values of R_C are shown for speeds less than 63 mph. For speeds of greater than 63 mph, only R_H is used.

Except for CO, R_C is typically the smallest at the lowest average speed shown at 40 mph and approaches a value of 1 as speed increases to 80 mph. For CO, emission rates under cruise are approximately the same values as those under acceleration for each speed mode; thus, R_C is less sensitive to speed than for other pollutants and generally remains approximately constant.

For speeds of 70 and 80 mph, R_H generally is greater than 1 for CO and CO_2. R_H is the most sensitive to higher speed for CO_2, which is also highly correlated with the rate of fuel consumption.

The corrected emission factor represents an estimate of the emission factor at constant speed for the indicated speed. The effect of R_C on the corrected emission factor is significant for NO_x and CO_2 for speeds of 40 to 60 mph.

The NO_x emission factor is insensitive to the high-speed correction factor. For example, the NO_x emission factor is 3% lower than base emission factor at 80 mph. For low speeds, the corrected emission factor at 40 mph is 14% lower than the base emission factor.

For HC, both correction factors have generally less influence compared to the other pollutants. For example, the corrected emission factor is 2% lower than the base emission factor at 60 mph. However, at 80 mph, the corrected emission factor is 16% lower than the base emission factor.

For CO, the correction factors are relatively insensitive for speeds ranging from 40 to 70 mph, while the high-speed correction factor is the dominant influence on the corrected emission factor for a speed of 80 mph. At 80 mph, the corrected CO emission factor is 44% higher than the base emission factor. For CO_2, which is indicative of fuel consumption, the corrected emission factor is approximately 24% lower at 40 mph and 51% higher at 80 mph.

CONCLUSIONS

The assessment of near-roadway air quality and human exposure to air pollutants is expected to receive increasing attention in both the research and regulatory communities. For example, there is increasing interest in quantification of near-roadway CO concentrations to support the technical basis for revising the National Ambient Air

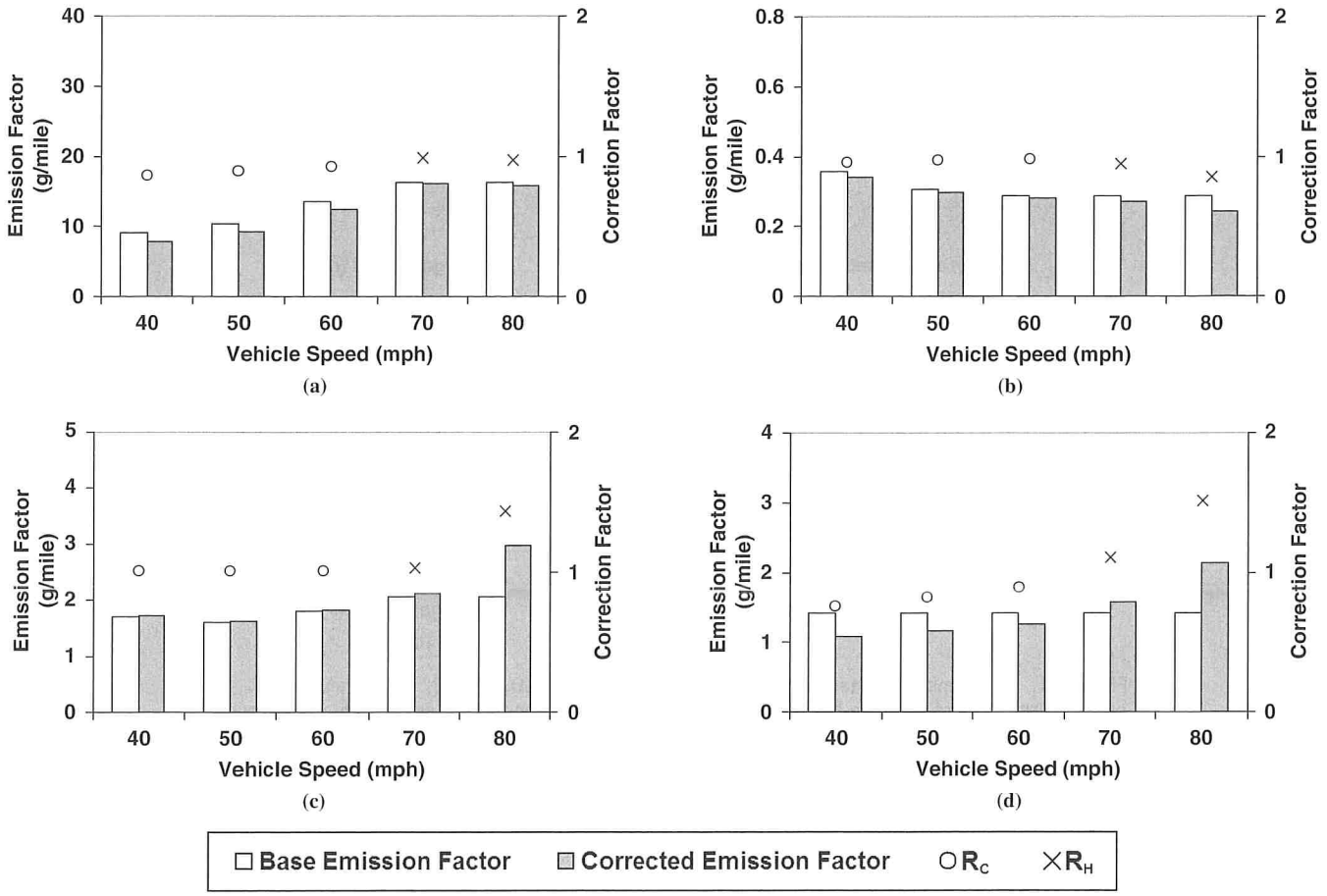

FIGURE 5 Comparison of base emission factors from MOBILE6 with corrected emission factors based on constant- and high-speed correction factors (R_C and R_H) for (*a*) NO_x, (*b*) HC, (*c*) CO, and (*d*) CO_2.

Quality Standards. Hence, factors that lead to variability in on-road emissions and that influence near-roadway air quality and exposure are of increasing concern.

The methodology demonstrated here can be applied to estimate emission factors for real-world link-based situations in which vehicles are driving at constant speed, high average speed, or both. A similar methodology can be applied with the expected final release of EPA's MOVES model, which also will have modal emission rates that can be weighted to represent a wide variety of driving cycles. The key limitations of this work are the relatively small sample sizes of data for some of the speed–acceleration modes and the limited sample of vehicles for which second-by-second data were available for a wide variety of driving cycles. However, since these data are used only to estimate relative changes, they are considered to provide robust insights. The correction factors developed here are representative of vehicles subject to moderate emissions standards. However, the data may not be representative of vehicles certified to the most recent stringent Tier 3 and 4 emissions standards that are equipped with diesel particulate filters or selective catalytic reduction. Over time, these data limitations are expected to be addressed as second-by-second data become available from a variety of sources, including in-use measurements with portable emission measurement systems.

There is currently a lack of second-by-second data for particulate matter emissions because there is not yet an accepted method for such measurements. This data gap could be filled by development of new measurement methods or by using real-time measurement techniques to allocate cycle average filter-based measurements to a second-by-second basis.

The key findings are that distance-based emission rates for diesel vehicles are estimated to be significantly different at high constant speed compared to estimates that are obtained from the MOBILE6 model. This is particularly the case for CO and CO_2 emission factors. For example, at a constant speed of 80 mph, the estimated emission factors are approximately 40% to 50% higher than those estimated using MOBILE6. For NO_x and HC emission factors, the differences are less pronounced, and the high constant-speed emission factors are estimated to be slightly lower than those obtained using MOBILE6.

Other useful findings are that diesel vehicle emission rates at constant speed tend to be lower than those at transient speeds for NO_x, HC, and CO_2, except at very high speed. For very high speeds, and for CO emission rates at all speeds, there is little difference in emission rates when comparing transient versus constant speed operations. The findings for NO_x, HC, and CO_2 imply that traffic management or driver behavior efforts that lead to constant-speed vehicle operations could reduce emissions and fuel use by as much as 15% to 30% without any change in vehicle miles traveled.

The results obtained using speed–acceleration modal emission rate models enable assessment of transient versus constant speed operations and of operations at varying constant speeds. An implication of the latter is that distance-based emission and fuel use rates tend

to be the lowest for moderate ranges of speed, such as 30 to 60 mph. Although these insights are not new, they are derived using a different methodology than that which underlies the MOBILE6 model and thus provide additional confidence regarding the robustness of the insights.

The methodology demonstrated here is applicable to the estimation of emissions on short segments of highway for which vehicles may be driving at approximately constant speed. Such estimates are useful as part of assessment of emissions and air quality in the near vicinity of a roadway.

ACKNOWLEDGMENT

This work has been supported in part by a grant from the National Science Foundation.

REFERENCES

1. U.S. Environmental Protection Agency. *Air Pollutant Emissions Trend Data.* http://www.epa.gov/ttn/chief/trends. Accessed May 20, 2007.
2. Davis, S. C., and L. F. Truett. Sales and Impact of Class 2b Trucks. In *Transportation Research Record: Journal of the Transportation Research Board, No. 1842,* Transportation Research Board of the National Academies, Washington, D.C., 2003, pp. 1–8.
3. *Integrated Science Assessment for Carbon Monoxide (First External Review Draft).* EPA600-R-09-019. U.S. Environmental Protection Agency, Research Triangle Park, N.C., 2009.
4. Giannelli, R. A., J. H. Gilmore, L. Landman, S. Srivastava, M. Beardsley, D. Brzezinski, G. Dolce, J. Koupal, and G. Shyu. *Sensitivity Analysis of MOBILE6.0.* U.S. Environmental Protection Agency, Washington, D.C., 2002.
5. Frey, H. C., N. M. Rouphail, and H. Zhai. Link-Based Emission Factors for Heavy-Duty Diesel Trucks Based on Real-World Data. In *Transportation Research Record: Journal of the Transportation Research Board, No. 2058,* Transportation Research Board of the National Academies, Washington, D.C., 2008, pp. 23–32.
6. Frey, H. C., A. Unal, and J. Chen. *Recommended Strategy for On-Board Emission Data Analysis and Collection for the New Generation Model.* U.S. Environmental Protection Agency, Ann Arbor, Mich., 2002.
7. Yoon, S., H. Li, J. Jun, J. H. Ogle, R. L. Guensler, and M. O. Rodgers. Methodology for Developing Transit Bus Speed–Acceleration Matrices for Load-Based Mobile Source Emission Models. In *Transportation Research Record: Journal of the Transportation Research Board, No. 1941,* Transportation Research Board of the National Academies, Washington, D.C., 2005, pp. 26–33.
8. Coelho, M. C., H. C. Frey, N. M. Rouphail, H. Zhaid, and L. Pelkmans. Assessing Methods for Comparing Emissions from Gasoline and Diesel Light-Duty Vehicles Based on Microscale Measurements. *Transportation Research Part D,* Vol. 14, No. 2, 2009, pp. 91–99.
9. *Mobile Source Observation Data: User Guide and Reference.* EPA420-B-04-004. U.S. Environmental Protection Agency, Ann Arbor, Mich., 2004.
10. Browning, L. *Update Heavy Duty Engine Emission Conversion Factors for MOBILE6: Analysis of BSFCs and Calculation of Heavy-Duty Engine Emission Conversion Factors.* EPA420-R02-005. U.S. Environmental Protection Agency, Ann Arbor, Mich., 2002.
11. *Draft Motor Vehicle Emission Simulator (MOVES) 2009 User Guide.* EPA-420-B-09-008. U.S. Environmental Protection Agency, Ann Arbor, Mich., 2009.
12. Beardsley, M. *Development of Speed Correction Cycles.* EPA420-R-01-042. U.S. Environmental Protection Agency, Washington, D.C., 2001.
13. *User's Guide to MOBILE6.1 and MOBILE6.2: Mobile Source Emission Factor Model.* EPA420-R-03-010. U.S. Environmental Protection Agency, Ann Arbor, Mich., 2003.
14. Frey, H. C., K. Zhang, and N. M. Rouphail. Fuel Use and Emissions Comparisons for Alternative Routes, Time of Day, Road Grade, and Vehicles Based on In-Use Measurements. *Environmental Science & Technology,* Vol. 42, No. 7, 2008, pp. 2483–2489.
15. Flagan, R. C., and J. H. Seinfeld. *Fundamentals of Air Pollution Engineering.* Prentice Hall, Englewood Cliffs, N.J., 1988.
16. Ropkins, K., R. Quinn, J. Beebe, H. Li, B. Daham, J. Tate, M. Bell, and G. Andrews. Real-World Comparison of Probe Vehicle Emissions and Fuel Consumption Using Diesel and 5% Biodiesel (B5) Blend. *Science of the Total Environment,* Vol. 376, No. 2007, 2007, pp. 267–284.
17. Park, S., H. A. Rakha, M. Farzaneh, J. Zietsman, and D.-W. Lee. Development of Fuel and Emission Models for High-Speed Heavy-Duty Trucks, Light-Duty Trucks, and Light-Duty Vehicles. Presented at 87th Annual Meeting of the Transportation Research Board, Washington, D.C., 2008.
18. Rakha, H., K. Ahn, and A. Trani. Development of VT-Micro Model for Estimating Hot Stabilized Light Duty Vehicle and Truck Emissions. *Transportation Research Part D,* Vol. 9, No. 1, 2004, p. 49.
19. Weinblatt, H., R. G. Dulla, and N. N. Clark. Vehicle Activity-Based Procedure for Estimating Emissions of Heavy-Duty Vehicles. In *Transportation Research Record: Journal of the Transportation Research Board, No. 1842,* Transportation Research Board of the National Academies, Washington, D.C., 2003, pp. 64–72.

Any opinions, findings, and conclusions or recommendations expressed in this material are those of the authors and do not necessarily reflect the views of the National Science Foundation.

The Transportation and Air Quality Committee peer-reviewed this paper.

Effects of Transportation and Land Use Policies on Air Quality

A Case Study in Austin, Texas

Elena C. McDonald-Buller, Alba Webb, Kara M. Kockelman, and Bin (Brenda) Zhou

The effects of land use and transportation policies on emissions, ozone concentrations, and a metric for population exposure were investigated for Austin, Texas. Three distinct transportation and land use scenarios were examined with a gravity-based land use model and a standard travel demand model: a business-as-usual scenario, a road pricing policy that included a flat-rate carbon-based tax and congestion pricing of all Austin-area freeways, and an urban growth boundary policy. Two scenarios, a business-as-usual scenario and a flat-rate carbon-based tax and congestion pricing policy, were also examined with a novel, parcel-level land use change and land use intensity model and a standard travel demand model. Transportation and land use policies were predicted to have substantial effects on travel and on emissions of ozone precursors. Emissions of ozone precursors decreased markedly for all 2030 scenarios because of the implementation of more stringent federal motor vehicle emission control programs. Transportation and land use policies were predicted to lead to greater reductions of emissions of ozone precursors relative to the business-as-usual scenario. The effects of such policies on ozone concentrations and population exposure vary. Lower exposure was predicted for the road pricing scenarios, but a penalty appeared to exist in the form of relatively higher exposure predicted for the urban growth boundary on some days. This analysis indicates the potential complexity of planning for urban growth and equity and the need for integrated modeling and policy evaluation efforts.

Land use and land cover changes caused by urbanization affect air quality through changes in biogenic and anthropogenic emissions, heat and energy balances and urban climate, and dry deposition of pollutants. Evaluating the impacts of urbanization on future emissions, air quality, and human exposure to pollution requires consideration of transportation, land use, and environmental policies, technological advances, and changes in demographics and human activity patterns. Previous studies have examined the effects of uncertainty in population and employment control totals on vehicle emissions (*1*) as well as the effects of certain land use and transport policies (*2*) on such emissions. Other studies have examined the effects of land use change on future air quality by isolating the impacts due to changes in surface meteorology and anthropogenic and biogenic emissions under one or more growth scenarios (*3–5*).

Song et al. (*5*) explored the impacts of alternative regional development patterns on anthropogenic and biogenic emissions of ozone precursors and ozone concentrations using four visions of future land use in Austin, Texas. Although all visions were based on an assumed doubling of population in 20 to 40 years from 2001, they assumed different spatial patterns of development ranging from a continuation of the region's historical trend of low-density, separate-use development; to corridor-oriented development; to high-density, balanced-use development and redevelopment in existing areas. Emissions and their spatial allocation were determined for each development pattern and used to predict hourly ozone concentrations under the same meteorological conditions. Differences in hourly ozone concentrations due to changes in emissions between 2007 and the future case scenarios were primarily the result of more stringent federal motor vehicle emission control programs, including the Environment Protection Agency's (EPA's) Tier 2 rules and the 2007 heavy-duty highway rule. These differences in the magnitude of emissions produced greater changes in air quality than differences in regional development patterns between the four scenarios, although the effects of urbanization patterns were distinguishable. Using the same four visions of future growth, McDonald-Buller et al. (*6*) found that concentrated high-density development in existing towns with balanced-use zoning produced lower exposure to high ozone concentrations in the Austin area than a more typical urban sprawl pattern.

Future emission scenarios prepared for air quality planning typically account for changes in the magnitude of emissions due to recognized environmental regulations, technological changes, and forecasted population growth, but do not consider regional transportation and land use policies. The five-county Austin–Round Rock metropolitan statistical area (MSA), including Travis, Williamson, Bastrop, Hayes, and Caldwell Counties, is representative of many rapidly growing urban areas in the United States that are challenged with improving air quality that is on the cusp of attainment with the National Ambient Air Quality Standard (NAAQS) for ozone while considering the spatial patterns and equity of future growth. In the work of Song et al. (*5*), the air quality impacts of different urban growth scenarios based on a community-driven visioning process known as Envision Central Texas (ECT) were compared. In our continued focus on the Austin–Round Rock MSA, two integrated transportation–land use models (ITLUMs) that were developed by Zhou and Kockelman (*7*)

E. C. McDonald-Buller and A. Webb, Center for Energy and Environmental Resources, University of Texas at Austin, 10100 Burnet Road, Building 133, M/S R7100, Austin, TX 78758. K. M. Kockelman, Department of Civil, Architectural, and Environmental Engineering, University of Texas at Austin, 6.9 E. Cockrell Jr. Hall, Austin, TX 78712-1076. B. Zhou, Central Connecticut State University, Room 21208, Copernicus Hall, New Britain, CT 06050. Corresponding author: E. C. McDonald-Buller, ecmb@mail.utexas.edu.

Transportation Research Record: Journal of the Transportation Research Board, No. 2158, Transportation Research Board of the National Academies, Washington, D.C., 2010, pp. 28–35.
DOI: 10.3141/2158-04

and Zhou et al. (*8*) are used in conjunction with the comprehensive air quality model with extensions (CAMx; *9*) to evaluate the impacts of transportation and land use policies on emissions of nitrogen oxides (NO_x) and volatile organic compounds (VOCs) and daily maximum and hourly episodic ozone concentrations. Three policies were considered: a business-as-usual (BAU) scenario, congestion pricing plus carbon tax (CPCT) scenario, and an urban growth boundary (UGB) scenario.

INTEGRATED TRANSPORTATION–LAND USE MODELING

Year 2030 travel conditions and household and employment distributions for the Austin–Round Rock MSA were predicted with two ITLUMs, as described in detail by Zhou et al. (*8*) and by Zhou and Kockelman (*7*), and are thus only briefly reviewed here. The first utilizes a gravity-based land use model (G-LUM) that is a variation of Steven Putman's Integrated Transportation–Land Use Package and a reasonably standard sequential travel demand model (TDM) largely based on Smart Mobility's specification. The second, a new land use change and land use intensity (LUC-LUI) model, examines land use change at the parcel level and applies systems of equations for land use intensity (household and employment counts by type) at the level of travel analysis zones (TAZs).

Figure 1*a* shows the interactions between the three G-LUM components and the TDM. In this integrated modeling framework, the employment allocation (EMPLOC) model runs before the residential allocation (RESLOC) model, followed by the land use density (LUDENSITY) model and the TDM. The EMPLOC model output (employment by category by zone) serves as an input to the RESLOC. Predicted household and employment levels (by category and type) are LUDENSITY's primary inputs. The TDM is applied immediately after allocating households and jobs (and estimating land consumption levels), in order to update travel times between zones and the relative attractiveness of each zone. The model system predicts the spatial distributions of six household types [categorized by number of workers (0, 1, and 2+) and presence of children] and three employment categories (basic, retail, and service jobs). Model data requirements and calibration are described by Zhou et al. (*8*). The models were applied at 5-year intervals to obtain 2030 forecasts with the inclusion of several restrictions: (*a*) households and jobs in each TAZ were not allowed to fall by more than 5% in any (5-year) time interval; (*b*) growth in these counts was limited by land availability; and (*c*) in fully developed TAZs, households and jobs were not allowed to increase by more than 5% per time interval.

In addition to the G-LUM, a hybrid land use model system consisting of two model components operated on individual parcel and zonal levels was applied to the five-county Austin area. Figure 1*b* shows the model components and their relationship. The land use change (LUC) model determines how individual parcels evolve: whether an undeveloped parcel will subdivide into several smaller parcels during a specified time interval (e.g., 5 years in this study) (the subdivision model), how big these subdivided parcels are (the parcel size model), and what land use types will emerge on each individual parcel (the land development model). Land use change is generally associated with increases (or decreases) of land use intensity levels (household and employment counts), and the effect is aggregated at the level of TAZs to provide key inputs to a standard TDM. A land use intensity (LUI) model allocates households and employment by type, using a seemingly unrelated regression with

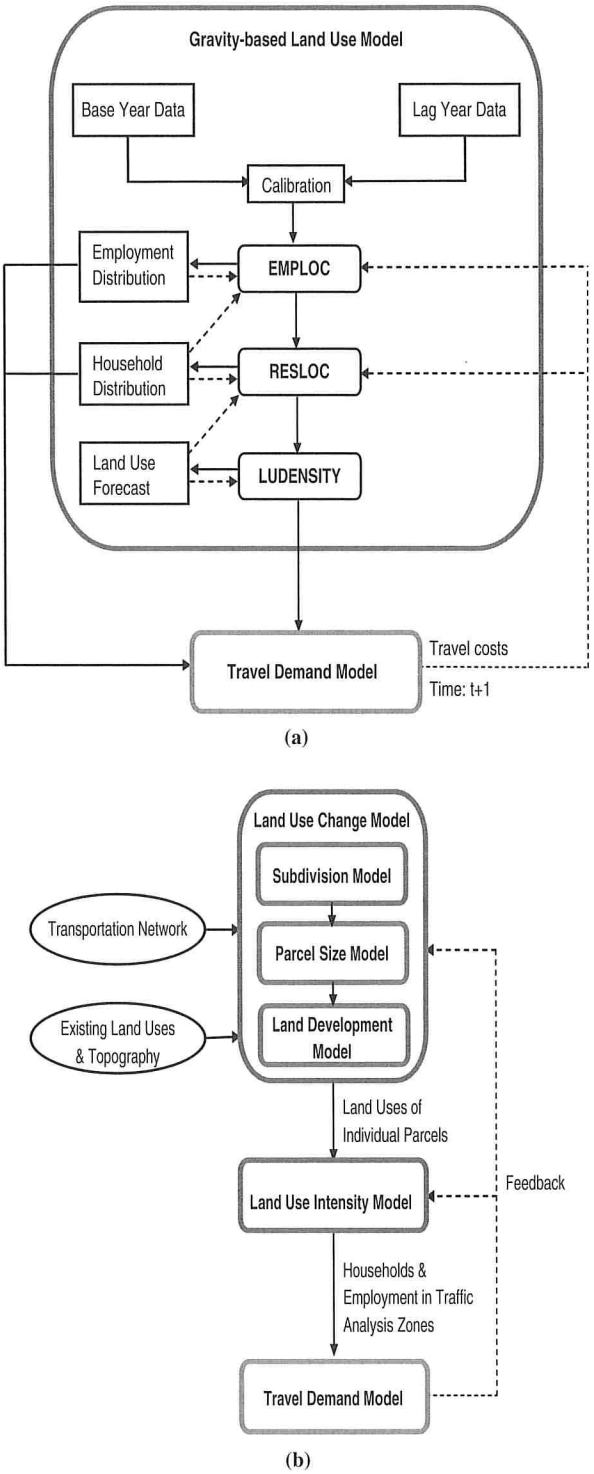

FIGURE 1 Model logic of (*a*) gravity land use model and (*b*) land use change and land use intensity model.

two spatial processes. Data availability and model specification, calibration, and application are described in detail by Zhou and Kockelman (*7*). The LUC model, the LUI model, and a TDM formed a new integrated model that was applied to investigate the spatial distribution of households and jobs, along with travel conditions in 2030 across the Austin–Round Rock MSA. Iterative adjustments in the

land development model's alternative-specific constants according to regionwide land use forecasts and adjustments of household and job counts to match control totals, due to the inability to embed "targets" into the model system, were among the restrictions required to obtain reasonable results. The transportation and land use policy scenarios were simulated through year 2030 at 5-year intervals.

Three transportation and land use policies were considered, as described in Zhou et al. (*8*) and briefly reviewed here. The BAU scenario assumed that development trends observed over the 5-year calibration would continue without imposition of new policies. The road pricing (CPCT) scenario combined congestion pricing with a gas (or carbon) tax. A congestion charge was set to equal the implicit cost of marginal delay (imposed per added vehicle mile traveled, assuming a $6.75/person hour value of travel time) on all freeway segments in the network, and the carbon tax was assumed to be 4.55 cents per mile on all links in the network. The BAU and CPCT scenarios were applied with both the G-LUM and the LUC-LUI models. The UGB scenario restricted all types of new development to a predefined set of largely contiguous zones, centered on existing population centers. Developable zones were defined as TAZs having two or more job equivalents per acre and any TAZs touching their boundaries; a job equivalent is one job or 0.714 households, since the region has 0.714 households per job. Zones outside this "boundary" were not permitted any new residential, basic, or commercial development as described by Zhou et al. (*8*). This scenario was applied within the G-LUM, but could not be applied in the LUC-LUI model because the spatial econometric models used are not readily adapted to zone exclusions, such as zoning constraints or prior knowledge of development (*10*).

EMISSION INVENTORIES

Methodology

Biogenic emissions of hydrocarbons dominate the overall emission inventory in eastern Texas, but their spatial distribution is heterogeneous (*11, 12*). Portions of central Texas, including the Austin area, represent transition zones where both biogenic and anthropogenic emissions are significant, and accurately characterizing the spatial distribution of biogenic emissions is an important element in understanding air quality and the effectiveness of emission control strategies. Urbanization patterns and the accompanying changes in vegetative cover can alter a region's biogenic emissions.

The Global Biogenic Emissions and Interactions System (GloBEIS) Version 3.1 was used to develop biogenic emission inventories for a September 13 to September 20, 1999, modeling episode (*5, 13*). The photochemical modeling domain was a nested regional and urban scale 36-km/12-km/4-km grid with 12 vertical layers from the surface to 3.9 km; the five-county Austin area was included within the 4-km domain. GloBEIS and similar models rely on accurate spatial mappings of land cover and on meteorological parameters, including temperature, photosynthetically active radiation, wind speed, and humidity, to obtain biogenic emission estimates. Biogenic emission estimates were developed for the ITLUM scenarios using the methodology described by Song et al. (*5*) for the ECT scenarios. According to this approach, ECT planners estimated the fraction of impervious cover for each ECT land use type, which was used to adjust the fraction of original vegetation expected to exist in that land use category. Assumptions about the remaining vegetation after development were based on visual studies of development impacts on tree cover using orthophotography from 1995 and 2002 and on local knowledge of development practices (*5*). However, in contrast to the ECT land use and land cover databases, which included estimates of impervious cover for each land use type, the classifications used in the G-LUM and LUC-LUI models did not directly provide information that could be used to estimate the fraction of original vegetation remaining after application of each scenario. Instead, the classifications used in the models were mapped to one of the ECT development types as shown in Tables 1 and 2. Each TAZ polygon

TABLE 1 Assumed Fraction of Vegetative Cover Remaining After Development for Each G-LUM and Corresponding ECT Classification

Gravity Land Use Model (G-LUM) Classification	Envision Central Texas (ECT) Classification	Assumed Fraction of Vegetative Cover Remaining
CBD residential	Downtown	0.023
CBD basic employment	Downtown	0.023
CBD commercial employment	Downtown	0.023
Urban residential	Town	0.171
Urban basic employment	Activity center	0.042
Urban commercial employment	Activity center	0.042
Suburban residential	Residential subdivision	0.363
Suburban basic employment	Industrial–office park	0.144
Suburban commercial employment	Industrial–office park	0.144
Rural residential	Rural housing	0.763
Rural basic employment	Industrial–office park	0.144
Rural commercial employment	Industrial–office park	0.144

TABLE 2 Assumed Fraction of Vegetative Cover Remaining After Development for Each LUC-LUI and Corresponding ECT Classification

Land Use Change-Land Use Intensity (LUC-LUI) Model Classification	ECT Classification	Assumed Fraction of Vegetative Cover Remaining
CBD LLSF	Downtown	0.023
CBD SF	Downtown	0.023
CBD MF	Downtown	0.023
CBD commercial/office	Downtown	0.023
CBD industrial	Downtown	0.023
CBD civic	Downtown	0.023
Urban LLSF	Large lot	0.493
Urban SF	Residential subdivision	0.363
Urban MF	Town	0.171
Urban commercial/office	Activity center	0.042
Urban industrial	Activity center	0.042
Urban civic	Activity center	0.042
Suburban LLSF	Large lot	0.493
Suburban SF	Residential subdivision	0.363
Suburban MF	Town	0.171
Suburban commercial/office	Industrial/office park	0.144
Suburban industrial	Industrial/office park	0.144
Suburban civic	Industrial/office park	0.144
Rural LLSF	Rural housing	0.763
Rural SF	Rural housing	0.763
Rural MF	Town	0.171
Rural commercial/office	Industrial/office park	0.144
Rural industrial	Industrial/office park	0.144
Rural civic	Industrial/office park	0.144

NOTE: LLSF = large-lot single family; SF = single family; MF = multifamily.

TABLE 3 Year 2001 Housing Units and Year 2030 Projected Households (HHs) for Each ITLUM Scenario by County (in thousands)

Austin Area County	2001 Housing Units (U.S. Census)	Average Household Size (U.S. Census)	G-LUM BAU HHs	G-LUM CPCT HHs	G-LUM UGB HHs	LUC-LUI BAU HHs	LUC-LUI CPCT HHs
Bastrop	22.7	2.87	64.4	65.5	49.4	65.2	62.6
Caldwell	12.2	2.98	30.4	31.4	26.0	55.7	55.0
Hays	37.9	2.92	87.0	87.0	73.3	94.3	93.7
Travis	353.3	2.53	512.2	510.6	582.5	495.3	496.7
Williamson	98.1	2.88	237	236	200	220	223
Total	524	—	931	931	931	931	931

was classified as central business district (CBD), urban, suburban, or rural on the basis of the following calculation:

$$DF_{TAZ} = P_{TAZ} + B\left(\frac{E_{TAZ}}{A_{TAZ}}\right)$$

where

DF = density factor,
P = population in the TAZ,
E = employment in the TAZ,
A = acreage of the TAZ, and
B = ratio of the study area population to the study area employment (*14*).

The area was classified as CBD if $DF_{TAZ} \geq 50$; as urban if $50 > DF_{TAZ} \geq 10$; as suburban if $10 > DF_{TAZ} \geq 1$; and as rural if $1 > DF_{TAZ} \geq 0$. The reclassified ITLUM scenarios were then overlaid on the original land cover data for the region from Wiedinmyer et al. (*11, 12*) and used to modify the original vegetation density which was used in GloBEIS to obtain estimates of biogenic emissions.

Dry deposition, which is the dominant physical loss mechanism for air pollutants in central Texas, is a strong function of land use and land cover type and is most frequently estimated based on the model of Wesely (*15*). Deposition rates are estimated as a series of mass transfer resistances to deposition. Land cover estimates for input into the dry deposition algorithms of CAMx were developed using the reclassified ITLUM scenarios and the methodology described by Song et al. (*5*).

Forecasts of the growth of point source emissions have been small relative to other anthropogenic sources in the region; hence, these emissions were assumed to be constant through 2030. Anthropogenic emission estimates for on-road mobile, nonroad mobile, and area sources were developed for the ITLUM scenarios using the methodology of Song et al. (*5*). MOBILE6.2 was used to calculate emission factors (grams per mile) for VOCs, carbon monoxide, and NO_x and included default federal motor vehicle control programs for the year 2030. Population and household count data for each scenario were used in conjunction with the EPA's NONROAD model version 2005 to obtain 2030 nonroad mobile source inventories.

Area source emission inventories for each scenario were developed by projecting 2007 base-year area emissions using human population growth and applying federal and state emission standards (*5*). Typically, for Texas and other states that routinely prepare and update state implementation plans, spatial allocation factors and surrogates remain the same between the base year and future attainment year. Song et al. (*5*) accounted for the spatial differences in emissions from the different development patterns under the ECT scenarios. A similar approach was applied in this work in order to spatially allocate nonroad and area sources emissions under the ITLUM policy scenarios. Housing and population values used in the projections and spatial allocation of anthropogenic emissions for the ITLUM scenarios are summarized in Tables 3 and 4, respectively. As expected, the different land use models result in different housing and population projections at the county level, which will influence emission estimates.

Inventory Summaries and Comparisons

Predictions of biogenic and anthropogenic emissions for the ITLUM scenarios were compared to predictions from a 2007 base case largely based on emission inventories developed for Austin's Early Action Compact. A summary of vehicle miles traveled (VMT) and NO_x and VOC emissions from major source sectors for the 2007 base case and each ITLUM scenario is presented in Table 5. Similar results are presented for the 2007 Base Case and ECT scenarios, based on work by Song et al. (*5*) and Webb et al. (*10*), in Table 6 for comparison purposes.

TABLE 4 2001 Human Population and Year 2030 Projected Human Population for Each ITLUM Scenario by County (in thousands)

Population	2001 (U.S. Census)	G-LUM BAU	G-LUM CPCT	G-LUM UGB	LUC-LUI BAU	LUC-LUI CPCT
Bastrop	61.5	185	188	142	187	179.6
Caldwell	33.8	90.6	93.6	77.4	166.1	163.9
Hays	104	254.1	254	214	275.2	273.7
Travis	842.3	1,295.9	1,291.8	1,473.6	1,253.1	1,256.7
Williamson	277	681	679.7	575	634.2	641.2
Total	1,319	2,507	2,507	2,482	2,516	2,515

TABLE 5 Emissions of VOC and NO_x (tpd) for 2007 Base Case and 2030 ITLUM Scenarios

	2007 Base Case VMT = 45[a]		G-LUM BAU VMT = 85[a]		G-LUM CPCT VMT = 71[a]		G-LUM UGB VMT = 70[a]		LUC-LUI BAU VMT = 84[a]		LUC-LUI CPCT VMT = 71[a]	
Category	VOC	NO_x	VOC	NO_x	VOC	NO_x	VOC	NO_x	VOC	NO_x	VOC	NO_x
On-road mobile	34	62	23	24	19	20	19	20	22	24	19	20
Nonroad mobile	22	22	23	9	23	9	23	9	23	9	23	9
Area	111	10	224	22	226	22	215	20	254	23	254	23
Point	3	3	3	3	3	3	3	3	3	3	3	3
Biogenic	211	20	150	20	151	20	206	20	201	20	202	20

[a]VMT is given in units of 10^6 miles per day in the five-county Austin area.

Biogenic sources and, because they have been projected using human population, area sources are predicted to remain the most significant sources of VOC emissions in the five-county area. Zhou and Kockelman (*7*) and Zhou et al. (*8*) found that the CPCT and BAU scenarios result in similar land use patterns, with CPCT predicted to influence travel behavior but not location choice. The biogenic emissions predictions for the BAU and CPCT scenarios for each model are consistent with this finding. However, biogenic emission estimates for the G-LUM BAU and G-LUM CPCT scenarios are considerably lower than for the LUC-LUI scenarios. The G-LUM scenarios forecast large changes in undeveloped land, particularly in rural zones, resulting in large reductions in vegetative cover as compared to the base case. The increased development rates, due to model limitations and no constraints on maximum developable land, result in unrealistic predictions of vegetative cover loss and overpredictions of urbanization in those zones. In contrast, the G-LUM UGB scenario predicts concentrated growth in households and employment within the predefined boundary, resulting in very modest consumption of vegetative cover and changes in biogenic emissions primarily within Travis County and southern Williamson County. With the exceptions of the G-LUM BAU and CPCT scenarios, the range of differences in the magnitude of biogenic hydrocarbons between the ITLUM scenarios and the 2007 base case was comparable to the 2% to 6% reductions in daily biogenic emissions between the ECT four scenarios and the 2007 base case across the five-county Austin MSA.

Area source VOC emissions in Austin were primarily due to solvent utilization, service stations, and industrial processes, while NO_x emissions were associated with agricultural production and stationary source fuel combustion. The relative contribution of emissions from these source categories did not change in future years. However, the magnitude of emissions increased relative to the 2007 base case because area sources emissions increased with population growth.

Emissions from most on-road and nonroad mobile source categories decreased for the ITLUM scenarios relative to the base case because of more stringent federal emission controls. Nonroad mobile source NO_x emissions for all ITLUM scenarios were approximately 9.4 tpd and were nearly identical to the ECT scenarios, suggesting that implementation of EPA's Tier 4 engine standards has a more significant influence than regional development patterns and the imposition of policies. VOC emissions remain nearly the same or increase slightly between the 2007 base case and the 2030 ITLUM and ECT scenarios, largely attributed by Song et al. (*5*) to the growth in lawn and garden equipment, which tracked population growth.

The G-LUM BAU, LUC-LUI BAU, and ECT A (a continuation of the current trend of low-density, segregated-use development) scenarios predicted nearly a doubling of VMT (i.e., 85% to 90% increase) by 2030, relative to the 2007 base case. VMT differences for the CPCT, UGB, and ECT B, C, and D scenarios relative to the 2007 base case indicated that transportation and land use policies as well as smart growth styled development can have substantial impacts on travel, increasing VMT by only 48% to 60%. VOC and NO_x emissions decreased markedly for all 2030 scenarios due to the implementation of more stringent federal motor vehicle emission control programs, including the EPA's Tier 2 and heavy-duty 2007 rules (*5*). Smart growth strategies and transportation and land

TABLE 6 Emissions of VOC and NO_x (tpd) for 2007 Base Case and 2030 ECT Scenarios from Song et al. (*5*) and Webb et al. (*10*)

	2007 Base Case VMT = 45[a]		ECT A VMT = 82[a]		ECT B VMT = 72[a]		ECT C VMT = 70[a]		ECT D VMT = 66[a]	
Category	VOC	NO_x	VOC	NO_x	VOC	NO_x	VOC	NO_x	VOC	NO_x
On-road mobile	34	62	22	18	19	16	19	16	17	14
Nonroad mobile	22	22	23	10	24	10	24	10	23	10
Area	111	10	214	21	238	22	262	24	236	22
Point	3	3	3	3	3	3	3	3	3	3
Biogenic	211	20	199	20	205	20	205	20	208	20

NOTE: ECT scenario emissions are calculated for a future year of 2030. ECT Scenario A assumes low-density, segregated-use development based on extensive highway provision; ECT Scenario B assumes concentrated, contiguous regional growth within 1 mi of transportation corridors; ECT Scenario C concentrates growth in existing and new communities with distinct boundaries; and ECT Scenario D assumes high-density development in existing towns and cities with balanced-use zoning.
[a]VMT is given in units of 10^6 miles per day in the five-county Austin area.

TABLE 7 Daily Maximum 1-h Ozone Concentrations for Base Case and Differences in Daily Maximum Ozone Concentrations Relative to Base Case

Episode Day	Base Case Daily Max. O_3 Conc. (ppb)	G-LUM BAU	G-LUM CPCT	G-LUM UGB	LUC-LUI BAU	LUC-LUI CPCT
9/15	80.5	−4.1	−4.9	−4.4	−4.9	−5.6
9/16	72.0	−1.5	−1.6	−2.2	−2.1	−2.2
9/17	85.8	−6.5	−6.5	−6.4	−6.9	−6.9
9/18	86.2	−3.9	−3.9	−4.1	−4.1	−4.1
9/19	90.4	−6.0	−7.3	−5.5	−6.1	−7.5
9/20	90.5	−8.3	−9.7	−8.0	−8.6	−10.1

use policies were predicted to lead to greater reductions of emissions of both ozone precursors. For the G-LUM, CPCT and UGB policies were predicted to lead to approximately a 16% decrease in emissions of VOC and NO_x relative to the BAU scenario. Similarly, the LUC-LUI model predicted approximately a 15% decrease of both NO_x and VOC emissions for the CPCT scenario relative to the BAU scenario. Song et al. (*5*) found reductions in NO_x and VOC emissions for the ECT B (corridor-oriented development), ECT C (clustered development in new and existing areas), and ECT D (high-density mixed-use development and redevelopment) scenarios ranging from 13% to 22%, relative to ECT A, which represented a continuation of current development trends.

AIR QUALITY MODELING AND EXPOSURE PREDICTIONS

The ITLUM scenarios were compared to each other as well as to the predictions from the 2007 base case based on their impacts on daily maximum 1-h ozone concentrations, hourly episodic ozone concentrations, and population exposure. CAMx simulations for the ITLUM scenarios were identical to those of the 2007 base case except for changes in biogenic and anthropogenic emissions and dry deposition velocities.

Predicted 1-h averaged daily maximum ozone concentrations for the 2007 base case ranged from 72 ppb to 90 ppb across the episode. Differences in daily maximum 1-h ozone concentrations due to the combined changes in dry deposition, biogenic emissions, and anthropogenic emissions from on-road mobile, nonroad mobile, and area sources for the ITLUM scenarios ranged from −10 to −2 ppb with typical values of −5 ppb as shown in Table 7. On most episode days, reductions in the daily maximum 1-h averaged ozone concentrations due to the CPCT and UGB scenarios were comparable to or slightly greater than the reductions between the BAU scenarios and the 2007 base case.

Maximum and minimum differences in 1-h ozone concentrations that occurred across the region regardless of time of day or magnitude were also evaluated. Figure 2 shows the range of changes in 1-h ozone concentrations between the ITLUM scenarios and the 2007 base case due to changes in biogenic and anthropogenic emissions and dry deposition for each scenario. Similar to the findings of Song et al. (*5*), increases occurred primarily during the morning hours not during afternoon periods with peak ozone concentrations and are associated with reductions in on-road mobile source emissions along transportation corridors in the Austin urban core that result in less titration of ozone by NO_x emissions. Maximum decreases of as much as 16 ppb were predicted in the LUC-LUI scenarios. The G-LUM UGB scenario resulted in decreases of as much as 14 ppb as compared to

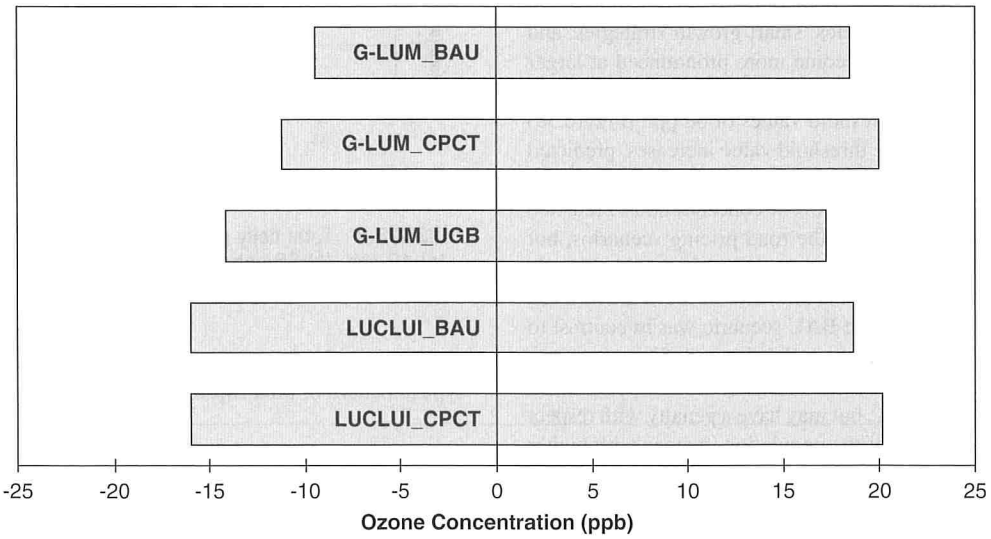

FIGURE 2 Range of changes in hourly ozone concentrations (ppb) between ITLUM scenarios and base case across five-county Austin area.

9.5 ppb in the G-LUM BAU scenario. Differences in hourly ozone concentrations between the future development scenarios and a 2007 base case were more pronounced than differences due to regional transportation and land use policies. However, evaluated with the findings of Song et al. (*5*), the magnitude of the impacts of transportation and land use policies and smart growth-oriented strategies on ozone concentrations is generally within the range of several parts per billion and has the potential to be significant particularly in regions on the cusp of attainment with the NAAQS.

In addition to metrics based on ozone concentration, McDonald-Buller et al. (*6*) examined total daily population-weighted exposure above a threshold ozone concentration (parts per billion) for the ECT scenarios:

$$M_{\text{pop}} = \sum_h \sum_g \frac{p_g}{p_t} s_{g,h}$$

where

p_t = total population in the five-county Austin area for the scenario,
p_g = population in each grid cell g, and
$s_{g,h}$ = ozone concentration (ppb) over the threshold c_{thresh} for each grid cell g at hour h or

$$s_{g,h} = \begin{cases} 0 & c_{g,h} \le c_{\text{thresh}} \\ c_{g,h} - c_{\text{thresh}} & c_{g,h} > c_{\text{thresh}} \end{cases}$$

With the same approach for each ITLUM scenario, this metric was evaluated for various threshold values and estimated for each grid cell, summed over the Austin-area modeling domain and over all hours of the day. Although population exposure-based metrics do not affect a region's attainment status, they do facilitate a more comprehensive assessment of the impacts of urban growth strategies.

As shown in Figure 3*a*, for a threshold value of 40 ppb, all ITLUM scenarios exhibited greater exposure than the base case because of additional increases in ozone and population in newly developed areas. This finding was consistent with results for the ECT scenarios at a 40-ppb threshold concentration, indicating an overall increase in exposure with population growth. The impacts of land use and transportation policies, smart growth strategies, and regulatory emissions controls become more pronounced at larger threshold ozone levels. Figure 3 shows the variation in exposure over the episode for higher threshold values of 60 ppb (Figure 3*b*) and 80 ppb (Figure 3*c*). As the threshold value increases, predicted exposure generally decreased for the ITLUM scenarios relative to the base case consistent with lower peak ozone concentrations. Predicted exposure was generally lower for the road pricing scenarios, but higher for the urban growth boundary scenario where population was more concentrated. Interestingly, the influence of the G-LUM UGB policy on exposure relative to the BAU scenario was in contrast to the impacts on ozone concentrations and emissions of its precursors; the UGB appeared to offer benefits for reducing emissions and ozone concentrations as well as VMT, but may have a penalty with respect to the proximity and density of the population in areas with higher ozone concentrations. McDonald-Buller et al. (*6*) found that consistent with the trends in daily maximum ozone concentrations, population exposure to ozone concentrations above a 60-ppb threshold was lower for the future ECT development scenarios. Concentrated high-density development in existing towns with balanced-use zoning (ECT D) produced lower exposure to high ozone concentrations than a more typical pattern of urban sprawl (ECT A).

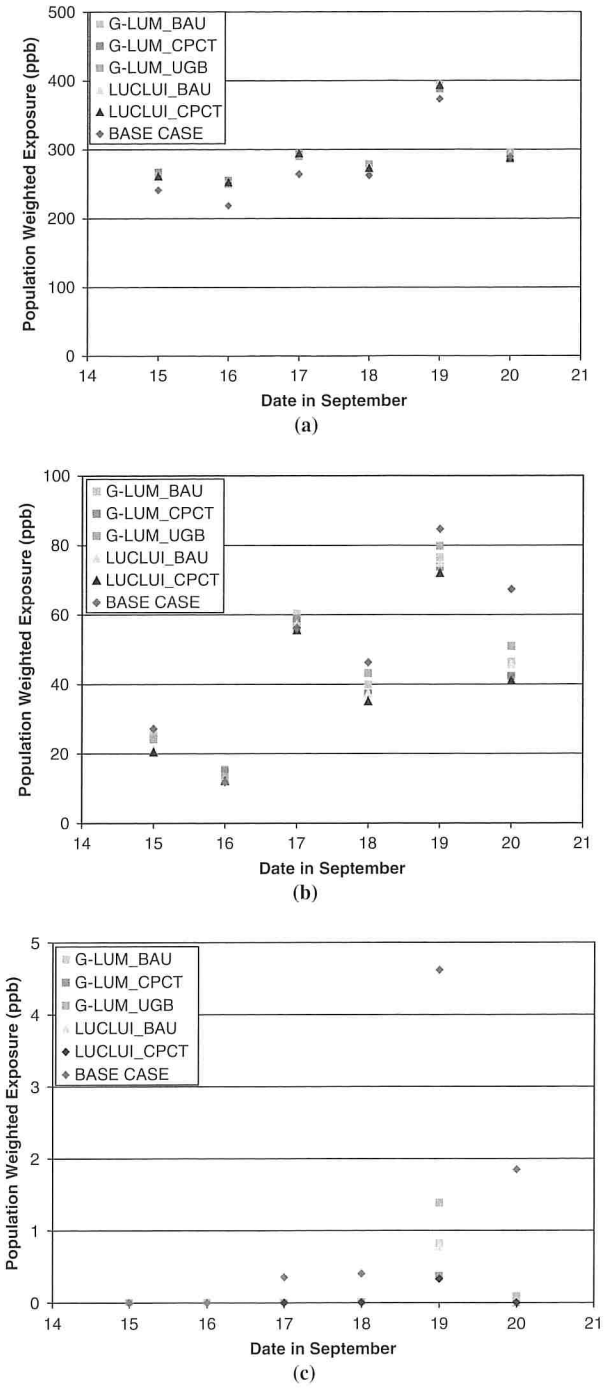

FIGURE 3 Total daily population-weighted exposure using a (*a*) 40-ppb, (*b*) 60-ppb, and (*c*) 80-ppb threshold for ITLUM scenarios and 2007 base case.

CONCLUSIONS

The impacts of land use and transportation policies on emissions, ozone concentrations, and a metric for population exposure were examined using Austin, Texas, as a case study. Austin is typical of

many urban areas of the United States that are on the cusp of nonattainment with the NAAQS for ozone. Three transportation and land use scenarios were investigated using a G-LUM and a standard TDM: a BAU scenario, a road pricing policy that included a flat-rate CPCT of all Austin-area freeways, and UGB policy. Two scenarios, a BAU scenario and a flat-rate CPCT policy were also investigated using a novel, parcel-level LUC-LUI model and a standard TDM. The prices, tolls, and boundary locations considered in this work represented reasonable scenarios if such policies were to be pursued by community stakeholders.

Transportation and land use policies were predicted to have substantial impacts on travel and emissions of ozone precursors. The BAU scenario predicted an 85% to 90% increase in VMT in 2030 relative to a 2007 base case. In contrast, the increase in VMT under the road pricing and UGB policies was only 60%. Emissions of ozone precursors decreased markedly for all 2030 scenarios due to the implementation of more stringent federal motor vehicle emission control programs, but transportation and land use policies were predicted to lead to even greater reductions, by about 15%, of emissions relative to the BAU scenario.

The impacts of such policies on ozone concentrations and population exposure suggested varying effects. Daily maximum 1-h ozone concentrations were predicted to decrease under the future scenarios with changes ranging from –10 ppb to –2 ppb, with typical values of –5 ppb. The benefits of transportation and land use policies and smart growth-oriented strategies for reducing ozone concentrations were generally within the range of several parts per billion, which suggests that these policies have the potential to be significant particularly in regions on the cusp of attainment with the NAAQS. Lower exposure was typically predicted for the road pricing scenarios, but a penalty appeared to exist with relatively higher values of exposure predicted for the UGB on some episode days. Future work should explore the impacts of urban growth and transportation and land use policy scenarios on greenhouse gas emissions, examine new scenarios (such as density floors on new development), allow for new vehicle and power-generation technologies, and accommodate other land use model specifications.

The results of this analysis indicate the potential complexity of planning for urban growth and equity and the need for integrated modeling and policy evaluation efforts. This project was conducted by a team with expertise spanning urban and regional planning, transportation and land use modeling, emission inventory development, and air quality modeling. Although the primary team members had long histories of working with the State of Texas and Austin-area stakeholders, this project was the first that synthesized their efforts. While expertise in these areas is not unique within the realm of many metropolitan planning organizations, departments of transportation, city governments, and state environmental agencies, there is a need for better collaboration between fields during community and regulatory decision-making processes to allow more comprehensive assessments of urbanization and its environmental impacts.

ACKNOWLEDGMENT

This research was funded by the U.S. Environmental Protection Agency.

REFERENCES

1. Rodier, C., and R. Johnston. Uncertain Socioeconomic Projections Used in Travel Demand and Emissions Models: Could Plausible Errors Result in Air Quality Nonconformity? *Transportation Research Part A,* Vol. 36, 2002, pp. 613–631.
2. Rodier, C., R. Johnston, and J. Abraham. Heuristic Policy Analysis of Regional Land Use, Transit, and Travel Pricing Scenarios Using Two Urban Models. *Transportation Research Part D,* Vol. 7, 2002, pp. 243–254.
3. Wang, X. M., W. S. Lin, L. M. Yang, R. R. Deng, and H. Lin. A Numerical Study of Influences of Urban Land-Use Changes on Ozone Distribution Over the Pearl River Delta Region, China. *Tellus B,* Vol. 59, No. 3, 2007, pp. 633–641.
4. Civerolo, K., C. Hogrefe, B. Lynn, J. Rosenthal, J. Y. Ku, W. Solecki, W. Cox, C. Small, C. Rosenzweig, R. Goldberg, K. Knowlton, and P. Kinney. Estimating the Effects of Increased Urbanization on Surface Meteorology and Ozone Concentrations in the New York City Metropolitan Region. *Atmospheric Environment,* Vol. 41, No. 9, 2007, pp. 1803–1818.
5. Song, J., B. Parmenter, A. Webb, D. Allen, and E. McDonald-Buller. Impacts of Urbanization on Emissions and Air Quality: Comparison of Four Visions of Austin, Texas. *Environmental Science and Technology,* Vol. 42, No. 19, 2008, pp. 7294–7300.
6. McDonald-Buller, E., J. Song, A. Webb, and D. Allen. Regional Visions of Urbanization in Austin, Texas, and the Impacts on Air Quality and Population Exposure Metrics. *Proc., Air & Waste Management Association Annual Meeting,* Portland, Ore., June 2008.
7. Zhou, B., and K. M. Kockelman. Lessons Learned in Developing and Applying Land Use Model Systems: Parcel-Based Example. In *Transportation Research Record: Journal of the Transportation Research Board, No. 2133,* Transportation Research Board of the National Academies, Washington, D.C., 2009, pp. 75–82.
8. Zhou, B., K. M. Kockelman, and J. D. Lemp. Applications of Integrated Transport and Gravity-Based Land Use Models for Policy Analysis. In *Transportation Research Record: Journal of the Transportation Research Board, No. 2133,* Transportation Research Board of the National Academies, Washington, D.C., 2009, pp. 123–132.
9. *User's Guide to the Comprehensive Air Quality Model with Extensions (CAMx)–Version 4.03.* ENVIRON International Corporation, Novato, Calif., 2004.
10. Webb, A., J. Song, D. Allen, E. McDonald-Buller, B. Zhou, S. Gadda, J. Lemp, S. Tirumalachetty, K. Kockelman, and B. Parmenter. *Predicting the Relative Impacts of Urban Development Policies and On-Road Vehicle Technologies on Air Quality in the United States: A Case Study in Austin, Texas.* Final report submitted to the U.S. EPA (STAR Grant No. RD83183901), Dec. 2008.
11. Wiedinmyer, C., I. W. Strange, M. Estes, G. Yarwood, and D. T. Allen. Biogenic Hydrocarbon Emission Estimates for North Central Texas. *Atmospheric Environment,* Vol. 34, No. 20, 2000, pp. 3419–3435.
12. Wiedinmyer, C., A. Guenther, M. Estes, I. Strange, G. Yarwood, and D. T. Allen. A Land Use Database and Examples of Biogenic Isoprene Emission Estimates for the State of Texas, USA. *Atmospheric Environment,* Vol. 35, No. 36, 2001, pp. 6465–6477.
13. Yarwood, G., G. Wilson, S. Shepard, and A. Guenther. *User's Guide to the Global Biosphere Emissions and Interactions System–Version 3.1.* ENVIRON International Corporation, Novato, Calif., 2003.
14. Alliance-Texas Engineering Group. *City of Pflugerville Refined Transportation Model Development Report,* Nov. 2003.
15. Wesely, M. L. Parameterization of Surface Resistances to Gaseous Dry Deposition in Regional-Scale Numerical Models. *Atmospheric Environment,* Vol. 23, No. 6, 1989, pp. 1293–1304.

This research has not been subjected to the U.S. Environmental Protection Agency's peer and policy review and therefore does not necessarily reflect the views of the agency, and no official endorsement should be inferred.

The Transportation and Air Quality Committee peer-reviewed this paper.

Bus Technology Meta-Analysis

Hilda Martínez, Jorge Macias Mora, and Alper Unal

This paper analyzes data obtained from international studies that compared natural gas, diesel, and hybrid technologies for buses to determine differences in particulate matter (PM_{10}), nitrogen oxides (NO_x), nonmethane hydrocarbon (NMHC), carbon monoxide (CO), greenhouse gas, and air toxic emissions. The results presented here are for 90-passenger 12-m buses. Two types of comparisons were made: technology and fuel. The comparison revealed that buses using ultra-low-sulfur diesel (ULSD) with diesel particulate filters (DPF) and buses using compressed natural gas (CNG) with oxidation catalysts (OC) had the lowest emissions of PM_{10} and CO; CNG with OC had lower NO_x and greenhouse gases emissions, while ULSD with DPF had lower NMHC emissions. Posttreatment technologies are presented as a low-cost option to reduce emissions. Hybrid diesel buses were found to be the technology that has the lowest emissions for most of the studied pollutants.

The Mexico City, Mexico, Metropolitan Area (ZMVM in Spanish), according to Instituto Nacional de Estadística, Geografía e Informática (*1*), houses approximately 19,232,000 people and has a slight annual growth rate of 0.5%. Despite this slight demographic growth, urban development proceeds on the basis of a low-density, area-related, high-demand model. It is obvious that if this development process were to continue in Mexico City, within the next 25 years more municipalities would be incorporated into the metropolitan area, increasing both its total population and its transportation needs.

According to the EMBARQ Center for Sustainable Transportation's (CTS's) prospective statistics, there is an average of 52,400,953 daily trips (including nonmotorized trips) in the metropolitan area. Mexico City's inhabitants transport themselves at a rate of 2.7 trips per day per person, which puts the city within the parameters of medium development. If the approximately 13,305,684 daily nonmotorized trips (based on calculations made by CTS) are excluded, public transportation represents 69.05% of the total daily trips, providing service to the majority of the metropolitan area population.

Transportation greatly affects personal exposure to air pollution because of the closeness to the emissions sources (i.e., motorized vehicles) and the duration of the trips. Acute respiratory infections, asthma (*2*) and chronic obstructive pulmonary disease, are the illnesses usually related to air pollution, specifically caused by particulate matter (PM_{10} and $PM_{2.5}$) and ozone (*3*). The CTS in collaboration with the National Institute for Ecology (INE, in Spanish) calculates that between 50% and 80% of daily exposure to particles in Mexico City occurs during transportation (*4*).

A joint investigation between INE and CTS analyzed users' exposure in transportation under normal operation conditions and found concentrations averaging 152 $\mu g/m^3$ and 167 $\mu g/m^3$ ($PM_{2.5}$) and 212 $\mu g/m^3$ and 206 $\mu g/m^3$ (PM_{10}) for buses and microbuses, respectively (*4*). These concentrations prove to be much greater than the microenvironmental concentrations in direct-impact open spaces, because measurements were taken at the beginning (north) and at the end (south) of the route, with the following concentrations found: 86 $\mu g/m^3$ and 66 $\mu g/m^3$ of $PM_{2.5}$ and 110 $\mu g/m^3$ and 80 $\mu g/m^3$ of PM_{10} (*4*), respectively. Average concentrations inside buses and microbuses were almost twice as high as those outside. Official Mexican air quality standard NOM-025-SSA1-1993 stipulates that the maximum average values allowed for a 24-h period are 120 $\mu g/m^3$ and 65 $\mu g/m^3$ for PM_{10} and $PM_{2.5}$, respectively.

The metropolitan area has shown a decrease in ozone concentrations in the past few years. According to Mexico City's Ministry of the Environment, ozone concentration has decreased from 0.32 ppm in 1991 to 0.16 in 2006 (*5*). Despite the significant advance in diminishing the ozone levels, the number of days on which children are exposed to concentrations exceeding the air quality standard still worries investigators. This effect is especially severe in the southwest region of the valley, where, in 2005, levels were above the standard for 120 to 157 days of the year (*5*).

The population most vulnerable to ozone concentration and its effects are children and the elderly. Children are more vulnerable because they spend more time in the open than adults do and their breathing is quicker, which potentially exposes them to higher concentrations of air pollutants.

The World Health Organization estimates that 5 million children die each year worldwide due to because of pollution-related illnesses. For the Mexico Valley Metropolitan Area, where 30% of the population is under 15, this problem is very significant (*1*).

A total of 440,000 children who live in this area were exposed during almost half the year to concentrations of ozone above 0.110 ppm on average. In addition, the geographical area where the standard was exceeded for 60 to 120 days during 2005 in the metropolitan area houses 3.9 million infants (*5*). These numbers suggest that there is still a long way to go.

According to the World Asthma Association, 46% of the children in Mexico City suffer from asthma or allergic rhinitis. Each year, 500,000 new cases are registered and, according to the Social Security Department, this problem represents a direct cost of more than $50 million annually, which is probably an underestimation.

The serious cardiovascular problems brought about and worsened by pollution (*6*) and the relation between air pollution and the incidence of cancer through hydrocarbons (HC) in the population (*7*) cannot be ignored. HC emissions have well-known, highly mutagenic properties and must be considered, even though the magnitude of this relation is still unclear.

Center for Sustainable Transportation—EMBARQ, Mexico City, Felipe Carrillo Puerto #54 P.B., Villa Coyoacan, Mexico, D.F. C.P. 04000. Corresponding author: J. M. Mora, jmacias@ctsmexico.org.

Transportation Research Record: Journal of the Transportation Research Board, No. 2158, Transportation Research Board of the National Academies, Washington, D.C., 2010, pp. 36–43.
DOI: 10.3141/2158-05

METHODOLOGY FOR META-ANALYSIS

This study reviewed 12 previous reports that compared different compressed natural gas (CNG), diesel, and hybrid technologies. These investigations have been published in peer-reviewed journals and were chosen because of their consistent methodology and the validity of their arguments. These studies were conducted by different researchers under different testing conditions. A total of 14 CNG buses were analyzed, along with 29 CNG with oxidation catalysts (OC) buses, 28 conventional diesel buses (300 ppm of sulfur content), 12 ultra-low-density diesel (ULSD) buses, 21 ULSD with diesel particulate filters (DPF) buses, and 8 hybrids, totaling 112.

The main objective is to condense emission measurements from these investigations and analyze their data. The objective is not to compare these studies against each other because they were conducted under different conditions. This paper presents a general overview on emissions performance of these reported technologies with the given uncertainty and variability. However, the authors strongly suggest a comparison study in which buses with different technologies are compared under controlled conditions.

The analysis presents emissions measurements from buses under different driving conditions. The measurements took into account not only a variety of buses, technologies, and engines, but also the driving cycles used in each investigation.

Data were obtained for bus models from 1997 to the present. Samples were taken for cycles ranging from relaxed to aggressive driving. Most of the buses studied were approximately 12 m long, although some articulated buses (less than 10%) were included. To homogenize data, the emissions were transformed using a factor based on the standard capacity of the buses. They were indexed to emissions for 90 passengers or for 12-m-long buses. For the most part, the exact passenger capacity of the buses was unknown. It was assumed that there would be 140 passengers for 15-m buses, 160 for 18-m buses, and 90 for 12-m buses.

Variability in the conditions of the samples can be regarded as an advantage, because it allowed the authors to closely examine different conditions in which these buses are used. Delays in the introduction of new technologies in developing countries are taken into account by including older models in the analysis. Likewise, by considering all driving cycles, the authors cover the different driving styles and conditions that can be found in different cities.

The analysis focuses on the study of the variability in different technological options. The emissions produced by different technologies in use are not stable or constant. By centering the study on the variability tendencies, a more precise image of the trend can be obtained, and the behavior of different technologies under various weights, technological, maintenance, and driving conditions can be analyzed.

The first variability measurement presented for analysis is interquartile range (IQR). IQR is a statistical measure that is equal to the difference between the first and third quarter (or upper and lower 25th percentile). Thus, 25% of the data are less than or equal to the first quarter, while 25% are more than or equal to the third. IQR includes approximately half of the observations. This measurement avoids the need to establish suppositions about the probability distribution of the data (such as normal or log-normal distribution) while allowing a clear view of the spread and can be graphically presented using a box-and-whisker plot. For comparison purposes, a chart was prepared assuming normal distribution of the data, which allows the use of confidence interval comparisons.

COMPARISON OF EMISSIONS BY FUEL AND CONTROL TECHNOLOGIES

This section presents the results obtained using two methods: the first based on interquartile range, and the second using confidence intervals of 90%. Using IQR, we obtained box-and-whisker plots. Box-and-whisker or box plots are built in a box the same length as the IQR, and tails or whiskers are added to determine out-of-range data. Any observation under 1.5 times the IQR of the first quarter or over 1.5 times the IQR of the third quarter will be considered out of range (outlier). In box plots, the least and the greatest values that were not considered are indicated as out-of-range data and are joined to the box by a vertical line or whisker.

For interval confidence charts, descriptive statistics are obtained and the data that are two standard deviations above and below the initial average (outliers) are eliminated. Once the outliers are eliminated, the confidence intervals are calculated. The intervals, as well as the average emissions, are reported in corresponding charts. Figure 1 presents the general descriptive statistics, comparative IQR, general statistics, and 90% confidence interval for PM_{10}.

Spread in the results is particularly evident for conventional diesel, which had very high IQR and standard deviation. Figure 1 shows the interquartile ranges and the median, giving a clear image of the data that is possibly out of range. The horizontal lines that divide the boxes in two symbolize the position of the medians. The upper limit of the boxes represents the third quarter and the lower limit the first quarter. IQR, therefore, shows 50% of the data, which are at the center, and is represented by the length of the boxes.

Figure 1 clearly shows the difference in emissions for CNG, CNG with OC, ULSD with DPF, and hybrid technologies. These four technologies show drastically lower emission levels than conventional diesel, even ULSD with no posttreatment equipment.

With the introduction of ULSD, emissions for diesel technologies lower to less than half of conventional diesel. The reductions added by the particle trap (DPF) reinforce the results of the CTS-EMBARQ field test in Mexico City, with a 78% reduction compared to ULSD alone and a 90% reduction for conventional diesel.

By the data provided in the studies mentioned, CNG proved to be, without the need for any posttreatment equipment, a clean fuel concerning PM_{10}. The introduction of posttreatment in CNG buses further reduces these emissions. The adoption of CNG, CNG with OC, ULSD with DPF, and hybrid technologies is a substantial improvement (90% to 97%) with respect to the status quo, conventional diesel.

The cleanest options for this pollutant are CNG buses with OC, which had an emission average of 0.01 g/km, and diesel hybrid technology, with an average of 0.08 g/km. Both technologies had very similar variations for their confidence intervals.

Nitrogen Oxides

Nitrogen oxides (NO_x) are important because, with hydrocarbons, they are the main precursors of ozone formation. The data analyzed in this investigation are shown in Figure 2.

It is worth noticing the emission increase in diesel technologies with the introduction of DPF particle traps. This increase can be due to the inverse relation in the treatment of PM_{10} and NO_x. The particle trap requires that the gases maintain an elevated temperature to function optimally in the elimination of particles. Conversely, NO_x diminish when exhaust fumes are at lower temperatures.

	No. Buses	Median	Average	Standard Deviation	IQR
CNG	10	0.025	0.052	0.084	0.019
CNG + OC	14	0.008	0.009	0.007	0.010
D. Conv	11	0.280	0.309	0.155	0.207
ULSD	7	0.131	0.140	0.025	0.030
ULSD + DPF	17	0.029	0.057	0.080	0.024
Hybrid	8	0.012	0.011	0.007	0.007

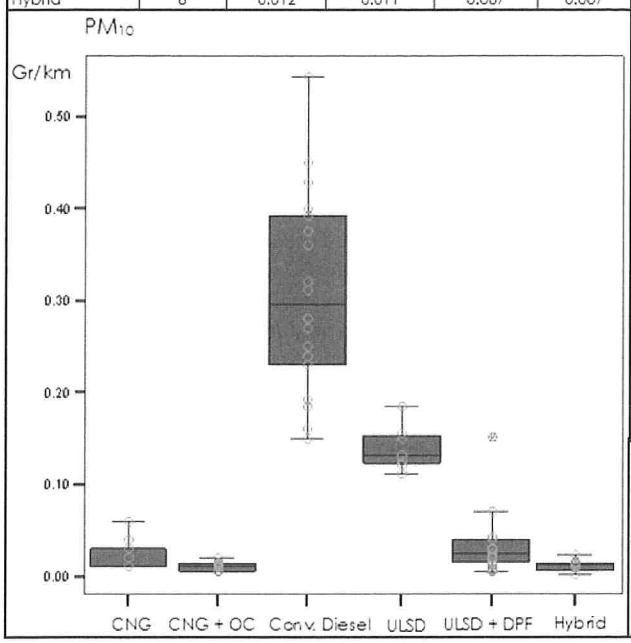

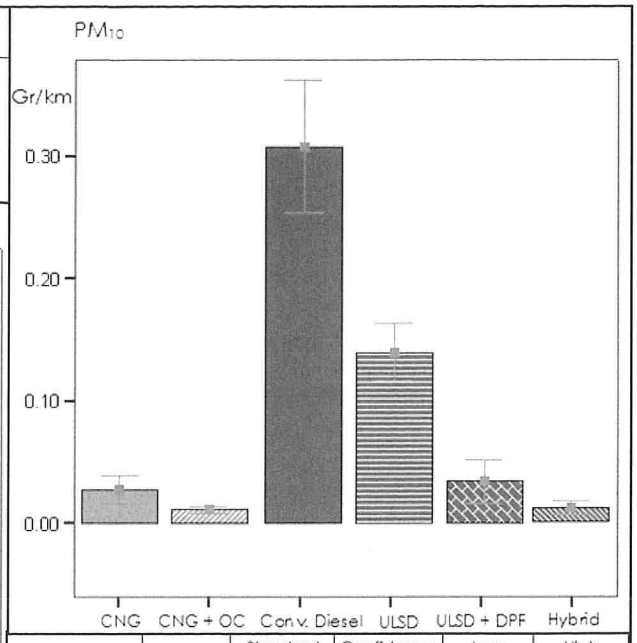

	Average	Standard Deviation	Confidence Interval	Low Range	High Range
CNG	0.027	0.016	0.008	0.044	0.060
CNG + OC	0.010	0.005	0.002	0.008	0.011
D. Conv	0.308	0.110	0.038	0.272	0.347
ULSD	0.140	0.025	0.016	0.124	0.155
ULSD + DPF	0.033	0.034	0.013	0.044	0.070
Hybrid	0.011	0.007	0.004	0.007	0.015

FIGURE 1 Results for PM_{10}.

	No. Buses	Median	Average	Standard Deviation	IQR
CNG	13	11.87	15.76	11.72	9.204
CNG + OC	27	6.84	7.21	4.43	5.577
D. Conv	20	10.78	11.20	8.76	9.225
ULSD	9	8.20	6.99	5.55	7.830
ULSD + DPF	21	11.12	10.44	4.78	6.876
Hybrid	8	5.85	5.99	1.67	1.909

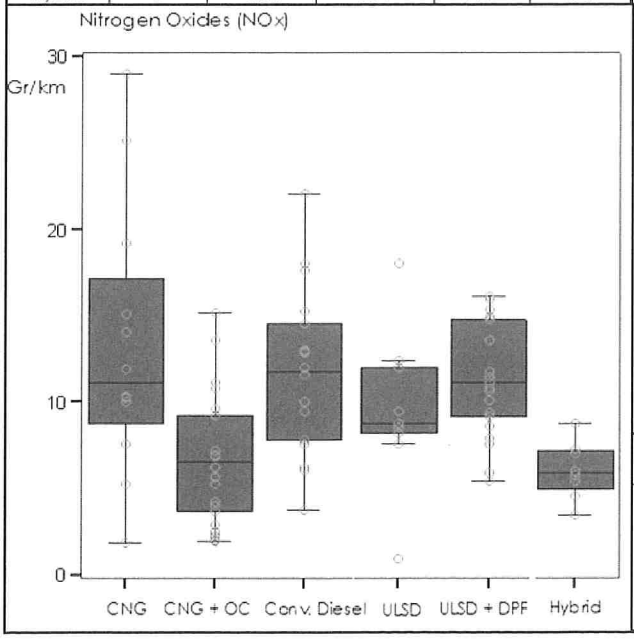

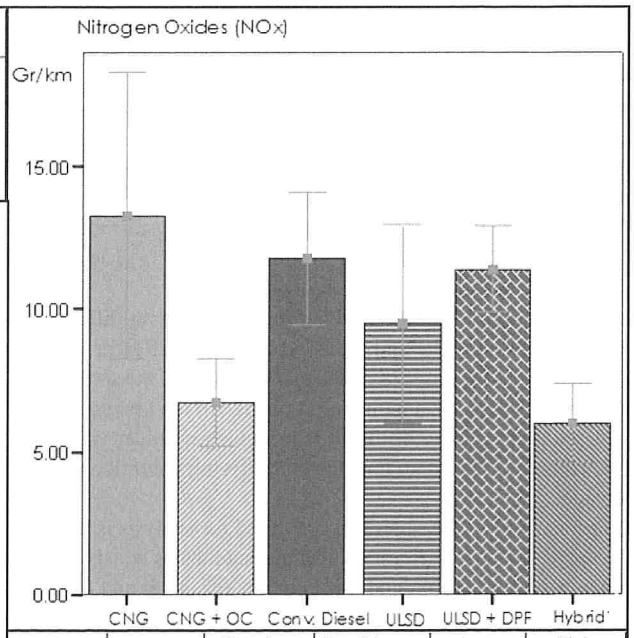

	Average	Standard Deviation	Confidence Interval	Low Range	High Range
CNG	13.279	7.90	3.47	9.80	16.75
CNG + OC	6.751	3.80	1.25	5.50	8.00
D. Conv	11.77	4.67	1.92	9.84	13.69
ULSD	9.51	4.58	2.38	7.13	11.90
ULSD + DPF	11.41	3.37	1.24	10.17	12.65
Hybrid	5.99	1.75	0.96	5.03	6.95

FIGURE 2 Results for NO_x.

The magnitude of the increase is more visible in the confidence interval of Figure 1. The figure shows the limits of the confidence interval for the high and the low ranges. It can be seen by taking the averages that the demand for higher temperatures for the functioning of DPF increases NO_x by 20% compared with ULSD technology. The best combustion, provided by the OC in CNG technology, provides a reduction of an average of 49% compared to emissions for CNG with no posttreatment device.

Based on the comparison, hybrid diesel technology is the one with the lower grams per kilometer emissions of NO_x, representing a value that is practically half of the emissions present in conventional and ULSD with a particle trap. In general, hybrids and CNG buses with a catalyst are the cleanest options for NO_x.

Nonmethane Hydrocarbons

Nonmethane hydrocarbons (NMHCs) are relevant because they are constituted by some toxic, cancer-causing, or mutagenic gases. For the NMHC evaluation, a total of 64 measurements were taken into account, since the CNG technology without an OC was not analyzed. The data used for each technology are represented by its general descriptive statistics in Figure 3.

The analysis shows that greater NMHC levels prevail for the CNG technology with OC. It is also clear, as can be deduced from the figure, that this technology (with an interquartile range of 0.37) presents the greatest scattering of the analyzed technologies.

Conversely, diesel technologies have very low hydrocarbon emission levels. It is relevant to point out the existing emission reduction when DPF are introduced, because these also include a catalyst. As can be seen in Figure 3, ULSD buses emit only 0.26 g/km of HC. The introduction of DPF with a catalyst reduces the average to 0.04 g/km, a significant (85%) reduction.

It is clear that hybrid technology has the lowest nonmethane hydrocarbon emissions (0.014 g/km) representing a 95.3% reduction compared with conventional diesel. It is also important to point out the low dispersion of the data presented by diesel with DPF and hybrids compared with those present in CNG.

Unfortunately, the authors could not find enough data on NMHC to include CNG without OC in the emission analysis. The analysis of total hydrocarbons shows a reduction of 42% of the emissions with the addition of a catalyst. It is to be expected that a similar proportion would be found for NMHC reduction.

Carbon Monoxide

The role of posttreatment systems is also important for carbon monoxide (CO) emissions. The average emissions and data dispersion are drastically reduced with the introduction of OC for CNG technologies and particle traps for diesel technologies, which can be seen in Figure 4.

The use of a catalyst (OC) lowers CNG emissions from 11.32 to 0.72, a reduction of 94%. At the same time, the standard deviation is reduced. Likewise, the particle trap with a catalyst reduces CO emissions by 84% compared with ULSD.

ULSD with DPF buses have the lowest CO emissions, 30% less than CNG with OC. Despite this relative difference, emissions from

	No. Buses	Median	Average	Standard Deviation	IQR
CNG + OC	15	0.65	0.71	0.39	0.369
D. Conv	11	0.30	0.42	0.59	0.298
ULSD	15	0.26	0.26	0.09	0.136
ULSD + DPF	15	0.04	0.06	0.08	0.075
Hybrid	8	0.01	0.01	0.01	0.012

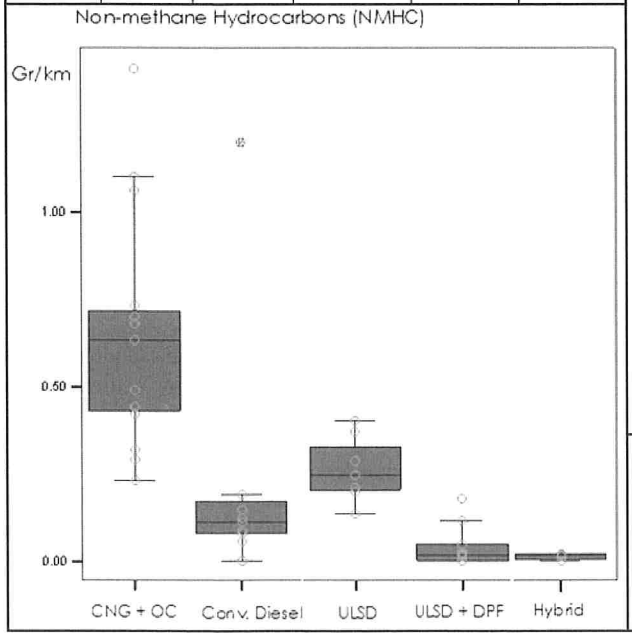

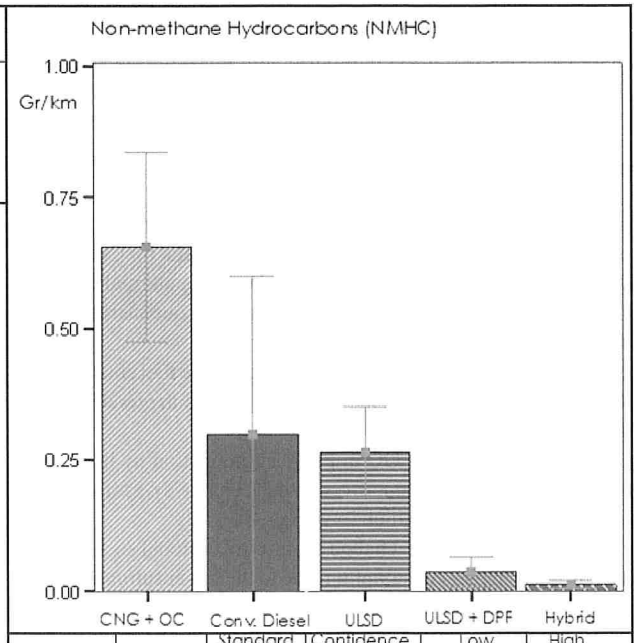

	Average	Standard Deviation	Confidence Interval	Low Range	High Range
CNG + OC	0.655	0.327	0.112	0.543	0.767
D. Conv	0.298	0.449	0.213	0.085	0.511
ULSD	0.264	0.095	0.055	0.209	0.319
ULSD + DPF	0.036	0.050	0.020	0.016	0.056
Hybrid	0.013	0.008	0.005	0.008	0.017

FIGURE 3 Results for NMHC.

	No. Buses	Median	Average	Standard Deviation	IQR
CNG	13	7.15	17.20	24.51	18.086
CNG + OC	27	0.33	0.90	1.23	1.132
D. Conv	20	3.50	3.59	2.61	2.925
ULSD	9	1.40	3.15	4.02	0.801
ULSD + DPF	21	0.21	0.72	1.20	0.812
Hybrid	8	0.63	0.72	0.40	0.374

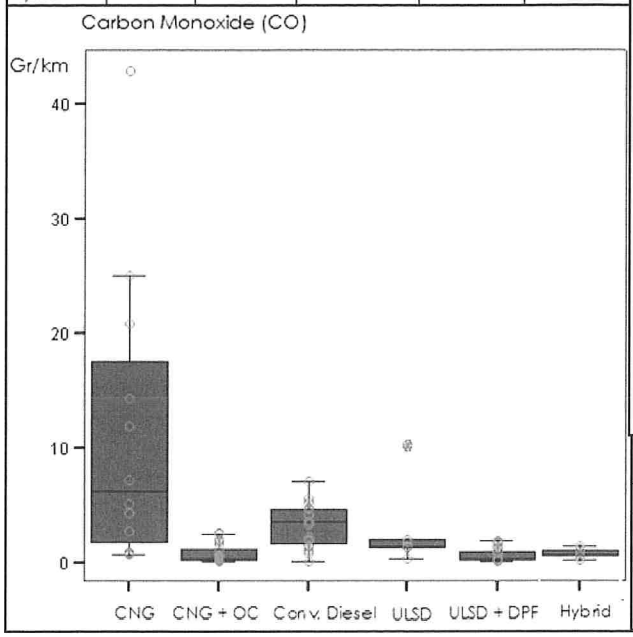

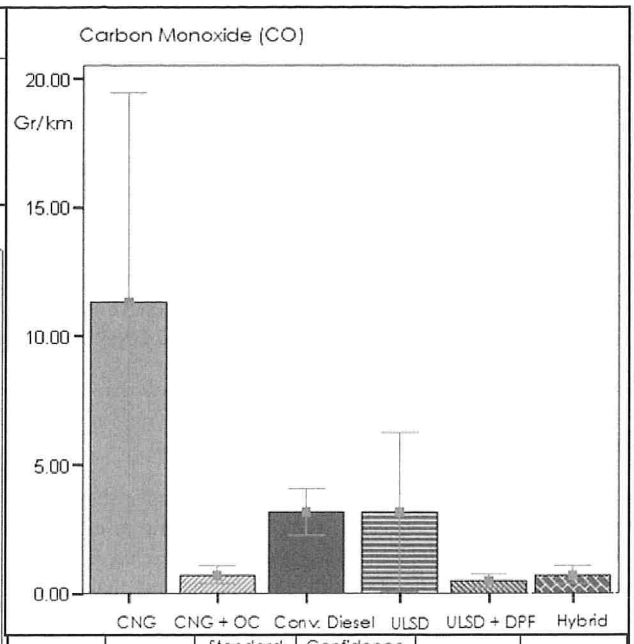

	Average	Standard Deviation	Confidence Interval	Low Range	High Range
CNG	11.32	12.78	6.07	5.25	17.38
CNG + OC	0.72	0.84	0.27	0.45	0.99
D. Conv	3.17	1.88	0.71	2.46	3.88
ULSD	3.15	4.02	2.20	0.95	5.35
ULSD + DPF	0.49	0.61	0.22	0.27	0.72
Hybrid	0.72	0.40	0.23	0.49	0.95

FIGURE 4 Results for CO.

CNG with OC, ULSD, ULSD with DPF, and hybrid technologies are within significantly low emission ranges.

Greenhouse Gases

To analyze greenhouse gases (GHG), both carbon dioxide (CO_2) and methane (CH_4) were considered. The warming potential for CH_4 was considered to be 21 times that of CO_2. The heating potential of the emissions for each technology was obtained (in CO_2 equivalents) and the results are shown in Figure 5.

In general, GHG emissions are closely related to the fuel consumption of different technologies. This relation explains the tendencies seen in Figure 5.

For CNG, the presence of OC improves combustion by helping the gas mix with oxygen. This improves both the engine's performance and its methane emissions, which lower considerably.

In reference to diesel, the change from conventional to ULSD means an increase in fuel consumption, due to the lower sulfur levels. In general, the processing required to reduce sulfur to 15 ppm also reduces the aromatics content and density of diesel fuel, resulting in a reduction in energy content (BTU/gal). A 1% reduction is expected, which may affect kilometers per liter. Figure 5 shows this increase, with average emissions of 1,177 g/km for conventional diesel and 1,332 g/km for ULSD. This effect diminishes once the out-of-range data are removed, as shown in Figure 5 for GHG.

The introduction of particle traps also increases fuel consumption requirements, considerably increasing GHG emissions. The DPF increases its fuel usage due, in great part, to the filter regeneration phase. The increase shown in Figure 5 for emissions with DPF is 43% compared to ULSD alone.

Conversely, fuel savings in hybrid technology allow for emissions of 1,068 g/km. This is the technology that produces the least GHG emissions, 19% less than CNG with OC, and 35% less than ULSD with particle traps.

Toxic Air Pollutants

The toxic air pollutants analyzed are acetaldehyde and formaldehyde. Unfortunately, the data pool gathered was quite limited and lacked measurements of aldehydes for hybrid technology, therefore failing to report emissions on this technology.

Acetaldehyde

Acetaldehyde is considered a probable human carcinogen (*8*) and at higher levels of exposure it can cause coughing, pulmonary edema, and necrosis (*9*). A total of 31 measurements for five technologies were taken into consideration.

Because of the low number of pooled observations, the IQR spread shown in Figure 6 is quite big. This is quite visible for CNG and for ULSD, with IQR values of 70 and 87, respectively. Conversely, conventional diesel shows the smallest IQR spread and low levels of emission of acetaldehyde.

CNG and ULSD have the highest average of acetaldehyde emission. Conventional diesel had a comparable emission level as CNG with OC. The switch from conventional diesel to ULSD is no guarantee

	No. Buses	Median	Average	Standard Deviation	IQR
CNG	13	1620	1922	916	434
CNG + OC	23	1340	1355	267	339
D. Conv	16	1104	1177	307	457
ULSD	7	1200	1332	330	351
ULSD + DPF	19	1821	1685	450	677
Hybrid	9	1194	1116	245	224

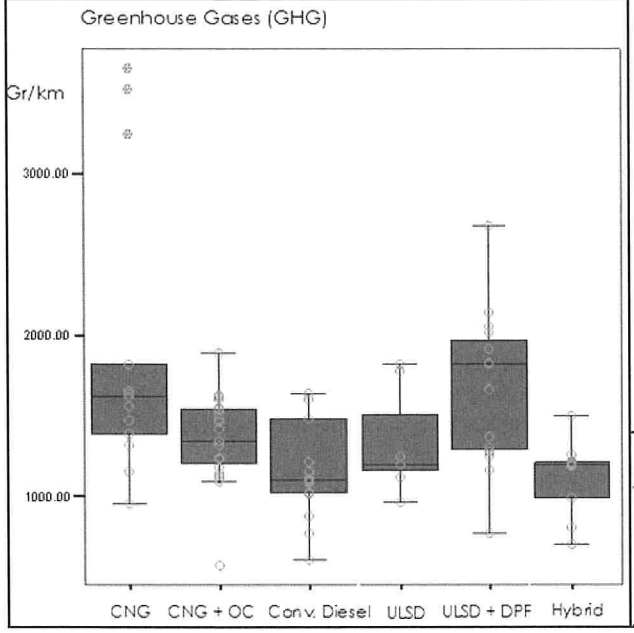

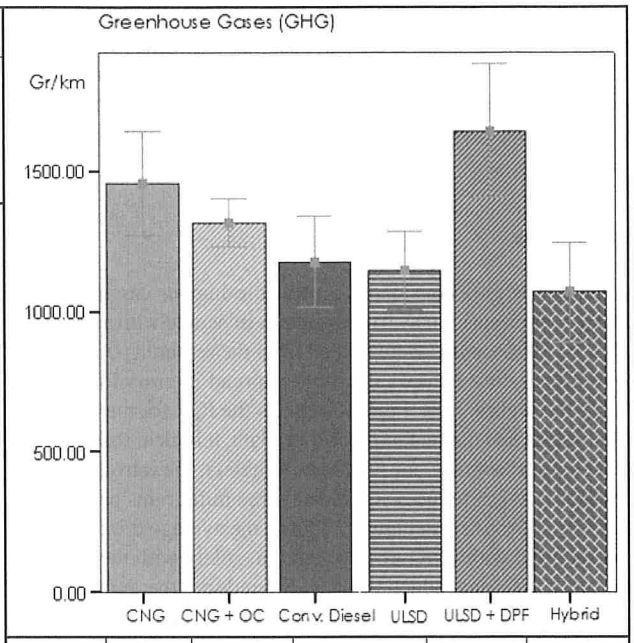

	Average	Standard Deviation	Confidence Interval	Low Range	High Range
CNG	1457.32	259.27	113.98	1343.34	1571.29
CNG + OC	1316.32	166.04	55.75	1260.57	1372.07
D. Conv	1177.19	306.51	126.04	1051.15	1303.23
ULSD	1146.67	112.57	58.55	1088.11	1205.22
ULSD + DPF	1641.75	412.07	155.50	1486.25	1797.24
Hybrid	1068.34	211.92	116.19	952.15	1184.53

FIGURE 5 Results for GHG.

	No. Buses	Median	Average	Standard Deviation	IQR
CNG	3	10.00	56.67	80.83	70
CNG + OC	11	7.00	20.29	23.13	34.5
D. Conv	6	18.65	19.55	1.92	3
ULSD	5	34.00	52.70	48.41	87
ULSD + DPF	6	3.50	6.23	7.13	10.35

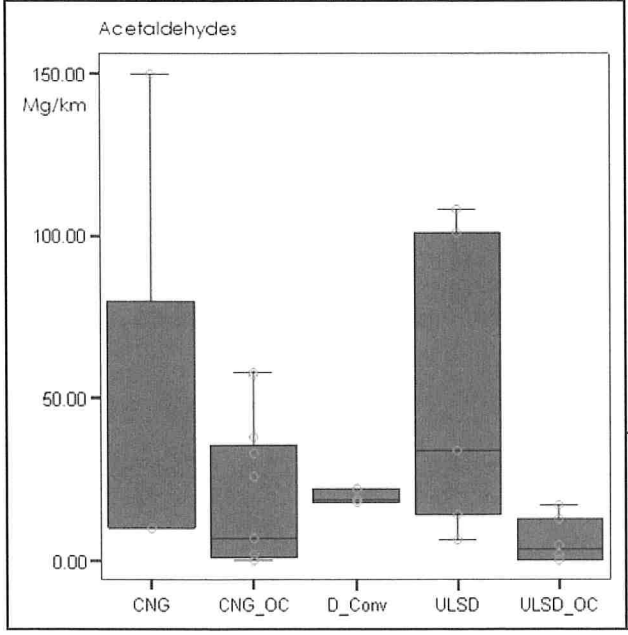

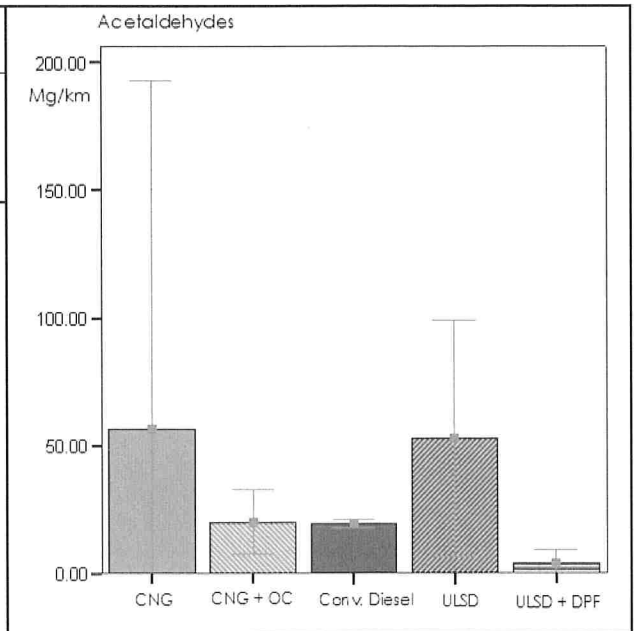

	Average	Standard Deviation	Confidence Interval	Low Range	High Range
CNG	56.67	80.83	53.81	2.85	110.48
CNG + OC	20.29	23.13	10.06	10.23	30.35
D. Conv	19.55	1.92	13.13	6.42	32.68
ULSD	52.70	48.41	38.77	13.93	91.47
ULSD + DPF	4.08	5.36	3.00	1.08	7.08

FIGURE 6 Results for acetaldehyde.

of lower emissions as proved from the figure. In order for ULSD to be cleaner, the introduction of a particulate filter is required.

CNG and ULSD without posttreatment did not emit less acetaldehydes than conventional diesel and no gain is obtained merely by switching to an alternative fuel; again the real gain comes from posttreatment.

Formaldehyde

Formaldehyde is also considered a probable human carcinogen. At high concentrations it may trigger attacks in people with asthma. A total of 44 observations were pooled from the research papers.

Conventional diesel shows the higher spread in emissions, by presenting the highest IQR. Figure 7 reflects the IQR for the different technologies and the scatter plot for the data. It is clear that CNG offers the highest average emissions; nonetheless, the introduction of an oxygen catalyst reduces significantly the milligrams per kilometer of formaldehyde. As Figure 7 shows, the average diminishes from 683 mg/km with CNG to 17.95 mg/km solely with the introduction of OC. The introduction of ULSD reduces the amount of formaldehyde compared with conventional diesel and it is furthered reduced with the introduction of DPF.

CONCLUSIONS

This study analyzed data obtained from international studies that compare natural gas, diesel, and hybrid technologies for buses to identify differences in particulate matter, nitrogen oxides, nonmethane hydrocarbon, carbon monoxide, GHG, and air toxic emissions. The main objective is to condense emission measurements from these investigations and to provide a general overview on emissions performance of the presented technologies with the given uncertainty and variability. However, the authors strongly suggest a comparison study where buses with different technologies are compared under the same controlled conditions. In this study the following conclusions were obtained:

- Emission certificates proved to be a good indicator for emission reductions in PM_{10}, NO_x, CO, and HC, but not for GHG, which did not show any reduction between the lower and the higher European levels.
- Within the experimental data, conventional diesel had greater variation in its results for PM_{10} emissions. CNG without posttreatment had a greater IQR for CO and NO_x emissions data, as well as a high variation for PM_{10}. The CNG with OC option had greater variability for NMHC, as did the ULSD with DPF for GHG.
- The technology that presented the lowest emissions for all the categories analyzed was diesel hybrid technology. One of the main reasons is that most buses with this technology are recent models, in addition to less fuel consumption. Particle emissions are also reduced due to particle traps.
- Hybrid buses presented between 18% and 27% less fuel consumption, which together with ULSD fuel can be one of the best options in the market.
- CNG with OC buses proved to have lower PM_{10} and NO_x emissions than ULSD with DPF buses; however, their emission of NMHC, CO, and air toxins is greater. Despite this relative comparison,

	No. Buses	Median	Average	Standard Deviation	IQR
CNG	3	683.65	683.65	31.08	31.08
CNG + OC	18	14.50	20.68	20.32	25.51
D. Conv	6	45.00	41.34	27.42	45.51
ULSD	6	38.50	33.00	20.62	26.00
ULSD + DPF	11	4.18	5.35	4.72	6.39

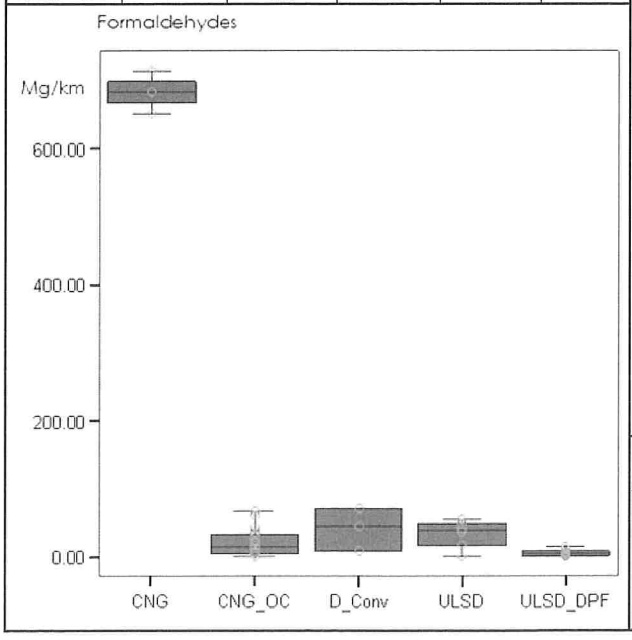

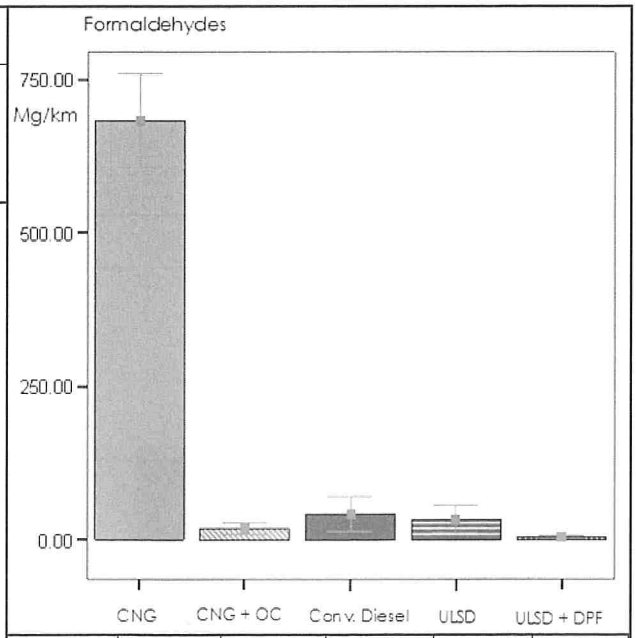

	Average	Standard Deviation	Confidence Interval	Low Range	High Range
CNG	683.65	31.08	649.24	34.42	1332.89
CNG + OC	17.95	17.23	7.16	10.79	25.12
D. Conv	41.34	27.42	27.76	13.58	69.10
ULSD	33.00	20.62	22.16	10.84	55.16
ULSD + DPF	4.38	3.65	2.28	2.10	6.67

FIGURE 7 Results for formaldehyde.

both technologies represent a significant advance compared to conventional diesel. It is observed that with the right control equipment both CNG and ULSD buses have very low emissions. A cost–benefit analysis is recommended to choose the best technological option for criteria pollutants.

- In relation to climate change and GHG emission, hybrid technology proved to have the lowest emissions because of lower fuel consumption associated with the fact that the engine works with both an electric and a diesel motor. CNG technologies, on average, have greater emissions than conventional and ULSD without DPF.
- The studies included in this investigation only measure exhaust emissions and do not include life-cycle analysis. To evaluate total environmental impact of a technological change correctly, it is necessary to expand the chain of emissions vertically, up to the source, via life-cycle analysis.

REFERENCES

1. Instituto Nacional de Estadística, Geografía e Informática (National Institute for Statistics, Geography and Computing). II Conteo de Población y Vivienda, 2005. Estados Unidos Mexicanos. Resultados Definitivos. (II Population and Housing Count, 2005, Mexico, Definitive Results). Mexico, 2006.
2. Zmirou, D., S. Gauvin, I. Pin, I. Momas, F. Sahraoui, J. Just, Y. Le Moullec, F. Brémont, S. Cassadou, P. Reungoat, M. Albertini, N. Lauvergne, M. Chiron, and A. Labbé. Traffic Related Air Pollution and Incidence of Childhood Asthma: Results of the Vesta Case-Control Study. *Journal of Epidemiology and Community Health,* Vol. 58, 2004, pp. 18–23.
3. Anderson, H. R., C. Spix, S. Medina, J. P. Schouten, J. Castellsague, G. Rossi, D. Zmirou, G. Touloumi, B. Wojtyniak, A. Ponka, L. Bacharova, J. Schwartz, and K. Katsouyanni. Air Pollution and Daily Admissions for Chronic Obstructive Pulmonary Disease in 6 European Cities: Results from the APHEA Project. *European Respiratory Journal,* Vol. 10, 1997, pp. 1064–1071.
4. Wöhrnschimmel, H., et al. *Evaluación de la Exposición Personal a Contaminantes Atmosféricos en Pasajeros de Vehículos de Transporte Público.* Centro de Transporte Sustentable, Instituto Nacional de Ecología, Mexico City, 2004.
5. *La Calidad del Aire en la Zona Metropolitana del Valle de México: Informe del Estado y Tendencias de la Contaminación Atmosférica* (Air Quality in Mexico Valley Metropolitan Area: Report on the State and Tendencies of Air Pollution). Secretaria del Medio Ambiente del GDF (Ministry of the Environment for the Federal District), Mexico City, 2007.
6. Pope III, C. A., R. T. Burnett, G. D. Thurston, M. J. Thun, E. E. Calle, D. Krewski, and J. J. Godleski. Cardiovascular Mortality and Long-Term Exposure to Particulate Air Pollution: Epidemiological Evidence of General Pathophysiological Pathways of Disease. *Circulation,* Vol. 109, 2004, pp. 71–77.
7. Boffetta, P., N. Jourenkova, and P. Gustavsson. *Cancer Risk from Occupational and Environmental Exposure to Polycyclic Aromatic Hydrocarbons,* Vol. 8, No. 3. Springer, Netherlands, 1997.
8. U.S. Department of Health and Human Services. *Registry of Toxic Effects of Chemical Substances* (RTECS, online database). National Toxicology Information Program, National Library of Medicine, Bethesda, Md., 1993.
9. U.S. Environmental Protection Agency. *Health Assessment Document for Acetaldehyde.* EPA/600/8-86-015A. Environmental Criteria and Assessment Office, Office of Health and Environmental Assessment, Office of Research and Development, Research Triangle Park, N.C., 1987.

The Transportation and Air Quality Committee peer-reviewed this paper.

Analysis of Real-World Lead Vehicle Operation for Modal Emissions and Traffic Simulation Models

Eric Jackson and Lisa Aultman-Hall

New models and data are needed in microscopic traffic simulation tools to allow effective use with newer modal tailpipe emissions models. Traffic simulation models offer the ability to simulate large, second-by-second vehicle operation data sets as input for emissions models. However, more data are needed to improve simulation of second-by-second vehicle speed. This research analyzes and models the vehicle dynamics of unconstrained drivers in real-world driving situations based on road geometry. Vehicle dynamics data were collected by using an instrumented vehicle driven by 22 volunteers over a 17-mi predetermined test route. The objective of this research was to analyze and model the nonrandom speed variations in unconstrained lead drivers. The results of this study suggest that horizontal and vertical curvatures have a significant impact on the second-by-second operation of an unconstrained lead vehicle. Furthermore, these nonrandom changes in speed are important considerations since they can produce considerable variations in the level of tailpipe emissions.

Estimating vehicle emissions based on second-by-second vehicle operation creates a significant motivation to link microscopic traffic simulation models to more accurate operating mode–based regional mobile emissions models. Because the collection of a large, representative, second-by-second vehicle operation data set for every traffic circumstance is not realistic, the use of microscopic traffic simulation models to replicate the real-world second-by-second driver behavior for hundreds of vehicles and traveling patterns is ideal. The simulated vehicle driving cycle data could be integrated into a mobile emissions model, such as the new version of the U.S. Environmental Protection Agency's (EPA) MOVES, to allow for improvements in emissions modeling of project-level transportation alternatives or traffic conditions. Unfortunately, few real-world vehicle driving cycle data sets exist, especially for lead vehicles (following vehicles have long been modeled with the use of car-following theories that predate widespread use of computer traffic simulations). Moreover, detailed models to incorporate second-by-second vehicle operating mode data into traffic simulation models are limited. This paper investigates the second-by-second variation of lead vehicle dynamics in a real-world, on-road data set as a function of road geometry.

E. Jackson, Connecticut Transportation Institute, University of Connecticut, 270 Middle Turnpike, Unit 5202, Storrs, CT 06269. L. Aultman-Hall, Transportation Research Center, School of Engineering, University of Vermont, Farrell Hall, 210 Colchester Avenue, Burlington, VT 05405. Corresponding author: E. Jackson, e.jackson@engr.uconn.edu.

Transportation Research Record: Journal of the Transportation Research Board, No. 2158, Transportation Research Board of the National Academies, Washington, D.C., 2010, pp. 44–53.
DOI: 10.3141/2158-06

RESEARCH MOTIVATION

Two factors motivate this research: the feasibility of collecting on-road, second-by-second vehicle operations data with readily available technology and the desire to integrate microscopic computer traffic simulation models for use with modal tailpipe emissions models. Microscopic simulation models typically use car-following theory to capture the temporal changes in an individual vehicle's velocity and thus its location in response to the vehicle it is following, the lead vehicle (*1*). Brackstone and McDonald identified five groups of car-following models: Gazis–Herman–Rothery, collision-avoidance, linear, psychophysical, and fuzzy logic. While these models are used to describe the behavior of the following car, few research efforts have studied and modeled the behavior of the lead vehicle. Default lead vehicle behavior is modeled as a constant speed until it approaches another vehicle. This assigned "desired" speed typically varies between individual simulated vehicles (on a normal distribution) and is often a function of the speed limit or free-flow speed of a given link.

Some models, such as PARAMICS, have optional subroutines that alter this vehicle speed, including lead vehicle speed, as a function of roadway characteristics (such as horizontal curvature when it is coded into the network), but these advanced options are rarely used, presumably not only because few network databases have curvature and grade coded, but also because there is a lack of real-world vehicle operating data to calibrate these functions. Recent work (*2, 3*) has indicated that assumptions regarding car-following rules make differences to emissions estimates and also to the overall aggregate traffic conditions predicted by microscopic traffic simulation models. Researchers have alluded to the need to collect lead vehicle data (*2*), but, to date, only a few studies have done so (*4, 5*).

BACKGROUND

Second-by-Second Vehicle Speed Variation

Previous studies have investigated the impacts of curvature on vehicle dynamics. The majority of research efforts that focused on the impacts of roadway geometry on driver behavior and speed used observational techniques to collect data for analysis. Most of these studies used radar, LIDAR, or pneumatic tubes to record vehicle speeds at finite locations (*6, 7*). One limitation with these approaches is that driver behavior may be significantly affected by the driver's perception of law enforcement or the presence of observers. Another limitation is the finite locations of speed data collection and a continuous time series of second-by-second speeds cannot be obtained.

Past curvature studies have been limited because second-by-second speed and acceleration profiles were not easily attainable.

Existing studies have suggested that roadway geometry has a significant impact on the speed profiles of vehicles (*4–7*). Figueroa and Tarko used regression models to determine that there are "transition" sections approaching and exiting horizontal curves where speed changes are suspected to take place. They concluded that 66% of the deceleration events and 72% of the acceleration events in their data set occurred on the tangent sections approaching and exiting horizontal curves (*6*).

However, Figueroa and Tarko did not consider vertical curvature in their analysis. Research conducted by Gibreel et al. is one of the few studies to consider the three-dimensional highway alignments in predicting operating speeds. Their research suggests that by including vertical curvature into regression equations there is a 33% increase in model accuracy, implying that future operating speed models should include three-dimensional alignments (*7*). However, the study conducted was limited in the number of curves studied. Only two types of alignment combinations were studied: sag vertical curve combined with circular horizontal curve and crest vertical curve combined with circular horizontal curve. They concluded that future research is necessary to establish a more robust three-dimensional model for operating speed prediction.

This paper extends previous work on curvature impacts on vehicle operation in two ways: (*a*) by investigating a range of curves and (*b*) by using an instrumented vehicle to collect a second-by-second real-world velocity profile. Instrumented vehicles are now in more widespread use to capture vehicle operations to study the impacts of horizontal curvature on driver speed behavior (*5*). The study by Nie and Hassan contributes several key findings relevant to this paper: (*a*) the effects of road geometry on driver speed vary with road type (i.e., two-lane rural highway vs. local connector roads); (*b*) driver speed selection is highly correlated with the geometric features; (*c*) drivers were more cautious on continuous curves than on isolated curves with long approach and departure tangents; (*d*) drivers do not maintain a constant speed; and (*e*) acceleration and deceleration events take place on curved sections.

Traffic Simulation Models

Previous traffic simulation research has focused on more aggregate calibration and the comparison of different computer models, all having some degree of success. These studies have been conducted with many different simulation programs but recently include the following most often: VISSIM, CORSIM, PARAMICS, and AIMSUM (*8–19*). Traffic simulation models offer the potential to generate large amounts of second-by-second data from individual vehicles while keeping the costs of data collection low. Because it is impractical to collect real-world tailpipe data for hundreds of drivers on a full range of facility conditions, traffic simulation model validation and calibration are critical to ensure that the simulation model accurately represents the real-world system. The validation and calibration of these models are not trivial tasks, because the nonstationary and auto-correlated nature of traffic flow complicates the process (*20–22*).

For tailpipe emissions modeling, the microscopic traffic simulation models offer great potential because simulated 1-s vehicle operation data could be used as input for operating mode–based emissions models. However, in order to be useful for future mode-based emissions models, traffic simulation models will need to produce results that are much more detailed than average speed. For example, the EPA's MOVES model is incorporating vehicle-specific power (VSP) into the model to predict emissions estimates. However, MOVES and current traffic simulation models do not incorporate true road grade. Therefore, an accurate calculation of VSP for a realistic range of real-world conditions is impossible given the current modeling structure. Furthermore, the vehicle dynamics generated by these simulation packages need to be evaluated to ensure that the second-by-second model output is realistic.

This research proposes using second-by-second real-world data, collected from multiple drivers, to study unconstrained lead vehicle operation. This research is important because it contributes to improving the interface between traffic simulation models and the next generation of modal emissions models: measuring real-world 1-s vehicle dynamics and comparing them to corresponding simulated conditions.

DATA COLLECTION

The overall objective of this data collection effort was to obtain onboard, on-road, real-world vehicle operations as well as tailpipe emissions data on a 17-mi predefined test route in northeast Connecticut. The data used in this analysis were collected between October 11 and October 27, 2006, with an instrumented light-duty minivan driven by 22 different volunteer drivers. The drivers who participated in the study were recruited from the University of Connecticut community via e-mail and personal communication. All drivers were asked to drive the route at least twice in a row. These drivers included undergraduates, graduate students, and faculty members with between 1 and 40 years of driving experience.

Test Route

The route chosen for this research was selected to contain multiple road types (freeways, rural two-lane highways, and local stop-controlled roads) and varying degrees of both vertical and horizontal curvature. The Connecticut Department of Transportation (ConnDOT) collected and provided the route geometric data using an ARAN photologging van. The ARAN van is equipped with a set of gyroscopes to collect detailed road geometry such as curvature and grade. Grade and curvature data were collected continuously and recorded every 10 m along the entire length of the test route. According to the manufacturer, the ARAN system is capable of providing grade and curvature data at "rod and level" accuracy and meets the FHWA regulations for curve classification (*23*).

Vehicle Instrumentation

The 1999 Toyota Sienna minivan was instrumented to collect spatial location, vehicle and engine operating parameters, and tailpipe emissions data simultaneously. Spatial location data were collected using Global Positioning System (GPS) receivers. The Garmin 16 HVS antenna (*24*) was used to synchronize all instruments to GPS time. The Garmin GPS unit has a published positional accuracy rate of less than 49 ft, velocity accuracy at steady-state speed of 0.12 mph, and a reacquisition time of less than 2 s.

An AutoEnginuity ST01 ScanTool collected vehicle velocity, engine load, and engine revolutions per minute from the vehicle's

onboard computer. Vehicle acceleration data were collected using a Crossbow CXLO2LF3 accelerometer mounted on the roof. This accelerometer is a three-axis accelerometer with a measurable range of –2 *g* to +2 *g* and a 50-Hz response rate. The accelerometer selected for this research has a low noise density and a reported accuracy of ±0.01 V (0.2 mph/s). The GPS receiver and ScanTool were powered by the vehicle, while the accelerometer was powered through the data collection port of the desktop computer. Real-world onboard gas and particulate tailpipe emissions data were also collected simultaneously but are not used in this analysis. The van was also equipped with a forward-facing video camera to record driving conditions experienced by the driver.

Data Preparation

Data from each of the instruments were merged into one master database. The GPS data from the ARAN van, and the GPS data from the instrumented minivan allowed the grade and vehicle operations data sets to be joined based on spatial location in ArcGIS. Therefore, every record in the vehicle operations data set was assigned a grade (in percent) and horizontal curvature (radius in meters) based on the ARAN data point that was closest to it in proximity.

Other research studies have identified surrogate variables that can be calculated to describe how a vehicle is operating. One such variable is VSP. VSP is a measure of engine power demand that is calculated from the measured velocity, acceleration, and road grade (*25*). The joining of road grade to the emissions data set allows the calculation of VSP when investigating causal factors in vehicle emissions. VSP is highly correlated to increased concentrations of gas-phase vehicle emissions (*25–28*). VSP for each second of data was calculated using Equation 1 (*25*):

$$\text{VSP} = 1.1(v * a) + 9.81(\text{grade} * v) + 0.213(v) + 0.000305(v^3) \quad (1)$$

where

v = velocity (m/s),
a = acceleration (m/s^2), and
grade = rise/run [i.e., arctan (slope in degrees)].

However, the calculation of a variable from three different sources propagates errors. Specifically, when calculating VSP, potential sources of measurement error [velocity (at ±1 mph), acceleration (at ±0.2 mph/s), and grade (no reported error)] are multiplied, added, and cubed. While the propagation of error has been limited by instrumentation selection, it cannot be eliminated.

To analyze the true unconstrained or free-flow driving of an individual, constrained versus unconstrained driving was noted in the data. The data from the forward-facing video camera were used to determine if the test vehicle was constrained by a vehicle, traffic control device, or obstacle. The times (HH:MM:SS) at which the driver became constrained (Tc_s) and the second the driver became unconstrained (Tc_e) were recorded. The time displayed on the camera was adjusted to match the time recorded by the GPS to ensure the camera was synchronized with the other instruments. For this paper, data where the vehicle was considered unconstrained were extracted and used in the analysis of the real-world lead vehicle operations. A driver was classified as constrained at time Tc_s to time Tc_e if one of the four following criteria was met:

1. If the driver was following another vehicle with less than 5-s headway or if a vehicle ahead of the instrumented vehicle applied their brakes. Actual headways were not recorded using instruments, but estimated using landmarks along the roadway to determine the time interval between the lead vehicle and the test vehicle.
2. If an intersection with a red or amber signal was visible at any point during the approach to an intersection. The vehicle was classified as constrained at the instant a red or amber traffic signal was visible in the frame of the camera.
3. If there were roadside obstructions that were not part of the typical road geometry. For instance, if there were construction signs warning of roadwork ahead, the data would be considered constrained.
4. If there were any abnormal conditions encountered by a driver that had a noticeable impact on the operation of the test vehicle. For example, if an instrumented van was approaching the intersection with a driveway and it was obvious that the test vehicle reacted to the possibility that someone would pull out in front of it, then the vehicle would be classified as constrained.

While the ARAN van provides point-based curvature, other curvature characteristics were hypothesized to impact driver behavior. With the calculated radius from the ARAN data, more descriptive statistics were generated to describe each curve along the test route. The first calculated variable was length of curve (LC). Knowing where the tangent sections start and end allowed the identification of the starting and ending station of each curve; then by simple subtraction the LC was calculated.

With the LC known, the deflection angle (DA) for each curve could be calculated using the given radius (R), substituting into Equation 2 (*29*), and making unit conversions. The curve deflection angle represents the degree at which the tangent section of the roadway deviates into the turn. The deflection angle is important because the larger the deflection angle, the more severe the turn and presumably the more significant a curve's impact on unconstrained velocity.

$$\text{DA} = \left\{ \left[\frac{R}{\text{LC}} \right] * 57.3 \right\} \div 2 \quad (2)$$

The lengths of tangent sections approaching and departing a curve are also hypothesized to have an impact on the variation in unconstrained velocity. The tangent sections of the horizontal alignment provide motorists with a clear view of the road ahead (given small grades) and the ability to travel at higher speeds between curves. It is hypothesized that longer tangent sections allow drivers to accelerate to a "comfortable" cruising speed before needing to decelerate to a perceived safe speed to negotiate an upcoming curve. Therefore, the length of the tangent approaching (LT_A) and the length of the tangent departing (LT_D) a curve were added to the data set by simply subtracting the stations of the beginning of tangent from the end of tangent. Finally, the data were reduced further into two subsets based on their location on subsections of the test route. The first criteria were defined based on a uniform posted speed limit along the entire section of the section. The second main criteria were that major intersections were not included that may alter the behavior of a driver. With these criteria in mind, two portions of the test route were selected for further analysis. The "curves section" (Figure 1) of the test route contains multiple horizontal curves of varying radii and limited grades. Radii ranged from 153 m up to 2,000 m, while grades in this section were limited to –5% to 5%. Analysis of this section of the test route (State Route 32) focuses on the effects of horizontal curvature on unconstrained second-by-second velocities since grades are relatively small. According

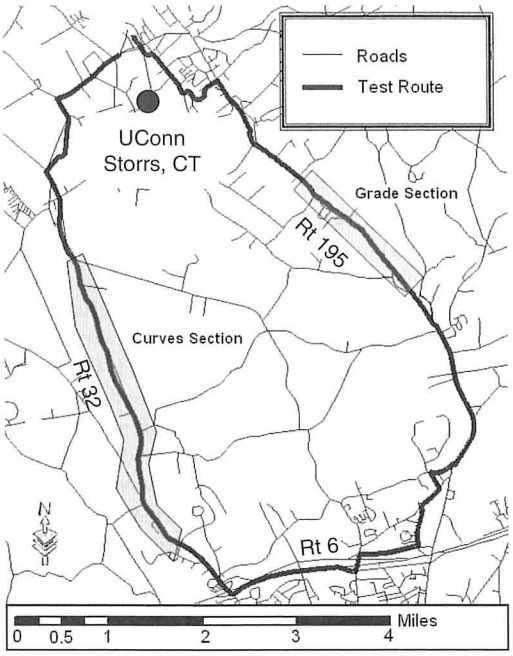

FIGURE 1 Test route subsections.

to AASHTO (*29*), "It is generally accepted that nearly all passenger cars can readily negotiate grades as steep as 4 to 5 percent without an appreciable loss in speed below that normally maintained on level roads."

AASHTO goes on to say that once grades go above +3% (upgrades), there begins to be a slight impact on speeds and the impact progresses with an increase in grade. Because there are grade impacts on speed, the "grade section" (Figure 1) of the test route (Route 195) was selected as a second study section due to the large degree of vertical curvature (grades range from –8% to 11%) and limited variation in horizontal alignment (only two horizontal curves in this section, both with radii greater than 1,000 m). This section of the test route will focus on investigating the effects of grade on unconstrained vehicle velocity. Figure 1 identifies these sections along the test route.

DATA ANALYSIS

Analysis of the video data indicated that 45.4% of the data were classified as constrained while 54.5% of the data were classified as unconstrained (or a lead vehicle). With more than half of the data classified as unconstrained, these data suggest that second-by-second lead vehicle operation accounts for a significant portion of the overall travel on this rural test section. However, it should be noted that data were collected from 9 a.m. to 2 p.m. on multiple days, thus missing the morning and afternoon peak travel periods. This may have biased the percent time unconstrained because of the lower number of vehicles on the road during off-peak travel times. Therefore, the percent time unconstrained cannot be applied to all time periods without further study.

Curve Section Analysis

To ensure that the variation seen in vehicle velocity is not specific to one vehicle, time series plots were overlaid for the curves section (Figure 2). The *x*-axis is the distance along the test route (chainage in miles) and *y*-axis is the individual vehicle's velocity along the subsection of the test route. The drivers plotted in Figure 2 were unconstrained for the entire length of the curve subsection. The majority of drivers increase their velocity from chainage (in miles) 3.4 to 3.6 mi and then there is a gradual decrease from 3.6 to 3.9 mi.

To test statistically if the test runs had similar patterns in velocity profiles, a correlation analysis was conducted between drivers. The mean speed was approximately 45 mph, with a standard deviation of 2.4 mph. The speed limit on this section of road is 40 mph, and 24 of the 25 series have a mean speed above 40 mph.

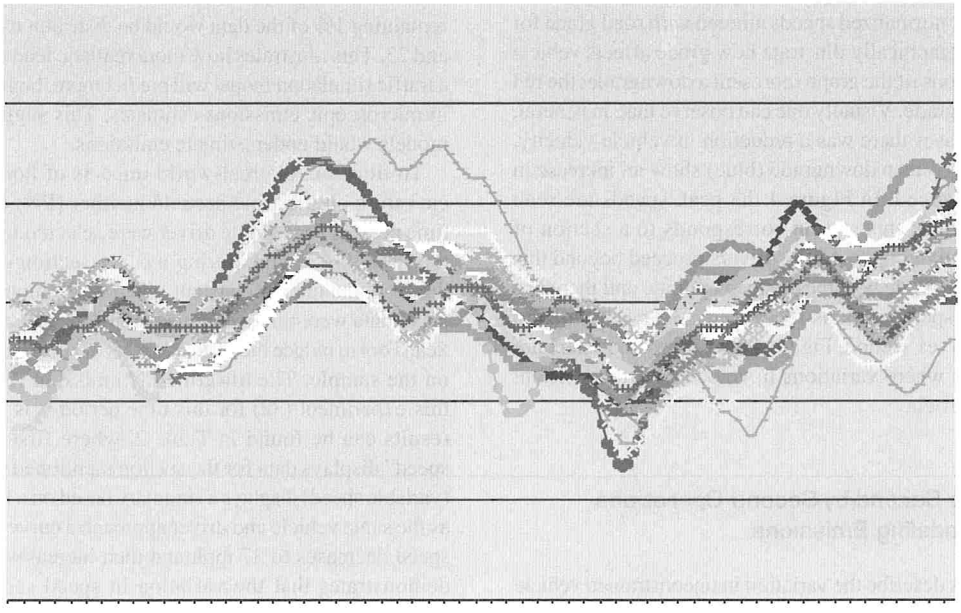

FIGURE 2 Time series plots for multiple test runs.

Speed Normalization to Account for Driving Style

To account for the differences in mean driving speed between the individual test runs, the second-by-second speed data for each series was divided by the mean speed for that individual series. The data were normalized to aid in reducing the impacts of an individual's driving style on the data. This produces a ratio of actual speed over the mean and preserves the temporal and spatial patterns in the speed data. To aid in analysis and to produce a vertical axis that is easy to interpret, the speed ratio was multiplied by the mean speed of the all drivers on that section of the test route (44.7 mph).

The correlation analysis was then repeated for the normalized data. This analysis resulted in a mean overall Pearson correlation coefficient of 0.78 to 0.89. Overall, this analysis suggests that the patterns in vehicle velocity with respect to location are present and consistent between test runs and drivers. This variation in the second-by-second velocities is not random and should be accounted for in traffic simulation models.

Curve Section Analysis

Using the subset of 25 unconstrained test runs, box plots (Figure 3) were generated for raw speeds and normalized speeds for every 10th of a mile in the curve section. The box plots allowed for a graphical analysis to determine if sections of the test route had speeds that were statistically different from other sections on the test route. From these plots there are sections on the test route that are significantly different from the others (i.e., boxes at locations do not overlap with other sections). Specifically, speeds at chainage 3.55 and 3.93 mi are statistically different from each other even though the speed limit stays the same.

Grade Section Analysis

A similar analysis was conducted for the grade section. A subset of runs were used in this analysis because only 11 of the test runs had continuous unconstrained driving on the grade section. Figure 4 shows the box plot of normalized speeds aligned with road grade for the grade section to graphically illustrate how grade affects vehicle speed. The blue sections of the graph represent a downgrade; the red areas represent an upgrade. Visually one can observe that, in general, as uphill grade increases there was a reduction in vehicle velocity, while segments with a steep downgrade (blue) show an increase in normalized vehicle speed. In Figure 4 the peak speeds are seen at chainage 13.0 (mile); this station corresponds to a section of the route with a negative grade. As the drivers proceed beyond this point on the route, the grade becomes a steep upgrade and there is a resulting decrease in speed (stations 13.15 mi to 13.3 mi). Similar to the results for the curves section, Figure 4 also shows that there are sections of the route where variations in velocity were consistent with location on the route.

Impact of Vehicle Second-by-Second Operations on Accurately Modeling Emissions

The previous sections describe the variation in unconstrained vehicle velocity and identify the second-by-second variations. This section evaluates the impact of incorporating accurate variations in lead vehicle operations for traffic simulation-based emissions analysis. Research into the correlation of vehicle emission rates and the operating mode of a vehicle has prompted several researchers to develop a system of binning operational data based on the velocity and acceleration of the vehicle at a given time, often 1 s. Most simply, the classes of operating modes have been divided into four "bins": idle, acceleration, cruise, and deceleration. Models or estimates of vehicle emissions are "looked up" or grouped by operating bin. The definitions for each bin as outlined by Frey et al. (*30*) were applied to each second of valid data in this analysis to see if vehicles on horizontal and vertical curves would be coded in different bins, thus resulting in different emissions estimates in an emissions model. However, the four-bin system is now rarely used. The more sophisticated vehicle operating binning system currently used in the new EPA MOVES model was also applied (*31*). This new binning method (using VSP and speed) has increased the need for more accurate second-by-second vehicle operation data (i.e., VSP).

The binning analysis of unconstrained driving suggested that when using the traditional four-bin system, the variation in real-world lead vehicle 1-s speeds on the horizontal and vertical curve sections in this study is not large enough to produce significant differences in the percent time spent in each operating mode. In this case, the lead vehicles would be classified as cruising 95% of the time, whereas the traffic simulation data would predict 100% of time was cruise. This suggests that for unconstrained driving on rural arterial segments, away from intersections, the speed profiles generated by traffic simulation may be adequate for modal binning if using the traditional four-bin system.

Table 1 outlines the VSP, speed-based binning definitions used in MOVES2009 that were applied to the data collected for this research (*31*). When data with a constant velocity in unconstrained conditions (representative of lead vehicle velocity generated by typical traffic simulation models) are binned using the EPA definitions in Table 1, 100% of the data would be assigned to bin number 22. However, when applying the EPA's VSP speed binning system to the on-road, onboard data along sections A and B for time periods where vehicles were classified as lead vehicles, data would be assigned to seven different bins: 42% of the data were assigned to bin 22, 40% were assigned bin 0, and 17% were assigned to bin 33. The remaining 1% of the data would be distributed over bins 11, 12, 21, and 23. This illustrates how more realistic lead vehicle operations in a traffic simulation model will predict more, higher emitting VSP bins in microscopic emissions estimates. This suggests that the current models would underestimate emissions.

To illustrate the real-world impacts of horizontal and vertical curvature on ultrafine particle number (PN) emissions, two 30-s time periods for a single driver were selected from this data set. For the first 30-s period, during a curve section of the test route, the driver maintained a constant speed of 43 mph (±1 mph). The first 5 s of data were removed after a constant speed was reported by the ScanTool to reduce the history effects of acceleration and deceleration on the sample. The ultrafine PN emission rate measured during this experiment (*32*) for this time period was summarized and the results can be found in Table 2, where first data row "constant speed" displays data for the section mentioned above. The next row (variable speed) displays a summary based on a following 30 s of data as the same vehicle and driver approach a curve. For this section, the speed decreases to 37 mph and then increases to 47 mph. Table 2 demonstrates that the variation in speed seen in unconstrained driving can have an impact on the range and scale of ultrafine particles emitted. The constant speed section has a mean that is a factor

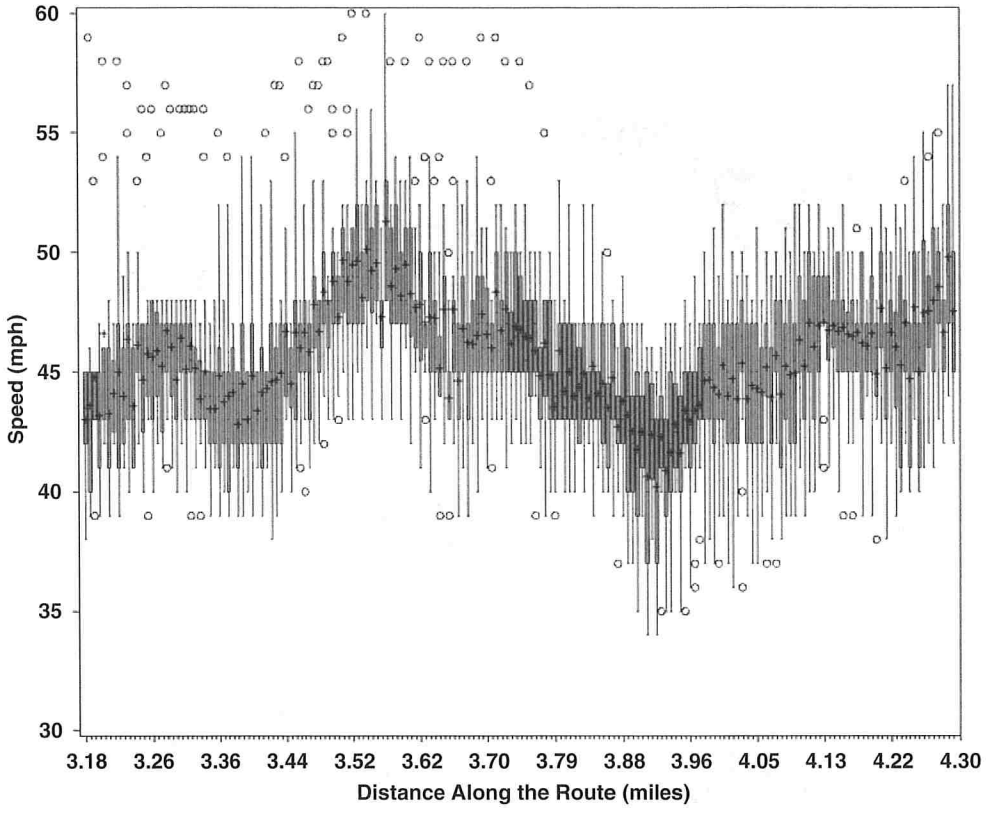

(a)

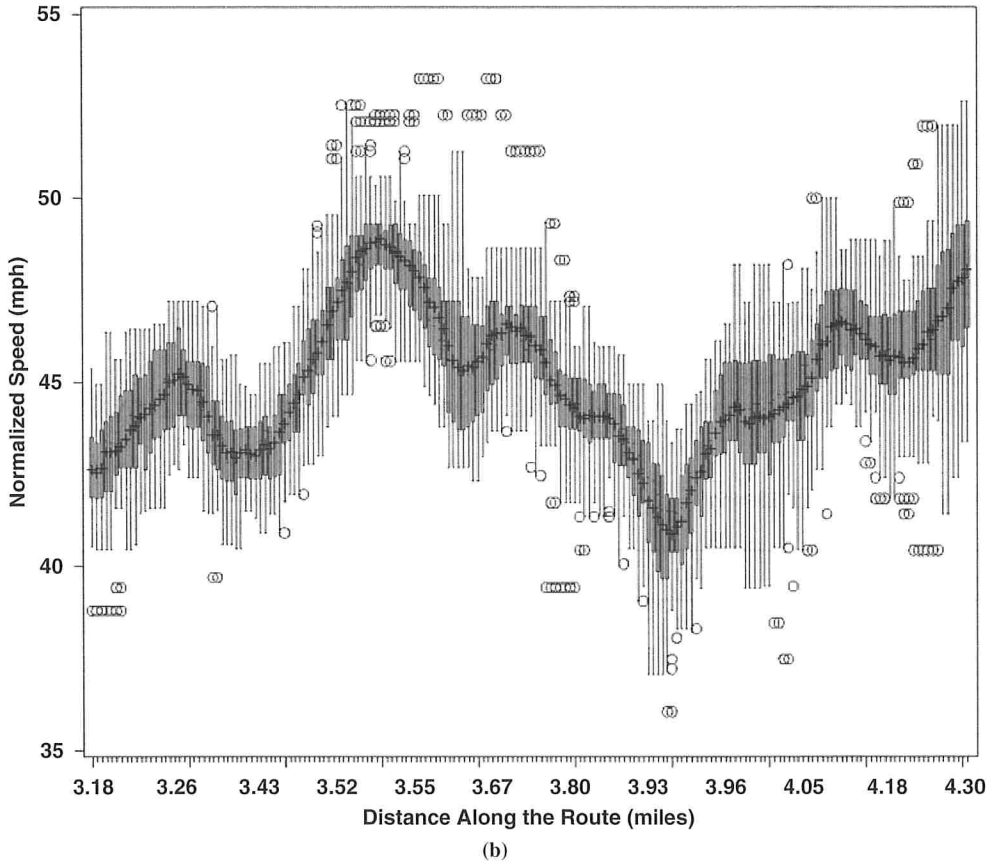

(b)

FIGURE 3 Curve section: (*a*) raw and (*b*) normalized speed box plot.

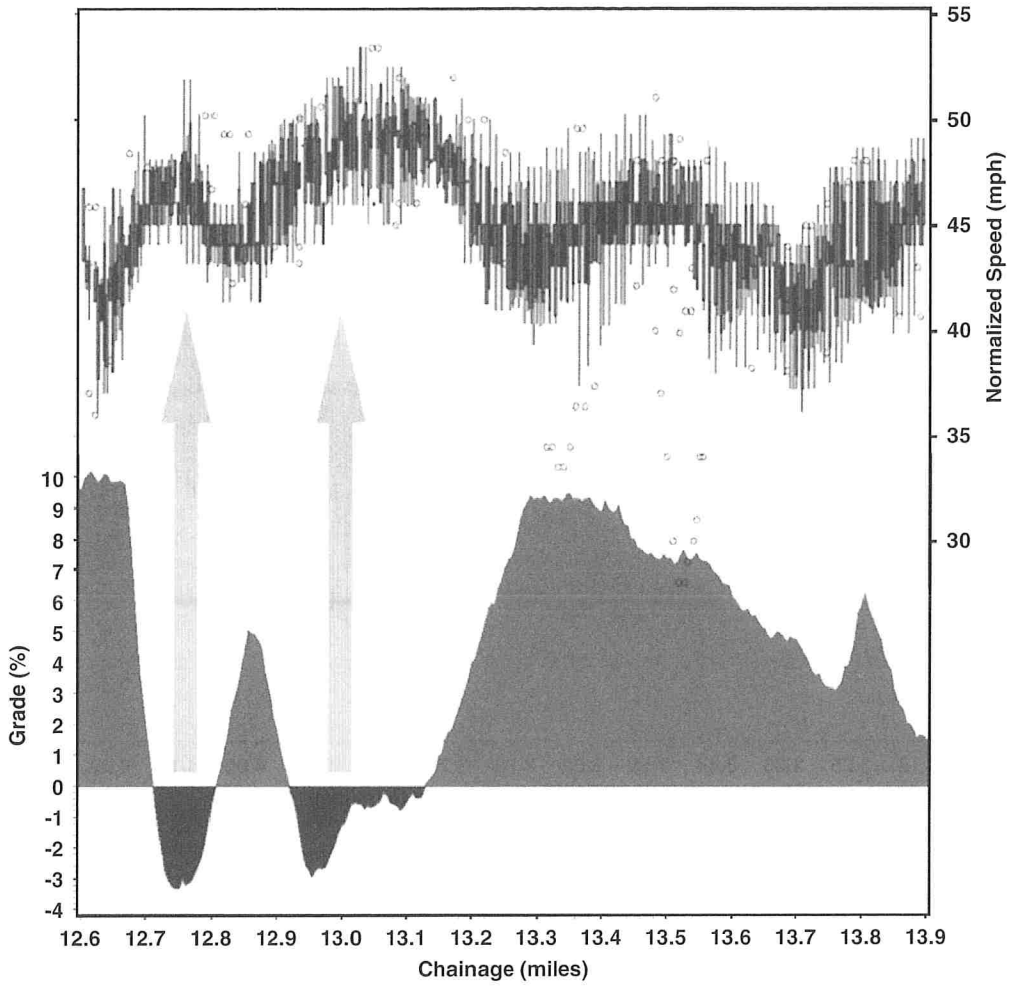

FIGURE 4 Grade section: normalized speeds box plot.

of 10 smaller than the variable speed section and a much smaller standard deviation than the variable speed section.

Table 2 suggests that if a lead vehicle is assigned a constant speed in a traffic simulation model, the emissions impact from that inaccurate assumption could result in an underestimation of the true emissions rate. Furthermore, based on car-following theories and equations used in traffic simulation, slight variations in lead vehicle behavior will influence operation of vehicles following the lead vehicle. Overall this suggests that variations in second-by-second lead vehicle operation will increase second-by-second PN emissions for the lead vehicles as well as all other vehicles in the traffic simulation.

TABLE 1 EPA MOVES2009 Activity Binning Definitions (*31*)

VSP/Instantaneous Speed	0–25 mph	15–50	>50
<0 kW/tonne	Bin 11	Bin 21	—
0–3	Bin 12	Bin 22	—
3–6	Bin 13	Bin 23	—
6–9	Bin 14	Bin 24	—
9–12	Bin 15	Bin 25	—
≥12	Bin 16	Bin 26	Bin 36
6–12	—	—	Bin 35
<6	—	—	Bin 33

NOTE: braking = bin 0; idle = bin 1.

MODELING LEAD VEHICLE DYNAMICS

Preliminary models were developed to describe the variation in second-by-second velocity of a vehicle for the curve section and for the grade section independently. Ordinary linear regression analysis assumes that the error variance is the same for all observations. For

TABLE 2 Comparison of Real-World PN Emissions by Speed Variation

	Mean (#/s)	Max. (#/s)	Min. (#/s)	Standard Deviation (#/s)
Constant speed	7,900,000	19,000,000	2,000,000	5,200,000
Variable speed	75,000,000	350,000,000	960,000	110,000,000

NOTE: # = number of particles.

this data set, the error variance is not constant (heteroscedastic) and the ordinary least-squares estimates are inefficient. An autoregressive error model was necessary to address these issues of autocorrelation in the time series data set. The form of this model is represented in Equations 3 and 4.

$$\Delta V_t = \alpha + \beta_1 x_1 + \beta_2 x_2 + \cdots + \beta_k x_k + \mu_t \quad (3)$$

$$\mu_t = \phi_1 \mu_{t-1} + \phi_2 \mu_{t-2} + \epsilon_t \quad (4)$$

where

ΔV_t = second-by-second deviation from the mean speed (V_t);
α = constant (set to zero);
β_k = parameter estimate;
$x_{1,k}$ = inverse radius, length of curve, distance from curve, distance to curve;
μ = error estimate;
ϕ = parameter estimates for the first- and second-order error estimates; and
ϵ = normally distributed error term with mean of zero and standard deviation of σ^2 IN(0,σ^2).

An autoregressive model was developed by using speed deviation as the dependent variable. The autoregressive model was further enhanced by specifying a second-order (NLAG = 2) autoregressive error term. Because the dependent variable had a mean of zero, the model was fit without an intercept (i.e., intercept = 0). Multiple iterations of the modeling procedure were performed to remove parameters that were not statistically significant to the model ($\alpha = .05$). A correlation analysis determined that none of the predictors used in model development were highly correlated. The maximum correlation coefficient of .61 was found between LC and change in curvature (DA).

Modeling Results: Grade Section

Recall that the grade section of the route has few horizontal curves but significant grades (up to 12%). The objective of this first model was to investigate the impacts of grade on speed. The generated model has a total R^2 of 0.90 and a root-mean-square error of 0.834 mph. Since there were only two horizontal curves on this section, none of the parameters relating to horizontal geometry were found to be significant to the prediction of second-by-second speeds. Grade was determined to be the only independent variable for this section of the test route that was statistically significant. Equations 5 and 6 represent the final model, which indicates that with every 1% increase in grade there will be a 0.33-mph decrease in vehicle velocity. For example, on a 5% upgrade, one could expect a 1.6-mph decrease in mean speed. Conversely, on a 6% downgrade, one could expect an increase in speed of 1.9 mph above the mean travel speed. This analysis indicates that grade can affect the second-by-second speed of a vehicle.

$$\Delta V_t = -0.33(\text{grade}) + \mu_t \quad (5)$$

$$\mu_t = -0.97\mu_{t-1} + 0.046\mu_{t-2} + \epsilon_t \quad (6)$$

Modeling Results: Curve Section

A second-order autoregressive error model with an intercept set to zero was developed for the curve section data by using the same modeling techniques. The resulting model had a total R^2 of 0.86. Table 3 contains the statistically significant predictors and their estimated coefficients. Figure 5 contains a time series plot of single unconstrained driver's data with the actual and predicted speeds plotted.

TABLE 3 Full Model Independent Variables for Curve Section

Variable (in km)	DF	Estimate	Standard Error	t-Value	Approx. Pr > |t|
Inverse radius	1	–0.700	0.015	–4.70	<.0001
Length of curve	1	2.815	0.522	5.39	<.0001
Distance from curve	1	0.322	0.033	9.84	<.0001
Distance to curve	1	0.833	0.221	3.77	.0002

For the curve section of the test route, grade was determined not to be significant when considering the second-by-second speed deviation. Unlike on the grade section of the test route, the grades on the curve section are mild (range from –5% to 4%). This could account for grade not being significant in the curve section model. This conclusion fits with the observations made by AASHTO (*29*) that grades up to 4% or 5% do not cause an "appreciable" loss in speed. The curve section model also indicates that the metrics of a curve and distance from the curve can be used to model the mean change in velocity.

SUMMARY AND CONCLUSIONS

The objective of this research was to quantify and model the second-by-second variation of lead vehicle operations in a real-world, on-road data set as a function of horizontal and vertical curvature. The initial analysis of vehicle operation on the route demonstrated that there are significant variations in speed along the test route and these variations are systematic with location along the route. Because following vehicles are reacting to the second-by-second operation of the lead vehicle, it is important that simulated lead vehicle dynamics are accurate. Therefore, there is a need to develop a method to describe this variation so future simulation models would be able to incorporate realistic lead vehicle behavior.

Analysis of the grade section shows that grade has a significant impact on vehicle operation. Steep grades can affect lead vehicle behavior and should be incorporated into current traffic simulation models to aid in the modeling real-world vehicle velocity. However, grades of less than 5% do not appear to have a significant impact on speeds. The findings suggest that, for grade sections, for every 1% change in grade there will be a 0.33-mph change in vehicle velocity. For example, a grade of +7% would result in a reduction in mean travel speed of 2.3 mph. The curve analysis indicates that the degree of curvature and distance to and from a curve have a significant impact on mean vehicle speed.

The focus on velocity was to demonstrate that there are non-random variations in vehicle speeds that can be associated with road geometry. This paper has demonstrated that horizontal and vertical curvatures contribute to dynamic operation for lead vehicles. The second-by-second operations of these lead vehicles in turn have a significant impact on the second-by-second patterns of the following vehicles based on accepted car-following theories. Therefore, if vehicle dynamics data from traffic simulation output are going to be used for mobile source emissions modeling, it is critical that lead vehicle operations be modeled accurately.

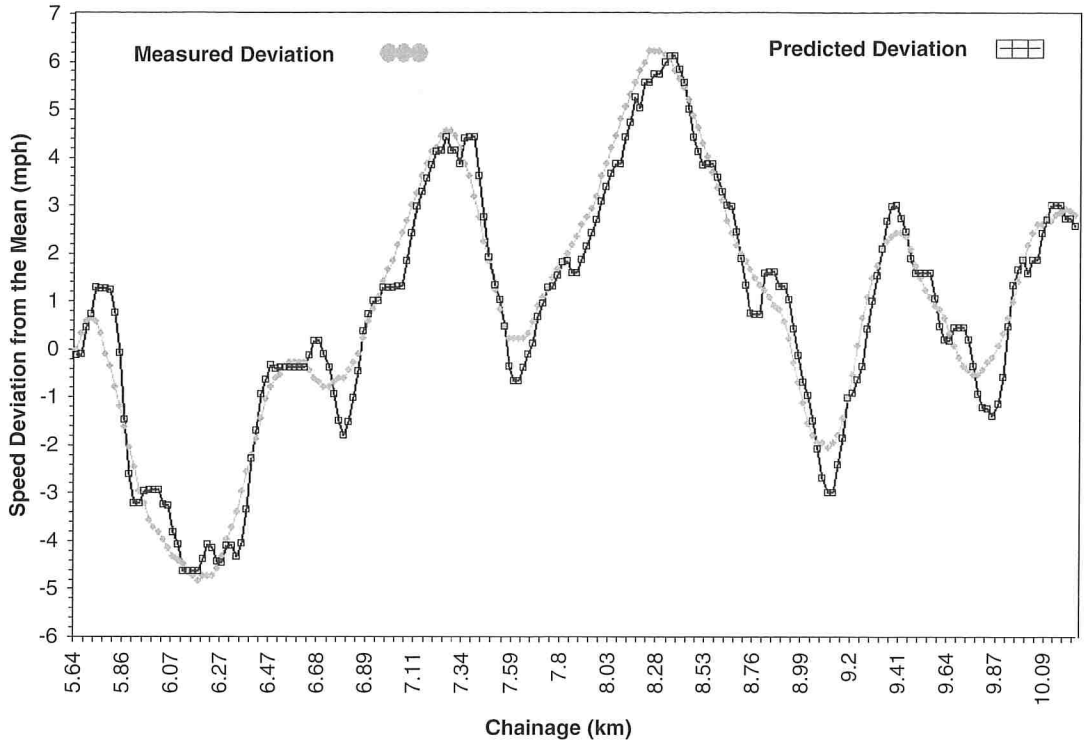

FIGURE 5 Actual and predicted speeds for a single run.

The current trend in mobile emissions modeling suggests that future models (including the current EPA MOVES model) will utilize second-by-second vehicle operation data for all vehicles in the fleet to create an accurate estimate of emissions for the transportation network. However, current microscopic traffic simulation models were not designed to provide data of the required accuracy. Of particular importance is the exclusion of vertical curvature (or grade) in both traffic simulation and emissions modeling which prevents the accurate calculation of VSP, which much recent research has identified as a key predictor of second-by-second vehicle emissions. We therefore recommend that the next steps in the collection of data for calibration and estimation of new vehicle dynamics models be focused on grade.

ACKNOWLEDGMENTS

Research was conducted in cooperation with Britt Holmén and Yingge Qu with funding from the National Science Foundation.

REFERENCES

1. Brackstone, M., and M. McDonald. Car-Following: A Historical Review. *Transportation Research Part F,* Vol. 2, No. 4, 1999, pp. 181–196.
2. Rakha, H., M. Snare, and F. Dion. Vehicle Dynamics Model for Estimating Maximum Light-Duty Vehicle Acceleration Levels. In *Transportation Research Record: Journal of the Transportation Research Board, No. 1883,* Transportation Research Board of the National Academies, Washington, D.C., 2004, pp. 40–49.
3. Rakha, H., and B. Crowther. Comparison of Greenshields, Pipes, and Van Aerde Car-Following and Traffic Stream Models. In *Transportation Research Record: Journal of the Transportation Research Board, No. 1802,* Transportation Research Board of the National Academies, Washington, D.C., 2002, pp. 248–262.
4. Levison, W. H., and B. H. Kantowitz. Measuring the Operational Effects of Highway Geometrics: Beyond Spot Speeds. *Transportation Human Factors,* Vol. 2, No. 3, 2000, pp. 265–278.
5. Nie, B., and Y. Hassan. Modeling Driver Speed Behavior on Horizontal Curves of Different Road Classifications. Presented at 86th Annual Meeting of the Transportation Research Board, Washington, D.C., 2007.
6. Figueroa, A. M., and A. P. Tarko. Free-flow Speed Changes in the Vicinity of Horizontal Curves. *Proc., 3rd International Symposium on Highway Geometric Design,* Chicago, Ill., Transportation Research Board of the National Academies, Washington, D.C., 2005, pp. 1–19.
7. Gibreel, G., S. M. Easa, and I. El-Dimeery. Prediction of Operating Speed on Three-Dimensional Highway Alignments. *Journal of Transportation Engineering,* Vol. 127, No. 1, 2001, pp. 20–30.
8. Schmidt, K. Dynamic Traffic Simulation Testing. *Traffic Technology International,* Jan. 2000, pp. 54–57.
9. Boxill, S., and L. Yu. *An Evaluation of Traffic Simulator Models for Supporting ITS Development.* Technical Report 167602-1. Center for Transportation Training and Research, Texas Southern University, Houston, Oct. 2000.
10. Sommers, K. 1996. *Comparative Evaluation of Freeway Simulation Models.* MS thesis. University of Minnesota, 1996.
11. Bloomberg, L., and J. Dale. Comparison of VISSIM and CORSIM Traffic Simulation Models on a Congested Network. In *Transportation Research Record: Journal of the Transportation Research Board, No. 1727,* TRB, National Research Council, Washington, D.C., 2000, pp. 52–60.
12. Prevedouros, P. D., and Y. Wang. Simulation of Large Freeway and Arterial Network with CORSIM, INTEGRATION, and WATSim. In *Transportation Research Record: Journal of the Transportation Research Board, No. 1678,* TRB, National Research Council, Washington, D.C., 1999, pp. 197–207.
13. Milam, R. T., and F. Choa. Recommended Guidelines for the Calibration and Validation of Traffic Simulation Models. *Proc., 8th TRB Conference on the Application of Transportation Planning Methods,* Corpus Christi, Tex., 2001, pp. 178–187.
14. Wang, Y., and P. Prevedouros. Comparison of INTEGRATION, TSIS/CORSIM, and WATSim in Replicating Volumes and Speeds on Three

Small Networks. In *Transportation Research Record 1644,* TRB, National Research Council, Washington, D.C., 1998, pp. 80–92.
15. Kim, K.-D. and L. R. Rilett. Simplex-Based Calibration of Traffic Microsimulation Models with Intelligent Transportation Systems Data. In *Transportation Research Record: Journal of the Transportation Research Board, No. 1855,* Transportation Research Board of the National Academies, Washington, D.C., 2003, pp. 80–89.
16. Jayakrishnan, R., J. Oh, and A. Sahraoui. *Calibration and Path Dynamics Issues in Microscopic Simulation for Advanced Traffic Management and Information Systems.* UCI-ITS-WP-00-22. Institute of Transportation Studies, University of California, Irvine, 2000.
17. Park, B., and J. D. Schneeberger. Microscopic Simulation Model Calibration and Validation: Case Study of VISSIM Simulation Model for a Coordinated Actuated Signal System. In *Transportation Research Record: Journal of the Transportation Research Board, No. 1856,* Transportation Research Board of the National Academies, Washington, D.C., 2003, pp. 185–192.
18. Sacks, J., N. M. Rouphail, B. Park, and P. Thakuriah. Statistically-Based Validation of Computer Simulation Models in Traffic Operation and Management. *Journal of Transportation and Statistics,* Vol. 5, No. 1, 2002, pp. 1–15.
19. Akçelik, R., and M. Besley. Operating Cost, Fuel Consumption, and Emission Models in aaSIDRA and aaMotion. Presented at 25th Conference of Australian Institutes of Transport Research (CAITR 2003), University of South Australia, Adelaide, Australia, 2003.
20. Zhang, Y., and L. E. Owen. Systematic Validation of a Microscopic Traffic Simulation Program. In *Transportation Research Record: Journal of the Transportation Research Board, No. 1876,* Transportation Research Board of the National Academies, Washington, D.C., 2004, pp. 112–120.
21. Nam, E. K., C. A. Gierczak, and J. W. Butler. Comparison of Real-World and Modeled Emissions Under Conditions of Variable Driver Aggressiveness. Presented at 82nd Annual Meeting of the Transportation Research Board, Washington, D.C., 2003.
22. Sivanandan, R., and H. Rakha. Vehicle Aggregation Impacts on Fuel Consumption and Emissions Estimates. Presented at 82nd Annual Meeting of the Transportation Research Board, Washington, D.C., 2003.
23. Roadware. Roadware ARAN brochure. http://www.roadware.com/_lib/pdf/datasheet.icon_sheet.pdf. Accessed June 5, 2007.
24. Garmin International Inc. GARMIN GPS 16 and GPS 17. Olathe, Kans., 2002.
25. Jimenez, J. *Understanding and Quantifying Motor Vehicle Emissions with Vehicle Specific Power and TILDAS Remote Sensing.* PhD dissertation. Massachusetts Institute of Technology, 1999.
26. Huai, T., T. Durbin, T. Younglove, G. Scora, M. Barth, and J. Norbeck. Vehicle Specific Power Approach to Estimating On-Road NH3 Emissions from Light-Duty Vehicles. *Environmental Science and Technology,* Vol. 39, No. 24, 2005, pp. 9595–9600.
27. Kuhns, H., C. Mazzoleni, H. Moosmuller, D. Nikolic, R. Keislar, P. Barber, Z. Li, V. Etyemezian, and J. Watson. Remote Sensing of PM, NO, CO and HC Emission Factors for On-Road Gasoline and Diesel Engine Vehicles in Las Vegas, NV. *Science of the Total Environment,* Vol. 322, No. 1–3, 2004, pp. 123–137.
28. Pokharel, S., G. A. Bishop, and D. H. Stedman. 2001. *On-Road Remote Sensing of Automobile Emissions in the Los Angeles Area: Year 2.* University of Denver final report to the Coordinating Research Council, Inc. Available at http://www.crcao.com.
29. *A Policy on Geometric Design of Highways and Streets.* AASHTO, Washington, D.C., 2001.
30. Frey, C., A. Unal, N. Rouphail, and J. Coylar. On-Road Measurement of Vehicle Tailpipe Emissions Using a Portable Instrument. *Journal of the Air and Waste Management Association,* Vol. 53, 2003, pp. 992–1002.
31. *Draft Motor Vehicle Emission Simulator (MOVES) 2009: Software Design and Reference Manual.* U.S. Environmental Protection Agency, Washington, D.C., 2009. http://www.epa.gov/otaq/models/moves/420b09007.pdf. Accessed July, 28, 2009.
32. Jackson, E. D., Y. Qu, B. Holmen, and L. Aultman-Hall. Driver and Road Type Effects on Light-Duty Gas and Particulate Emissions. In *Transportation Research Record: Journal of the Transportation Research Board, No. 1987,* Transportation Research Board of the National Academies, Washington, D.C., 2006, pp. 118–127.

The Transportation and Air Quality Committee peer-reviewed this paper.

Using Portable Emission Measurement Systems for Transportation Emissions Studies

Comparison with Laboratory Methods

Huan Liu, Matthew Barth, George Scora, Nicole Davis, and James Lents

Portable emission measurement systems (PEMS) are increasingly being used in a variety of transportation research projects to determine the impact of real-world vehicle emissions. One of the key questions that remain is how well these systems perform compared with testing that occurs in controlled laboratory conditions. To help answer this question, three PEMS were carefully evaluated for both gasoline and diesel light-duty vehicles in a dynamometer test facility. The evaluation was focused on the systems' accuracy, time correspondence, and suitability for measuring transient emissions. Both cumulative mass emissions and modal emissions for carbon monoxide (CO), hydrocarbons (HC), oxides of nitrogen (NO_x), and carbon dioxide (CO_2) were measured for three gasoline and three diesel vehicles on three widely varying driving cycles. All of the PEMS proved to be both reasonably accurate and precise. The CO_2 emissions measured by the PEMS were in excellent agreement (within 98%) with measurements from the laboratory system. Other pollutants measured were found to be in reasonable agreement (within 20% or better) for NO_x and HC on diesel vehicles and CO on gasoline vehicles. The second-by-second emission rate measured with the PEMS matched well with the corresponding laboratory modal analyzer data for CO_2, NO_x, and CO under all driving cycles. Transient emissions of all pollutants agreed within 10% of the two systems for more than 6,000 data points from each vehicle. The results suggest that when properly set up and calibrated, PEMS are capable of measuring emissions from both gasoline and diesel vehicles to an accuracy within 20% of conventional laboratory modal analyzer systems.

In recent years, portable emission measurement systems (PEMS) have become increasingly used in a variety of transportation research projects to determine the impact of real-world vehicle emissions. For example, researchers use PEMS to measure emissions in a target area, such as the toll area (*1*), the high-occupancy-vehicle lane (*2*), the arterial signal area (*3*), or even the whole city (*4*). Researchers also use PEMS to measure emissions on target vehicles, such as heavy-duty vehicles (*5, 6*) or biodiesel vehicles (*7*). In part of the multisponsored Kansas City Light-Duty Vehicle Emission Study, PEMS units were found to compare favorably to dynamometer results and were used to collect emission factors and activity data from light-duty vehicles (*8*). PEMS are also used as a tool to bridge the gap in transportation and emissions models (*9, 10*). In addition, several vehicle emissions models depend on PEMS measurements, such as the international vehicle emissions model (*11*). It is now relatively straightforward to purchase commercial PEMS from different manufacturers and to install the units in a variety of different vehicle types. Most PEMS require very careful setup and maintenance during the tests. One of the key questions that remain is how well these systems perform compared with testing that occurs in controlled laboratory conditions.

The focus of this study is on the comparison of emission results from different PEMS and a light-duty chassis dynamometer facility with a full-flow constant volume sampling system. The goal of this study was to determine whether PEMS can be utilized as a tool for either emissions inventory development or in-use compliance.

Currently, PEMS are used to collect vehicle emission rates as a complementary method to federal test procedures. On-road emission testing requires different methodologies than traditional approaches of testing in the laboratory. One of the key advantages of PEMS is that they can capture real-world scenarios without trying to repeat these scenarios in the laboratory. Furthermore, using PEMS can result in lower costs and time for measuring mobile emissions.

There are other ongoing studies to evaluate whether PEMS can be used to test real-world emissions for the purposes of compliance, regulation, or decision making (*12–16*). Most of these studies focus on oxides of nitrogen (NO_x) and carbon dioxide (CO_2) from diesel vehicles.

In this study, both gasoline and diesel light-duty vehicles were tested under different driving conditions. A total of six in-use vehicles were recruited and tested on a single-roll 122-cm (48-in.) dynamometer over three different driving cycles. For each of these cycles, second-by-second tailpipe CO_2, NO_x, carbon monoxide (CO), and hydrocarbon (HC) emissions data were collected. For diesel vehicles, particulate matter (PM) emission data were collected as well. All the data were utilized to compare PEMS output with output from the laboratory quality analyzers for the key exhaust gas components.

H. Liu, College of Engineering, Center for Environmental Research and Technology, University of California, Riverside, 1084 Columbia Avenue, Riverside, CA 92507, and International Sustainable Systems Research Center, 605 South Palm Street, Suite C, La Habra, CA 90631. M. Barth and G. Scora, College of Engineering, Center for Environmental Research and Technology, University of California, Riverside, 1084 Columbia Avenue, Riverside, CA 92507. N. Davis and J. Lents, International Sustainable Systems Research Center, 605 South Palm Street, Suite C, La Habra, CA 90631. Corresponding author: H. Liu, huanliu@cert.ucr.edu.

Transportation Research Record: Journal of the Transportation Research Board, No. 2158, Transportation Research Board of the National Academies, Washington, D.C., 2010, pp. 54–60.
DOI: 10.3141/2158-07

TABLE 1 Measurement Capabilities of Individual Instruments

	Pierburg	PEMS1	PEMS2	PEMS3
HC	FID[a]	FID	FID	FID
CO	NDIR[b]	NDIR	NDIR	NDIR
CO_2	NDIR	NDIR	NDIR	NDIR
NO_X	CLD[c]	NDUV[d]	NDUV	NDUV
PM	Not measured	Not measured	Ionize and collect by size	Not measured
Flow	Constant	Pressure differential	Pressure differential	Pressure differential
Sample	Dilute exhaust	Raw exhaust	Raw exhaust	Raw exhaust

[a]Flame ionization analyzer. THC (total hydrocarbon), C_3, and CH_4 were recorded.
[b]Nondispersive infrared analyzer (NDIR).
[c]Chemiluminescence analyzers (CLA).
[d]Nondispersive ultraviolet (NDUV): the NO and NO_2 constituents of NO_x can be measured simultaneously and independently.

EXPERIMENTAL PROCEDURES

Instrumentation

All tests were conducted at the Vehicle Emissions Research Laboratory at the University of California, Riverside, equipped with a Burke E. Porter 48-in. single-roll electric dynamometer (*17*). For these tests, second-by-second measurements were obtained for HC, CO, NO_x, and CO_2 using two types of instruments. A Pierburg AMA-4000 bench was used as a laboratory whole flow measurement system (*18*). The concentrations were measured and then converted into mass emissions rates by multiplying by the density and the time-aligned exhaust flow rate (*19*). Three PEMS were evaluated with their flow meter system. The PEMS include a Semtech G (PEMS1), a Semtech D with a Dekati Mass Monitor for PM (PEMS2), and a Semtech DS (PEMS3). The measurement capabilities from each PEMS and Pierburg differed as summarized in Table 1.

PEMS1 was used only for gasoline vehicles and PEMS2 was used only for diesel vehicles. The PEMS3 and Pierburg instruments were both used throughout the entire testing procedure.

The Pierburg system utilizes measurements for both methane and propane. Only propane was used as an audit for PEMS. The Semtech G only measures nonmethane hydrocarbons.

Figure 1 presents a flow diagram for the overall emissions testing system. The exhaust flow in the PEMS dilution device is measured with a Dwyer differential pressure transducer, which is accurate to 0.25% of full scale. The differential pressure gauge is used to measure the pressure difference between P2 and P3 shown in Figure 2. A microfilter produces particle-free air to be diluted with the exhaust sample. The exhaust sample and dilution air are heated to 110°C to avoid water and organic condensation. The dilution level reaches values from 20:1 to 30:1 depending on the vehicle tested and the exhaust flow rate.

Test Vehicles

Six vehicles were selected and tested in this study. This fleet included three gasoline vehicles and three diesel vehicles. Table 2 describes the vehicles.

Procedure

Three different driving cycles were used in this study: (*a*) the Federal Test Procedure (FTP) (40 CFR Parts 86–99), (*b*) the high-speed US06 cycle (*20*), and (*c*) a specially designed modal emission cycle (MEC01) (*21*).

A complete FTP test was selected as a standard certification testing procedure to provide baseline information about a vehicle's emissions, which could be used as a reference to compare with existing tests of other vehicles. The US06 is a high-acceleration

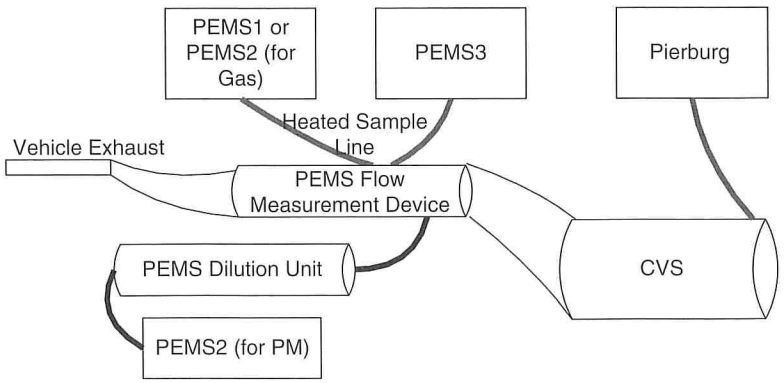

FIGURE 1 Flow diagram for overall emissions testing system (CVS = constant volume sampling).

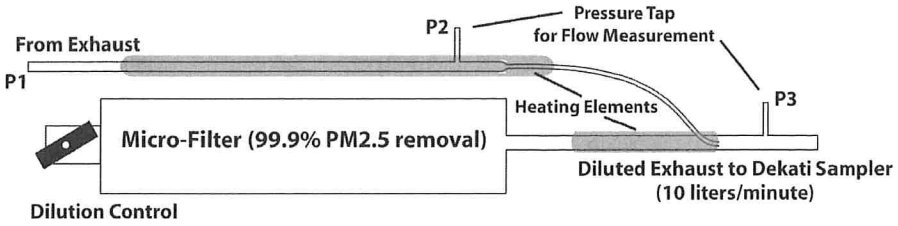

FIGURE 2 PEMS flow measurement and dilution device.

aggressive driving schedule that is often identified as part of the "Supplemental FTP" driving schedule. The MEC01 cycle was designed to exercise a vehicle across a variety of modal events and includes rapid load reduction and long deceleration events. The MEC01 also includes a set of constant speed cruises, speed fluctuation driving, and constant power driving. Details of the MEC01 cycle are given in a previous paper (*21*).

RESULTS

Steady-State Correlation

The cumulative mass emissions (CMEs) for each driving cycle were calculated and compared. By comparing the pollutants' emissions, the bias for a given pollutant and driving cycle could be determined. The correlation plots for pollutants between the PEMS and Pierburg instruments are provided in Figures 3 and 4. The smallest CMEs were produced under the FTP cycle followed by the US06 cycle. The MEC cycle produced the most emissions.

PEMS1 and PEMS3 were used for gasoline vehicles. Comparisons between the two data sets showed regression line slopes between 0.91 and 1.24 and R^2 correlations greater than 0.95 for CO_2 and CO for all PEMS. This result is quite reasonable because all PEMS units tested and the Pierburg analyzer use a nondispersive infrared analyzer to measure CO and CO_2. NO_x is 30% lower for PEMS than for Pierburg. However, it should be noted that the difference in CMEs for NO_x between PEMS and Pierburg is less than 2 g per cycle. NO_x emissions are much lower than other pollutants, which may lead to a high percent difference, but still low absolute difference between measured values. The HC CMEs from gasoline vehicles are almost incomparable between PEMS and Pierburg because target components tested are different. Considering that different flow measurement systems will introduce some differences into the system, the results illustrated the reliable CMEs measurement capability of PEMS.

Figure 4 provides the CMEs results for all gaseous pollutants from diesel vehicles when the PEMS are compared with Pierburg. The results showed excellent linear relationships between CO_2 and NO_x for all PEMS (regression slopes >0.88 and <1.01), with good R^2 correlations (>0.93) as well. A unique finding in this research is that HC measured by PEMS also has a relatively good relationship with Pierburg (regression slopes >1.01 and <1.24). Compared with PEMS2, PEMS3 performed better in the MEC cycle, so the regression slope was improved from 1.23 to 1.01. For all pollutants under the FTP and US06, PEMS2 and PEMS3 showed good agreement with Pierburg. The MEC cycle always produced the highest emissions and introduced some differences for CO and HC measurements. Pierburg measured lower CO emissions than all PEMS, with deviations in the range of 30% to 100%. However, the correlation results between the PEMS and Pierburg instruments still showed good R^2 values (>0.92) for all PEMS for CO, which is evidence of the stability of the instruments.

Comparison of Two PEMS for Diesel Vehicle on Basis of Instantaneous Data

Figures 5 and 6 show scatter plots with trend lines for the instantaneous emission data from PEMS instruments and the Pierburg analyzer for diesel vehicles. PEMS2 shows significant correlation with Pierburg for CO, CO_2, and NO_x emissions, as illustrated in Figure 5. PEMS2 matched Pierburg measurements, even in the high emission cycle. The deviation is 1% for CO_2, 15% for NO_x emissions, and 30% for CO. It should be noted that most of the data points for CO emissions are clustered around the low end of the CO emission range with only a few points populating the higher end of the range.

Figure 6 provides the scatter plots for PEMS2 versus PEMS3. These two pieces of equipment utilize the same measurement technique and both perform well. PEMS2 and PEMS3 demonstrated similar capability to measure transient emissions. Both of these PEMS units

TABLE 2 Description of Tested Vehicles

ID	Maker	Model	Fuel	Year	Engine Size (L)	GVWR (lb)	Curb Weight (lb)
1	Ford	Escort	G	1996	2.0	3,400	2,478
2	GMC	Pickup truck	G	2002	4.3	4,900	3,050
3	Ford	Expedition	G	2005	5.4	7,100	5,352
4	Chevrolet	Silverado	D	2005	6.6	6,400	3,900
5	Chevrolet	Silverado	D	2006	6.6	9,700	5,700
6	Mercedes	300D	D	1984	3.0	3,300	2,400

NOTE: GVWR = gross vehicle weight rating.

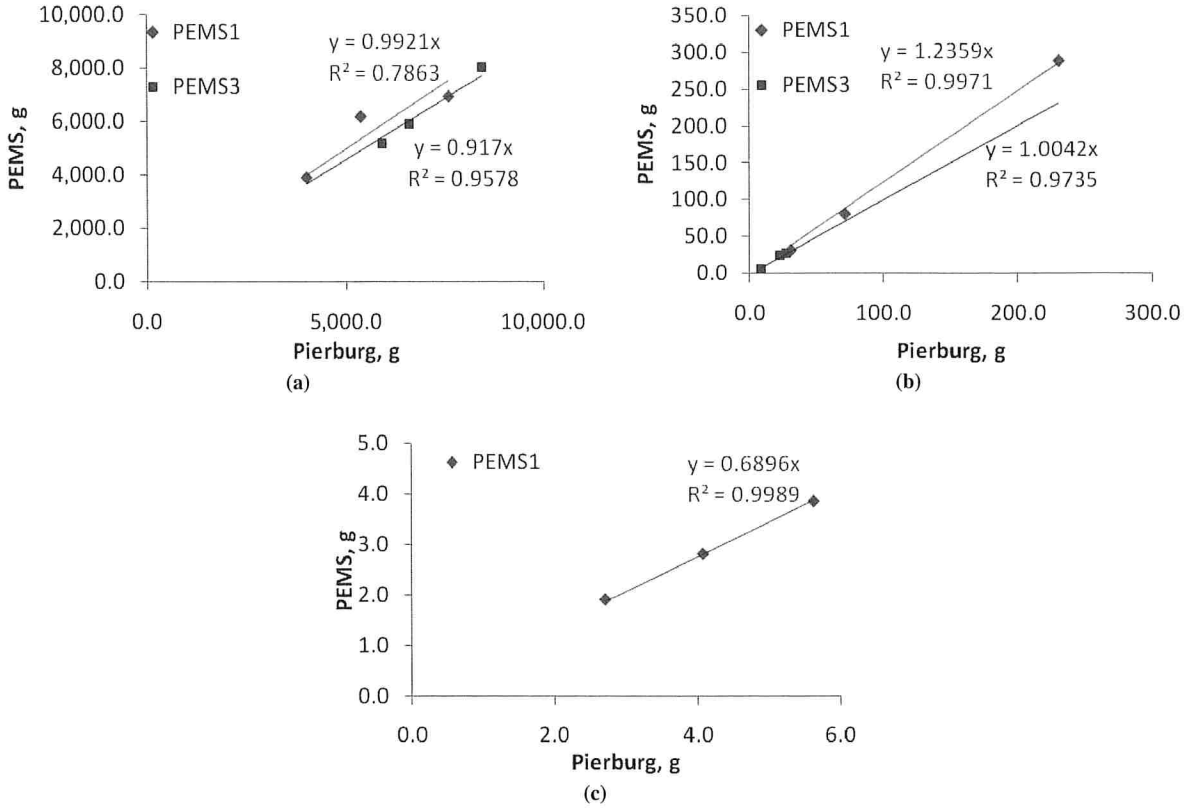

FIGURE 3 Correlation plot of CMEs for gasoline vehicles: (*a*) CO_2, (*b*) CO, and (*c*) NO_x.

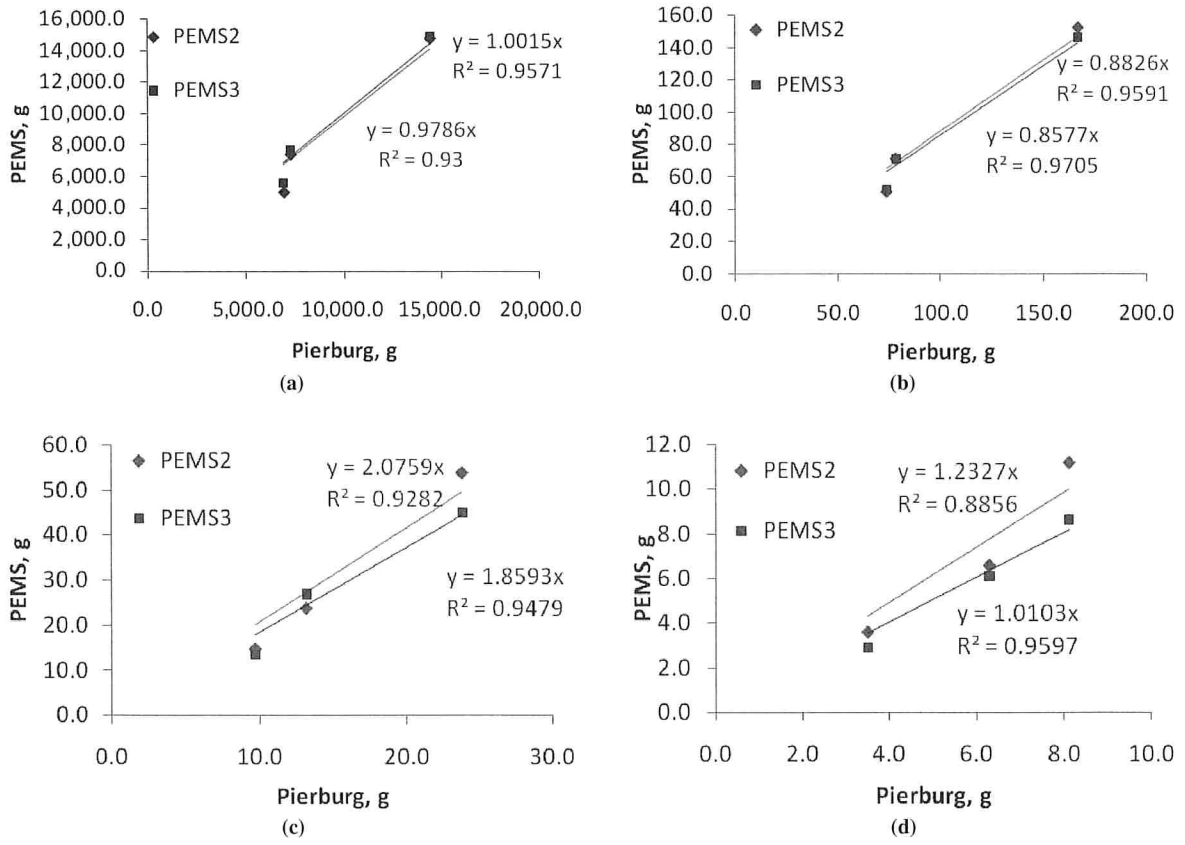

FIGURE 4 Correlation plot of CMEs for diesel vehicles: (*a*) CO_2, (*b*) NO_x, (*c*) CO, and (*d*) HC.

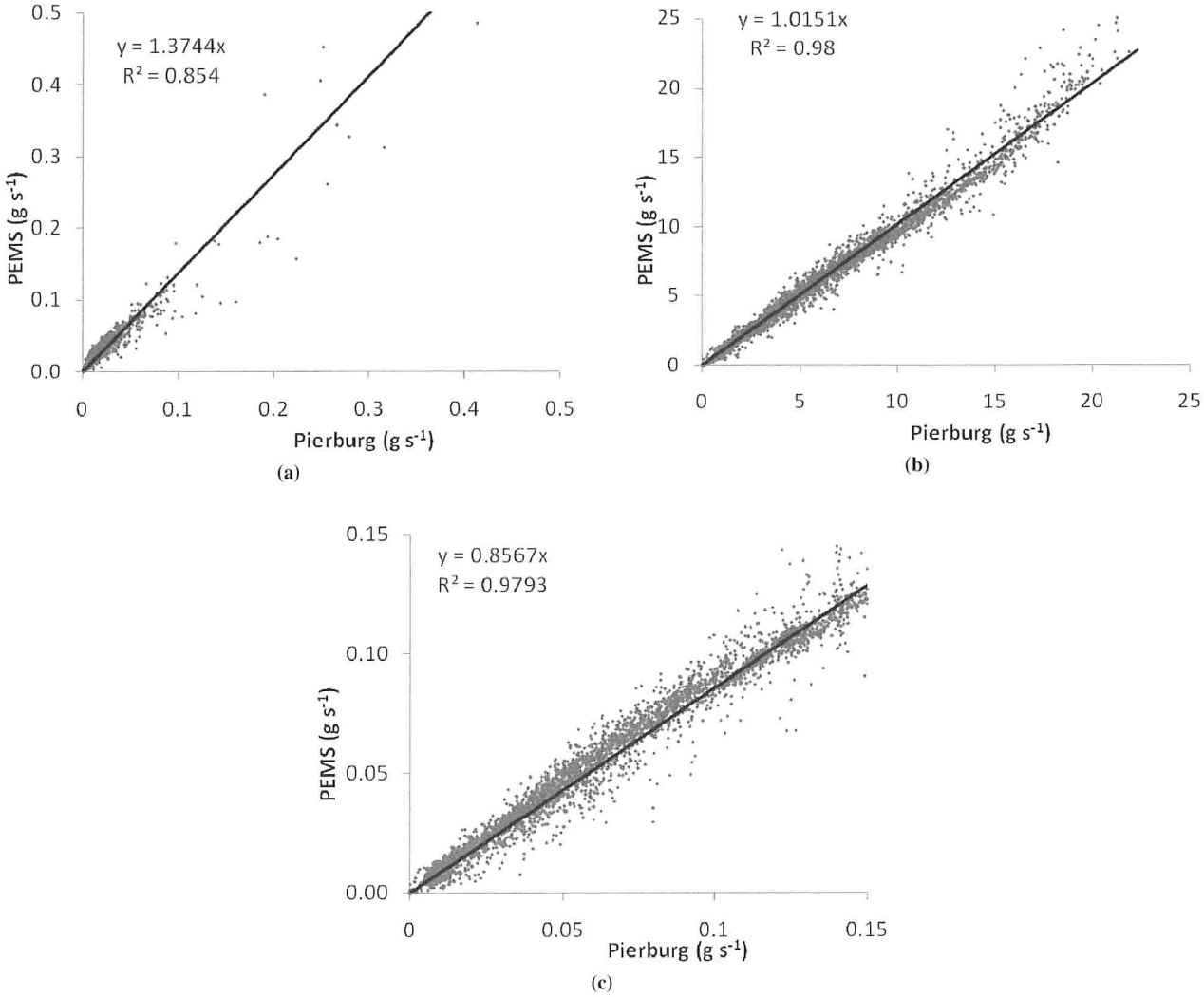

FIGURE 5 Comparison of instantaneous emission rates of diesel test vehicles for PEMS2 and Pierburg: (*a*) CO, (*b*) CO_2, and (*c*) NO_x.

are stable in the full measurement range, from very low concentrations above the detection limit to the highest concentration that occurred during testing. NO_x plots showed scatter in a larger range than other pollutants, but both the slope of the trend line (0.93) and the correlation coefficient ($R^2 = 0.92$) are acceptable. The variance and measurement correlation values for all the PEMS units fulfilled the primary objective of vehicle emission testing.

The transient mass correlation could be used for evaluating the following aspects: response time, variety, peak value, and base value. For all pollutants, PEMS1 and Pierburg have precise response to the emission change. Profiles from these two systems match each other well on both the response time and the value. PEMS1 and Pierburg show a similar peak value for CO_2 and NO_x, but some high CO peaks were only captured by PEMS1. Also, PEMS1 has higher CO_2 measurements during idle than Pierburg.

Pierburg, PEMS2, and PEMS3 show good performance for the diesel test. The time alignment, emission trace, peak value, and base value all matched well for CO_2, NO_x, and CO. PEMS2 and PEMS3 show closer results for HC than PEMS2 does compared with Pierburg. The HC measurements using the PEMS were in good agreement with each other.

The predictive performance of all three PEMS is good. In general, all emission data series exhibited similar trends for PEMS and Pierburg, including CO, CO_2, HC, and NO_x exhaust emissions during the whole combined driving cycle.

DISCUSSION OF RESULTS AND CONCLUSION

The goal of this study was to provide a snapshot of the capabilities of PEMS for transportation-related emission research. The results show that PEMS have quick and precise response to most pollutants for most driving cycles.

PEMS showed good capacity to be used for capturing emission changes in the microtraffic research. PEMS have strong linear relationships to the laboratory modal system for all pollutants on both response time and value. All the correlation results between the PEMS and laboratory modal system showed good R^2 values (0.85, 0.98, and 0.98). PEMS and Pierburg get similar peak values for CO_2 and NO_x, but some high value peaks were only captured by PEMS. For normal traffic activity, PEMS are reliable. PEMS were evaluated to be as good as laboratory modal system under most driving conditions. As

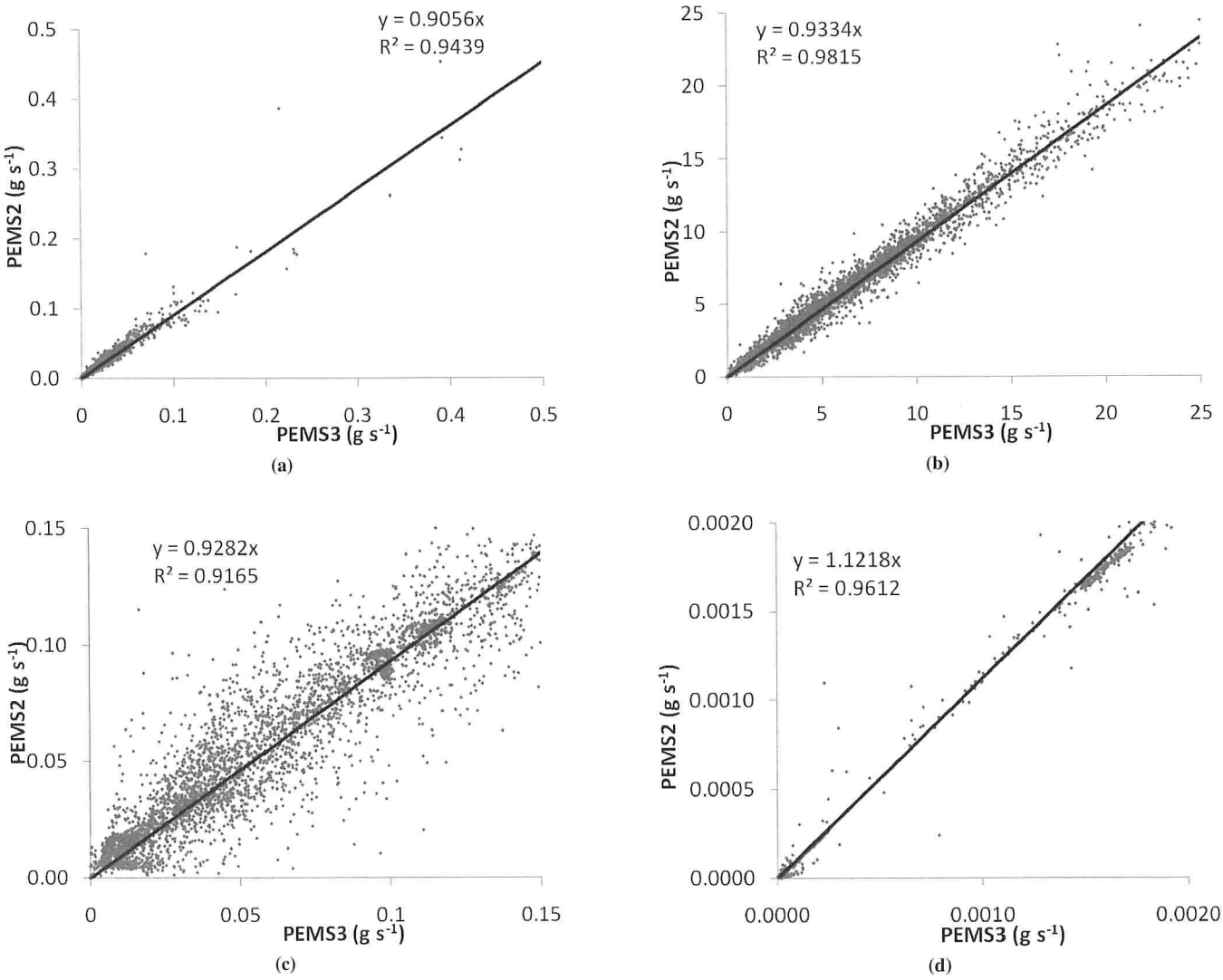

FIGURE 6 Comparison of instantaneous emission rates of diesel test vehicles for PEMS2 and PEMS3: (*a*) CO, (*b*) CO_2, (*c*) NO_x, and (*d*) HC.

an example, for normal to aggressive driving cycles, such as FTP and US06, the PEMS showed agreement with the laboratory modal system within 5% for HC. For the MEC01 cycle, PEMS get 20% higher HC than the laboratory modal system.

The agreement between PEMS and the laboratory modal system also varied depending on the pollutant. PEMS showed agreement within 3% for CO_2 and 15% for NO_x with diesel vehicles and within 10% for CO_2 on gasoline vehicles. HC and CO emission levels were relatively low for testing, and the PEMS showed larger deviations. Table 3 gives a suggestion value of systematic variation, which could be used to estimate possible departure. However, it should be noted that this value is generated based on the driving cycle mentioned in the procedure section.

TABLE 3 Systematic Variations Under the FTP-US06-MEC01 Cycle (%)

	HC	CO	NO_X	CO_2
PEMS1	—	13.4	−30.6	1.4
PEMS2	15.2	85.9	−16.1	−7.6
PEMS3	−4.4	77.5	—	−3.3

ACKNOWLEDGMENTS

The authors acknowledge the contribution and support of Tom Durbin, Kurt Buhmiller, Bill Welch, and Harshit Aggrawal of CE-CERT, UC Riverside, for performing the emissions measurements.

REFERENCES

1. Song, G., L. Yu, and X. Zhang. Emission Analysis at Toll Station Area in Beijing with Portable Emission Measurement System. In *Transportation Research Record: Journal of the Transportation Research Board, No. 2058,* Transportation Research Board of the National Academies, Washington, D.C., 2008, pp. 106–114.
2. Krimmer, M., and M. Venigalla. Measuring Impacts of High-Occupancy-Vehicle Lane Operations on Light-Duty-Vehicle Emissions: Experimental Study with Instrumented Vehicles. In *Transportation Research Record:*

Journal of the Transportation Research Board, No. 1987, Transportation Research Board of the National Academies, Washington, D.C., 2006, pp. 1–10.
3. Unal, A., N. M. Rouphail, and H. C. Frey. Effect of Arterial Signalization and Level of Service on Measured Vehicle Emissions. In *Transportation Research Record: Journal of the Transportation Research Board, No. 1842,* Transportation Research Board of the National Academies, Washington, D.C., 2003, pp. 47–56.
4. Qiao, F., Z. Wang, and L. Yu. On-Road Vehicle Emissions in Beijing, China: Experimental Study Using Portable Emission Measurement System. Presented at 86th Annual Meeting of the Transportation Research Board, Washington, D.C., 2007.
5. Weinblatt, H., R. G. Dulla, and N. N. Clark. Vehicle Activity-Based Procedure for Estimating Emissions of Heavy-Duty Vehicles. In *Transportation Research Record: Journal of the Transportation Research Board, No. 1842,* Transportation Research Board of the National Academies, Washington, D.C., 2003, pp. 64–72.
6. Yoon, S., M. O. Rodgers, J. R. Pearson, and R. L. Guensler. Engine and Weight Characteristics of Heavy-Duty Diesel Vehicles and Improved On-Road Mobile Source Emissions Inventories: Engine Model Year and Horsepower and Vehicle Weight. In *Transportation Research Record: Journal of the Transportation Research Board, No. 1880,* Transportation Research Board of the National Academies, Washington, D.C., 2004, pp. 99–107.
7. Frey, H. C., and K. Kim. Comparison of Real-World Fuel Use and Emissions for Dump Trucks Fueled with B20 Biodiesel Versus Petroleum Diesel. In *Transportation Research Record: Journal of the Transportation Research Board, No. 1987,* Transportation Research Board of the National Academies, Washington, D.C., 2006, pp. 110–117.
8. Kishan, S., S. Fincher, M. Sabisch, A. Burnette, M. Zmud, R. Santos, and S. Bricka. *Late Model Vehicle Emissions and Fuel Economy Characterization Study: Addendum to the Kansas City Exhaust Characterization Study.* Final Report for EPA Contract #GS 10F-0036K. Sept. 26, 2005.
9. Frey, H. C., N. M. Rouphail, and H. Zhai. Speed- and Facility-Specific Emission Estimates for On-Road Light-Duty Vehicles on the Basis of Real-World Speed Profiles. In *Transportation Research Record: Journal of the Transportation Research Board, No. 1987,* Transportation Research Board of the National Academies, Washington, D.C., 2006, pp. 128–137.
10. Yoon, S., H. Li, J. Jun, J. H. Ogle, R. L. Guensler, and M. O. Rodgers. Methodology for Developing Transit Bus Speed–Acceleration Matrices for Load-Based Mobile Source Emissions Models. In *Transportation Research Record: Journal of the Transportation Research Board, No. 1941,* Transportation Research Board of the National Academies, Washington, D.C., 2005, pp. 26–33.
11. Davis, N., J. Lents, M. Osses, N. Nikkila, and M. J. Barth. Development and Application of an International Vehicle Emissions Model. In *Transportation Research Record: Journal of the Transportation Research Board, No. 1939,* Transportation Research Board of the National Academies, Washington, D.C., 2005, pp. 157–165.
12. Johnson, K. C., T. D. Durbin, D. R. Cocker III, W. J. Miller, D. K. Bishnu, H. Maldonado, N. Moynahan, C. Ensfield, and C. A. Laroo. On-Road Comparison of a Portable Emission Measurement System with a Mobile Reference Laboratory for a Heavy-Duty Diesel Vehicle. *Atmospheric Environment,* Vol. 43, No. 18, 2009, pp. 2877–2883.
13. Zhang, K., and C. Frey. Evaluation of Response Time of a Portable System for In-Use Vehicle Tailpipe Emissions Measurement. *Environmental Science & Technology,* Vol. 42, No. 1, 2008, pp. 221–227.
14. U.S. Environmental Protection Agency, California Air Resources Board, and Engine Manufacturers Association. *Test Plan to Determine PEMS Measurement Allowances for the Gaseous Emissions Regulated Under the Manufacturer-Run Heavy-Duty Diesel Engine In-Use Testing Program,* May 20, 2005.
15. Dearth, M. A., J. W. Butler, A. Colvin, C. Gierczak, S. Kaberline, T. Korniski, and D. Semtech. *The Chassis Roll Evaluation of a Commercial Portable Emission Measurement System (PEMS).* SAE Technical Paper 2005-01-0673, 2005.
16. Durbin, T. D., K. Johnson, D. R. Cocker, J. W. Miller, H. Maldonado, A. Shah, C. Ensfield, C. Weaver, M. Akard, N. Harvey, J. Symon, T. Lanni, W. D. Bachalo, G. Payne, G. Smallwood, and M. Linke. Evaluation and Comparison of Portable Emissions Measurement Systems and Federal Reference Methods for Emissions from a Back-Up Generator and a Diesel Truck Operated on a Chassis Dynamometer. *Environmental Science & Technology,* Vol. 41, No. 17, 2007, pp. 6199–6204.
17. Durbin, T. D., J. T. Pisano, T. Younglove, C. G. Sauer, S. H. Rhee, T. Huai, J. W. Miller, G. I. MacKay, A. M. Hochhauser, M. C. Ingham, R. A. Gorse, L. K. Beard, D. DiCicco, N. Thompson, R. J. Stradling, J. A. Rutherford, and J. P. Uihlein. The Effect of Fuel Sulfur on NH_3 and Other Emissions from 2000–2001 Model Year Vehicles. *Atmospheric Environment,* Vol. 38, No. 17, 2004, pp. 2699–2708.
18. Brezonick, M. New Generation Emissions Test Bench From Pierburg: Product Announcement. *Diesel Progress North American Edition,* 2009.
19. Barth, M., F. An, T. Younglove, G. Scora, C. Levine, M. Ross, and T. Wenzel. *Development of a Comprehensive Modal Emissions Model.* Final report by the University of California, College of Engineering, Center for Environmental Research and Technology, Riverside, Calif., for the National Cooperative Highway Research Program Under Contract NCHRP 25-11, 2000.
20. *Support Document to the Proposed Regulations for Revisions to the Federal Test Procedure: Detailed Discussion and Analysis.* Office of Air and Radiation, U.S. Environmental Protection Agency, 1995.
21. Barth, M., T. Younglove, T. Wenzel, G. Scora, F. An, M. Ross, and J. Norbeck. Analysis of Modal Emissions from a Diverse In-Use Vehicle Fleet. In *Transportation Research Record 1587,* TRB, National Research Council, Washington, D.C., 1997, pp. 73–84.

The Transportation and Air Quality Committee peer-reviewed this paper.

TAMNROM-3D

Three-Dimensional Eulerian Model to Simulate Air Quality near Highways

Sri Harsha Kota, Qi Ying, and Yunlong Zhang

Most models for the study of near-road air quality are based on either steady-state Gaussian equations or Lagrangian puff formulations to describe nonreactive pollutant concentrations at receptor sites. The accuracy of the dispersion calculation is often limited because of simplifications that are necessary to derive the analytical solutions. The general source–receptor structure of these models limits their capabilities to treat rapid chemical and physical processes that were recently observed in the near-road environment. A new three-dimensional (3-D) Eulerian near-road air quality model, the Texas A&M Near-Road Model (TAMNROM-3D), was developed. The enhanced pollutant turbulent diffusion caused by moving vehicles is handled in TAMNROM-3D by a revised vehicle-induced turbulence parameterization scheme. The performance of TAMNROM-3D on nonreactive tracer dispersion is evaluated with the SF_6 data set collected by General Motors during a 1975 sulfate dispersion experiment. Predicted concentrations show good agreement with observations under different wind conditions. Model performance statistics are compared favorably with those reported by the ROADWAY-2 model. Sensitivity studies indicate that the model is robust to reasonable uncertainties in the model parameters and input data.

Emissions from highway vehicles significantly affect local and regional air quality (*1, 2*) and contribute to global climate change (*3*). It is estimated that approximately 11% of the population of the United States lives within 100 m from highways (*4*). Epidemiological studies have indicated an increase in lung and respiratory-related diseases with a decrease in the distance of residences from roadways (*5*). Quantitative evaluation of the pollutant levels near highways using numerical near-road air quality models is a necessary complement to air quality monitoring programs to provide essential data for traffic planning (*6, 7*), congestion mitigation (*8*), and human health studies to link personal air pollution exposure to health effects (*9*).

Models to predict air quality near highways differ in their approaches in representing emissions from the vehicles, the pollutant dispersion processes, and level of details in treating chemical and physical processes. Depending on the different approaches to model the atmospheric dispersion process, existing near-road air quality models can be grouped into three major categories: steady-state Gaussian models, Lagrangian models, and Eulerian models.

Zachry Department of Civil Engineering, Texas A&M University, 3136 TAMU, College Station, TX 77843. Corresponding author: Q. Ying, qying@civil.tamu.edu.

Transportation Research Record: Journal of the Transportation Research Board, No. 2158, Transportation Research Board of the National Academies, Washington, D.C., 2010, pp. 61–68.
DOI: 10.3141/2158-08

Several models used in near-road air quality studies are based on the steady-state Gaussian solution to the atmospheric dispersion equation for point or line sources to determine nonreactive air pollutants near highways (*10–12*). For pollutants undergoing fast chemical reactions, semiempirical methods, such as assuming a first-order decay, are often adopted (*13*). Additional turbulent diffusion caused by moving vehicles on the highways significantly affects the dispersion of air pollutants. This process is handled differently in different Gaussian models. For example, the CALINE models account for the dispersion due to vehicle-induced turbulence (VIT) with an additional heat flux in the stability class calculations (*10*). The UCD2001 model accounts for VIT by simply assuming that pollutants emitted from vehicles are immediately well mixed within the mixing zone that extends 3 m laterally from the roadway and 2.5 m above the roadway (*11*). Sahlodin et al. applied a computational fluid dynamics model to estimate the increase in the Gaussian dispersion parameters due to the additional turbulence created by the moving vehicles (*14*).

Lagrangian models have also been used in near-road air quality applications. In the TRAQSIM model developed at University of Central Florida (*12*), emissions from individual highway vehicles are simulated as discrete air parcels as the vehicles move on the highway. The pollutant concentrations in the air parcel at receptor locations are described by the Gaussian puff equation. The effect of VIT on dispersion is accounted for by an additional contribution term to the dispersion parameters using a parameterization developed by Eskridge et al. (*15–17*). Similar to the steady-state Gaussian models, detailed treatment of chemical and physical transformation processes is not included in the TRAQSIM model.

Eulerian chemical transport model (CTM) is a natural extension to the Lagrangian approach to determine the spatial and temporal distribution of pollutants near highways. In Eulerian models, space and time are discretized and concentrations of air pollutants are determined by numerically solving the equations that govern the transport, transformation, and removal of air pollutants based on first principles. The Eulerian approach has been widely used in regional air quality models, but its application to near-road air quality studies are few because of the difficulty in accurately accounting for the VIT. Rao et al. formulated a two-dimensional Eulerian model ROADWAY-2 for pollutant dispersion near highways (*18, 19*). The ROADWAY-2 model directly predicts wind and turbulent diffusion parameters using a turbulent kinetic energy closure model with adjustments for the turbulence production in vehicle wakes based on the Eskridge parameterizations (*15, 17*). The model performance has been evaluated using SF_6 measurements from the sulfate dispersion experiment conducted by General Motors (GM). However, the ROADWAY-2 model only includes simple nitrogen oxide (NO_x) chemistry but does not include a complete treatment of the photochemistry and particle microphysics.

For a complete evaluation of air quality near highways, it is necessary to simultaneously determine the spatial and temporal distribution of multiple air pollutants and accurately simulate the chemical and physical processes during their dispersion to downwind locations. This paper describes the formulation of a new three-dimensional (3-D) Eulerian near-road air quality model, the Texas A&M Near-Road Model (TAMNROM-3D) and the initial evaluation of the model with GM's SF_6 data set. The uniqueness of the model is the inclusion of a new turbulence parameterization for the VIT in a general 3-D air quality model.

MODEL DESCRIPTION

TAMNROM-3D is a 3-D Eulerian air quality model that simulates the emission, dispersion, transformation, and removal of gas and particulate air pollutants emitted from highway vehicles. The model includes a revised SAPRC-99 photochemical mechanism to simulate six air toxics from mobile sources: benzene, 1,3-butadiene, formaldehyde, acetaldehyde, acrolein, and methyl *tert*-butyl ether. The inputs needed to run TAMNROM-3D include (*a*) gridded wind, temperature, and atmospheric turbulent diffusion coefficients; (*b*) gridded pollutant emission rates; and (*c*) gridded vehicle density and vehicle speed.

A simple meteorology preprocessor is developed to interpolate the meteorology observations to the model domain and calculate the atmospheric turbulent diffusivity at each grid cell. Gridded emissions from vehicles are prepared with an emission preprocessor based on the U.S. Environmental Protection Agency's MOBILE6 model. TAMNROM-3D does not include a traffic simulation module. Thus the vehicles' velocity, density, and fleet composition on each highway section represented in the model need to be derived from existing traffic simulation models. Details of the gas-phase photochemical mechanism, the emission preprocessor, and the treatment of particles will be described in a separate paper. In this paper, the governing equations of the TAMNROM-3D model and the solution procedures are described in more detail.

Governing Equations

The fundamental equation that describes the transport, chemical transformation, and removal of air pollutants in the atmosphere is the reactive chemical transport equation, shown in Equation 1 for Cartesian coordinates:

$$\frac{\partial C_j}{\partial t} = -\frac{\partial (u_i C_j)}{\partial x_i} + \frac{\partial}{\partial x_i}\left(K_i \frac{\partial C_j}{\partial x_i}\right) + R_j + S_j - L_j \qquad i = 1, 2, 3 \quad (1)$$

where

C_j = concentration (ppb/s) of an arbitrary air pollutant j as a function of space and time,
t = time,
i = three directions in the Cartesian coordinates,
u = wind speed (m/s),
K = turbulent diffusion coefficient (m^2/s),
R = rate of formation of the pollutant due to chemical reactions (ppb/s),
S = increase of pollutant concentration due to emission (ppb/s), and
L = loss rate (ppb/s).

To account for the turbulence produced in vehicle wakes to the dispersion of pollutants, TAMNROM-3D implements the two-dimensional VIT parameterization scheme developed by Bäumer et al. (20) with slight modifications for a 3-D model framework. The scheme assumes that the overall turbulent diffusivity (K_i) in the atmosphere near highways can be estimated by the addition of the background atmospheric turbulent diffusivity ($K_{i,\text{atm}}$) and the additional diffusivity due to moving vehicles ($K_{i,\text{mv}}$), as shown in Equation 2:

$$K_i = K_{i,\text{atm}} + K_{i,\text{mv}} \quad (2)$$

$K_{i,\text{atm}}$ is calculated in the model with the planetary boundary layer similarity theory as described in Garratt (*21*) and Jacobson (*22*), based on the interpolated vertical wind and temperature profiles. The Bäumer scheme suggests that $K_{i,\text{mv}}$ can be parameterized as a simple function of the extra turbulent kinetic energy (TKE) created due to the moving vehicles (*16*), as illustrated in Equation 3:

$$K_{i,\text{mv}} = \bar{L}_i e_m^{0.5} \quad (3)$$

The turbulence characteristic length scale $\bar{L}_i$ is taken as the average length of all the vehicles along direction i in a given grid cell; e_m, the TKE due to vehicle movement, is determined in the Bäumer scheme by solving the prognostic equation of TKE (*23*), as illustrated in Equation 4:

$$\frac{\partial e_m}{\partial t} = -\frac{\partial (u_i e_m)}{\partial x_i} + \frac{\partial}{\partial x_i}\left(K_i \frac{\partial e_m}{\partial x_i}\right) + P - \epsilon \qquad i = 1, 2, 3 \quad (4)$$

where P and ϵ are the TKE production and dissipation rate, respectively. P and ϵ are estimated in Equations 5 (*20*) and 6 (*23*):

$$P = \frac{1}{2\Omega_1}\left(n_{\text{pc}} c_{d,\text{pc}} \bar{W}_{\text{pc}} \bar{H}_{\text{pc}} \bar{V}_{\text{pc}}^3 + n_{\text{hd}} c_{d,\text{hd}} \bar{W}_{\text{hd}} \bar{H}_{\text{hd}} \bar{V}_{\text{hd}}^3\right) \quad (5)$$

$$\epsilon = c_1 \frac{e_m^{1.5}}{z} \quad (6)$$

where

n = vehicle density (number of vehicles per grid cell);
c_d = vehicle drag coefficient;
$\bar{W}$, $\bar{H}$, and $\bar{V}$ = mean vehicle width, height, and velocity; and
Ω_1 = volume of a model grid cell.

Since the dimensions and speed of the vehicles in a grid cell can be significantly different for passenger cars (pc) and heavy-duty vehicles (hd), their contributions to TKE production is estimated separately. For Equation 6, it can be seen that the dissipation of TKE is inversely proportional to height (z) above surface (*23*). c_1 is a proportionality constant determined through experiments.

Theoretically, the mean wind speed and direction near highways are also affected by the wakes of the passing vehicles. However, in the current model, this wake effect is neglected. Monte Carlo simulations are performed to evaluate the sensitivity of the predicted concentrations to the wind velocity and turbulent diffusivities. The sensitivity studies are discussed in a later section. No specific treatment of the rise of the exhaust plume from the tailpipe is included in the current model. All emissions from the tailpipe are immediately well mixed in the first model layer and are transported to the higher layers through vertical diffusion. It is expected that large K values near the surface should be able to move the pollutants fast enough so that the buoyancy effect can be neglected. This might not be the case when

the atmosphere is very stable due to temperature inversion or small VIT. Future modification of the model will include a proper treatment of the buoyancy effect.

Solution of the Governing Equations

The TAMNROM-3D model can be used to simulate both steady-state and transient pollutant concentrations near highways. Bäumer et al. (*20*) did not describe the solution techniques for this coupled system, so the authors' solution method is described briefly below.

In the transient applications, TAMNROM-3D can take emission and meteorology inputs at user-specified time resolution and Equations 1 to 6 are solved simultaneously with proper initial and boundary conditions. The time resolution of the inputs needs to be on the order of a few minutes or less to make meaningful transient predictions because the predicted concentration fields will reach steady state in a few minutes under typical metrological conditions and domain size (~500 m) if the emission does not change rapidly.

A more typical application is to use the model with hourly emission and meteorology data to predict the steady-state concentrations. In this case, the model first solves Equations 2 to 5 until e_m reaches steady state. Equation 1 is then solved for all species using the updated K fields. The convergence criterion for e_m is shown in Equation 7:

$$\left|\frac{e_m^t - e_m^{t-\Delta t}}{e_m^t + e_m^{t-\Delta t}}\right| < 5\times10^{-6} \qquad \text{for all grid cells} \tag{7}$$

Operator splitting technique (*24*) was employed to solve Equations 1 and 4. The diffusion and advection terms were solved using the Crank–Nicolson method (*25*) and the piecewise parabolic method (*26*), respectively.

MODEL EVALUATION

In this initial model performance study, the ability of the model to predict the dispersion of a nonreactive tracer using the new VIT parameterization discussed previously was evaluated using GM's SF_6 data set. The sensitivity of the predicted concentrations to the model inputs and key model parameters is also discussed. The ability of the model to predict reactive pollutants such as NO, NO_2, and air toxics using the SAPRC-99 photochemical mechanism will be evaluated in a separate paper.

Model Setup to Simulate GM Experiment

GM in 1975 conducted a series of experiments to study the possible human exposure to sulfate near roadways (*27*). SF_6 and sulfate data were collected and only the SF_6 data set is used in this study. The study was undertaken at a 10-km-long looped four-lane testing track at Milford, Michigan, in September and October for 17 days during the morning hours, with four 30-min sampling periods per day. The vehicle fleet comprised 17 pickup trucks, equipped with SF_6 cylinders, and 352 passenger cars that were driven at 80 km h^{-1} by trained drivers. The meteorological conditions and concentrations of SF_6 were measured at six towers and two stands placed in a straight line, as shown in Figure 1. SF_6 concentration data were collected at 0.5, 3.5, and 9 m above the ground, and wind speed and direction were collected at 1.5, 4.5, and 10.5 m on each of those towers. SF_6 concentrations were also measured at the two stands, S1 and S2,

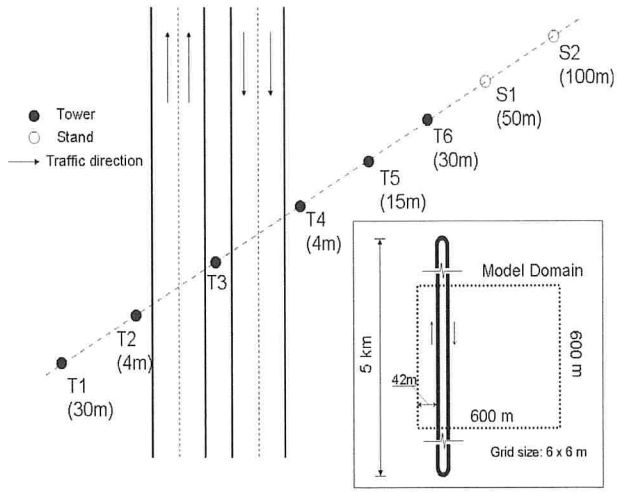

FIGURE 1 Schematic of four-lane testing track at GM and towers and stands where meteorological data and SF_6 concentrations were measured (inset: overview of looped track and the model domain).

which were 0.5 m above surface. Temperature data were collected at 1.5, 4.5, and 10.5 m on Towers 1 and 5. The distances of the towers and stands to the centerline that passes Tower 3 in the middle of the north- and southbound tracks are also shown on the figure.

The inset in Figure 1 shows the rectangular model domain of 600 × 600 m used in this study. The model domain is divided into 100 × 100 grids in the horizontal directions with a grid size of 6 × 6 m. The vertical domain extends to 40 m above surface and is divided into 11 layers. The vertical spacing of grid cells varies from 1 m near the surface to 10 m at the top. The four-lane highway is placed at 42 m from the left boundary and the width of each lane is taken as 6 m, the width of a grid cell. The north- and southbound tracks are separated by 6 m.

For each model simulation, 30-min averaged wind speed and direction measured at the same height from the six towers were averaged and then interpolated vertically. The resulting wind profile is assigned to each vertical column in the model. Temperature at each grid cell was assigned in a similar manner. The interpolated wind speed and temperature were used to estimate the atmospheric diffusivity at each grid cell. Based on the vehicle speed, SF_6 emitter density and the reported emission rate, the emission rate of SF_6 in each highway grid cell is estimated. It was assumed that SF_6 is evenly and continuously emitted from all highway grid cells. In the east and west boundaries, SF_6 concentration was set to zero in the upwind direction and a zero concentration gradient was assumed for the downwind boundary. Because only a small fraction of the entire highway is included in the model domain, periodical boundary condition was used in the north–south boundaries. For example, the south boundary condition of SF_6 for each column is set to be equal to the predicted concentration of SF_6 at the northernmost grid cell of that column.

Results of Base Case Model

The vehicle drag coefficients ($c_{d,\mathrm{pc}}$ and $c_{d,\mathrm{hd}}$) and the TKE dissipation rate (c_1) are empirical parameters used in the production and

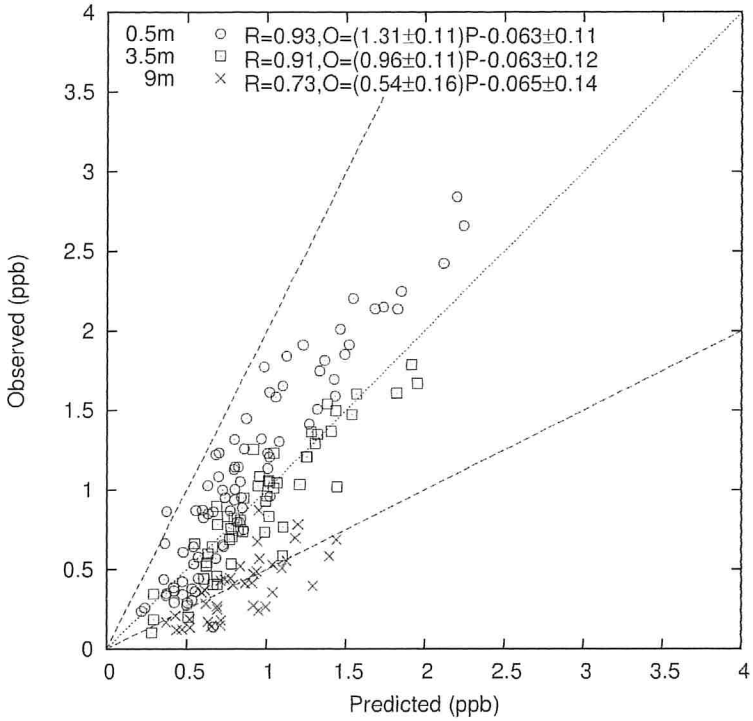

FIGURE 2 Predicted and observed concentrations of SF_6 for all simulated cases at three different elevations (O = observation; P = prediction). Uncertainties shown in the slopes and intercepts reflect the 95% confidence interval of these values.

dissipation terms (Equations 5 and 6, respectively). Since the GM experiments did not include any heavy-duty vehicles, only the drag coefficient for passenger cars ($c_{d,pc}$) needs to be determined. Proper values for the two empirical constants, $c_{d,pc}$ and c_1, were determined through a series of model simulations with different $c_{d,pc}$ and c_1 combinations to minimize the sum of the squared residuals (SSR) between the prediction and observations using the entire GM data set. The best values for $c_{d,pc}$ and c_1 are 0.4 and 8×10^{-3}, respectively.

The experiments were divided in three categories. Category A (225° to 315° from north), Category B (315° to 337.5° and 202.5° to 225°), and Category C (337.5° to 22.5° and 157.5° to 202.5°) represent wind directions that are perpendicular, oblique, and parallel to the highway, respectively. Since the design of the GM experiment assumed a dominant westerly wind and only two samplers were placed to west of the road, easterly wind cases were not included in the analysis.

Figure 2 shows the paired comparison of the observed and predicted SF_6 concentrations for 12 selected 30-min sampling experiments. Four experiments were selected for each wind direction category. The total number of data points included in the figure is 240. The correlation coefficient (R), slope, and interception for a linear fit between predicted and observed concentrations are 0.812, 1.16 (±0.11, 95% confidence interval), and –0.168 (±0.12), respectively. This suggests that the slope is statistically close to 1 and the intercept is close to 0. Most of the data points fall between the 2:1 and 1:2 lines. The data points were grouped based on the height where the observations were made. The linear fit parameters with 95% confidence interval and the correlation coefficients for each group are also shown on Figure 2. Highest concentrations generally occur at the surface and the model slightly underpredicts these concentrations. The model performance appears to be best for the concentrations measured at 3.5 m above surface. At 9 m above surface, the model overpredicts the concentrations.

The model performance was further evaluated using statistical measures of fractional bias (FB) and normalized mean squared error (NMSE). Table 1 shows the comparison of the FB and NMSE from TAMNROM-3D and ROADWAY-2 models, which also reported model performance with GM's SF_6 data set. Both models slightly underpredict the concentrations under perpendicular wind conditions with a similar model performance. TAMNROM-3D performs significantly better for oblique wind cases with a small overprediction. Both models perform well under parallel wind conditions. Further analysis showed that 90% of the TAMNROM-3D predictions

TABLE 1 FB and NMSE for TAMNROM-3D and ROADWAY-2

	TAMNROM-3D		ROADWAY-2	
Wind Category	FB	NMSE	FB	NMSE
Perpendicular (A)	–0.07	0.15	–0.11	0.30
Oblique (B)	0.05	0.15	–0.55	0.52
Parallel (C)	0.05	0.12	0.12	0.10
Overall	0.001	0.13	–0.18	0.29

NOTE: $FB = 2(\bar{P} - \bar{O})/(\bar{O} + \bar{P})$, $NMSE = (\bar{P}_i - \bar{O}_i)^2/(\bar{O} \times \bar{P})$, where $\bar{O}$ and $\bar{P}$ are mean observed and predicted concentrations.

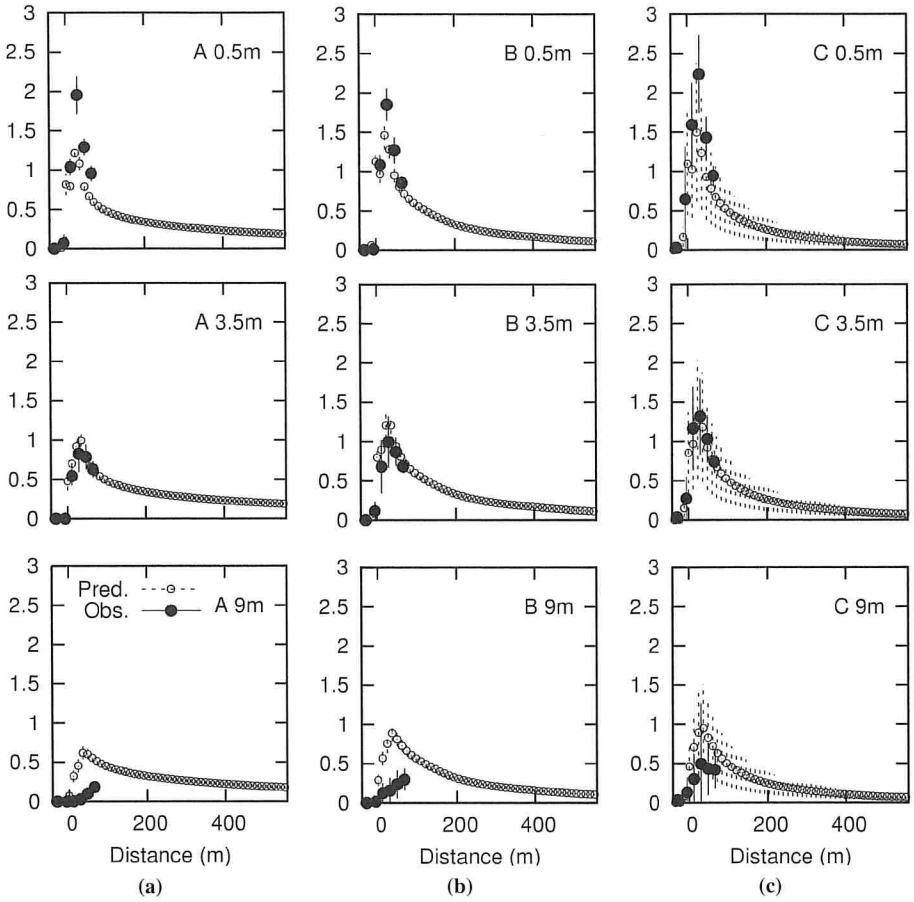

FIGURE 3 Observed and predicted spatial distribution of SF_6 concentrations averaged over all data points analyzed at 0.5, 3.5, and 9 m above the surface for wind categories A, B, and C (units are parts per billion).

were within a factor of 2 of the observed concentrations, compared to 80% for the ROADWAY2 model. Overall, TAMNROM-3D satisfactorily reproduced the SF_6 experiments at all wind directions. A similar comparison with the UCD 2001 model indicated that the TAMNROM-3D performs similar to the UCD 2001 model, which performs better than CALINE models (*11*).

Figure 3 shows the observed and predicted concentrations for wind categories—perpendicular (A), oblique (B), and parallel (C)—at three elevations above the surface along the downwind distance from the simulated highway. Error bars on each data point represent standard deviation from the mean value. Averaged over all cases, the predicted peak SF_6 concentrations at 0.5 m are in the range of 1.2 to 1.5 ppb for three wind categories. The observed concentrations are around 2 to 2.2 ppb. The difference between the prediction and observation decreased at downwind locations. At 3.5 m, the model predictions agree well with observations at all locations. The observed spatial gradients of SF_6 are also well reproduced. Both predictions and observations show that highest concentrations occur when the wind is parallel to the highway. The panels on the third row show that the model overpredicts the concentrations at 9 m above surface. Errors in the predicted diffusivity fields or wind fields are the likely causes for this overprediction.

Figure 4 illustrates the importance of the VIT parameterization in predicting pollutant concentrations in a near-road environment.

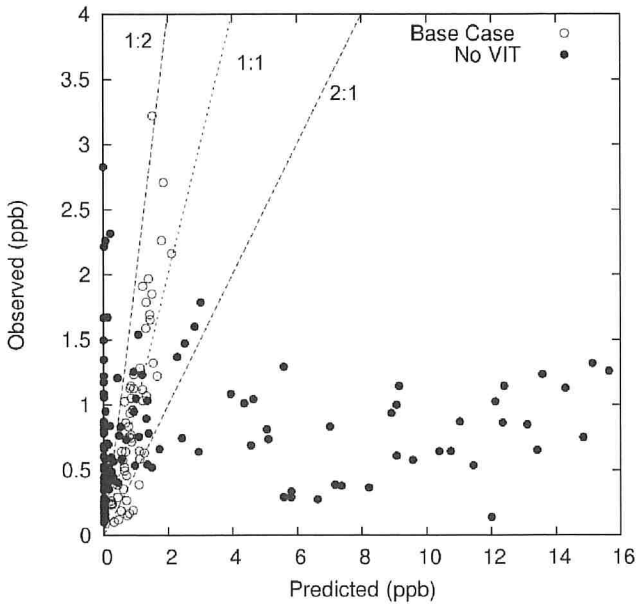

FIGURE 4 Predicted SF_6 concentrations compared with observations when VIT is not considered (base case results with VIT also shown).

Open circles show the comparison of the base case predictions with observations as shown in Figure 2. The filled circles are the predicted SF_6 concentrations when the VIT is not included in the dispersion calculation (i.e., only advection and diffusion due to atmospheric turbulence were included). Without VIT, the concentrations are significantly over- and underpredicted. A close look at the model results shows that surface concentrations are significantly overpredicted, while concentrations at 3.5 and 9 m are generally underpredicted.

Sensitivity Analysis

Meteorology Inputs

A Monte Carlo technique was used to estimate the uncertainty in predicted SF_6 concentrations due to uncertainty in wind speed and diffusivity. One hundred simulations were conducted for a representative case in each wind category using randomly generated wind speeds and diffusivities that follow a normal distribution curve with a standard deviation of 30% around the original wind speed and diffusivity. Typical uncertainty of the wind speed and direction measurements is only a few percent. However, using average wind in this simulation and the vertical interpolation scheme may introduce additional uncertainties. Although wind speed and turbulent diffusivity are related, they were treated as independent variables in this analysis. The mean values and standard deviations for the predicted SF_6 concentrations at monitor locations were determined from all the simulations and were compared to observations in Figure 5*a*. The mean values from the Monte Carlo simulation agree with the base case predictions. The error bars on predictions represent 1 SD (σ) from the mean and the error bars on observations indicate a measurement accuracy of $\pm 3\%$ (1σ) (*27*). Thirty percent uncertainties in the meteorology lead to uncertainties of 0.1 to 0.2 ppb in most cases. The magnitude of the uncertainty appears not to be correlated with the absolute value of the predicted concentration. The data points with smaller uncertainty of the predicted values are from the parallel wind case, which can be understood easily.

Vehicle Drag Coefficient and TKE Dissipation Rate

Vehicle drag coefficient and TKE dissipation rate directly affect the intensity of TKE created by moving vehicles and thus indirectly affect the overall turbulent diffusivity and the pollutant concentrations. In order to better understand the sensitivity of the predicted concentrations to the selection of the vehicle drag coefficient ($c_{d,\mathrm{pc}}$) and the proportionality constant (c_1), another set of Monte Carlo simulations was conducted by assuming an uncertainty of 50% for both parameters.

Similar to the meteorology inputs study, 100 simulations were conducted for a representative case in each wind category using randomly generated positive values for $c_{d,\mathrm{pc}}$ and c_1 that follow a normal distribution curve with a standard deviation of 50% around the original $c_{d,\mathrm{pc}}$ and c_1 values of 0.4 and 8×10^{-3}, respectively. If either c_1 or $c_{d,\mathrm{pc}}$ was negative, this simulation was skipped. Thus, approximately 5% of simulations were neglected from the analysis. The predicted mean values of the SF_6 concentrations from the Monte Carlo simulations were compared with the base case predictions and no deviation was detected. It can be seen from Figure 5*b* that the uncertainties in c_1 and $c_{d,\mathrm{pc}}$ more effectively affect the concentrations near the surface when the concentrations are high but not significantly at 9.5 m above surface with generally low concentrations.

An additional simulation using the default $c_{d,\mathrm{pc}}$ and c_1 values of 0.3 and 0.1 as reported by Bäumer et al. (*20*) leads to slightly worse model performance. The R, slope, and interception values are 0.76, 1.59 ($\pm$ 0.22), and –0.27 ($\pm$ 0.17), respectively. This suggests that the proper $c_{d,\mathrm{pc}}$ and c_1 values are likely dependent on aerodynamic properties of vehicles and also metrology conditions. The lower $c_{d,\mathrm{pc}}$ value reported by Bäumer et al. might be due to less aerodynamic drag of the vehicles made in 1990s than of the vehicles made in 1970s. Although $c_{d,\mathrm{pc}}$ can be estimated with relative high confidence, more near-road data sets need to be analyzed in future studies to better estimate c_1 under various meteorology conditions. In the absence of observation data to fit the two parameters, the default values should be used as a first-order estimate.

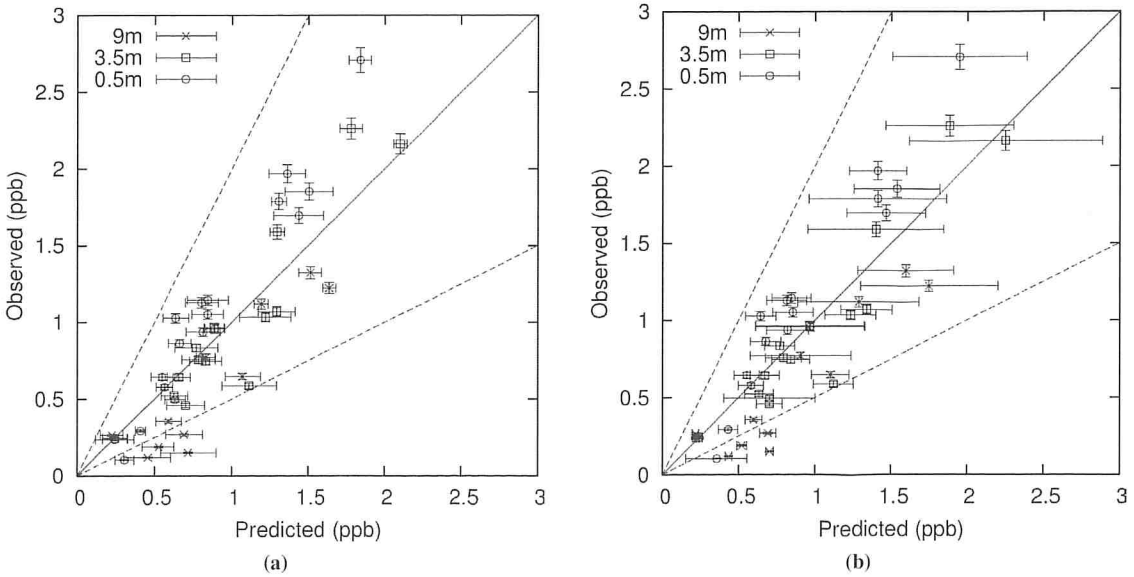

FIGURE 5 Uncertainty of predicted SF_6 concentrations because of (*a*) 30% uncertainties in the wind speed and atmospheric turbulent diffusivity and (*b*) 50% uncertainties in the model parameters $c_{d,\mathrm{pc}}$ and c_1.

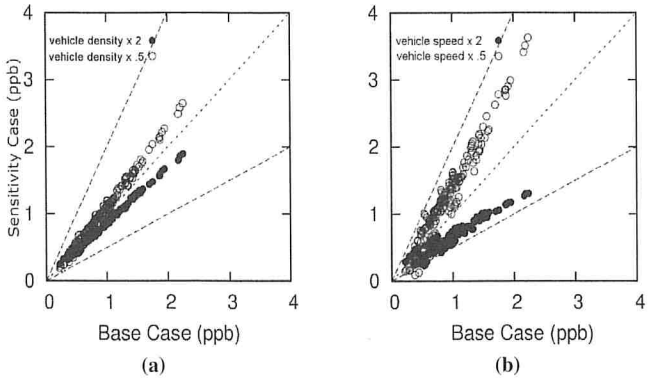

FIGURE 6 Sensitivity of predicted SF_6 concentrations to change in (*a*) vehicle density and (*b*) speed (other parameters are unchanged).

Vehicle Speed and Density

This section explores the variability of the model results due to variation in the vehicle speed and density. Figure 6*a* shows the change in predictions when the vehicle density in each grid cell is doubled or halved keeping the vehicle speed and SF_6 emission rate at each grid cell constant. The peak concentrations changed by only approximately ±20%, indicating that the model is less sensitive to the vehicle density alone. Figure 6*b* shows the sensitivity of the model to vehicle speed, when the vehicle density and the emission rate of SF_6 remain constant. It can be seen from the figure that doubling the vehicle speed by a factor of 2 leads to a reduction of the peak concentrations by approximately 50% compared to the base case. Similarly, a decrease in vehicle speed by 50% increases the peak concentrations by approximately a factor of 2. As expected, the model is more sensitive to the vehicle speed than the vehicle density because the TKE production is linearly proportional to the vehicle density but proportional to vehicle speed cubed.

Vertical Grid Resolution

In Eulerian models, space is discretized into a finite number of grid cells. Generally, higher grid resolution will lead to more accurate predictions. However, higher-resolution simulations are slower and require more computation resources. The sensitivity of the predicted concentrations to the vertical grid resolution is studied here by using a finer vertical grid setup. The number of vertical layers is increased from 11 to 30. The first 20 layers have a resolution of 1 m and the remaining 10 layers have a resolution of 2 m. Figure 7 shows the predicted vertical profiles of SF_6 concentrations averaged using all the data points at Tower 4. The results from the coarse grid are slightly lower than the fine-resolution results when the wind is parallel (Category A) or oblique (Category B) to the highway, with differences less than 5%. The fine-resolution results agree very closely with the low-resolution results for parallel cases (Category C).

DISCUSSION OF RESULTS

TAMNROM-3D is not designed to be another operational model for routine near-road air quality simulation but a tool to assist traffic planning and advanced near-road air quality research. For example, the model can be used to estimate the potential air quality impact of a proposed roadway based on the estimated traffic flow and prevailing wind. Traffic flow can be modeled and meteorology observations are available from regional or local monitoring stations. TAMNROM-3D needs to be further validated with additional near-road air quality data sets under different meteorology, traffic, and emission conditions to better understand the range of the proportional constant c_1. A guideline of selecting the proper c_1 value should be developed before the model can be applied by transport planning agencies.

The authors will integrate chemical and physical processes in the model to simulate the detailed transformation of air pollutants emitted from roadways. For example, recent theoretical and experimental studies have shown that size, chemical composition, and number concentration of the ultrafine particles emitted from highway vehicles change rapidly as they are transported away from the highway due to gas-to-particle partitioning of semivolatile organic compounds and coagulation processes (*2, 28, 29*). These processes are difficult to be properly included in the current near-road air quality models but can be implemented in a 3-D Eulerian modeling framework.

ACKNOWLEDGMENTS

This research is supported by the University Transportation Center for Mobility at the Texas Transportation Institute, funded by the U.S. Department of Transportation's University Transportation Centers program. The authors thank Tony Held for providing the

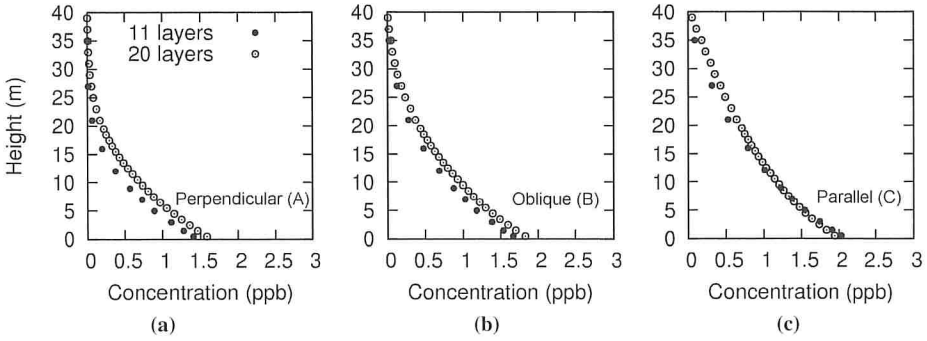

FIGURE 7 Comparison of vertical SF_6 concentration profiles at Tower 4 predicted by base case model and the model with finer vertical resolution (first 20 layers).

GM data set and useful discussions and three anonymous reviewers for suggestions that improved the quality of the paper.

REFERENCES

1. Gray, H. A., and G. R. Cass. Source Contributions to Atmospheric Fine Carbon Particle Concentrations. *Atmospheric Environment,* Vol. 32, No. 22, 1998, pp. 3805–3825.
2. Zhu, Y., W. C. Hinds, S. Kim, S. Shen, and C. Sioutas. Study of Ultrafine Particles Near a Major Highway with Heavy-Duty Diesel Traffic. *Atmospheric Environment,* Vol. 36, No. 27, 2002, pp. 4323–4335.
3. Lloyd, A. C., and T. A. Cackette. Diesel Engines: Environmental Impact and Control. *Journal of the Air and Waste Management Association,* Vol. 51, No. 6, 2001, pp. 809–847.
4. Brugge, D., J. Durant, and C. Rioux. Near-Highway Pollutants in Motor Vehicle Exhaust: A Review of Epidemiologic Evidence of Cardiac and Pulmonary Health Risks. *Environmental Health,* Vol. 6, No. 1, 2007, p. 23.
5. Venn, A. J., S. A. Lewis, M. Cooper, R. Hubbard, and J. Britton. Living Near a Main Road and the Risk of Wheezing Illness in Children. *American Journal of Respiratory and Critical Care Medicine,* Vol. 164, No. 12, 2001, pp. 2177–2180.
6. Boriboonsomsin, K., and M. J. Barth. Evaluating Air Quality Benefits of Freeway High-Occupancy Vehicle Lanes in Southern California. In *Transportation Research Record: Journal of the Transportation Research Board, No. 2011,* Transportation Research Board of the National Academies, Washington, D.C., 2007, pp. 137–147.
7. Savonis, M. J. Toward a Strategic Plan for Transportation–Air Quality Research, 2000–2010. In *Transportation Research Record: Journal of the Transportation Research Board, No. 1738,* TRB, National Research Council, Washington, D.C., 2000, pp. 68–73.
8. Adler, K., M. Grant, and W. Schroeer. Emissions Reduction Potential of the Congestion Mitigation and Air Quality Improvement Program: A Preliminary Assessment. In *Transportation Research Record 1641,* TRB, National Research Council, Washington, D.C., 1998, pp. 81–88.
9. Gauderman, W. J., H. Vora, R. McConnell, K. Berhane, F. Gilliland, D. Thomas, F. Lurmann, E. Avol, N. Kunzli, M. Jerrett, and J. Peters. Effect of Exposure to Traffic on Lung Development from 10 to 18 Years of Age: A Cohort Study. *Lancet,* Vol. 369, No. 9561, 2007, pp. 571–577.
10. Benson, P. E. A Review of the Development and Application of the CALINE3 and 4 Models. *Atmospheric Environment Part B: Urban Atmosphere,* Vol. 26, No. 3, 1992, pp. 379–390.
11. Held, T., D. P. Y. Chang, and D. A. Niemeier. UCD 2001: An Improved Model to Simulate Pollutant Dispersion from Roadways. *Atmospheric Environment,* Vol. 37, No. 38, 2003, pp. 5325–5336.
12. Kim, B. Y., R. L. Wayson, and G. G. Fleming. Development of the Traffic Air Quality Simulation Model. In *Transportation Research Record: Journal of the Transportation Research Board, No. 1987,* Transportation Research Board of the National Academies, Washington, D.C., 2006, pp. 73–81.
13. Zannetti, P. *Air Pollution Modeling—Theories, Computational Methods and Available Software.* Van Nostrand Reinhold, New York, 1990.
14. Sahlodin, A. M., R. Sotudeh-Gharebagh, and Y. Zhu. Modeling of Dispersion Near Roadways Based on the Vehicle-Induced Turbulence Concept. *Atmospheric Environment,* Vol. 41, No. 1, 2007, pp. 92–102.
15. Eskridge, R. E., F. S. Binkowski, J. C. R. Hunt, T. L. Clark, and K. L. Demerjian. Highway Modeling. Part II: Advection and Diffusion of SF6 Tracer Gas. *Journal of Applied Meteorology,* Vol. 18, No. 4, 1979, pp. 401–412.
16. Eskridge, R. E., and J. C. R. Hunt. Highway Modeling. Part I: Prediction of Velocity and Turbulence Fields in the Wake of Vehicles. *Journal of Applied Meteorology,* Vol. 18, No. 4, 1979, pp. 387–400.
17. Eskridge, R. E., and R. S. Thompson. Experimental and Theoretical-Study of the Wake of a Block-Shaped Vehicle in a Shear-Free Boundary Flow. *Atmospheric Environment,* Vol. 16, No. 12, 1982, pp. 2821–2836.
18. Rao, K. S. ROADWAY-2: A Model for Pollutant Dispersion Near Highways. *Water, Air, & Soil Pollution: Focus,* Vol. 2, No. 5, 2002, pp. 261–277.
19. Rao, K. S., R. L. Gunter, J. R. White, and R. P. Hosker. Turbulence and Dispersion Modeling Near Highways. *Atmospheric Environment,* Vol. 36, No. 27, 2002, pp. 4337–4346.
20. Bäumer, D., B. Vogel, and F. Fiedler. A New Parameterisation of Motorway-Induced Turbulence and Its Application in a Numerical Model. *Atmospheric Environment,* Vol. 39, No. 31, 2005, pp. 5750–5759.
21. Garratt, J. R. *The Atmospheric Boundary Layer.* Cambridge Atmospheric and Space Science Series. Press Syndicate of the University of Cambridge, New York, 1994.
22. Jacobson, M. Z. *Fundamentals of Atmospheric Modeling.* Cambridge University Press, New York, 1998.
23. Stull, R. B. *An Introduction to Boundary Layer Meteorology.* Kluwer Academic Publishers, Dordrecht, Netherlands, 1988.
24. McRae, G. J., W. R. Goodin, and J. H. Seinfeld. Development of a Second-Generation Mathematical Model for Urban Air Pollution. Part I: Model Formulation. *Atmospheric Environment (1967),* Vol. 16, No. 4, 1982, pp. 679–696.
25. Crank, J., and P. Nicolson. A Practical Method for Numerical Evaluation of Solutions of Partial Differential Equations of the Heat-Conduction Type. *Proceedings of the Cambridge Philosophical Society,* Vol. 43, 1947, pp. 50–67.
26. Corlella, P., and P. R. Woodward. Piecewise Parabolic Method (PPM) for Gas-Dynamical Simulations. *Journal of Computational Physics,* Vol. 54, No. 1, 1984, pp. 174–201.
27. Cadle, S. H., et al. *Results of the General Motors Sulfate Dispersion Experiment.* General Motors Research Laboratories, Warren, Mich., 1976.
28. Clements, A. L., Y. Jia, A. Denbleyker, E. McDonald-Buller, M. P. Fraser, D. T. Allen, D. R. Collins, E. Michel, J. Pudota, D. Sullivan, and Y. Zhu. Air Pollutant Concentrations Near Three Texas Roadways. Part II: Chemical Characterization and Transformation of Pollutants. *Atmospheric Environment,* Vol. 43, No. 30, 2009, pp. 4523–4534.
29. Zhang, K. M., A. S. Wexler, Y. F. Zhu, W. C. Hinds, and C. Sioutas. *Evolution of Particle Number Distribution Near Roadways. Part II: The "Road-to-Ambient" Process. Atmospheric Environment,* Vol. 38, No. 38, 2004, pp. 6655–6665.

The Transportation and Air Quality Committee peer-reviewed this paper.

Comprehensive Field Study of Fuel Use and Emissions of Nonroad Diesel Construction Equipment

H. Christopher Frey, William Rasdorf, and Phil Lewis

Limited field data are available for analyses of fuel use and emissions of nonroad diesel construction equipment. This paper summarizes the results of field research that used a portable emissions monitoring system to collect fuel use and emissions data from eight backhoes, six bulldozers, three excavators, four generators, six motor graders, three off-road trucks, one skid-steer loader, three track loaders, and five wheel loaders while they performed various duty cycles. These tests produced approximately 119 h of field data for petroleum diesel and approximately 48 h for B20 biodiesel. Engine attribute data including horsepower, displacement, model year, engine tier, and engine load were collected to determine these factors' influence on fuel use rates and emission rates of nitrogen oxides, hydrocarbons, carbon monoxide, carbon dioxide, and opacity. Mass per time fuel use rates were developed for each item of equipment, as were mass per time and mass per fuel used emission rates for each pollutant. For petroleum diesel, fuel use and emission rates of each pollutant were found to increase with engine displacement, horsepower, and load and to decrease with model year and engine tier. The results were qualitatively similar for B20 biodiesel. Fuel-based emission rates were found to have less variability and less sensitivity to engine size and load than time-based emission rates. Where possible, development of emission inventories based on fuel consumed, rather than time of activity, is preferred.

There are more than 2 million items of diesel construction and mining equipment in the United States that consume almost 6 billion gallons of diesel fuel per year (*1*). This equipment emits nitrogen oxides (NO_x), hydrocarbons (HC), carbon monoxide (CO), particulate matter (PM), and carbon dioxide (CO_2). Fuel use and emissions estimates for construction equipment are typically based on steady-state engine dynamometer tests using uninstalled stationary engines in a laboratory; however, these tests do not represent in-use equipment activity. There is a need to determine fuel use and emission rates based on in-use measurements. Field data can be used to quantify construction equipment activity and the influence of equipment duty cycles on fuel use and emissions.

North Carolina State University recently completed two field studies that quantified the fuel use, emissions, and engine performance data of 39 items of diesel-powered construction equipment as they performed common construction duty cycles on job sites (*2, 3*). The equipment includes eight backhoes, six bulldozers, three excavators, four generators, six motor graders, three off-road trucks, one skid-steer loader, three track loaders, and five wheel loaders. These items were tested while fueled with petroleum diesel. Furthermore, five of the backhoes, all six motor graders, and four of the wheel loaders were also tested with B20 biodiesel, for a total of 54 field measurements. This research has produced an unprecedented database of real-world fuel use and emissions field data for diesel construction equipment. Although portions of these data are published in specific case studies, there has not yet been a comprehensive overview of trends within these extensive data.

The objective of this paper is to report and assess trends in this large body of field data. The results include engine size, engine model year, and engine tier; engine performance data related to engine load; representative duty cycles of the work performed by the equipment at the job site; and the related fuel use rates and emission rates of NO_x, HC, CO, CO_2, and PM. These data can be used to develop and improve diesel emission inventories, evaluate diesel emissions reduction programs and regulations, model diesel equipment fuel use and emissions, assess air quality impacts of alternative fuels, estimate CO_2 emissions from diesel construction equipment, and develop fuel and emission inventories for construction projects.

RELATED WORK

There has been a lack of field data for in-use fuel consumption and emissions characteristics of construction equipment. The Environmental Protection Agency (EPA), West Virginia University, and Clean Air Technologies International, Inc. (CATI) have conducted onboard in-use measurements of emissions from construction equipment (*4–6*). Not all of these data were quality assured nor are they all available for public use. Furthermore, it is not possible to investigate the relationship between the activity duty cycles versus fuel use and emissions based on these data.

Abolhasani et al. (*7*) evaluated the fuel use and emissions of excavators performing duty cycles in the field. Frey et al. (*8*) performed a comparison of petroleum diesel versus B20 biodiesel emissions from backhoes, motor graders, and wheel loaders performing field activities based on field data. Frey et al. (*9*) characterized the field activity, fuel use, and emissions of selected motor graders fueled with petroleum diesel and B20 biodiesel. Lewis et al. (*10*) examined requirements and incentives for reducing emissions from construction equipment and also advocated the use of field emissions data versus emissions data obtained from engine dynamometer tests. Lewis et al. (*11*) discussed the development and use of an emissions inventory

Department of Civil, Construction, and Environmental Engineering, North Carolina State University, Raleigh, NC 27695-7908. Corresponding author: H. C. Frey, frey@ncsu.edu.

Transportation Research Record: Journal of the Transportation Research Board, No. 2158, Transportation Research Board of the National Academies, Washington, D.C., 2010, pp. 69–76.
DOI: 10.3141/2158-09

for a fleet of backhoes, front-end loaders, and motor graders to make fleet management decisions related to replacing older equipment with newer equipment. Pang et al. (*12*) quantified the tailpipe emissions and fuel cycle energy use for petroleum diesel and B20 biodiesel to support a comprehensive comparison of the difference in total fossil energy use, greenhouse gas emissions, and air pollutant emissions for substitution of B20 in place of petroleum diesel. Frey and Bammi (*13*) developed probabilistic emission factors for NO_x and HC based on engine dynamometer data from nonroad mobile sources including construction, farm, and industrial engines. Frey et al. (*14*) used field data from dump trucks to develop link-based emission factors for NO_x, HC, CO, and PM. Although these were highway vehicles, this type of equipment is used extensively in construction and can be used to estimate the overall impact of emissions from construction activities.

METHODOLOGY

This section provides a brief overview of the field data collection and analysis process. Detailed documentation of these procedures is provided by Frey et al. (*3*) and Rasdorf et al. (*15*).

Field Data Collection

An onboard portable emissions monitoring system (PEMS) was used to gather engine, fuel use, and emissions data directly from in-use construction equipment. The PEMS used was the Montana System manufactured by CATI (*16*). The PEMS was secured to the body of the equipment. Sensors were connected to the engine to collect engine performance data related to engine speed, intake air temperature, and engine load. Tailpipe exhaust samples were drawn continuously to measure exhaust concentrations of NO_x, HC, CO, CO_2, and PM. These data were collected on a second-by-second basis, typically for 3 h or more.

The original field data (referred to as "raw data") underwent a rigorous quality assurance process to determine whether any errors or problems existed. This process is documented in detail by Frey et al. (*3*). If any errors were found, they were corrected when possible. If the errors could not be corrected, the affected data were removed. The purpose of the quality assurance process was to produce a valid set of data (referred to as "processed data").

Engine Attributes

Engine attributes that affect performance, fuel use, and emissions include engine size, engine age, engine tier, and engine load. Engine size is quantified based on rated horsepower and displacement. This information was collected in the field and verified with the engine manufacturer's specifications, found in publications such as the *Caterpillar Performance Handbook* (*17*).

As engines increase in age, their performance may deteriorate (*18*). Consequently, engines may produce more emissions as they get older. Engine age was represented by the engine model year. Engine hours of operation are another attribute that can be used to measure engine age; however, insufficient data were collected for engine hours and therefore are not reported.

In 1994, EPA adopted an engine tier classification system for all new nonroad diesel engines. Engine tiers are emission standards that require diesel engines manufactured after a specified date to meet the performance levels specified in the standards. The EPA engine tier classifications include successive Tier 1, Tier 2, Tier 3, Tier 4 Transitional, and Tier 4 Final, which are effective in reducing emissions in a phased sequence from 1996 to 2013. Engine tiers are essentially a hybrid engine attribute based on engine size (horsepower rating) and engine age (model year). The engine tier of each item of equipment was recorded.

Engine load affects the fuel use and emission rates of construction equipment. The variables that were monitored by the PEMS include engine speed measured in revolutions per minute (rpm), engine intake air temperature (IAT) measured in degrees Celsius, and pressure-based engine load measured by manifold absolute pressure (MAP) in units of kilopascals (kPa).

Of the variables that were monitored, MAP has been consistently identified as highly correlated with fuel use and emission rates (*3*) and is often used as a surrogate for engine load. Since the equipment had various ranges of MAP values, the values were normalized on a consistent basis to enable comparisons between engines. The recorded second-by-second MAP values for a specific item of equipment were normalized according to the following equation:

$$MAP_{nor} = \frac{MAP - MAP_{min}}{MAP_{max} - MAP_{min}}$$

where

MAP_{nor} = normalized MAP for a measured MAP for a specific item of equipment,
MAP = measured MAP for a specific item of equipment,
MAP_{min} = minimum MAP for a specific item of equipment, and
MAP_{max} = maximum MAP for a specific item of equipment.

Normalized MAP values range from zero to one, thus representing a percentage of in-use engine loads.

Representative Duty Cycles

The duty cycle of the equipment used for a construction activity has its own distinct sequence of activities that affect the engine performance, fuel use, and emissions characteristics. A representative duty cycle for each item of equipment that was monitored during field data collection was defined. Although it is possible to describe the equipment's duty cycle in great detail, these representative duty cycles were intended only to provide the general nature of the work being performed by the equipment. Each duty cycle was subdivided into activity modes, including idling, moving, or working with an attachment such as a bucket or a blade. The representative duty cycles were used to evaluate relationships among equipment activity, engine performance data, and fuel use and emission rates.

Average Fuel Use and Emission Rates

Second-by-second equipment fuel use was computed on a mass per time basis of grams per second (g/s), based on the measured engine variables and exhaust composition. The average fuel use for each item of equipment is reported in units of gallons of fuel used per hour (gal/h). The PEMS also measured the second-by-second emission rate of each pollutant on a mass per time basis of grams per second.

The average mass per time emission rate of each pollutant for each item of equipment is reported in units of grams per hour.

Fuel-based emission rates, which quantify the mass of emissions per unit of fuel consumed, were estimated based on a carbon balance of the exhaust composition and the fuel properties. The average of the mass per fuel used emission rates for each item of equipment is reported in units of grams per gallon of fuel used (g/gal).

The term "fuel-based emission factors" only refers to estimating emissions per unit of fuel consumed (grams of pollutant per gallon of fuel consumed), as opposed to estimating emissions per unit of engine shaft output (grams per brake horsepower-hour, g/bhp-h) as has been the typical practice using engine dynamometers. It is not possible to measure engine shaft output during actual operations; therefore, g/bhp-h emission factors are not a convenient basis for developing practical emission inventories. Furthermore, the results of this research will indicate that fuel-based emission factors have less variability than time-based (gram of pollutant emitted per hour of operation) emission factors. Since one objective of this work is to support improved emission inventories, the most convenient form of an emission factor can be selected, irrespective of the regulatory framework used for engine certification testing. A fuel-based emission factor can be developed for any fuel and thus does not imply or exclude any particular regulatory approach.

The average fuel use and emission rates of each pollutant were measured for all 39 items of equipment while they were fueled with petroleum diesel. Furthermore, five backhoes, six motor graders, and four wheel loaders were tested a second time while fueled with B20 biodiesel, thus providing a basis for comparison of fuel use and emission rates of construction equipment while using different types of fuel. The methodology used to collect the data was the same for each fuel type.

RESULTS

This section provides the results of the field data collection for the equipment that was tested. These results include engine attributes, representative duty cycles, and average fuel use and emission rates. Analyses of trends in the data are also provided.

Field Data Collection

The 54 tests yielded more than 665,000 s (185 h) of raw data. After the quality assurance process, nearly 604,000 s (168 h) of processed data remained. Approximately 9% of the raw data were deemed invalid by the quality assurance process and were not included in the final processed data set; thus, approximately 91% of the data collected in the field were available for use. Of the processed data, approximately 119 h were associated with equipment fueled with petroleum diesel and approximately 48 h were associated with B20 biodiesel.

The PEMS estimated accurate emissions data for NO_x, CO, and CO_2. The emission rates of these pollutants are of the same magnitude of those found in other data sources, such as the EPA NONROAD model (*1, 19*). The HC data tend to be biased low. The PM detection method for the PEMS is analogous to opacity. The field measurements are useful for relative comparisons of PM emission rates for different fuels or equipment types, but not for characterization of the absolute magnitude of PM emissions. The PM data reported here could be low by an order of magnitude according to previous comparisons of the opacity-based measurements to other PM data. Battelle (*20*) provides a detailed evaluation of the reporting accuracy of the PEMS.

Engine Attributes

Table 1 summarizes the engine attributes of the tested equipment. The rated horsepower of the equipment ranged from 44 hp for a skid-steer loader to 306 hp for an off-road hauler truck. The engine displacement ranged from 2.0 L for a skid-steer loader to 14.2 L for a bulldozer. The engine model years ranged from 1988 to 2007, with one engine from the 1980s, 12 engines from the 1990s, and 26 engines from the 2000s; thus, the majority of the engines were less than 10 years old when they were tested. Engine Tiers 0 through 3 were represented in the data set, with six Tier 0 engines, 19 Tier 1 engines, 13 Tier 2 engines, and one Tier 3 engine. The latter was a new motor grader that recently had been placed into service. Engine loads and their relationship to duty cycles are discussed in the following section.

TABLE 1 Summary of Engine Attributes

Equipment	Horsepower (HP)	Displacement (liters)	Model Year	Engine Tier
Backhoe 1	88	4.0	2004	2
Backhoe 2	88	4.2	1999	1
Backhoe 3	88	4.2	2000	1
Backhoe 4	97	3.9	2004	2
Backhoe 5	90	4.2	1997	0
Backhoe 6	90	4.2	2001	1
Backhoe 7	99	4.5	1999	1
Backhoe 8	97	4.5	2004	2
Bulldozer 1	89	5.0	1988	0
Bulldozer 2	95	3.9	2002	1
Bulldozer 3	90	5.0	2003	1
Bulldozer 4	175	10.5	1998	1
Bulldozer 5	285	14.2	1995	0
Bulldozer 6	99	4.2	2005	2
Excavator 1	254	8.3	2001	1
Excavator 2	138	6.4	2003	2
Excavator 3	93	3.9	1998	1
Generator 1	90	4.5	2002	1
Generator 2	150	6.8	2004	2
Generator 3	200	6.8	2004	2
Generator 4	177	6.8	2003	2
Motor Grader 1	195	8.3	2001	1
Motor Grader 2	195	7.1	2004	2
Motor Grader 3	195	8.3	2001	1
Motor Grader 4	167	8.3	1990	0
Motor Grader 5	160	8.3	1993	0
Motor Grader 6	198	7.2	2007	3
Off-Road Truck 1	306	9.6	2005	2
Off-Road Truck 2	285	10.3	1998	1
Off-Road Truck 3	285	10.3	1998	1
Skid Steer Loader 1	44	2.0	2003	1
Track Loader 1	121	7.2	1998	1
Track Loader 2	70	4.5	1997	0
Track Loader 3	127	7.2	2006	2
Wheel Loader 1	149	5.9	2004	2
Wheel Loader 2	130	5.9	2002	1
Wheel Loader 3	130	5.9	2002	1
Wheel Loader 4	126	5.9	2002	1
Wheel Loader 5	133	6.0	2005	2
Maximum	306	14.2	2007	3
Minimum	44	2.0	1988	0

Representative Duty Cycles

The representative duty cycle for each item of tested equipment is summarized in Table 2 for the equipment fueled with petroleum diesel and in Table 3 for the equipment fueled with B20 biodiesel. These duty cycles were related to grading and earthwork activities commonly performed on construction sites, such as moving soil, moving rock, moving building materials, loading trucks, rough grading, fine grading, excavating soil, clearing and grubbing, and shaping soil stockpiles. For motor graders, the resurface duty cycle refers to a dirt road maintenance activity that involved smoothing ruts in the road surface while using the full length of the motor grader's

TABLE 2 Summary Data for Petroleum Diesel

			Average Time-Based Fuel & Emission Rates						Average Fuel-Based Emission Rates[a]			
Equipment	Duty Cycle	Load (%)	Fuel (gal/h)	NO_x (g/h)	HC (g/h)	CO (g/h)	CO_2 (g/h)	Opacity (g/h)	NO_x (g/gal)	HC (g/gal)	CO (g/gal)	Opacity (g/gal)
BH 1	Load truck	5	0.5	60	14	25	4,791	0.1	124	34	65	0.2
BH 2	Move material	16	1.1	112	9	35	10,535	1.1	99	12	38	1.1
BH 3	Move soil	19	0.8	73	7	15	8,360	1.3	82	10	23	2.1
BH 4	Move soil	20	0.5	64	6	5	4,611	0.3	172	14	11	0.8
BH 5	Load truck	23	1.8	206	27	154	18,175	2.1	111	15	80	1.1
BH 6	Load truck	30	2.1	222	24	73	20,795	2.2	106	12	35	1.1
BH 7	Move soil	19	0.8	112	7	52	8,035	0.7	164	13	61	0.8
BH 8	Move soil	19	0.5	69	6	10	4,764	0.4	168	17	27	0.9
	Average	19	1.0	115	13	46	10,008	1.0	128	16	43	1.0
BD 1	Rough grade	23	1.7	252	16	63	16,658	2.3	180	17	59	1.3
BD 2	Fine grade	14	0.9	92	14	28	8,540	0.7	119	22	52	0.6
BD 3	Fine grade	14	1.4	228	18	91	14,221	2.3	165	19	123	1.5
BD 4	Rough grade	27	3.4	613	39	131	34,311	2.9	214	18	51	1.0
BD 5	Stockpile	48	10.1	1,913	33	240	100,647	N/A[b]	204	9	56	N/A[b]
BD 6	Stockpile	18	1.1	104	24	44	11,166	0.9	94	24	41	0.8
	Average	24	3.1	534	24	100	30,924	1.8	163	18	64	1.0
EX 1	Clear & grub	21	2.8	319	13	37	28,503	3.2	145	9	23	1.0
EX 2	Move rock	52	2.5	189	19	71	25,077	1.7	73	7	27	0.7
EX 3	Excavate soil	40	1.9	214	20	27	19,401	1.5	132	16	26	0.8
	Average	38	2.4	241	17	45	24,327	2.1	117	11	25	0.8
GE 1	Generate	62	0.8	92	9	54	7,589	0.6	120	12	71	0.8
GE 2	Generate	46	1.1	72	19	137	10,533	0.9	67	18	128	0.9
GE 3	Generate	N/A[b]	1.4	90	24	238	13,320	1.8	65	18	170	1.3
GE 4	Generate	50	1.4	121	19	121	13,532	1.6	88	14	88	1.2
	Average	53	1.2	94	18	138	11,244	1.2	85	16	114	1.1
MG 1	Resurface	53	5.5	643	53	67	54,615	4.9	129	16	17	1.0
MG 2	Shoulder	10	1.7	192	50	48	16,956	1.0	148	43	29	0.5
MG 3	Shoulder	42	2.5	275	152	29	25,085	2.8	131	77	20	1.1
MG 4	Resurface	27	2.9	596	95	141	28,845	2.3	215	43	72	0.7
MG 5	Shoulder	20	2.6	423	26	134	26,013	1.9	179	15	113	0.7
MG 6	Resurface	38	2.5	163	21	17	24,893	1.8	86	10	7	0.7
	Average	32	3.0	382	66	73	29,401	2.5	148	34	43	0.8
OT 1	Haul soil	14	2.4	298	22	121	23,543	2.2	155	13	32	0.9
OT 2	Haul soil	4	1.7	246	15	41	16,904	1.5	181	13	27	0.9
OT 3	Haul soil	6	1.9	268	17	59	19,080	1.6	179	13	44	0.9
	Average	8	2.0	271	18	74	19,842	1.8	172	13	34	0.9
SS 1	Move material	54	0.9	74	12	17	8,721	0.5	97	17	29	0.6
	Average	54	0.9	74	12	17	8,721	0.5	97	17	29	0.6
TL 1	Fine grade	30	2.9	169	29	67	29,297	2.3	67	14	30	0.8
TL 2	Move material	44	2.9	514	22	38	28,738	2.1	159	10	17	1.0
TL 3	Stockpile	46	3.7	216	7	58	37,241	2.2	71	5	26	0.7
	Average	29	2.1	237	17	55	21,343	1.6	131	13	30	0.8
WL 1	Move soil	18	1.7	179	19	73	17,399	1.5	114	14	44	0.9
WL 2	Load truck	18	1.6	195	33	38	15,534	1.5	132	30	42	0.9
WL 3	Load truck	17	0.9	131	8	18	9,250	0.4	179	14	38	0.6
WL 4	Load truck	25	1.2	156	15	12	11,691	1.1	145	22	13	1.0
WL 5	Move soil	9	0.8	78	8	23	7,819	0.5	104	13	36	0.6
	Average	17	1.2	148	17	33	12,339	1.0	135	19	35	0.8
	Maximum	62	10.1	1,913	152	240	100,647	4.9	215	77	170	2.1
	Minimum	4	0.5	60	6	5	4,611	0.1	65	5	7	0.2

NOTE: BH = backhoe; EX = excavator; MG = motor grader; SS = skid-steer loader; WL = wheel loader; BD = bulldozer; GE = generator; OT = off-road truck; TL = track loader.

[a]Average fuel-based CO_2 emission rate for all equipment is 9,939 g/gal ± 2%.

[b]Data not available.

TABLE 3 Summary Data for B20 Biodiesel

Equipment	Duty Cycle	Load (%)	Average Time-Based Fuel & Emission Rates						Average Fuel-Based Emission Rates[a]			
			Fuel Use (gal/h)	NO_x (g/h)	HC (g/h)	CO (g/h)	CO_2 (g/h)	Opacity (g/h)	NO_x (g/gal)	HC (g/gal)	CO (g/gal)	Opacity (g/gal)
BH 4	Move soil	23	0.6	77	9	6	5,994	0.3	181	56	N/A[b]	1.8
BH 5	Load truck	29	1.8	213	25	125	18,290	2.0	114	14	66	1.1
BH 6	Move soil	23	2.0	178	19	64	19,575	2.1	91	10	33	1.1
BH 7	Move soil	20	1.2	111	42	105	11,388	1.6	139	33	73	1.2
BH 8	Move soil	15	0.4	69	2	6	4,346	0.3	202	3	16	0.5
	Average	22	1.2	129	19	61	11,919	1.3	145	23	47	1.1
MG 1	Resurface	48	5.1	561	62	64	49,997	4.2	129	15	22	0.9
MG 2	Shoulder	14	1.7	233	16	34	17,102	0.5	173	13	24	0.3
MG 3	Shoulder	31	3.8	364	47	53	36,710	2.1	122	18	22	0.4
MG 4	Shoulder	12	1.3	201	36	N/A[b]	12,658	0.0	131	32	N/A[b]	0.8
MG 5	Shoulder	30	3.4	600	47	92	33,443	1.9	195	24	57	0.6
MG 6	Resurface	30	2.7	166	55	28	26,869	1.4	100	34	12	0.5
	Average	28	3.0	354	44	54	29,463	1.7	142	23	27	0.6
WL 2	Move soil	17	1.0	126	8	28	9,637	0.7	151	19	53	1.8
WL 3	Move soil	16	1.2	166	22	16	11,735	0.6	170	27	22	0.6
WL 4	Move soil	22	2.2	253	30	38	21,130	1.6	132	21	29	0.7
WL 5	Move soil	20	1.5	137	8	37	14,495	1.0	103	8	33	0.6
	Average	19	1.5	171	17	30	14,249	1.0	139	19	34	0.9
	Maximum	48	5.1	600	62	318	49,997	4.2	202	56	313	1.8
	Minimum	12	0.4	69	2	6	4,346	0.0	100	3	12	0.3

[a]Average fuel-based CO_2 emission rate for all equipment is 9,749 g/gal ± 5%.
[b]Data not available.

blade; the shoulder duty cycle refers to a highway maintenance activity that involved grading roadway shoulders and ditches while using only the end portion of the motor grader's blade. The primary duty cycle of the generators was to provide a temporary source of electricity at a job site. Overall, there were 12 observed representative duty cycles during the 54 tests.

The average engine loads based on the normalized MAP values are summarized in Table 2 for the equipment fueled with petroleum diesel and in Table 3 for the equipment fueled with B20 biodiesel. The average engine loads correspond to each duty cycle.

For the equipment fueled with petroleum diesel, the skid-steer loader and generators have the highest overall average engine loads of 54% and 53%, respectively. The skid-steer loader average engine load, however, is based on one observation only; thus, there is no basis for comparison with other skid-steer loaders. Furthermore, generators are stationary equipment that does not move around a job site and therefore there is limited variability in engine load.

The lowest overall average engine load is 8% for the off-road hauler trucks; however, such a low average engine load should be interpreted with caution. The duty cycles observed for these off-road trucks included long idle times while the trucks were waiting to be loaded and then moving at low speeds for very short haul distances. Off-road trucks frequently operate at high speeds over long distances while hauling heavy payloads and can therefore generate very high engine loads. Thus, the overall average engine load for off-road trucks presented here is not representative of all off-road truck duty cycles.

Backhoes and wheel loaders have similar overall average engine loads of 19% and 17%, respectively. Both types of equipment are wheel-mounted tractors with comparable body styles and front-loader buckets that are used to perform similar duty cycles, including loading trucks, moving soil, and moving building materials. Bulldozers and track loaders also have similar overall average engine loads of 24% and 29%, respectively. These are track-type tractors with comparable body styles and work attachments that perform similar duty cycles, including rough grading, fine grading, stockpile shaping, and moving building materials. Although the average engine loads for these four types of equipment can be higher under extreme conditions, such as moving maximum payloads on an adverse grade, the average engine loads presented here are typical for the observed duty cycles.

Each of the three excavators was observed performing a separate duty cycle that had its own distinct average engine load. Based on these data, it is apparent that excavators can operate under a wide range of engine loads. For example, the average engine load of 21% for clearing and grubbing involved removing small-to-medium sized trees that did not require much effort from the engine. Conversely, the average engine load of 52% involved moving heavy rock, which required significant effort. For the excavating soil duty cycle, an average engine load of 40% was observed for the excavator while digging in common earth; however, the soil type may affect the engine load. A lower engine load would be expected for an excavator digging in sandy topsoil and a higher engine load would be expected for an excavator digging in hard-packed clay, although there was no opportunity to measure the engine loads for an excavating soil duty cycle for various soil types.

Motor graders were observed performing two separate duty cycles, including resurfacing and shouldering. Resurfacing had an average engine load of 39% and shouldering had an average engine load of 24%. The resurfacing duty cycle had a higher average engine load because the motor grader engaged the full length of its blade and thus had a higher resistance imposed by the ground. The shouldering duty cycle had a lower average engine load because only a fraction of the blade was engaged with the ground and thus had less resistance.

For the equipment fueled with B20 biodiesel, the overall average engine loads were quantitatively similar to the equipment fueled with

TABLE 4 Correlation Coefficients for Fuel Use and Emissions, and Engine Attributes for Petroleum Diesel

	Horsepower	Displacement	Model Year	Engine Tier	Engine Load
Time-based					
Fuel (gal/h)	0.50	0.72	–0.32	–0.33	0.39
NO_x (g/h)	0.45	0.70	–0.45	–0.47	0.26
HC (g/h)	0.26	0.34	–0.24	–0.22	0.18
CO (g/h)	0.40	0.53	–0.29	–0.23	0.23
CO_2 (g/h)	0.50	0.72	–0.32	–0.34	0.39
Opacity (g/h)	0.40	0.54	–0.31	–0.31	0.28
Fuel-based					
NO_x (g/gal)	0.29	0.40	–0.55	–0.52	–0.33
HC (g/gal)	0.04	0.04	–0.06	–0.05	–0.10
CO (g/gal)	0.00	0.04	–0.13	–0.10	–0.01
Opacity (g/gal)	–0.02	–0.02	–0.20	–0.25	0.03

petroleum diesel. Backhoes and wheel loaders had an overall average engine load of 22% and 19%, respectively (19% and 17%, respectively, for petroleum diesel). For motor graders, the overall average engine load for resurfacing was 39% (the same as petroleum diesel) and 22% for shouldering (24% for petroleum diesel). Thus, as expected, fuel type has no significant impact on average engine loads and the slight variability in average engine loads based on fuel type shown here can be attributed to the variation in the individual duty cycles that were measured.

Average Fuel Use and Emission Rates

The average time-based fuel use and emission rates and the average fuel-based emission rates are summarized in Table 2 for the equipment fueled with petroleum diesel and in Table 3 for the equipment fueled with B20 biodiesel. The average fuel use and emission rates for each item of equipment correspond to the duty cycle and engine attribute data, including horsepower, displacement, model year, engine tier, and engine load. Furthermore, the correlation coefficients for fuel use and emission rates versus engine attributes are presented in Tables 4 and 5 for the equipment fueled with petroleum diesel and B20 biodiesel, respectively.

Based on Table 4, the time-based fuel use and emission rates of each pollutant have a strong positive relationship with displacement and a moderate positive relationship with horsepower; thus, engine size has the greatest impact on time-based petroleum diesel fuel use and emission rates of NO_x, HC, CO, CO_2, and opacity. As examples, scatter plots for the relationships of fuel use and NO_x emission rates versus displacement are presented in Figure 1. These plots represent the linear increase in fuel use and NO_x emission rates as displacement increases. Although not shown, similar trends exist in the emission rates of the other pollutants.

Based on Table 5, the time-based fuel use and emission rates of NO_x, HC, CO_2, and opacity have a strong positive relationship with engine load; CO emission rates have a strong negative relationship with model year. Fuel use and NO_x, HC, and CO_2 emission rates also have a strong positive relationship with horsepower and displacement. Overall, engine load has the most significant impact on B20 biodiesel time-based fuel use and emission rates of NO_x, HC, CO_2, and opacity; model year has the most significant impact on CO emission rates.

Engine displacement was the most highly correlated factor for petroleum diesel fuel use and emission rates in part because there was large variability of a factor of more than 6, from 44 to 306 hp, in displacement among those data. For the equipment tested using B20 fuel, displacement varied by only a factor of approximately 2, from 90 to 198 hp. However, for the tests on B20 fuel, engine load varied by a factor of 4, from 12% to 48%. Hence, the identification of engine load as most highly correlated with fuel use rate and most of the emission rates for B20 is in part an artifact of the range of variation of this factor in the sample data set. As examples, scatter plots for the relationships of fuel use and NO_x versus engine load are presented in Figure 2. These plots represent the linear increase in fuel use and NO_x emissions with an increase in engine load. Although

TABLE 5 Correlation Coefficients for Fuel Use and Emissions, and Engine Attributes for B20 Biodiesel

	Horsepower	Displacement	Model Year	Engine Tier	Engine Load
Time-based					
Fuel (gal/h)	0.66	0.68	–0.13	–0.19	0.87
NO_x (g/h)	0.56	0.71	–0.41	–0.44	0.71
HC (g/h)	0.61	0.65	–0.31	–0.21	0.70
CO (g/h)	0.10	0.32	–0.85	–0.64	–0.13
CO_2 (g/h)	0.66	0.68	–0.13	–0.18	0.87
Opacity (g/h)	0.24	0.26	–0.06	–0.24	0.91
Fuel-based					
NO_x (g/gal)	–0.09	–0.03	–0.08	–0.02	–0.29
HC (g/gal)	–0.01	–0.05	–0.10	0.08	–0.02
CO (g/gal)	0.04	0.26	–0.77	–0.52	–0.34
Opacity (g/gal)	–0.54	–0.52	–0.05	–0.16	–0.02

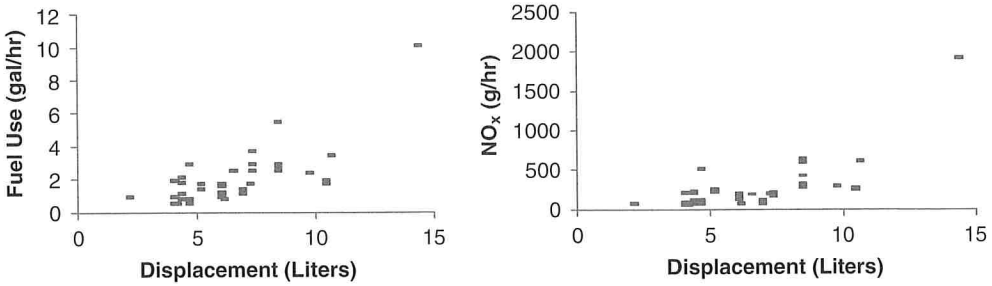

FIGURE 1 Time-based fuel use and emission rates, and displacement (petroleum diesel).

not shown, there are similar trends in the data for HC, CO_2, and opacity with respect to engine load; however, CO emission rates decrease as the model year increases.

As in Tables 4 and 5, there is a negative relationship of fuel use and emission rates versus model year and engine tier, regardless of fuel type. Although these relationships are relatively weak, they still imply that newer model engines and engine tier standards have been effective at reducing fuel use and emissions.

Based on Tables 4 and 5, fuel-based emission rates have relatively weak relationships with the measured engine attributes of horsepower, displacement, model year, engine tier, and engine load. This does not mean, however, that fuel-based emission rates are unreliable. In fact, fuel-based emission rates tend to have less variability than time-based emission rates and therefore are effective for emissions analyses. Based on the data in Table 2, the petroleum diesel fuel-based emission rates have coefficients of variation (standard deviation divided by the mean) that are lower than those of the time-based emission rates by approximately 73% for NO_x, 34% for HC, 14% for CO, and 42% for opacity; the average fuel-based emission rate of CO_2 for all equipment that was measured using petroleum diesel is approximately 9,900 g/gal ± 2%. Based on the data in Table 3, the B20 biodiesel fuel-based emission rates have coefficients of variation that are lower than those of the time-based emission rates by approximately 65% for NO_x, 8% for HC, 51% for CO, and 32% for opacity; the average fuel-based emission rate CO_2 for all equipment that was measured using B20 biodiesel is approximately 9,700 g/gal ± 5%. Overall, the relative range of variation for fuel-based emission rates is lower than for time-based emission rates.

A comparison of results between B20 and petroleum diesel for the 15 vehicles that were measured using both fuels needs to be done on a consistent basis for the same duty cycles for each type of equipment, in order to avoid the confounding effect of intertest variability in duty cycle. Frey et al. (*8*) developed and applied engine load-based modal models of fuel use and emission rates and, for each equipment item, used the same distribution of engine load, to enable comparison between the two fuels for the same duty cycle. On average over all 15 vehicles tested, time-based NO_x emission rates were 2% lower for B20 than for petroleum diesel, which is not a statistically significant result. However, time-based emission rates were lower by 18%, 26%, and 25% for PM, HC, and CO, respectively, which are significant.

CONCLUSIONS AND RECOMMENDATIONS

There is a need for accurate fuel use and emissions data for in-use nonroad diesel construction equipment. This type of information can be used to assess the environmental impacts of construction activities, particularly with regard to energy use and air quality. The work presented here provides a solid foundation for developing comprehensive data sets of fuel use and emissions information; however, more research needs to be done. The research that produced these results should be continued to observe more equipment of the same type in order to refine the current data and also gather data from other nonrepresented equipment types.

Fuel use and emissions field data collected by an onboard PEMS has an advantage over laboratory dynamometer testing in that the field data represent actual in-use conditions for the equipment as opposed to simulated conditions. Thus, PEMS data are useful for developing emission inventories that are representative of actual vehicle operations in the field; however, the methods and results presented here are not intended as a certification test or to replace existing certification tests. The field data results have been quality assured and benchmarked to independent data and are considered valid. These data should be used as a complement to existing emissions data, including the EPA NONROAD emission factors, in order to provide in-depth analyses of nonroad emission sources, including construction equipment.

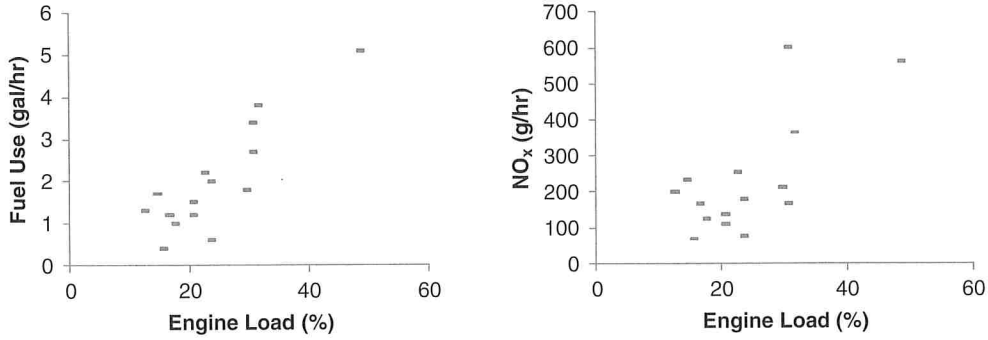

FIGURE 2 Time-based fuel use and emission rates, and engine load (B20 biodiesel).

The construction activities being performed by the equipment presented here were characterized by representative duty cycles; therefore, the corresponding fuel use and emissions for the construction activity itself can be compared to the quantity of work completed by the equipment. By linking construction quantities to fuel use and emissions, it is possible to establish fuel use and emission factors based on construction quantities, such as the cubic yards of excavation per gallon of fuel used by an excavator or the grams of pollutant emitted per mile of roadway shoulder scraped by a motor grader. These emission factors can then be used to estimate the fuel use requirements and the pollutants emitted for a construction project based on a quantity takeoff from a set of construction plans and specifications.

Petroleum diesel and B20 biodiesel fuel use and time-based emission rates, in most cases, have a strong positive relationship with engine displacement, horsepower, and load. For both fuels, time-based fuel and emission rates were inversely proportional to model year and engine tier. These types of trends should be investigated further and used for modeling fuel use and emissions as a function of equipment type, engine size, engine load, and model year or engine tier.

Fuel-based emission rates tend to have less variability than time-based emission rates. Hence, development of emissions inventories based on quantifying fuel consumed, rather than time of operation, is preferred where possible.

The data presented here may be used to evaluate fuel use and emission rates based on equipment type, fuel type, and engine attributes, including horsepower, displacement, model year, engine tier, and engine load. These comparisons permit fuel use and emissions considerations to be used when making fleet management decisions, such as selecting equipment for a specific activity or evaluating the equipment's useful life and deterioration rates. Fleet managers should consider the impact of fuel use and emissions when determining which equipment to use on a project and also when to retire, replace, or retrofit existing equipment.

The results presented here may be used as a basis for establishing emissions inventories of construction projects to help determine their emissions footprint. These types of emission inventories may be used to assess the environmental impact of construction projects at the local, state, regional, and national levels. Environmental planners and policy makers should consider such emissions inventories when developing pollution reduction strategies and regulations, particularly for the construction industry.

ACKNOWLEDGMENTS

This material is based on work supported by the National Science Foundation and the North Carolina Department of Transportation. Saeed Abolhasani, Hyung-Wook Choi, Kangwook Kim, and Shih-Hao Pang assisted with data collection and analysis.

REFERENCES

1. *User's Guide for the Final NONROAD2005 Model.* EPA-420-R-05-013. U.S. Environmental Protection Agency, Office of Transportation and Air Quality, Ann Arbor, Mich., 2005.
2. Frey, C., W. Rasdorf, K. Kim, S. Pang, P. Lewis, and S. Abolhasani. *Life Cycle Inventory and Impact Analysis Framework for Nonroad Construction Vehicles and Equipment (TSE03-L).* Research project for National Science Foundation, Arlington, Va., 2007.
3. Frey, C., W. Rasdorf, K. Kim, S. H. Pang, P. Lewis, and S. Abolhasani. *Real-World Duty Cycles and Utilization for Construction Equipment in North Carolina.* FHWA/NC/2006-55. Prepared by North Carolina State University for North Carolina Department of Transportation, Raleigh, 2008.
4. May, D., L. Fisher, C. Tennis, and T. Parrish. *Simple, Portable, On-Vehicle Testing (SPOT) Final Report.* Contract 86-C-01-106. Prepared by Analytical Engineering, Inc. for the U.S. Environmental Protection Agency, Columbus, Ind., 2002.
5. Gautam, M., D. Carder, N. Clark, and D. Lyons. *Testing for Exhaust Emissions of Diesel Powered Off-Road Engines.* APB Contract 98-317. Prepared by West Virginia University for the California Air Resources Board and the California EPA, Sacramento, 2002.
6. Vojtisek-Lom, M. *Real-World Exhaust Emissions from Construction Equipment at the World Trade Center #7 Site.* Prepared by Clean Air Technologies International, Inc., for Northeast States for Coordinated Air Use Management, Buffalo, N.Y., 2003.
7. Abolhasani, S., H. C. Frey, K. Kim, W. Rasdorf, P. Lewis, and S. H. Pang. Real-World In-Use Activity, Fuel Use, and Emissions for Nonroad Construction Vehicles: A Case Study for Excavators. *Journal of the Air and Waste Management Association,* Vol. 58, No. 8, 2008, pp. 1033–1046.
8. Frey, H. C., W. J. Rasdorf, K. Kim, S. Pang, and P. Lewis. Comparison of Real-World Emissions of B20 Biodiesel versus Petroleum Diesel for Selected Nonroad Vehicles and Engine Tiers. In *Transportation Research Record: Journal of the Transportation Research Board, No. 2058,* Transportation Research Board of the National Academies, Washington, D.C., 2008, pp. 33–42.
9. Frey, C., K. Kim, W. Rasdorf, S. Pang, and P. Lewis. Characterization of Real-World Activity, Fuel Use, and Emissions of Selected Motor Graders Fueled with Petroleum Diesel and B20 Biodiesel. *Journal of the Air and Waste Management Association,* Vol. 58, No. 10, 2008, pp. 1274–1287.
10. Lewis, P., W. Rasdorf, C. Frey, K. Kim, and S. Pang. Requirements and Incentives for Reducing Construction Vehicle Emissions and Comparison of Nonroad Diesel Engine Emissions Data Sources. *Journal of Construction Engineering and Management,* Vol. 135, No. 5, 2009, pp. 341–351.
11. Lewis, P., H. C. Frey, and W. J. Rasdorf. Development and Use of Emissions Inventories for Construction Vehicles. In *Transportation Research Record: Journal of the Transportation Research Board, No. 2123,* Transportation Research Board of the National Academies, Washington, D.C., 2009, pp. 46–53.
12. Pang, S., C. Frey, and W. Rasdorf. Life Cycle Inventory Energy Consumption and Emissions for Biodiesel Versus Petroleum Diesel Fueled Construction Vehicles. *Environmental Science and Technology,* Vol. 43, No. 16, 2009, pp. 6398–6405.
13. Frey, C., and S. Bammi. Probabilistic Nonroad Mobile Source Emission Factors. *Journal of Environmental Engineering,* Vol. 129, No. 2, 2003, pp. 162–168.
14. Frey, H. C., N. M. Rouphail, and H. Zhai. Link-Based Emission Factors for Heavy-Duty Diesel Trucks Based on Real-World Data. In *Transportation Research Record: Journal of the Transportation Research Board, No. 2058,* Transportation Research Board of the National Academies, Washington, D.C., 2008, pp. 23–32.
15. Rasdorf, W., C. Frey, P. Lewis, K. Kim, S. Pang, and S. Abolhasani. Field Procedures for Real-World Measurements of Emissions from Diesel Construction Vehicles. *Journal of Infrastructure Systems,* Vol. 16, No. 4, 2010 (in press).
16. *OEM-2100 Montana System Operation Manual.* Clean Air Technologies International, Inc., Buffalo, N.Y., 2003.
17. *Caterpillar Performance Handbook,* 35th ed. Caterpillar, Inc., Peoria, Ill., 2004.
18. Nichols, H., and D. Day. *Moving the Earth: The Workbook of Excavation.* McGraw-Hill Companies, Inc., New York, 2005.
19. *Exhaust and Crankcase Emission Factors for Nonroad Engine Modeling-Compression-Ignition.* EPA-420-P-04-009, NR-009c. U.S. Environmental Protection Agency, Ann Arbor, Mich., 2004.
20. *Environmental Technology Verification Report: Clean Air Technologies International, Inc. REMOTE On-Board Emissions Monitor.* Prepared by Battelle for the U.S. Environmental Protection Agency, Columbus, Ohio, 2003.

Any opinions, findings, and conclusions or recommendations expressed in this material are those of the authors and do not necessarily reflect the views of the National Science Foundation or the North Carolina Department of Transportation.

The Transportation and Air Quality Committee peer-reviewed this paper.

Mobile Source Air Toxic Emissions

Sensitivity to Traffic Volume, Fleet Composition, and Average Speed

Alexandra Timoshek, Douglas Eisinger, Song Bai, and Deb Niemeier

This study used a new emissions modeling tool, CT-EMFAC, to assess the sensitivity of mobile source air toxic (MSAT) emissions to changes in traffic volumes, speeds, and fleet composition. In addition, the choice of the speed calculation method, which is usually part of a postprocessing technique, was analyzed. The investigation employed a hypothetical 6.7-mi freeway segment located in southern California; activity data were derived from comparable real-world information obtained from the California Department of Transportation. Results show that emissions more than doubled in 2004 and increased by a factor of two to four in 2030 when traffic volumes increased 30% above base case conditions. The nonlinear shift in emissions was a function of decreased travel speeds and increased grams per mile emission rates that accompanied increased traffic volumes. Fleet composition (the proportion of trucks) was also shown to affect MSAT emissions, especially for diesel particulate matter and aldehydes. Under some scenarios, the choice of the speed calculation method had a greater effect on MSAT emissions than 26 years of fleet turnover. The analysis also showed that the type of speed calculation method used could result in large variations in MSAT emissions. Application of one speed calculation method resulted in calculated congested freeway speeds that did not fall below 10 mph. The speed calculation method chosen was highly influential in the 2030 case study when forecasted volumes reached levels at which speeds approached the 10 mph minimum allowed by the speed calculation method; this probably underpredicted emissions.

Mobile source air toxics (MSATs) are an important constituent of urban-scale and near-road pollution problems. According to the National-Scale Air Toxics Assessment, mobile sources were responsible for about 47% of total outdoor toxic emissions, almost 30% of the population cancer risk, and 77% of noncancer risk in 2002 (*1*). A growing body of literature has linked road proximity to increased pollutant concentrations and adverse health impacts (*2–5*). In the United States, approximately 37 million people live within 300 ft of a four-or-more-lane highway, railroad, or airport (*6*). In addition, although individual exposure to pollutants can vary with receptor distance from a road, it can also vary substantially for occupants in moving vehicles, depending on the quantity of emissions originating from other vehicles operating ahead of the vehicles in which the occupants are located (*4, 7*).

U. C. Davis–Caltrans Air Quality Project, Department of Civil and Environmental Engineering, University of California, Davis, One Shields Avenue, Davis, CA 95616. Corresponding author: D. Niemeier, dniemeier@ucdavis.edu.

Transportation Research Record: Journal of the Transportation Research Board, No. 2158, Transportation Research Board of the National Academies, Washington, D.C., 2010, pp. 77–85.
DOI: 10.3141/2158-10

Among MSATs, diesel particulate matter (DPM) causes special concern. The California Air Resources Board (CARB) has identified DPM as a toxic air contaminant (*8*) and the U.S. Environmental Protection Agency (EPA) has found that diesel exhaust presents a chronic respiratory hazard and is likely to be carcinogenic to humans (*9*). The Multiple Air Toxics Exposure Study III (MATES III), conducted in the greater Los Angeles, California, area in 2004 and 2005, found that diesel exhaust accounted for about 84% of the total air toxics risk (*10, 11*). In light of health concerns, regulatory agencies have sought to identify and minimize the risk and exposure to MSATs and to DPM in particular. In 2001, EPA identified priority MSATs and established control requirements focused on fuel content (*12*). In 2007, EPA updated its MSAT requirements and expanded the list of priority pollutants (*13*). In recent years, ambient MSAT concentrations have generally been decreasing and are projected to decline further through the 2020s due to existing state and federal regulations mandating cleaner burning fuels and more stringent light- and heavy-duty new-vehicle emission standards (*11, 14*).

Yet at the transportation project level, there is still an important need to produce reliable MSAT emissions forecasts. In 2006, FHWA published guidance that, in effect, requires project-level MSAT emissions assessments (*14*). The MOBILE 6.2 on-road vehicle emissions model is used to estimate MSAT emissions in 49 states. CARB's EMFAC2007 on-road emissions model is available for use in California; however, it does not estimate MSAT emissions. Similar in concept to MOBILE 6.2, EMFAC2007 emission factors are based on simulated vehicle trips (*15*). Although the models predict regional and general trends reasonably well, they are not sensitive to key traffic variables and are not well suited for analysis at the project level (*14*).

In response to the lack of a California-specific MSAT emissions modeling tool, the University of California, Davis, worked in collaboration with the California Department of Transportation (Caltrans) and CARB to develop the CT-EMFAC tool (*16*). CT-EMFAC estimates emissions for the six priority MSATs identified in EPA's 2001 MSAT rule and FHWA's 2006 MSAT guidance (DPM, formaldehyde, 1,3-butadiene, benzene, acrolein, and acetaldehyde), in addition to other key pollutants [total organic gases (TOG), carbon monoxide, nitrogen oxides, sulfur oxides, PM_{10}, or $PM_{2.5}$] and carbon dioxide. It may be applied at the project level with user inputs of speed-based vehicle miles traveled (*16*). CT-EMFAC allows, for the first-time, project-level assessment of California-based travel activity and associated MSAT emissions (more details on CT-EMFAC are provided in section on emissions modeling).

The purpose of this study was to employ CT-EMFAC and traffic data postprocessing techniques to further insight on the sensitivity of the transportation project parameters on MSAT emissions. The

work was motivated by a need to provide project analysts a deeper understanding of how to improve MSAT emissions assessments, as well as to expand and enhance consideration of project design options for reducing real-world operating emissions.

CASE STUDY AND METHODOLOGY

This analysis is based on a hypothetical freeway case study using real-world southern California activity data (volumes, fleet mix, and speeds). Base case emissions were modeled for 2 analysis years. The authors also tested the sensitivity of the base case emissions to calendar years, various fleet mix scenarios, traffic volumes, and travel speeds, with a specific focus on the impact of the types of speed calculation methods used in postprocessing techniques, on estimated project-level MSAT emissions.

Case Study Description

The study used a hypothetical 6.7-mi freeway project in Los Angeles County, California. The assumed freeway had three mixed-flow travel lanes operating in each direction. The analyses focused on peak period conditions in a 2004 base and a 2030 horizon year. Assessment of the peak period allowed the authors to test emissions sensitivity to various travel speeds and volumes, starting with the base case conditions of high volumes and low speeds. Annual emissions were forecasted for six priority MSATs: DPM, formaldehyde, 1,3-butadiene, benzene, acrolein, and acetaldehyde. Base case (2004 and 2030) travel volumes and fleet mix reflected real-world project conditions from recent southern California freeway improvement projects: a 26% overall increase in forecasted traffic volumes and a growing share of overall travel by medium-duty and larger trucks (from 9% of 2004 activity to 13% of 2030 activity).

Speed Postprocessing

Estimates of regional-scale travel activity are often postprocessed to yield more refined estimates of project-level travel speeds. Many speed postprocessing methods have been discussed in the literature (*17–20*); this study estimated project-specific travel speeds with two relatively simple and widely used speed postprocessing techniques (*20*). The first method, the Bureau of Public Roads (BPR) function, was developed in the 1960s; it can be used to obtain speeds on individual freeway links, as well as to determine average speed by functional class (*18*). As shown in Equation 1, the BPR function models the average highway speed (s) by adjusting the free-flow speed (s_f), as traffic volume (v) approaches roadway capacity (c).

$$s = \frac{s_f}{1 + a\left(\frac{v}{c}\right)^b} \tag{1}$$

where the two parameters, a and b, can be calibrated to reflect local conditions or specific roadway functional class (*20*). In this study, $a = 0.2$ and $b = 10$ were used for calculating average speeds on the freeway segments for this case study (*21*). The suitability of various parameters is not being tested, but rather the speed formula using a common setting for a and b.

The second method used to estimate congested freeway speeds was the Texas Transportation Institute (TTI) function (*18, 22, 23*). The basis of this method is the harmonic mean of free-flow speed and delay. The TTI speed calculation is

$$s = \frac{60}{\frac{60}{s_f} + \text{delay}} \tag{2}$$

where

$$\text{delay} = \min\left[Ae^{B(v/c)}, M\right] \tag{3}$$

$A = 0.015$,
$B = 3.5$, and
M = maximum number of minutes of delay per mile, (5 for high-capacity facilities such as the freeway segments assessed in this study).

The parameters used for calculating average speeds in this study (e.g., *a/b* of the BPR function and *A/B* of the TTI method) are based on values cited previously in the literature. It should be noted, however, that values may be different in practice based on local conditions. Both the BPR and TTI methods require input of volume, capacity, and free-flow speed. To develop speed estimates, all-vehicle traffic volume from the data set was translated into passenger car–equivalent flow rate (Vp) in passenger vehicles per hour per lane.

$$Vp = \frac{V}{\text{PHF} * N * f_{hv} * f_p} \tag{4}$$

where

PHF = peak hour factor (0.9),
N = number of lanes in both directions (6),
f_{hv} = heavy vehicle adjustment factor (0.96) (i.e., trucks were assumed to be equivalent to 1.5 passenger vehicles), and
f_p = driver population factor that is equal to 1 during peak hour commute (*17*).

Further assumptions were also made for the free-flow speed (65 mph) and the associated roadway capacity (2,350 vehicles per hour per lane) based on the *2000 Highway Capacity Manual*. Detailed activity data for the two case study analysis years are presented in Table 1.

TABLE 1 Base Case Traffic Activity Data for 2004 and 2030

	Year	
	2004	2030
Vehicle Mix		
Trucks (%)	9	13
Others (%)	91	87
Travel Activities		
Peak period volume (vph)	13,058	16,392
BPR speed (mph)	46	11
TTI speed (mph)	38	22

NOTE: Base case data are for a hypothetical 6.7-mi freeway, three lanes in each direction.

Emissions Modeling

The study used a new version of CT-EMFAC (Version 2.6, May 2008) to model project-level MSAT emissions (*14*). The program includes a database of year-specific composite emission factors corresponding to combinations of temperature, relative humidity, speed, vehicle class, and technology type specific to particular geographic areas in California. The minimum data needed to conduct an analysis include the analysis year, traffic volume, truck percentage, and average traffic speed. By varying the volume and truck percentage and the subsequent speed estimates, the emission sensitivity of the six priority MSAT pollutants could be evaluated using outputs from CT-EMFAC for each test scenario.

The model's input for the fleet composition consists of two groups: trucks (medium-duty and above) and others (passenger cars, light-duty trucks, various buses, motorcycles, and motor homes). The truck group includes both diesel and nondiesel trucks and the program automatically apportions the truck fleet into appropriate fuel-specific fractions for the region using default data from CARB's EMFAC2007 model. Consistent with CT-EMFAC, trucks are considered to be all medium-duty and above vehicles, regardless of fuel type. The output includes (grams per mile) emission factors by pollutant for 13 speed bins with 5 mph. These emission factors were linearly interpolated within a given speed bin to obtain continuous speed-based emission factors appropriate for this sensitivity study.

Emission factors for the five organic gaseous MSATs are calculated based on toxics speciation factors supplied by CARB. A speciation factor represents the ratio of emissions of a specific MSAT to TOG emissions. An emission factor for a particular MSAT can be obtained by multiplying the TOG emission factor by the speciation factor associated with the vehicle class, technology type, and fuel type. These calculations, embedded in the program, are specific to each calendar year, season, geographic area, and emission process (stabilized running exhaust, idling exhaust, and running loss). The DPM composite emission factors are calculated by taking a weighted average of all emission factors for diesel trucks. The factors are then combined with the percentages of diesel trucks and diesel nontrucks in the whole fleet to calculate fleet-average DPM composite emission factors.

The CT-EMFAC version employed here includes two important data limitations. At the time CT-EMFAC was developed, CARB did not have acrolein speciation factors applicable to diesel vehicles. Thus, CT-EMFAC (and, consequently, this study) reports acrolein emissions solely for gasoline-powered vehicles. Other studies have identified that diesel-powered vehicles emit acrolein (*24, 25*). Therefore, the results reported here should be considered a partial assessment of the sensitivity of acrolein emissions to varying fleet characteristics. Also due to a lack of data, CARB assumed that speciation factors for the five gaseous MSATs associated with the diesel fleet remain constant over time. In contrast, CARB's gasoline-vehicle speciation factors for gaseous MSATs declines over time (e.g., the fraction of gasoline vehicle TOG emissions equal to benzene declines from about 0.03 in 2004 to about 0.02 in 2030). Thus, for the MSAT data presented here, changes in diesel-vehicle emission factors over time for the five gaseous MSATs depend solely on changes in TOG emission factors.

RESULTS

The first two parts of the findings report information using speeds estimated with the TTI speed postprocessing technique. The results illustrate how volumes and fleet mix changes can alter forecasted travel speeds and MSAT emissions, holding the speed postprocessing technique constant. The third part of the results illustrates the sensitivity of forecasted travel speeds (and resulting emissions) to speed calculation postprocessing approaches.

MSAT Emissions Sensitivity to Calendar Year Changes

Scenarios for the 2004 and 2030 base cases were conducted using CT-EMFAC with speeds calculated by the TTI speed post-processing method. Figure 1 illustrates that despite a 26% increase in forecasted travel volumes and a shift toward a larger fraction of travel from trucks (see Table 1), base case emissions decline substantially over time.

MSAT Emissions Sensitivity Toward Traffic Activity and Fleet Mix

Next, MSAT sensitivity toward traffic volume and truck percent change was assessed. Sensitivity test parameter values (Table 2 and Table 3) were varied to simulate possible project scenarios (e.g., increased volumes because of new lane additions; increased truck percentage given future growth in goods movement; decreased truck percentage because of truck rerouting).

Since the assumed roadway capacity stayed constant throughout this study, volume-to-capacity ratios were higher than normal operating conditions under some scenarios with large traffic volume increases. These extreme conditions are designed for the purposes of testing emissions sensitivity, but are not likely to be observed in the real-world because of the highway improvement projects that target growing traffic volume demand.

Holding truck percentage constant, growth in traffic volume has a significant impact on speeds: up to 53% speed reductions were forecasted due to a 30% growth in volume by 2030. In contrast, variations in truck traffic percentage affected speed estimates only marginally. The impact of fleet mix on emissions of all six pollutants is shown in Figure 2.

Changes in fleet composition had little effect on calculated average speed but did result in substantial shifts in estimated DPM and aldehyde emissions. The relationship between DPM and truck activity is straightforward; the sensitivity of aldehyde emissions to fleet mix is also indicative of the relative importance of trucks to overall aldehyde emissions. Note that total emissions of the five gaseous MSATs became more sensitive to truck percentage over time. Trucks contributed more to the overall MSAT emissions by 2030 than in 2004 because their associated emissions declined less significantly than nontrucks (an artifact of data available when CT-EMFAC was created). Therefore, the same scale of truck percentage shift as in 2004 triggered a larger percentage shift in total MSAT emissions by 2030. Figure 3 shows MSAT emissions sensitivity to total traffic volume for 2004 and 2030.

By comparing Figures 2 and 3, it can be seen that, overall, MSAT emissions are more sensitive to changes in traffic volume than to changes in fleet composition. As illustrated in Figure 3, the volume-to-emissions relationship is nonlinear and by 2030 emissions increase more than 250% due to a 30% volume shift, as seen for aldehydes. The percent shift in emissions that is in excess of the percent shift in volume is a function of the resulting decrease in travel speeds that accompanies upward shifts in traffic volumes.

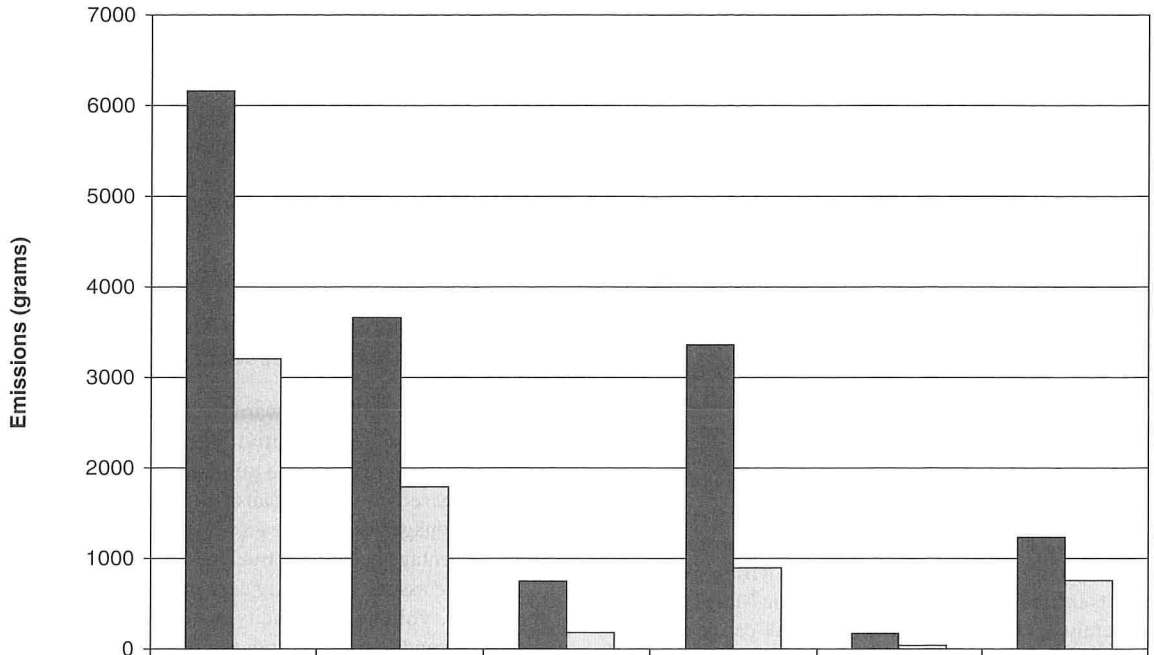

	DPM	Formaldehyde	Butadiene	Benzene	Acrolein	Acetaldehyde
2004	6160	3661	749	3361	171	1233
2030	3207	1791	179	895	39	755
% reduction	48	51	76	73	77	39

FIGURE 1 MSAT emissions comparison for 2004 and 2030 base case scenarios (reported acrolein emissions are those associated with gasoline-powered vehicles only).

TABLE 2 Sensitivity Analysis: Traffic Volume and Truck Percentage Data

	Year 2004			Year 2030		
Truck Change (%)	Truck (%)	Speed (mph)	Speed Change (%)	Truck (%)	Speed (mph)	Speed Change (%)
30	12	37	−2	17	21	−6
20	11	38	−1	15	21	−4
10	10	38	−1	14	21	−2
0% (base case)	9	38	0	13	22	0
−10	9	38	+1	11	22	+2
−20	8	39	+1	10	23	+4
−30	7	39	+2	9	22	+6

NOTE: Truck change means shifting the relative percent allocated to trucks above or below the base case, holding the overall volume constant. Speed, mph refers to the average speed for all vehicles (trucks and nontrucks). Speed estimates are based on the TTI method. Speed change reflects the total percent change from the base case.

TABLE 3 Sensitivity Analysis: Traffic Volume and Average Speed Data

	2004			2030		
Volume Change (%)	Volume (vph)	Speed (mph)	Speed Change (%)	Volume (vph)	Speed (mph)	Speed Change (%)
30	16,976	20	–46	21,310	10	–53
20	15,670	26	–32	19,670	10	–52
15	15,017	29	–24	18,851	13	–41
10	14,364	32	–16	18,031	15	–29
5	13,711	35	–8	17,212	18	–15
0% (base case)	13,058	38	0	16,392	22	0

NOTE: Volume change means increasing the amount of vehicles per hour by the percent stated above the base case, holding the truck percent constant. Speed, mph refers to the average speed for all vehicles (trucks and nontrucks). Speed estimates are based on the TTI method. Speed change reflects the total percent change from the base case.

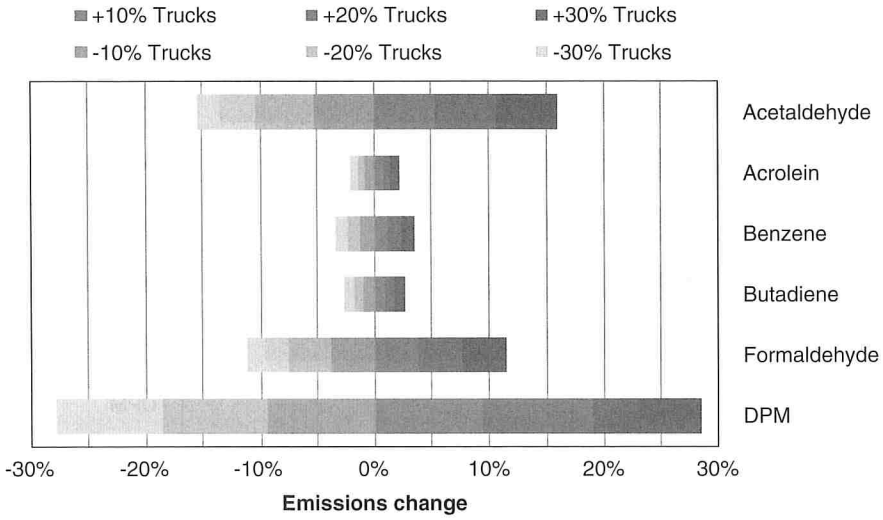

(a)

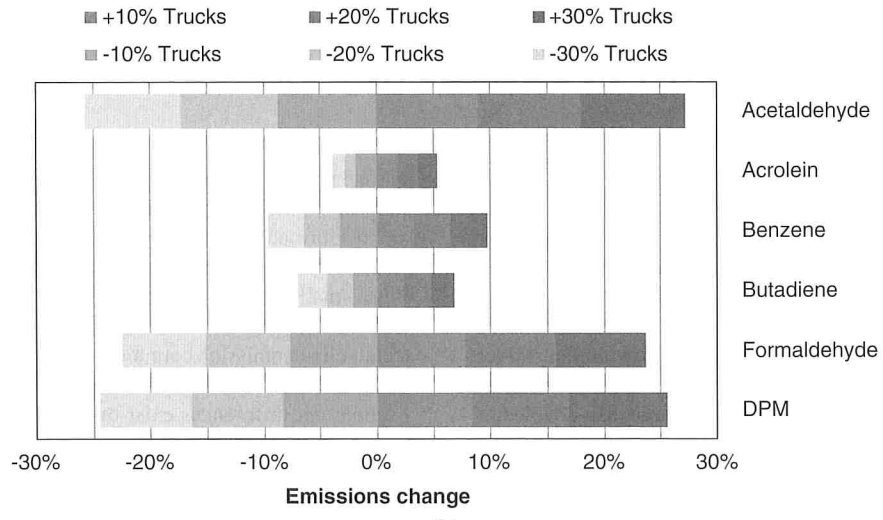

(b)

FIGURE 2 MSAT emissions sensitivity to fleet composition: (*a*) in 2004 and (*b*) in 2030. (Each increment represents a percent change in MSAT emissions associated with the corresponding truck percentage increase or decrease. Shifts in acrolein emissions are associated with gasoline-powered medium-duty and larger trucks.)

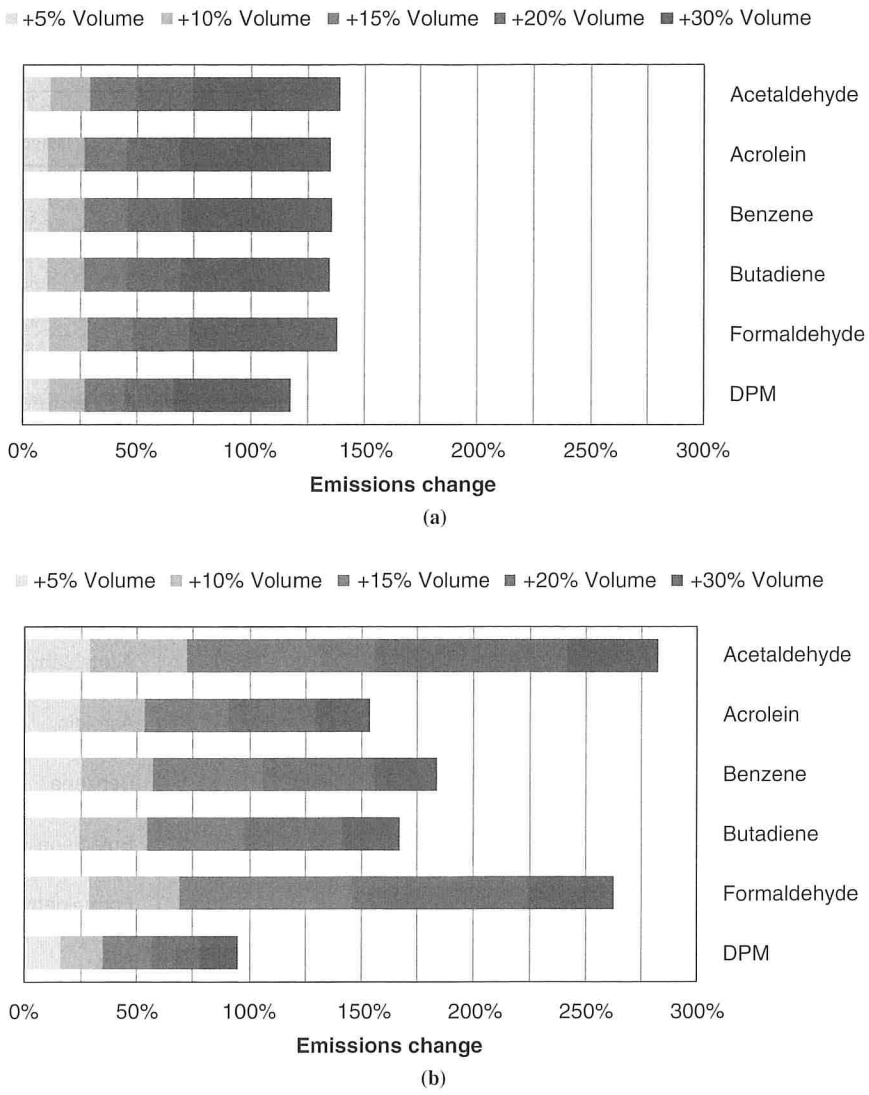

FIGURE 3 MSAT emissions sensitivity to traffic volume change: (*a*) in 2004 and (*b*) in 2030. (Each increment represents a percent change in MSAT emissions associated with the corresponding traffic volume increase. Shifts in acrolein emissions are associated with gasoline-powered medium-duty and larger trucks.)

The base case involved a 26% volume increase from 2004 to 2030, substantially lowering the average speed. However, the shift to cleaner operating vehicles over time overwhelmed the emissions increase because of reduced travel speeds, and overall emissions declined from 2004 to 2030. In contrast, within a given calendar year, volume shifts can have a large impact on speeds and emissions. In the 2030 scenario, testing a 30% overall increase in traffic volumes, travel speeds decreased from 22 mph in the base case to 10 mph with the higher volumes. In general, MSAT emissions more than doubled in 2004 and increased by a factor of two to four in 2030 with a 30% volume increase above the base case.

By 2030, the effect of speed on emissions is especially important for aldehydes. As shown in the subset of Figure 4*b*, aldehydes have emission factor curves with the steepest slopes, meaning a small decrease in speed will lead to a relatively high increase in grams per mile emissions. DPM emissions (virtually all of which are emitted by trucks) are less sensitive to total traffic volume change than other pollutants, which can be explained by the way the sensitivity analysis was performed. Shifts in acrolein emissions are associated with gasoline-powered medium-duty and larger trucks. Trucks represent only a small portion of the total fleet, so increasing the total volume adds more nontrucks than trucks. In contrast, formaldehyde and acetaldehyde emissions are a function of both truck and nontruck emissions, so the total volume impact is bigger.

Important differences exist over time in the incremental emissions impact of speed changes. In 2004, there are larger emissions impacts for each increment of additional activity and reduced speeds (year 2004 fleet emissions become increasingly more sensitive to speed changes as travel slows). However, this effect diminishes by 2030: as travel speeds slow, the incremental impact from those speed changes diminishes. Compare, as an illustration, the impact of a 30% volume increase to acetaldehyde emissions in 2004 and 2030. In 2004, the

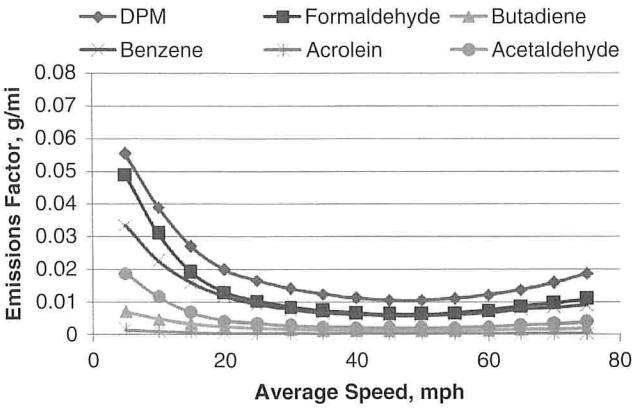

(a)

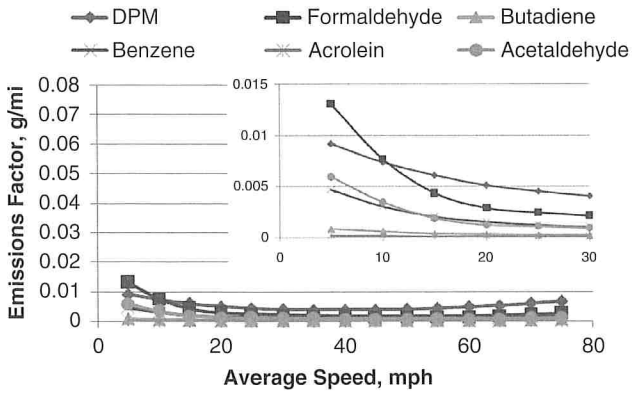

(b)

FIGURE 4 Speed effect on MSAT emission factors: (*a*) in 2004 and (*b*) in 2030. [Figure 4*b* shows an original plot and a magnified version (x = 30, y = 0.015)].

30% volume increment produces the largest incremental increase in emissions of the volume scenarios tested; in 2030, the 30% volume increment represents the smallest portion of the overall emissions increase (Figure 3). An explanation for this finding is related to the structure of the TTI formula used for speed calculation. As shown in Equation 3, the TTI approach assumes that the congested freeway speed estimates will generally not fall below 10 mph (i.e., the realistically possible minimum average highway speed is 10 mph). This assumption becomes particularly important by 2030 when travel volumes reach levels at which travel speeds are at the minimum allowed for the TTI method (Figure 5). The result, assuming the TTI formula overpredicts travel speeds in heavy congestion, is likely to be an underprediction in emissions.

MSAT Emissions Sensitivity to Speed Postprocessing Methods

It can be concluded from the previous sections that MSAT emissions are particularly sensitive to traffic speed. In turn, speeds can be especially sensitive to the method used to postprocess speed. To further investigate the importance of the method used in speed postprocessing, the authors evaluated how the selection of a speed postprocessing technique could affect emissions estimates, holding

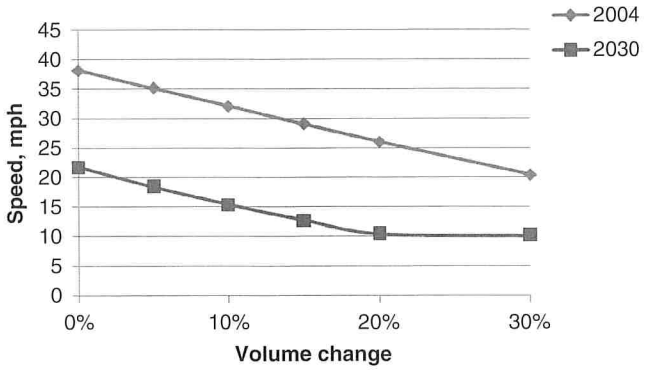

FIGURE 5 Speed sensitivity to traffic volume change for 2004 and 2030 (speeds are estimated on the basis of the TTI formula).

travel activity assumptions constant. To complete these assessments, assumed travel speeds were calculated by using the BPR formula, the resulting speeds were contrasted with those obtained using the TTI method, and the resulting emissions differences were modeled (Figure 6).

For the year 2004 base case, the difference between the two speed calculation methods is within 10%. For the 2030 base case, however, the BPR method resulted in substantially lower travel speeds (11 mph) compared to the TTI-based results (22 mph). As a result, BPR-based emissions ranged from 31% (DPM) to 62% (acetaldehyde) higher than the TTI results. For some pollutants, the difference between the two speed postprocessing methods in 2030 is larger than the corresponding emissions reduction that occurred over time because of fleet turnover. For example, applying the BPR methodology, the calculated emissions reduction for DPM over time is only about 18% (Table 4).

As illustrated by the results in Table 4, the choice of a speed postprocessing technique can have important implications for emissions estimates. Although this study did not examine the relative merits of various speed postprocessing techniques, there is literature that supports careful selection between speed postprocessing options (*18, 19, 21*).

CONCLUSION

MSAT emissions are highly sensitive to key transportation parameters and thus are potentially affected by transportation project design choices. This study used a newly developed emissions modeling tool (CT-EMFAC) to analyze DPM, formaldehyde, 1,3-butadiene, benzene, acrolein, and acetaldehyde emissions sensitivity to traffic volume, fleet composition, and average speed for years 2004 and 2030. The study found that emission estimates are more sensitive to speed changes than other input parameters. It is also critical to accurately forecast traffic volumes, which are the main determinant of estimated traffic speed.

The study findings reinforce known principles, such as the decline in fleet MSAT emissions over time, while emphasizing consideration of a forecasting process rarely discussed in the context of project-level emissions modeling: the selection of speed postprocessing techniques. In addition, traffic assumptions such as free-flow speeds and highway capacity also have an important

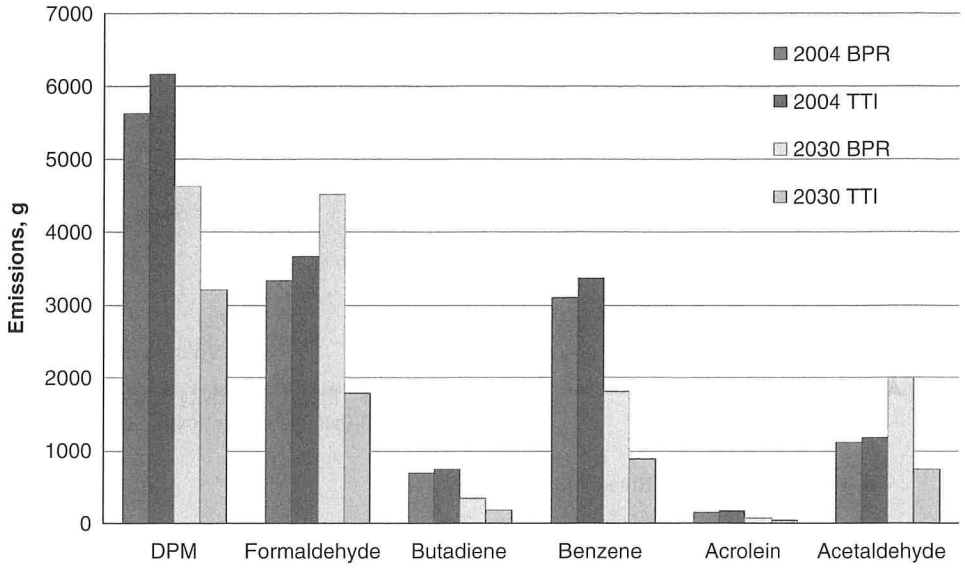

FIGURE 6 Speed postprocessing method effect on MSAT emissions (emissions modeled are for base case 2004 and 2030 scenarios).

effect on emission estimates because they further influence congested speed calculations.

Although CT-EMFAC reflects California's specific conditions (e.g., vehicle technology, fuel use, and fleet turnover), emission factor–speed curves are generally parabolic, so in concept the results of this sensitivity study can be useful for general cases in other states as well. Data limitations with respect to speciation information still exist in MSAT emissions modeling. A complete set of speciation factors, especially for diesel vehicles, are needed for improving MSAT emissions estimation. The quality of traffic activity data including volume and speed are important because MSAT emissions are sensitive to these variables; further research is needed to improve the accuracy of project-level travel activity forecasts for emissions modeling purposes.

TABLE 4 MSAT Emission Reductions Over Time and Difference Between TTI and BPR Speed Postprocessing Methods

	Emission Reductions Over Time (2004–2030)		Within-Year Differences Between Methods	
MSAT	BPR Function (%)	TTI Method (%)	2004 (%)	2030 (%)
DPM	18	48	9	31
Formaldehyde	–35	51	10	60
1,3-butadiene	50	76	8	48
Benzene	42	73	9	50
Acrolein	55	77	8	45
Acetaldehyde	–79	36	6	62

NOTE: Emissions are modeled for the base case scenarios. Shifts in acrolein emissions are associated with gasoline-powered medium-duty and larger trucks. Reported within-year differences are for TTI compared with BPR; for example, the TTI method resulted in 9% higher DPM estimates in 2004 than the BPR method.

ACKNOWLEDGMENTS

This research was partly funded through the UC Davis–Caltrans Air Quality Project. The authors gratefully acknowledge Mike Brady at Caltrans for overseeing the research effort.

REFERENCES

1. U.S. Environmental Protection Agency. *2002 National-Scale Air Toxics Assessment Technology Transfer Network,* Aug. 2009. http://www.epa.gov/ttn/atw/nata2002.html. Accessed Oct. 19, 2009.
2. English, P., R. Neutra, R. Scalf, M. Sullivan, L. Waller, and L. Zhu. Examining Associations Between Childhood Asthma and Traffic Flow Using a Geographic Information System. *Environmental Health Perspectives,* Vol. 107, No. 9, 1990, pp. 761–767.
3. Kim, J. J., S. Smorodinsky, M. Lipsett, B. C. Singer, A. T. Hodgson, and B. Ostro. Traffic-Related Air Pollution Near Busy Roads: The East Bay Children's Respiratory Health Study. *American Journal of Respiratory and Critical Care Medicine,* Vol. 170, 2004, pp. 520–526.
4. Zhu, Y., W. C. Hinds, S. Kim, S. Shen, and C. Sioutas. Study of Ultra-Fine Particles Near a Major Highway with Heavy-Duty Diesel Traffic. *Atmospheric Environment,* Vol. 36, 2002, pp. 4323–4335.
5. Health Effects Institute. *Mobile-Source Air Toxics: A Critical Review of the Literature on Exposure and Health Effects.* A Special Report of the Institute's Air Toxics Review Panel. Cambridge, Mass., 2007.
6. U.S. Census Bureau. *American Housing Survey 2004.* Table IA–6. http://www.census.gov/hhes/www/housing/ahs/ahs03/ahs03.html. Accessed May 10, 2009.
7. Fruin, S. A., A. M. Winer, and C. E. Rodes. Black Carbon Concentrations in California Vehicles and Estimation of In-Vehicle Diesel Exhaust Particulate Matter Exposures. *Atmospheric Environment,* Vol. 38, No. 25, 2004, pp. 4123–4133.
8. California Environmental Protection Agency. *The Toxic Air Contaminant Identification Process: Toxic Air Contaminant Emissions from Diesel-Fueled Engines,* Oct. 1998. http://www.arb.ca.gov/toxics/dieseltac/factsht1.pdf. Accessed July 11, 2009.
9. U.S. Environmental Protection Agency. *Health Assessment Document for Diesel Engine Exhaust.* Office of Research and Development, National Center for Environmental Assessment. Publication EPA/600/8-90/057F, 2002.

10. South Coast Air Quality Management District. *Multiple Air Toxic Exposure Study–II.* Final Report. Los Angeles, Calif., 2000.
11. South Coast Air Quality Management District. *Multiple Air Toxic Exposure Study–III.* Final Report. Los Angeles, Calif., 2008.
12. U.S. Environmental Protection Agency. Control of Emissions of Hazardous Air Pollutants from Mobile Sources. *Federal Register,* Vol. 66, No. 61, 2001, pp. 17229–17273.
13. U.S. Environmental Protection Agency. Control of Hazardous Air Pollutants from Mobile Sources. *Federal Register,* Vol. 72, No. 37, 2007, pp. 8427–8476.
14. Burbank, C. J. *Interim Guidance on Air Toxics in NEPA Documents.* Memorandum. FHWA, U.S. Department of Transportation, 2006.
15. Claggett, M., and J. Houk. 2008. Comparing MOBILE 6.2 and Emfac2007 Emission Factors. In *Transportation Research Record: Journal of the Transportation Research Board, No. 2058,* Transportation Research Board of the National Academies, Washington, D.C., 2008, pp. 51–57.
16. Wu, P., S. Bai, D. Eisinger, and D. Niemeier. *CT-EMFAC: A Computer Model to Estimate Transportation Project Emissions.* UC Davis-Caltrans Air Quality Project. Task Orders No. 61 and 67. Davis, Calif., 2007 (Update: Version 2.6, May 29, 2008).
17. *Highway Capacity Manual.* TRB, National Research Council, Washington, D.C., 2000.
18. ICF Consulting. *Sample Methodologies for Regional Emissions Analysis in Small Urban and Rural Areas.* Final Report. FHWA, U.S. Department of Transportation, 2004.
19. Bai, S., Y. Nie, and D. Niemeier. The Impact of Speed Post-Processing Methods on Regional Mobile Emissions Estimation. *Transportation Research Part D,* Vol. 12, 2007, pp. 307–324.
20. Dowling, R., W. Kittelson, A. Skabardonis, and J. Zegeer. *NCHRP Report 387: Planning Techniques to Estimate Speeds and Service Volumes.* TRB, National Research Council, Washington, D.C., 1997.
21. Skabardonis, A., and R. Dowling. Improved Speed-Flow Relationship for Planning Applications. In *Transportation Research Record 1572,* TRB, National Research Council, Washington, D.C., 1997, pp. 18–23.
22. Claggett, M., and T. L. Miller. Methodology for Evaluating Mobile Source Air Toxic Emissions: Transportation Project Alternatives. In *Transportation Research Record: Journal of the Transportation Research Board, No. 1987,* Transportation Research Board of the National Academies, Washington, D.C., 2006, pp. 32–41.
23. National Highway Institute. *Estimating Regional Mobile Source Emissions.* NHI Course 152071. FHWA, U.S. Department of Transportation, 2003.
24. Vermeire, T. *Environmental Health Criteria No. 127: Acrolein.* International Program on Chemical Safety. World Health Organization, 1991.
25. U.S. Department of Health and Human Services. *Toxicological Profile for Acrolein.* Public Health Service Agency for Toxic Substances and Disease Registry, 2007.

The Transportation and Air Quality Committee peer-reviewed this paper.

Particle Number and Size Distribution of Emissions During Light-Duty Vehicle Cold Start

Data from the Total Onboard Tailpipe Emissions Measurement System

Mitchell K. Robinson, Karen M. Sentoff, and Britt A. Holmén

Vehicle emissions during cold start are known to be significantly higher than after optimal vehicle operating temperatures are reached. There are limited data, however, on particle number and size distributions during cold start. Cold-start tailpipe emissions from a 1999 Toyota Sienna minivan were quantified at ambient temperatures between 20°C and 37°C using a novel system, the total onboard tailpipe emissions measurement system (TOTEMS), assembled to quantify the full suite of exhaust emissions from light-duty vehicles. TOTEMS particle number distributions were measured from 5.6 to 562 nm using an engine exhaust particle sizer (EEPS) and total 3- to 3,000-nm particle counts were measured using an ultrafine condensation particle counter (UCPC) with 1-s temporal resolution during cold start and warm-up driving. Second-by-second particle number distributions from five cold-start emissions tests showed similar particle emissions patterns, allowing for three different cold-start phases to be identified based on particle number emissions behavior. Cold-start duration ranged from 165 to 230 s and increased with decreasing ambient temperature. Different particle sizes during each phase were emitted for different lengths of time, with the most abundant particles in the nanoparticle (diameter <50 nm) range. The mean particle number distributions showed more than 99% of total particle number below 100 nm. Concentrations of ultrafine particles (<100 nm) during cold start were at least 10 to 100 times (EEPS), and as much as 1,000 times (UCPC), above hot-stabilized idle emissions. Observations also suggest the presence of tiny particles below 6 nm during cold start.

Recent evidence shows a strong relationship between fine particulate matter (PM) exposure and increased rates of lung diseases, cardiopulmonary diseases, and mortality (*1–4*), as well as decreased lung development in children (*5*). Vehicles are a major source of fine particles (particle diameter, Dp < 2.5 μm), ultrafine particles (Dp < 100 nm), and nanoparticles (Dp < 50 nm). However, vehicle emissions tests, typically performed under idealized lab conditions, are not wholly representative of the variability and emissions levels associated with real-world vehicle operating conditions. This study was conducted as part of a larger project initiated to better understand emissions from vehicles under real-world, on-road driving conditions. The larger project [see Holmén et al. (*6*) for more detailed description] is unique because total gas (28 species) and particulate (number distribution) tailpipe emissions are being collected for light-duty gasoline vehicles operating on a specified driving route in Vermont over four seasons of sampling. For the present study, 1-s data on particle size distributions from 5.6 to 562 nm and total particle number from 3 to 3,000 nm collected from a single vehicle are examined to quantify particle number emissions behavior during cold-start and warm-up driving after engine off-times greater than 12 h. A 12-h engine off-time is sufficient to cool the engine and catalyst to ambient temperature (*7, 8*).

Cold-start particle number emissions are significantly higher than emissions after a light-duty vehicle has warmed up to its normal operating temperature (*9*). However, few real-world data exist on particle number distributions during cold start. Extensive studies have been conducted to quantify cold-start gas-phase emissions (*8, 10*), but these studies are commonly limited to the criteria pollutants and lack high temporal resolution data for the full particle size distribution, often focusing on only gases or particle mass.

When operating efficiently, the three-way catalytic converter has been found to remove 75% of hydrocarbon particle precursors under low speed and load operating conditions (*9*). For the Environmental Protection Agency's FTP75 drive cycle, cold start produced more than 80% of the total hydrocarbon gaseous emissions (*11*), suggesting that increases may be expected for cold-start particle number emissions resulting from gas-to-particle nucleation. Understanding the magnitude of these cold-start emissions is important because many trips, especially in urban areas, are short and never allow the vehicle to reach optimal operating temperatures (*10*). Furthermore, most trips begin in urban environments, resulting in higher real-world emissions than predicted by existing models.

Previous studies have attempted to quantify the cold-start size distribution and composition of particle number emissions from light-duty vehicles. With the use of a direct injection gasoline engine and Cambustion's differential mobility analyzer, particle number emissions were found to decrease over time during engine warm-up, often with particle size decreasing as well (*12*). It was found that only 29% of particles were in the solid phase, elemental carbon between 5 and 10 nm and carbonaceous particles in the 30- to 80-nm range (*12*), meaning substantial nucleation occurred. One study noted particles

University of Vermont, 33 Colchester Avenue, Burlington, VT 05405. Corresponding author: M. K. Robinson, Mitchell.robinson@uvm.edu.

Transportation Research Record: Journal of the Transportation Research Board, No. 2158, Transportation Research Board of the National Academies, Washington, D.C., 2010, pp. 86–94.
DOI: 10.3141/2158-11

from gasoline engines are primarily in the 7- to 55-nm range during cold start (*13*). Now widely accepted, the low concentration of larger solid particles favors the formation of nuclei mode (diameter < 30 nm) particles (*14*) because of the small surface area available for gas-to-particle condensation. Also, many studies have focused more on diesel engines because they traditionally have had higher emissions rates, but diesel vehicles have lower cold-start emissions than gasoline vehicles (*15, 16*).

Decreases in ambient air temperature have been linked to increases in exhaust emissions that are an order of magnitude or more above hot-stabilized emissions (*15, 17–19*). Ambient temperatures between −20°C and +22°C showed cold-start emissions of many criteria pollutants [nitrogen oxides, carbon monoxide (CO), hydrocarbons (HC), and particle mass] were several times higher than hot-stabilized operation, with this effect magnified as ambient temperature decreased (*19*). One study documented that HC emissions were 26 g per start higher at −20°C than at +23°C (*16*). Another reported that HC emissions increased by a factor of 4 during cold starts when ambient temperature decreased from 32°C to −2°C (*18*). These changes in HC emissions could have a similar effect on nuclei mode particles because of the relationship between HC gas emissions and particle nucleation. Reported particle mass increased by a factor of 19 when cold-start temperature was decreased from 22°C to −7°C (*19*). However, a more recent study showed that particle mass was influenced little by ambient temperature (*15*), yet this result may have no relation to number emissions because particle number and mass seem to have little correlation (*20*). Mass is often reported because current regulations are mass-based (PM_{10} and $PM_{2.5}$), but particle size and number have the greatest effect on human health. Therefore, this study focused on particle number from 3 to 3,000 nm and quantified the distribution from 5.6 to 562 nm. Most particles measured in this study (nearly 100%) were below 300 nm in aerodynamic diameter.

METHODOLOGY

This section describes the vehicle and its operation during cold-start tests, the total onboard tailpipe emissions measurement system (TOTEMS) instrumentation and protocols relevant to this study, and laboratory instrument validation test procedures. All data for this study were collected with a minimum temporal resolution of 1-s and emissions were pulled directly from the tailpipe.

Test Vehicle and Emissions Data Collection

Individual emissions tests consisted of a single driver operating the vehicle under real-world driving conditions over a specific sequence of start-up operations and warm-up driving in Burlington, Vermont. One driver was used throughout the testing to minimize inconsistencies resulting from driver behavior. Before starting the vehicle, a series of quality assurance/quality control (QA/QC) measurements and operations were performed in order to collect accurate instrument and vehicle baseline data for each run. These QA/QC procedures included 3-h instrument warm-up, instrument blank data, and exhaust pipe tunnel blank data.

A gasoline-fueled 1999 Toyota Sienna minivan with a 194-horsepower, 3.0-L V-6 engine and a four-speed automatic transmission with LEV 1 emissions certification was used for all tests. At the time of testing, the minivan odometer ranged between 148,424 and 148,702 mi. Although an older vehicle was tested here, a 2005 study reported an 8.9-year median age of passenger cars. This was up from a median of 6.5 years in 1990. Furthermore, between 1990 and 2005, the median age of vehicles trended steadily up year to year, representing a sustained interest in emissions from these older vehicles (*21*). After completion of the blanks, the test vehicle's engine was started. The minivan then idled in park for a period of time before shifting into drive and traveling a 0.8-mi warm-up route to a gas station. Three traffic signals and two stop signs were encountered along the route. This activity was more than adequate for complete warm-up during the spring season data collection reported here. For this study, data are presented from engine start to engine stop at the gas station.

Total Onboard Tailpipe Emissions Measurement System

As described in more detail elsewhere (*6*), a suite of 20 instruments and accompanying data acquisition were assembled to collect second-by-second vehicle operation and tailpipe emissions data as test vehicles operate in the real world. This package, TOTEMS, collects emissions data on particle number and particle number distribution, as well as 28 gas species. In this paper, only the instrumentation and methodology relevant to particle emissions and characterization of cold-start vehicle behavior are described. An onboard battery system powered all instruments without drawing electrical power from the test vehicle. An automatic transfer switch was used to transfer onboard instrumentation from grid to battery power without shutting the instruments down, saving battery power while allowing adequate instrument warm-up.

Relative humidity and ambient temperature were monitored both inside and outside the vehicle using identical HOBOware pro v2 sensors. An AutoEnginuity ST01 ScanTool collected four engine parameters: engine load, vehicle speed, mass air flow, and engine revolutions per minute (RPM). Data acquisition cards were used to collect data for the following instruments via a Labview 7.0 interface: a type J thermocouple to monitor exhaust temperature at the end of the tailpipe, type T thermocouples to monitor temperature at the end of the heated line and the inlet of the emissions instruments, four differential pressure transducers to quantify exhaust flow rate, and four parameters monitoring the exhaust dilution system for particle measurements. The dilution system for particle measurement included two separate components, the matter engineering MD19-2E rotating disk mini-diluter and the TSI air supply evaporation tube (ASET 15-1), designed to work together providing first-stage (MD19-2E) and second-stage (ASET 15-1) dilution in one self-contained device. A total dilution ratio of 1:120 (raw exhaust: HEPA-filtered dilution air) was used throughout emissions testing.

Exhaust was transferred via a heated line (set to 191°C) from the tailpipe to the particle dilution system. Particle number emissions were quantified with two TSI, Inc., instruments: a Model 3090 engine exhaust particle sizer (EEPS) and a Model 3025A ultrafine condensation particle counter (UCPC). The EEPS counts (±20% accuracy) and sizes (± 10% accuracy) particles across 32 different bins from 5.6 to 562 nm (each bin records a specific range of particle sizes). The midpoint of each EEPS bin is the reported particle size based on aerodynamic diameter. The EEPS records particle number distribution data at a rate of 10 Hz, but values were aggregated to a 1-Hz rate and were recorded to the onboard PC using TSI EEPS Version 3.1.0 software. The UCPC counts particles from 3 to 3,000 nm with

a reported detection efficiency of 50% for 3-nm particles and 90% for particles greater than 5 nm. The total particle number concentration from the UCPC was recorded to the onboard PC using Aerosol Instrument Manager software (Version 8.1.0).

Antivibration platforms were constructed for both the EEPS and UCPC to minimize inaccuracy and instrument error due to noise resulting from vibration while driving. The instrument platform for the UCPC uses six natural rubber mounts, and because the UCPC is influenced little by vibrations, these mounts serve to help minimize instrument malfunctions that could result from being jostled. The EEPS is mounted on 10 silicone gel mounts, which reduced electrometer noise caused by driving by 64%.

The TOTEMS emissions measurement setup pulls engine exhaust from the tailpipe adapter through the 10-ft ⅜-in. inside diameter (ID) heated line at an exhaust sample flow rate of 13 L/min. The heated line (Atmoseal Model IGH-120-S-6/X-G13) is lined with smooth, flexible stainless steel pipe to minimize particle losses. At the end of the heated line is a four-way, stainless steel Swagelok fitting that splits the flow of undiluted exhaust to the emissions instruments: 12 L/min to the Fourier transform infrared spectrometer for gas analysis and 1.0 L/min to the dilution system for particle measurements. From the dilution system, particles are transported to the EEPS and UCPC via 42 in. of 1/4-in. ID conductive silicone tubing. The flow is split, first to the EEPS, then to the UCPC using two stainless steel Swagelok fittings. Data are collected on a Dell OptiPlex GX620 desktop PC outfitted with two National Instruments Model 6024E data acquisition cards and five serial ports.

EEPS and UCPC particle number emissions data were plotted for analysis using MATLAB Version R2008b. Instrument blanks were used in this program to calculate the lower detectable particle concentration limit for each EEPS size range. Because the EEPS operates on electrical principles, it is sensitive to noise. Therefore, using the prerun instrument blank for each run, the mean noise values for each of the 32 EEPS bins plus 3 standard deviations for each bin were calculated individually and subtracted from the EEPS concentrations. Noise quantification for the UCPC was unnecessary because it was not sensitive to noise.

Data Alignment for Instrument and Exhaust Flow Lags

All particulate number emissions data were aligned to the scantool data based on the "ignition on" point for reference. At this point, engine RPM changed from 0 (engine off) to the peak reading (ignition) in 1 recorded second of data. The EEPS and UCPC behaved similarly, where the concentrations jumped from background to maximum concentration in 1 recorded second. Therefore, the scantool and particle emissions data were time-aligned using the last point of 0 RPM and the last point for background particulates. No lag was assumed for exhaust temperature because it appeared to be sufficiently small (<0.5 s) to not affect data alignment.

Particle Number Instrument Comparison: Laboratory Tests

A comprehensive comparison between the EEPS and UCPC was conducted. From this comparison, it was determined that both particle instruments are necessary for quality assurance and to fully understand the second-by-second tailpipe particle emissions data. Laboratory tests were performed by generating constant concentrations (~3.5×10^4 #/cm^3) and varied concentrations (5.4×10^3 to 8.9×10^4 #/cm^3) of 10- to 100-nm particles, ensuring no detection bias toward either particle instrument. (The EEPS and UCPC have overlapping, but not identical, particle size measurement ranges.) Two types of particles were generated: a sodium chloride solution with a concentration of 0.2 g/L in deionized water and a 10:1000 (v/v) emery oil–isopropyl alcohol solution. Both solutions were atomized using a TSI Model 9302 atomizer and particle-free compressed air. From the atomizer, the NaCl aerosol passed through silica gel desiccant for drying. The desiccant was bypassed when using emery oil (drying not needed). Aerosol was transferred to the EEPS and UCPC through the dilution system (set to 80°C) using the same setup described for emissions testing. A total of 28 tests using sodium chloride particles and 14 tests using oil particles were performed. Particle type (emery oil versus sodium chloride) did not influence the total particle concentrations from either instrument. The in-lab comparison confirmed that both instruments have response times to enable analysis of cold-start data and that the EEPS instrument is capable of generating reproducible total particle concentrations.

The overall average percent difference between the EEPS and UCPC particle number concentrations was between 19% and 20%, with UCPC always higher. This was consistent regardless of particle composition and for both stable and varying particle concentrations. The instrument percent difference, which varied 5% to 25% during individual tests, results from the different measuring techniques of the two instruments and appears to be a consequence of the EEPS underpredicting concentration changes for the tested number concentrations.

Constant and transient dilution factor tests were performed to compare the instruments. The potentiometer on the ASET, which controls Stage 2 dilution, was always kept at 7.1. Constant concentration tests were performed stepwise by adjusting the MD19-2E potentiometer in increments of 10, beginning at 10% and ending at 100%. The potentiometer was kept at each increment for a minimum of 60 s. Transient tests were performed by rapidly changing the MD19-2E potentiometer to random values between 10% and 100%. Figure 1 shows typical results from both steady and transient concentrations. The instrument response of both the EEPS and UCPC was very consistent. Comparing the EEPS to the UCPC, the two instruments track very well together with nearly identical response curves. From Figure 1, the EEPS seems to underpredict concentration changes when compared to the UCPC for these laboratory test conditions. However, neither instrument appears to show a hysteresis effect. Under low concentrations (<5,000 particles per cm^3), the EEPS was much more variable, and therefore less accurate, due to electrometer noise. Emissions concentrations below 5,000 particles per cm^3 should therefore be interpreted with caution. The EEPS and UCPC had a consistent concentration difference, evident from similar percent differences calculated using constant concentration tests.

Defining Cold Starts

Although previous studies used catalyst light-off (*18*) or engine coolant temperature (*12*) to characterize cold starts, this study used particle number emissions behavior because of patterns observed in the data. Total cold-start duration was characterized by three separate phases based on significant changes in particulate emissions behavior. Figure 2 shows these different phases (RPM, vehicle speed, and exhaust temperature are included for reference) and the end of each

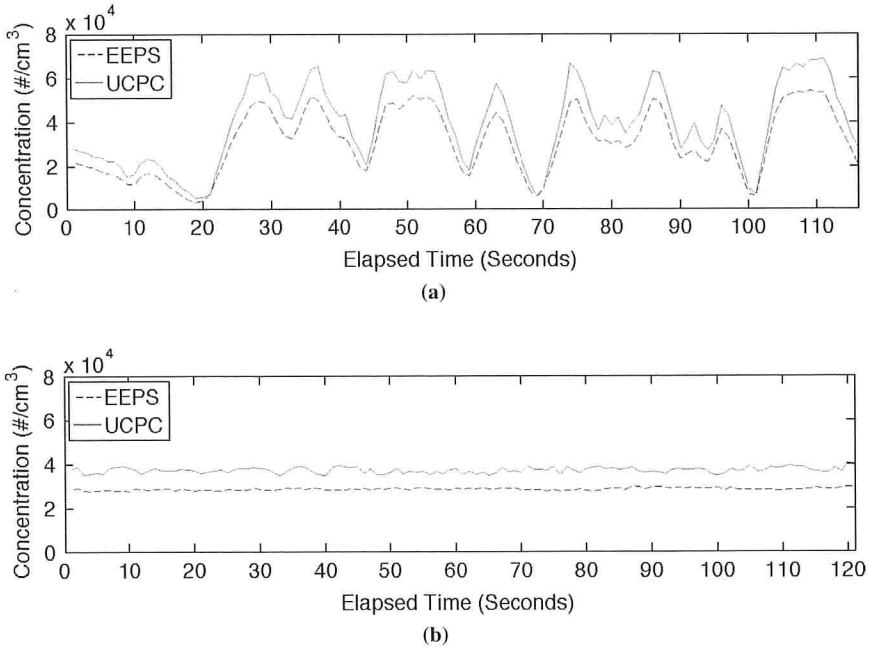

FIGURE 1 Laboratory tests compared the EEPS and UCPC under (*a*) transient concentrations and (*b*) constant concentration of laboratory-generated sodium chloride particles (# = number of particles).

phase is labeled. Flat tops on the UCPC curve in Figure 2 resulted when maximum concentration limits were reached. The UCPC max concentration limit of 99,900 is a major drawback when looking at engine emissions. Even with a high dilution ratio (1:120), the UCPC reached its maximum limit during much of the cold start. Use of a higher dilution ratio will cause lower concentrations to be undetected by the EEPS.

Cold-start emissions were defined to begin when the particle number concentration increased to three times greater than the tunnel blank background of 500 to 800 particles per cm^3 (EEPS) and 70 to 100 particles per cm^3 (UCPC) (Figure 2 at 4 s). Note that reported particle number concentrations were not corrected for losses in the transfer lines. Phase 1 of the cold starts occurred when the car was in park with the engine running; it is characterized by the highest total particle number emissions of each run. Phase 1 began at engine-on and depended on when the driver put the car in gear. Although not ideal for analysis, this is consistent with the variability associated with real-world driving.

Phase 2 of the cold start was characterized by vehicle operation—starting when the automatic transmission was shifted to drive

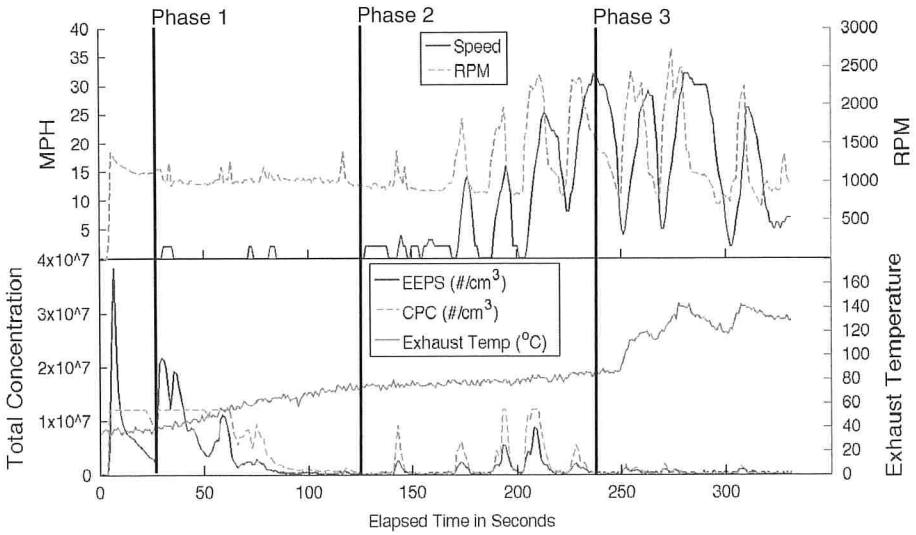

FIGURE 2 Total concentrations from the EEPS and UCPC during Run 1, corrected for dilution (bottom panel) (three vertical lines show cold-start phases; concentrations are in #/cm^3 and exhaust temperature is in °C).

(Figure 2 at 27 s). The end of Phase 2 was defined by emissions behavior, when Phase 2 idle particle concentrations dropped to levels comparable to hot-stabilized idle concentrations. The vehicle was moving during Phase 2, but predominately at idle-creep (<5 mph) in a parking lot setting.

Phase 3 was characterized by a particle emissions pattern showing elevated emissions during acceleration events (Figure 2 at 127 to 237 s). The end of Phase 3 occurred when particle concentrations satisfied three criteria: (*a*) total particle number concentrations were comparable to hot-stabilized idle [equivalent to ~2 times above EEPS instrument blank (1,400 #/cm^3) and ~250 times above UCPC instrument blank (100 #/cm^3), before accounting for dilution], where hot-stabilized idle concentrations were determined from traffic signal idling data collected later in the full driving route; (*b*) the smallest particles (5.6 to ~10 nm) in the measured EEPS distribution are no longer detectable; and (*c*) there were no longer significant increases in total number concentration as a result of mild to moderate RPM increases. Therefore, Phase 1 was driver behavior dependent, while Phases 2 and 3 were characterized by particle number emissions patterns.

EXPERIMENTAL RESULTS

The broader measuring range of the UCPC at both the large and small particle diameter ends [3 to 3,000 nm (UCPC) versus 6 to 560 nm (EEPS)] seems to indicate there are large numbers of particles formed during cold start that are outside the EEPS measurement range. This observation is drawn from the significant differences in particle number concentrations (at least a factor of 3) that are seen only during the cold start (Figure 2) but were not present while driving after the catalyst is hot or in the lab under controlled particle generation. The difference can most likely be attributed to the nucleation of small particles below the EEPS lower diameter limit of 5.6 nm. Significant particle numbers larger than 562 nm (EEPS maximum size) are unlikely in vehicle exhaust.

Cold-Start Total Particle Number Emissions Data

Cold-start data were collected on 5 separate days with the ambient temperature range from 20°C to 37°C for all starts. Table 1 summarizes the cold-start data. The actual total concentration difference between the EEPS and UCPC was even greater than documented in Table 1 because the UCPC reached its upper measurement range (9.99×10^4) for extended periods during the cold start, whereas the EEPS never reached its maximum limits (refer to Figure 2). Cold-start duration presented in Table 1 was determined from engine-on to the end of Phase 3.

Cold-Start Phases: Duration and Particle Modes

Figure 3 shows the contour plot of EEPS number distributions over the full duration of one cold start with corresponding vehicle speed, RPM, and exhaust temperature. Exhaust temperature was divided by 5 to achieve the same scale as vehicle speed in Figure 3; engine was switched on at 4 s, vehicle was put in gear at 27 s, and vehicle moved at idle-creep speed out of parking area, accelerating onto Colchester Avenue at 141 s. Data are presented as dN/dlogDp, which denotes the particle number concentration normalized to the individual diameter range on a given EEPS channel (or size bin) (i.e., Channel 1 is from 5.6 to 6.4 nm but Channel 32 is from 487 to 562 nm). Cold-start Phase 3 clearly shows particle concentrations spiking with increased RPM—which, in this case, indicates acceleration—for all particle sizes below 154 nm. This effect diminished as exhaust temperature gradually increased (see Figure 2, 140 to 237 s, for example).

Phase 1 lasted for 15 to 35 s and the highest measured concentrations were for particles between 8 and 60 nm. Particles larger than 20-nm diameter had extremely high concentrations for only about 5 s after engine start before dropping significantly; this behavior can most likely be attributed to enrichment at engine start (*9*). Even though the larger (>20 nm) particle concentrations dropped quickly in Phase 1, their concentrations remained as much as 100 times higher than hot-stabilized idle for the duration of Phase 1.

Phase 2 lasted 60 to 95 s with significant increases in number concentrations for particles from 5.6 to 200 nm in diameter. The highest concentrations, however, occurred for 10- to 30-nm particles and were two orders of magnitude above hot-stabilized idle concentrations. Increases in RPM during Phase 2 resulted in significant particle concentration increases (and subsequent emission rate increases) with particle diameters centered around 10 nm.

Phase 3 had variable particle number emissions that depended on driver behavior in urban traffic and lasted for 90 to 140 s. During Phase 3, when at idle (~700 RPM), the concentrations remained comparable to hot-stabilized idle concentrations. When RPM increased, which again indicates acceleration, 6- to ~154-nm particle concentrations increased with the highest concentrations at 10 and 30 nm. This is largely because the catalyst is unable to efficiently remove particle precursor vapors during Phase 3 because the catalyst is below its optimal operating temperature and decreased residence time. The particle number increase for sizes between 6 and ~154 nm occurred even under engine loads of 30% to 40% and acceleration of 2 to 3 mph/s. The emission of Phase 3 particles can likely be

TABLE 1 Summary of Cold-Start Emissions Data

Run No.	Cold-Start Duration (s)	EEPS Total Cold Start (#/cm^3)	CPC Total Cold Start (#/cm^3)	Avg. T (°C)	Avg. RH (%)
1	230	7.11E + 08	1.09E + 09[b]	20	28
2	165	3.50E + 08	6.68E + 08[b]	37	23
3	191	7.23E + 08	Instrument malfunction	25	42
4	201	5.13E + 08	8.35E + 08[b]	33	39
5	199	4.97E + 08	7.96E + 08[b]	32	37

[a]EEPS and UCPC data are the sum of particle number concentrations for the full cold-start duration (Phases 1–3 inclusive).
[b]Indicates the instrument reached its maximum concentration limit (9.99×10^4) during the cold-start period, meaning data are biased low.

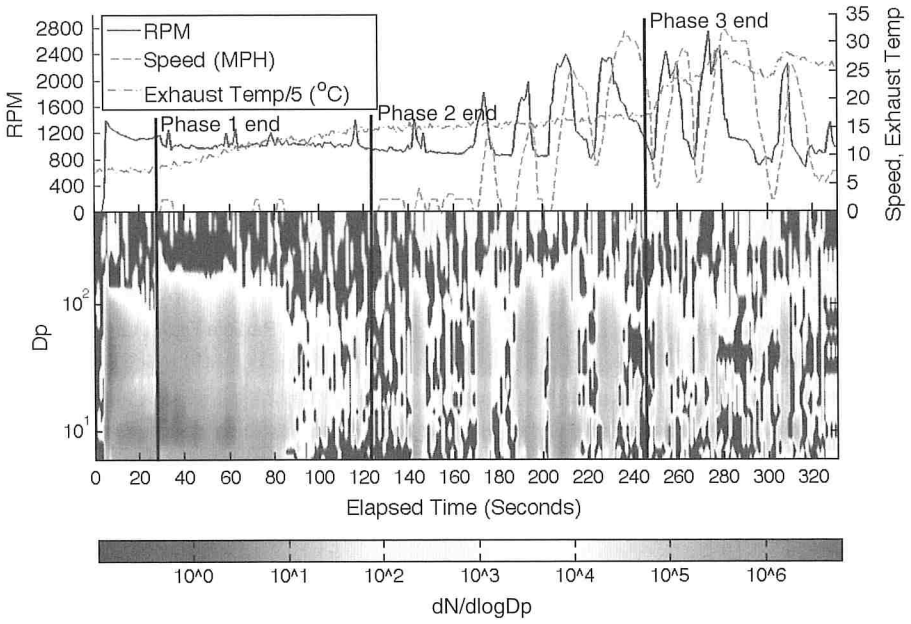

FIGURE 3 Contour plot of particle number distribution (bottom panel) over first 330 s of Run 1 test period, with time-aligned data on engine speed, vehicle speed, and exhaust temperature (upper panel).

attributed to enrichment during acceleration (>30 nm) events (*9*), mechanical release of particles (>30 nm), and increased flow rates (<30 nm). As exhaust flow rate increases, the catalytic converter becomes more inefficient due to reaction kinetics and shorter residence time in the catalyst. Although acceleration rates during the warm-up driving were relatively low (2 to 3 mph/s), even small increases in flow rate may be enough to cause significant increases in particulate number emissions if the catalytic converter is not operating at its optimal temperature. This may therefore indicate a gradual increase in the efficiency of the catalyst relative to its temperature until the optimal temperature is reached. The larger particles (>60 nm) observed throughout the cold start may, in part, be attributed to re-entrainment from the mechanical release of solid particles from the exhaust system caused by increased flow rates. At the end of Phase 3 (which is also the end of the cold start at 237 s on Figure 3), the smallest particles measured by the EEPS (5.6 to ~10 nm) are no longer detectable or have very low concentrations (see Figure 3, 237 to 330 s), indicating the catalyst is efficiently removing compounds that potentially nucleate to particles. As expected, the highest particle number concentrations occurred for particles in the nanoparticle (Dp < 50 nm) range, which accounted for over 97% of the particles over the entire cold start (Phases 1 to 3).

Mean Particle Size Distribution

EEPS data for each phase of the cold start over the five runs were averaged to evaluate changes in particle distribution over time after engine ignition. The particle number distributions changed consistently between phases of the cold start (Figure 4), but the particle diameter of the distribution "modes" was consistent run to run. In Figure 4, the solid line represents mean EEPS concentrations over five cold start runs and the error bars represent the overall range from five runs. Particle number distribution under hot-stabilized idle operation is included for reference; note that it has much lower concentrations and a chiefly bimodal distribution. The modes are the particle diameters of the distribution's peaks. Modes are typically assigned as sequential numbers based on particle diameter (*x*-axis), not the concentration (*y*-axis). In Figure 4, Mode 1 (10 nm) had the highest concentration, Mode 2 (18 nm) had the lowest concentration, and Mode 3 (50 nm) was intermediate in concentration. Mode 1 (10 nm) was present in all three phases of the cold start, but Mode 2 (18 nm) and Mode 3 (50 nm) were distinct only for Phases 1 and 3. Phase 1 had the highest variability in particle number for all particle diameters. During hot-stabilized idle operation (Figure 4, bottom), the greatest variability and highest emissions were for sizes between 8.65 and 11.55 nm, corresponding to Mode 1 of the cold-start distributions. Like Phase 2, hot-stabilized idle operation lacked a distinct Mode 2 (18 nm).

Magnitude and Duration of Different Particle Sizes During Cold Start

Concentrations from the EEPS were aggregated to 10 bins based on similar trends during cold start. EEPS sizing ranges are equally spaced on a log-scale, so the smallest ranges, and therefore the best resolution, are in the smallest particle sizes. Table 2 shows the different aggregate bin size ranges, the average particle concentration (magnitude) from all combined runs, and the temporal duration over which that particle size was detectable for each phase of the cold start. Concentrations from hot-stabilized idle operation are also provided for comparison. The duration of particles for each size range, except for particles from 5.6 to 7.5 nm, began at the beginning of each phase and lasted, on average, the length of time provided in Table 2. Particle sizes from 5.6 to 7.5 nm demonstrated slightly different behavior than all other sizes and therefore comprised the first aggregated bin. Particle number did not increase significantly after engine start for 3 to 5 s, then increased to the levels reported in Table 2. The particle number concentrations in Bin 1 also changed

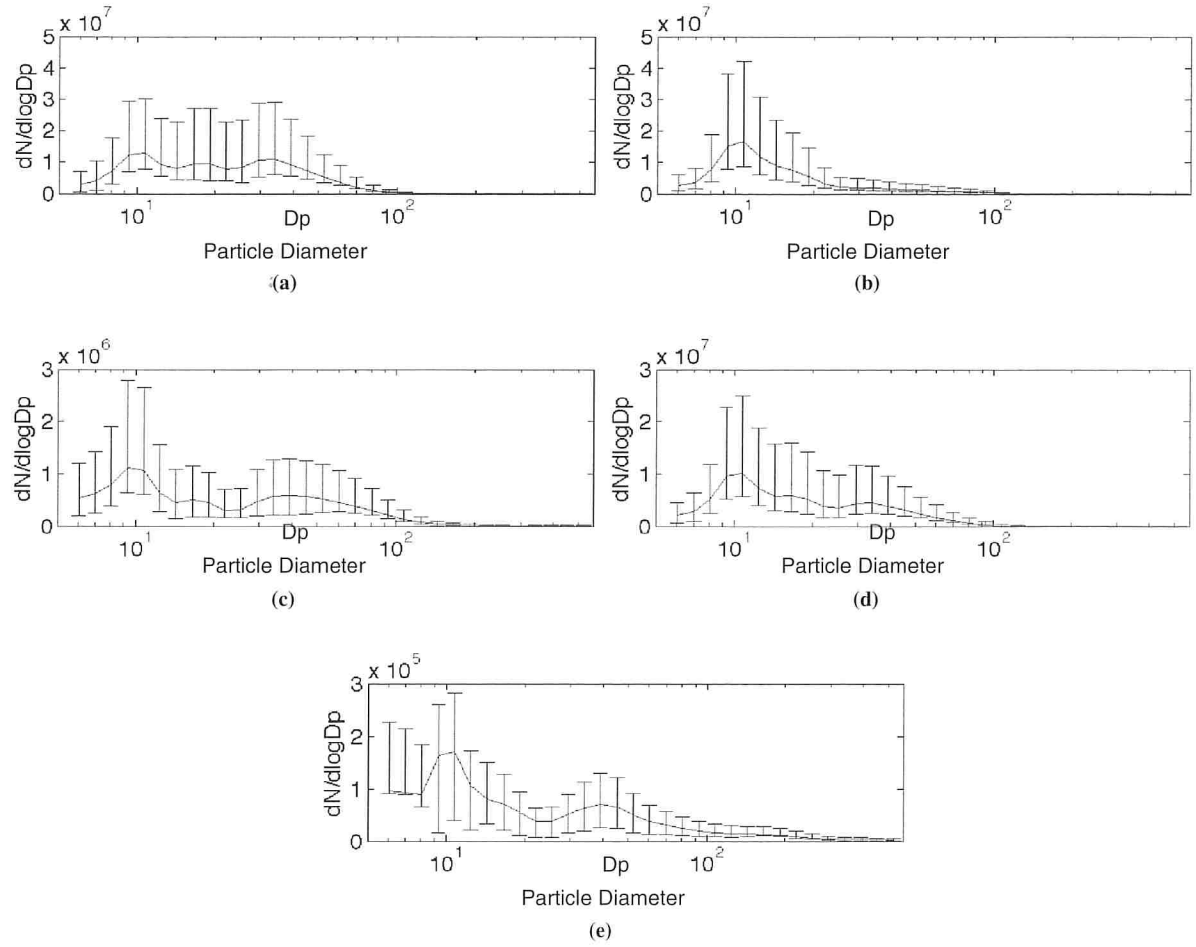

FIGURE 4 Cold-start mean particle number distributions (note different *y*-scales): (*a*) Phase 1, (*b*) Phase 2, (*c*) Phase 3, (*d*) entire cold start, and (*e*) hot-stabilized idle.

TABLE 2 Mean Particle Number Magnitude (#/cm^3) and Duration (s) for Three Cold-Start Phases and Hot-Stabilized Idle for Aggregated Particle Size Ranges

	Phase 1			Phase 2			Phase 3			Hot-Stabilized Idle
Particle Size Range	Magnitude	Duration	SD of Duration	Magnitude	Duration	SD of Duration	Magnitude	Duration	SD of Duration	Magnitude
5.6–7.5	4.52E + 05	24	6.56	3.83E + 05	43	28.02	6.78E + 04	91	36.06	7.20E + 03
7.5–10	1.23E + 06	27	4.73	1.43E + 06	42	27.54	1.14E + 05	91	37.15	1.31E + 04
10–13.3	1.38E + 06	27	4.73	1.76E + 06	42	27.54	1.01E + 05	93	27.41	1.72E + 04
13.3–17.8	1.10E + 06	20	5.13	1.01E + 06	42	27.54	5.56E + 04	97	31.33	1.30E + 04
17.8–23.7	1.09E + 06	20	5.13	5.48E + 05	27	26.10	4.26E + 04	97	31.33	6.93E + 03
23.7–31.6	1.19E + 06	15	2.65	2.50E + 05	25	28.02	4.66E + 04	92	24.01	9.31E + 03
31.6–48.7	1.74E + 06	16	2.73	2.85E + 05	25	28.02	1.05E + 05	97	15.28	2.69E + 04
48.7–75	6.62E + 05	12	2.31	1.87E + 05	27	26.10	8.30E + 04	100	36.06	1.84E + 04
75–100	7.79E + 04	6	1.73	5.91E + 04	20	10.41	3.04E + 04	60	52.92	6.38E + 03
100–562.3	2.05E + 04	2	1.15	3.49E + 04	7	2.52	1.93E + 04	40	57.74	7.75E + 03

very little through Phases 1 and 2, whereas sizes greater than 7.5 nm showed a clear end to Phase 1. Particle sizes between 7.5 and 100 nm showed very similar patterns in time series concentration, so these sizes were aggregated to eight bins based on the duration for which the particles were detectable. For example, in Table 2, Bin 7.5 to 10 nm and Bin 10 to 13.3 nm had nearly identical mean duration over each cold-start phase. During the aggregation process, particle sizes from the EEPS 32 size ranges demonstrating these similarities were combined. Larger particle size concentrations (i.e., diameters 100 to 562 nm), even when aggregated, were always at least two times (only representing ~1% of total number emissions) lower than other aggregated particle concentrations, so a more disaggregate approach was deemed unnecessary for this 10th bin.

Phase 3 was different from the first two phases because of the differing behavior during on-road driving (variable RPM, vehicle speed, and exhaust flow rate). Particle number increased for most particle sizes up to 154 nm (as shown in Figure 3) when RPM and flow rate increased, so the average durations of most aggregate size bins were quite similar in Phase 3. Also, Phase 3 concentrations were 1.6 to 17 times lower (depending on particle size) than those in Phases 1 and 2. This was a direct result of having generally low emissions during many episodes of idle operation from on-road travel under urban driving conditions. As was also indicated by Price et al. (*12*), mean particle size decreased through each phase, which is shown in Table 2 by smaller particles having longer durations. Lastly, the variability in cold-start duration, and subsequently total cold-start number emissions, is evident in the standard deviation. The standard deviation was typically larger for the smaller particles; this indicates greater variability from day to day in the time period over which the smallest particles were emitted.

Effect of Ambient Temperature

Although all data collected to date were for relatively warm days, with ambient temperatures between 20°C and 37°C (refer to Table 1 for ambient conditions), a trend was observed between ambient temperature and total cold-start duration. The maximum particle number concentrations emitted, as measured by the EEPS (the UCPC always reached its maximum concentration limit), were not influenced by the ambient temperature over the range of ambient temperatures sampled, but the sum of particles emitted throughout the entire duration of the cold start clearly indicated that, because of increased cold-start duration, cooler days resulted in greater total cold-start particle number emissions. The EEPS total particle number was two times higher for a 20°C day versus a 37°C day. Despite a shorter duration, the 25°C day cold-start emissions were slightly higher than the 20°C day by 2%. This is the only inconsistent day from the general trend. The observed effect of ambient temperature on cold-start emissions is consistent with previous work (*9, 12, 19*), including studies that only quantified gaseous emissions such as HC and CO (*17, 18*), which are precursors to particulate emissions (*9*).

CONCLUSIONS

Although this data set was small, based on only one vehicle, and measurements were performed with ambient temperature above 20°C, the value of second-by-second particle number distributions, which is rarely available in previous studies, is documented. High temporal resolution of the EEPS instrument allowed identification and quantification of shifting distributions between phases of the cold start. This means that a slower scanning mobility particle sizer instrument is inadequate for fully understanding particle behavior during the entire cold start. Also, all cold starts were performed with ambient temperatures above 20°C. Although there was clearly a relationship between cold-start duration and magnitude and ambient temperature, more data need to be collected in fall and winter months to determine how great an influence ambient temperature has on particle number distributions.

It is important to understand the distribution, as well as the magnitude and duration, of cold starts. Most exhaust particles (~99%) are less than 100 nm in diameter. For the minivan tests, three modes were present at 10 nm, 18 nm, and 50 nm, with the highest concentrations and longest duration occurring at 10 nm. Ambient temperature greatly influenced cold-start duration ranging from 165 to 230 s, where concentrations measured by the EEPS were 10 to 100 times greater than hot-idle concentrations. If the UCPC is considered, cold-start particle number concentrations were at times at least three orders of magnitude greater than hot-stabilized idle concentrations. This finding has implications for better understanding the health effects associated with particle number emissions from vehicles.

Instrument capabilities currently have serious limitations when quantifying vehicle particle number emissions. From this study, it is seen that the full particle number distribution cannot be collected from light-duty vehicles with the necessary particle size resolution using any single commercially available instrument. The increased difference between the EEPS and UCPC occurring during the cold start indicated significant numbers of particles outside the EEPS measuring range. Comprehensive multi-instrument studies must be conducted with representative vehicle types, fuels, maintenance levels, emissions control devices, vehicle age, and varying weather conditions to understand cold-start emissions.

ACKNOWLEDGMENTS

This project was funded by the U.S. Department of Transportation through the UTC research program at the University of Vermont Transportation Research Center under Signature Project 2.

REFERENCES

1. Brook, R. D., B. Franklin, W. Cascio, Y. Hong, G. Howard, M. Lipsett, R. Luepker, M. Mittleman, J. Samet, S. C. Smith, Jr., and I. Tager. Air Pollution and Cardiovascular Disease: A Statement for Healthcare Professionals From the Expert Panel on Population and Prevention Science of the American Heart Association. *Circulation,* Vol. 109, 2004, pp. 2655–2671.
2. Pope III, C. A., R. T. Burnett, M. J. Thun, E. E. Calle, D. Krewski, K. Ito, and G. D. Thurston. Lung Cancer, Cardiopulmonary Mortality, and Long-Term Exposure to Fine Particulate Air Pollution. *JAMA,* Vol. 287, No. 9, 2002, pp. 1132–1141.
3. MacNee, W., and K. Donaldson. Mechanism of Lung Injury Caused by PM10 and Ultrafine Particles with Special Reference to COPD. *European Respiratory Journal,* Vol. 21, Suppl. 40, 2003, pp. 47s–51s.
4. Pope III, C. A., R. T. Burnett, G. D. Thurston, M. J. Thun, E. E. Calle, D. Krewski, and J. J. Godleski. Cardiovascular Mortality and Long-Term Exposure to Particulate Air Pollution: Epidemiological Evidence of General Pathophysiological Pathways of Disease. *Circulation,* Vol. 109, 2004, pp. 71–77.
5. Gauderman, W. J., E. Avol, F. Gilliland, H. Vora, D. Thomas, K. Berhane, R. McConnell, N. Kuenzli, F. Lurmann, E. Rappaport, H. Margolis,

D. Bates, and J. Peters. The Effect of Air Pollution on Lung Development from 10 to 18 Years of Age. *New England Journal of Medicine,* Vol. 351, No. 11, 2004, pp. 1057–1067.
6. Holmén, B. A., K. M. Sentoff, M. K. Robinson, and P. Montane. University of Vermont Total Onboard Tailpipe Emission Measurement System Instrumentation Package for Real-World Monitoring of Conventional and Hybrid Light-Duty Vehicles. Presented at 89th Annual Meeting of the Transportation Research Board, Washington, D.C., 2010.
7. Favez, J.-Y., M. Weilenmann, and J. Stilli. Cold Start Extra Emissions as a Function of Engine Stop Time: Evolution Over the Last 10 Years. *Atmospheric Environment,* Vol. 43, No. 5, 2009, pp. 996–1007.
8. André, J.-M., and R. Joumard. *Modelling of Cold Start Excess Emissions for Passenger Cars.* INRETS Report LTE 0509, Bron, France, 2005.
9. Kittelson, D. B., W. F. Watts, J. P. Johnson, J. J. Schauer, and D. R. Lawson. On-Road and Laboratory Evaluation of Combustion Aerosols. Part 2: Summary of Spark Ignition Engine Results. *Journal of Aerosol Science,* Vol. 37, No. 8, 2006, pp. 931–949.
10. Blaikley, D. C. W., A. P. Smith, E. A. Feest, and A. H. Reading. *UG219 TRAMAQ—Cold Start Emissions. Summary Report.* AEA Technology, Oxfordshire, United Kingdom, 2001.
11. Xu, Z., J. Yi, S. Wolldridge, D. Reiche, E. Curtis, and G. Papaioannou. *Modeling the Cold Start of the Ford 3.5LV6 EcoBoost Engine.* Paper 2009-01-1493. SAE International, 2009.
12. Price, P., R. Stone, D. OudeNijeweme, and X. Chen. *Cold Start Particulate Emissions From a Second-Generation DI Gasoline Engine.* SAE Paper 2007-01-1931, 2007.
13. He, C. *Time-Resolved Emission Characteristics of Gasoline Vehicle Particle Number and Size Distributions.* Paper 2008-01-1750. SAE International, 2008.
14. Kasper, A., H. Burtscher, J. Johnson, D. B. Kittelson, W. F. Watts, U. Baltensperger, and E. Weingartner. *Particle Emissions From Si-Engines During Steady State and Transient Operating Conditions.* Paper 2005-01-3136. SAE International, 2005.
15. Weilenmann, M., J.-Y. Favez, and R. Alvarez. Cold-Start Emissions of Modern Passenger Cars at Different Low Ambient Temperatures and Their Evolution Over Vehicle Legislation Categories. *Atmospheric Environment,* Vol. 43, No. 15, 2009, pp. 2419–2429.
16. Weilenmann, M., P. Soltic, C. Saxer, A.-M. Forss, and N. Heeb. Regulated and Nonregulated Diesel and Gasoline Cold Start Emissions at Different Temperatures. *Atmospheric Environment,* Vol. 39, No. 13, 2005, pp. 2433–2441.
17. Li, H., G. Andrews, and D. Savvidis. *Impact of Ambient Temperatures on VOC Emissions and OFP During Cold Start for SI Car Real World Urban Driving.* Paper 2009-01-1865. SAE International, 2009.
18. Andrews, G. E., G. Zhu, H. Li, J. A. Wylie, A. Tomlin, M. Bell, and J. Tate. *The Effect of Ambient Temperature on Cold-Start Urban Traffic Emissions for a Real-World Si Car.* Paper 2004-01-2903. SAE International, 2004.
19. Ludykar, D., R. Westerholm, and J. Almén. Cold Start Emissions at +22, –7 and –20°C Ambient Temperatures from a Three-Way Catalyst (TWC) Car: Regulated and Unregulated Exhaust Components. *Science of the Total Environment,* Vol. 235, No. 1–3, 1999, pp. 65–69.
20. Kittelson, D. B. Engines and Nanoparticles: A Review. *Journal of Aerosol Science,* Vol. 29, No. 5/6, 1998, pp. 575–588.
21. Research and Innovative Technology Administration: Bureau of Transportation Statistics. www.bts.gov/publications/national_transportation_statistics/2005. Accessed Nov. 6, 2009.

The Transportation and Air Quality Committee peer-reviewed this paper.

Second-by-Second Characterization of Cold-Start Gas-Phase and Air Toxic Emissions from a Light-Duty Vehicle

Karen M. Sentoff, Mitchell K. Robinson, and Britt A. Holmén

Tailpipe pollutants from motor vehicles are linked to environmental concerns and human health issues. Gasoline engine ignition produces a significant portion of trip emissions, but few studies have quantified mobile source air toxic (MSAT) species for light-duty vehicles during cold start. Real-world tailpipe emissions were measured from a 1999 Toyota Sienna minivan with the University of Vermont total onboard tailpipe emissions measurement system. A Fourier transform infrared spectrometer measured 27 gas-phase emissions for cold start, extended idle, and warm-up driving at 1-s temporal resolution. Analysis demonstrated that (*a*) time to optimal function of emissions control devices was not indicated by one species, but varied for different pollutants; (*b*) extended idling after cold start produced elevated emissions for MSAT species as compared to warm-up driving; and (*c*) ambient temperatures ranging from 9.5°C to 38.4°C affected species from each emission category, with the exception of carbon dioxide. Carbon monoxide produced peak emissions three orders of magnitude higher than hot-stabilized conditions for an average of 90 s, regardless of operating conditions, while nitric oxide peak emissions were over an order of magnitude higher during warm-up driving than extended idle. Peak MSAT emissions, up to two orders of magnitude higher than hot-stabilized idle, were maintained or increased during extended idle and decreased to baseline within 100 to 200 s of warm-up driving. Results indicate extended idling after cold starts prolongs elevated concentrations of MSAT emissions, suggesting that recent policy efforts to reduce vehicle idling behavior could limit potential human exposure to the toxic exhaust constituents.

Vehicle emissions have widely known adverse environmental and human health effects, resulting from regulated and unregulated pollutant by-products of fuel combustion. Mobile source air toxics (MSATs) are of particular interest because they are identified as cancer-causing agents or potentially harmful to human health (*1*). Further, vehicle emissions models are predominantly informed by laboratory testing at baseline conditions, neglecting the influence of real-world conditions on engine operation and resulting emissions. Recent work to improve inventories and enhance the accuracy of emissions models has created a need for real-world data collection.

The data analyzed here were collected as part of a pilot study monitoring both particulate and gaseous emissions of real-world vehicles in northern climates, in line with the research aims of the Transportation Research Center at the University of Vermont. The overall objectives of this broader research are (*a*) to better characterize tailpipe emissions during real-world operation of vehicles on a second-by-second basis and (*b*) to speciate tailpipe exhaust from alternative vehicles operating under variable terrain conditions in a seasonal climate, with specific focus on unregulated compounds. The focus of this study is gas-phase emissions with particular attention on four of the recognized MSAT species during cold starts, an area that has received relatively little attention. This lack of research is surprising given that initial ignition of a gasoline engine from cold start requires fuel-enriched conditions that are known to produce a significant portion of trip emissions because the vehicle's exhaust aftertreatment (catalytic converter) is not yet warmed to operating temperature.

Real-world studies have utilized portable emission measurement systems (PEMS) to quantify tailpipe emissions while vehicles are in operation on the road network (*2–9*). Portable systems are advantageous over dynamometer laboratory tests for understanding the emissions resulting from real-world driving conditions. Many PEMS measure a small selection of emissions, limited to species regulated by Environmental Protection Agency emissions certification standards (*4, 8*). Other researchers have instrumented vehicles to develop more comprehensive speciation of emissions, implementing Fourier transform infrared spectrometers (FTIRs) to analyze real-world gas-phase emissions (*2, 3, 5–7, 9*). Though the PEMS employed by these institutions are capable of characterizing MSAT emissions (*7, 9*), only one group has pursued quantifying these over on-road, cold-start driving cycles (*6*). Additionally, low-emitting vehicles (typical of the most recent model year vehicles) require instrumentation capable of lower detection limits, compelling development of new PEMS. This study investigates use of FTIRs for onboard tailpipe emissions, alongside particle sizing and counting instrumentation (*10*).

Effects of variable terrain (*11*) and seasonal climate temperature ranges (*12–16*) influence the operation of vehicles, because passenger cars are designed to operate at maximum efficiency within typical temperature and terrain ranges. Second-by-second emissions measurements allow the transient effects encountered in real-world driving scenarios to be analyzed. To date, only temporal resolution significantly greater than 1 s have been achieved for FTIR onboard emissions quantification (*7, 9*), creating a need for higher temporal resolution real-world emissions data.

Pollutant concentrations emitted from the tailpipe of vehicles during cold starts are considerably higher than during travel, even with the influence of peaks occurring during on-road events (*2*).

University of Vermont, 33 Colchester Avenue, Burlington, VT 05405. Corresponding author: K. M. Sentoff, Karen.Sentoff@uvm.edu.

Transportation Research Record: Journal of the Transportation Research Board, No. 2158, Transportation Research Board of the National Academies, Washington, D.C., 2010, pp. 95–104.
DOI: 10.3141/2158-12

Ambient temperature is known to have a significant influence on cold-start emissions (*12, 14–16*). The enriched conditions following initial ignition of the engine produce high concentrations of hydrocarbons and carbon monoxide, which is amplified by colder conditions, as more fuel is required for colder, higher-density air combustion (*13*). Additionally, warm-up driving patterns immediately following engine ignition (after 12-h cold soak) affect the total level of emissions produced from cold starts. Speciation of cold-start exhaust in laboratory settings at varied temperatures based on real-world driving cycles has been reported, but little consideration has been paid to quantifying unregulated species for cold starts with an onboard system (*6*). Moreover, a significant gap in the literature exists in characterizing gaseous and particulate cold-start emissions simultaneously during real-world, on-road, warm-up driving. Groups conducting similar research have reported solely on gaseous cold-start emissions from light-duty gasoline vehicles and have found benzene, toluene, xylenes, and formaldehyde to be the dominant species (*6*). Toluene and xylene had elevated emissions at engine start, whereas benzene and formaldehyde reached peak emissions further into the driving cycle (*6*).

METHODOLOGY

A 1999 Toyota Sienna minivan was instrumented with the total onboard tailpipe emissions measurement system (TOTEMS) developed by researchers at the University of Vermont and discussed in detail in a separate paper (*17*). The instrumentation was utilized in a single vehicle as a proof of concept pilot study (*18*). The vehicle was equipped with a 3.0-L V6 engine and was rated as a low-emission vehicle according to California Air Resources Board Executive Order A-14-351. The specific model used in the study had an odometer reading of over 140,000 mi and was fueled with unleaded 87-octane gasoline from Gulf Oil L.P.

The pilot study cold-start gas-phase emissions data for 6 days of sampling are analyzed here in detail. Cold start was defined by an engine soak time of at least 12 h at ambient temperature before engine ignition. Particle number distributions for these cold starts are presented in a separate paper (*10*).

TOTEMS Instrumentation

TOTEMS is a portable emissions measurement system capable of measuring vehicle position, ambient conditions, engine operation, exhaust flow rate, exhaust temperature, and gas-phase and particle number tailpipe emissions at 1-Hz resolution while operating over real-world driving scenarios. The key aspects of TOTEMS relevant to gas-phase emissions measurement are described in the following sections.

Power Supply

Instrumentation was powered by two Lifeline absorbent glass mat lead-acid batteries rated to 12 V and 255 ampere-hours. These batteries deliver the power necessary to run TOTEMS through a Vector 2500-W power inverter. The system avoids utilizing the vehicle as a power source to prevent artificial load on the engine, in turn affecting emissions.

Vehicle Behavior

Data from the vehicle computer were acquired through an AutoEnginuity Scan Tool OBD-II Connector. The scan tool communicates with the vehicle to collect second-by-second operational parameters, including engine rotations per minute, vehicle speed, engine load, and mass air flow. In addition to the scan tool, acceleration in three directions was recorded by the Crossbow accelerometer.

Ambient Conditions

An Onset HOBO logger positioned on the roof rack of the vehicle acquired ambient temperature and relative humidity during sampling. System performance may be influenced by temperature; therefore, a second temperature and relative humidity logger was placed within the vehicle to monitor TOTEMS surrounding conditions.

Tailpipe Adapter and Exhaust Parameters

A custom-built tailpipe adapter was affixed to the end of the tailpipe of the test vehicle. The adapter extends the factory tailpipe to house (*a*) ports for sampling exhaust parameters, (*b*) a pitot tube, and (*c*) an exhaust sampling probe. A Type J thermocouple measured exhaust temperature. A pitot tube and differential pressure transducers measured static and dynamic pressure of the exhaust for conversion to exhaust flow rate based on laboratory calibration equations for the pitot tube (*18*). A perforated stainless steel sampling probe extended perpendicularly through the tailpipe adapter for delivery of exhaust samples to onboard emissions instrumentation. Samples were transferred into the vehicle through an Atmoseal smooth-walled flexible stainless steel heated line at 191°C to maintain the high exhaust sample temperature necessary for gas-phase species analysis.

Gas-Phase Emissions Measurement

An MKS Instruments MultiGas 2030 (MG2030) high-speed FTIR was used to characterize the gas-phase emissions from the tailpipe of the Toyota Sienna minivan. The FTIR instrument simultaneously quantified 27 species from the exhaust of the vehicle at 1-s resolution. Quantification for each compound was based on manufacturer calibrations, internal to the MultiGas 2000 software package. Exhaust composition was determined by analysis of infrared spectra. The manufacturer calibrations and exhaust composition guidelines were assumed accurate for the purpose of this analysis. Independent procedures to verify the manufacturer calibrations and method of exhaust speciation for gasoline exhaust complex mixtures are under development at the University of Vermont. Before the pilot study data collection, MultiGas response was verified using a calibration emissions mix of carbon monoxide, carbon dioxide, nitric oxide (NO), and a typical hydrocarbon surrogate, propane in a nitrogen balance. As shown in Table 1, the certified emissions mix concentrations were reasonably comparable to the resulting FTIR concentrations. The largest discrepancy between the certified mix and the MG2030 reported concentration was for carbon dioxide, at about a 10% difference.

Specifications and Setup The MultiGas instrument has a wavelength resolution of 0.5 cm^{-1} and a path length of 5.11 m, capable

TABLE 1 Percent Difference Between FTIR Response and Certified Emissions Mix Concentrations for Select Compounds

Compound (unit)	Concentrations		Percent Difference
	Emissions Mix	MKS MG2030	
CO (%)	8.04	7.98	−0.75
CO_2 (%)	12.22	10.94	−10.47
NO (ppm)	3,030	3,134.93	3.46
C_3H_8 (ppm)	3,230	3,120.38	−3.39

of 5-Hz data recording. A flow rate of 12 L/min through the FTIR was used to achieve 1-s sample residence time in the sample cell. Second-by-second resolution data enable analysis of the relationships between transient vehicle operation and resulting emissions. A slower recording rate, achieved by others utilizing similar methodologies but different instruments, may not capture the variability that driver behavior may induce on the engine operation and resulting tailpipe exhaust composition.

Sample flow through the MG2030 high-speed FTIR was maintained at 191°C and particle filtered to prevent damage to internal components. Potassium bromide windows and gold-plated mirrors within the sample cell can be attacked by water or accumulate particles, respectively; both interfere with analysis. The inlet of the FTIR was fixed with a 2.0-μm particulate filter certified for particle mass measurements in line with a 0.1-μm cartridge filter. The series of filters were insulated to ensure minimal heat loss across the stainless steel housings. Maintenance of the high temperatures prevented water condensation that could potentially change the composition of exhaust preceding analysis. It should be noted that the MultiGas instrument quantifies water vapor with each analysis point.

An SKC Leland Legacy battery-powered personal sampling pump pulled the necessary 12-L/min raw exhaust flow through the MultiGas instrument. Two water traps at the pump inlet prevented water damage or flow obstruction.

Compound Quantitation Limits As each exhaust emissions species was quantified according to a distinct calibration data set, the minimum concentration detection limits for the instrument are defined on an individual compound basis. The manufacturer specifies the calibration ranges and approximate accuracy of measure for each compound; however, sampling detection limits vary according to sampling rate. The goal of TOTEMS was to achieve the lowest detection limit possible for 1-s temporal resolution exhaust measurements. Individual compound detection limits for the FTIR were determined based on tunnel blank data collected before every run. Tunnel blanks were routinely collected as a part of the quality assurance and quality control procedure, from the flow of ambient air through the exhaust pipe and transfer lines while the vehicle's engine was off. Conceptually, these ambient air measurements provided a background measure and three times the standard deviation of tunnel blank average concentration was defined as the individual compound's detection limit (Table 2). For comparison, the last column of Table 2 shows

TABLE 2 Gas Species Detection Limits and Lower and Upper Quantitation Limits for the MKS MultiGas FTIR Instrument

Compound	Detection Limit (ppm or %)	Lowest Concentration Point (ppm or %)	Highest Concentration Point (ppm or %)	Autologic AutoGas Analyzer
Carbon monoxide	2.14	99.6	5,000	0–15
Carbon monoxide (%)	0.01	3.19	7.99	0–5,000 (as NO_x)
Nitric oxide	1.20	279	2,795	
Nitrogen dioxide	0.46	358	488	
Ammonia	0.32	12.73	2,995	
Sulfur dioxide	0.98	19.6	964.5	
Ethane	1.89	100.4	1,004	0–2,000 (as HC, propane surrogate)
Octane	1.12	20	1,000	
IsoOctane	1.01	20	1,000	
1,2,4-trimethylbenzene	4.16	20	1,000	
1,3,5-trimethylbenzene	1.89	100	1,000	
Ethylene	0.97	9.74	3,000	
Propylene	4.80	89.8	194	
1,2-propadiene	1.30	306	1,020	
2-methylpropene	1.68	150	500	
2-methyl-2-butene	10.26	19.57	19.57	
Ethanol	3.14	20	1,000	
Methanol	1.23	18.63	931.74	
Acetylene	1.43	101.6	1,016	
Propyne	4.38	50	500	
Formaldehyde	1.07	4.2	69	
1,3-butadiene	3.09	8.3	83.4	
Toluene	15.82	18.63	931.74	
m-Xylene	5.62	93.17	931.74	
Carbon dioxide (%)	0.08	4.6	23	0–20
Methane	1.10	414	3,143	
Nitrous oxide	0.30	146.9	200.1	
Water (%)	0.11	17.87	20.57	

the concentration range for the five-gas analyzer that the MultiGas replaced in the onboard measurement system (*19*). Note that the MultiGas allows real-time speciation of gases in vehicle exhaust unlike traditional five-gas analyzers [e.g., hydrocarbons and oxides of nitrogen (No_x) individual species in Table 2]. Additionally, a conventional five-gas analyzer is calibrated to an emissions mix, providing single calibration points for each gas surrogate on which to base measurements from the complex exhaust composition. In contrast, the MultiGas has a range of concentrations, presented in Table 2, used to interpolate the compound concentration in the tailpipe emissions sample.

Hydrocarbon Surrogate In addition to the compounds explicitly measured, a summation of a selection of hydrocarbons provided a surrogate for nonmethane hydrocarbons. Typically, a single hydrocarbon or the summations of a few hydrocarbons are quantified, but in this case a surrogate was developed based on variation in compound structure. Of the compounds selected, three have single-bonded carbons and three contain double-bonded carbons. In addition, the number of carbons varies for each of these compounds, incorporating the range of hydrocarbon structures. The hydrocarbon parameter (HC*) was developed to show the relative concentration of nonmethane hydrocarbons to other emissions and the relationship of HC* to ambient cold-start temperatures. The value for HC* was calculated as follows:

$$[HC^*] = [\text{ethane}] + [\text{octane}] + [\text{isooctane}] + [\text{2-methyl-2-butene}] + [\text{2-methylpropene}] + [\text{ethylene}]$$

where the brackets indicate the gas species concentration measured by the MultiGas in parts per million (ppm).

Summary of Cold-Start Sampling Phases

A total of six events were considered for the gas-phase exhaust species analysis (Table 3). Three warm-up driving events (indicated by "-WD") were comprised of engine cold start followed by driving under stop sign and signal-controlled conditions typical of urban arterial driving. Three other events consisted of a cold-start engine ignition followed by a period of extended idle (indicated by "-EI"), during which time the engine was running, but the transmission remained in park for varying lengths of time between approximately 900 and 3,000 s. Each of the sampling events was preceded by more than 12 h of cold soak that allowed all engine components and lubricants to reach ambient temperature. Temperature data from the Onset HOBO logger monitoring ambient conditions was averaged over the period from engine ignition to end of warm-up driving or extended idle for each sampling event, as tabulated in Table 3.

During extended idle conditions, the vehicle was running, but the transmission remained in park. For warm-up driving, the engine was started and driving commenced after a short idle period, less than 1 min. The warm-up driving route was a 0.8-mi section of a larger 35-mi test route to be used in future studies. Warm-up driving for this analysis included departure from the University of Vermont Transportation Air Quality laboratory and travel to the single gas station used for all gasoline refills for the study. Two traffic lights, three stop signs, and a steep downhill section provided varied conditions along the trip to the gas station.

RESULTS

Peak Cold-Start Emissions

Peak gas concentrations were examined for all species to evaluate the relative abundance of each pollutant during vehicle warm-up over either extended idle or warm-up driving conditions (see Figure 1). The range of peak emissions over the six events was compared to hot-stabilized emissions (indicated by blue stars in Figure 1) from sampling on-road following a full, 2.4-mi warm-up driving period. Of all the gas species measured, carbon monoxide (CO) had the highest concentrations during the six cold-start events, with the maximum detected concentration during Run 1-EI at over 83,000 ppm and minimum peak emissions observed in sampling Run 4-WD at approximately 26,000 ppm. Even this lower bound of CO peak concentration was more than two orders of magnitude higher than peak concentrations measured for most other compounds. For CO, this peak occurred almost instantaneously following engine ignition. Nitric oxide (NO), a significant component of the criteria pollutant NO_x, was also abundant. The peak emissions for NO did not occur immediately, but instead were elevated during the driving cycle. Other significant peak emissions included acetylene, methane, ethanol, ethylene, isooctane, octane, propylene, and toluene. Water was quantified as part of the emissions composition, producing approximately 12% stabilized water emissions on average, with the exception of the first event. The first event, Run 1-EI, with signifi-

TABLE 3 Cold-Start Sampling Data Collected

Event	Date	Ambient Temperature (°C)	Relative Humidity (%)	Phase of Sampling		
				Cold Start	Extended Idle	Warm-Up Driving
Run 1-EI	1-Apr-2009	9.5	50.1	X	X	
Run 2-WD	17-May-2009	20.3	25.9	X		X
Run 3-WD	21-May-2009	38.4	19.2	X		X
Run 4-WD	22-May-2009	24.6	39.0	X		X
Run 5-EI	24-Jun-2009	32.4	41.3	X	X	
Run 6-EI	25-Jun-2009	37.5	32.6	X	X	

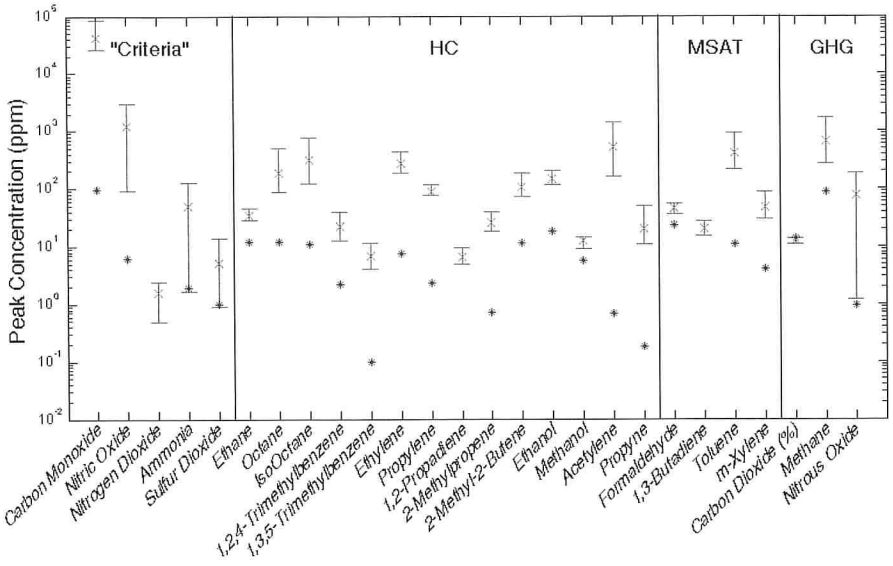

FIGURE 1 Maximum emissions concentration range (red cross and range bars) measured over six cold starts compared with typical stabilized idle emissions (blue star). The cross indicates the mean of maximum emissions, with range bars equivalent to maximum and minimum peak emissions for all six events. Missing blue stars for select compounds indicate that hot-stabilized idle emissions were below instrument detection limit.

cantly colder ambient temperatures, stabilized water concentrations at about 5%.

Cold-Start Emissions for Criteria Pollutants and Greenhouse Gases

Of the 27 gases measured, the temporal trend in concentration of two predominant emissions species, CO and carbon dioxide (CO_2), were assumed to indicate the relative operating efficiency of the vehicle's catalytic converter over time. As shown in Figure 2, immediately after engine start, carbon monoxide concentrations increased rapidly to the peak concentration and decreased back to baseline levels, on average, within 90 s of engine start. Cold-start CO emissions are typically associated with low air-to-fuel ratio, or fuel-enriched conditions, as well as a cold catalytic converter. Relatively quick warm-up of the catalytic converter under the test conditions and its increasing ability to oxidize CO to CO_2 as time elapsed from ignition are indicated by the increase in CO_2 that occurred after the time of CO peak emissions. The time to optimal efficiency of emissions control devices varied tremendously for other emissions species, specifically NO_x and MSATs.

For the warm-up driving tests (Figure 2, right panels), the end of the sampling period was indicated by engine off for refueling at the gas station, resulting in a drop in CO_2. The three extended idle cold starts without driving (Figure 3, left panels) produced steady CO and CO_2 emissions over the extended idle period.

Nitrogen species emissions patterns were different from CO (see Figure 3). Nitric oxide was emitted at an average of approximately 100 ppm with the initial cold start of the engine. Beyond the initial peak emission, NO concentrations depended on vehicle operation. During extended idle tests (Figure 3, left panels), the vehicle continued to emit relatively stable concentrations of NO and concentrations gradually increased at idle conditions beyond approximately 300 s after ignition. As soon as the vehicle was put into gear for driving (Figure 4, right panels), the NO concentrations increased to concentrations that exceeded the ignition peak. These higher NO concentration peaks were likely a result of engine loading. It was not until driving was continued for 100 to 200 s that the concentration peaks diminished significantly and other nitrogen species were present at low concentrations. The vehicle's catalytic converter was not able to convert the NO pollutant to other, less harmful compounds until close to the end of the warm-up driving. It is important to note that for Run 3-WD, the NO concentration pattern clearly depicts the initial shift into drive (indicated by the drive partition in Figure 3), the shift into park about 150 s later (indicated by the park partition), and the short period of idling that occurred while a Global Positioning System error was fixed.

Air Toxic Cold-Start Emissions

In general, air toxic species (defined here as formaldehyde, 1,3-butadiene, toluene, and xylenes) were emitted at elevated concentrations during cold-start sampling. Of the MSAT species quantified, the products of combustion (formaldehyde and 1,3-butadiene) behaved uniquely. When driving commenced as indicated by drive partitions (Figure 4, right panels), formaldehyde concentrations increased further to peak emissions levels and then decreased gradually to near baseline levels within 100 to 200 s of driving. During the extended idle conditions (Figure 4, left panels), formaldehyde concentrations did not decrease back to baseline levels, but continued to increase slightly during the entire cold start and idle sampling period. The pattern of formaldehyde emissions indicates that the extended idle conditions were not sufficiently warming up the catalyst that would otherwise diminish formaldehyde emissions. In contrast,

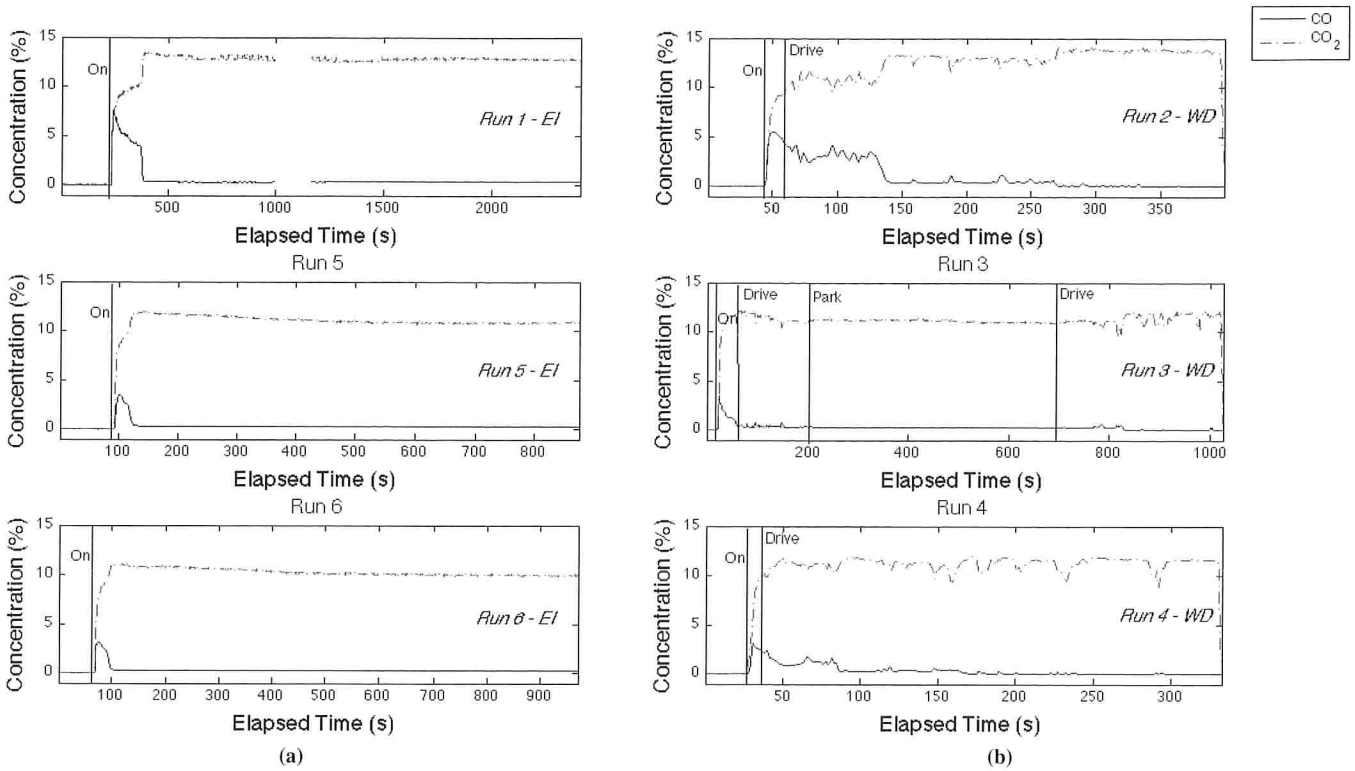

FIGURE 2 Second-by-second CO and CO_2 emissions during cold-start runs: (*a*) cold starts with extended idle and (*b*) cold starts with warm-up driving.

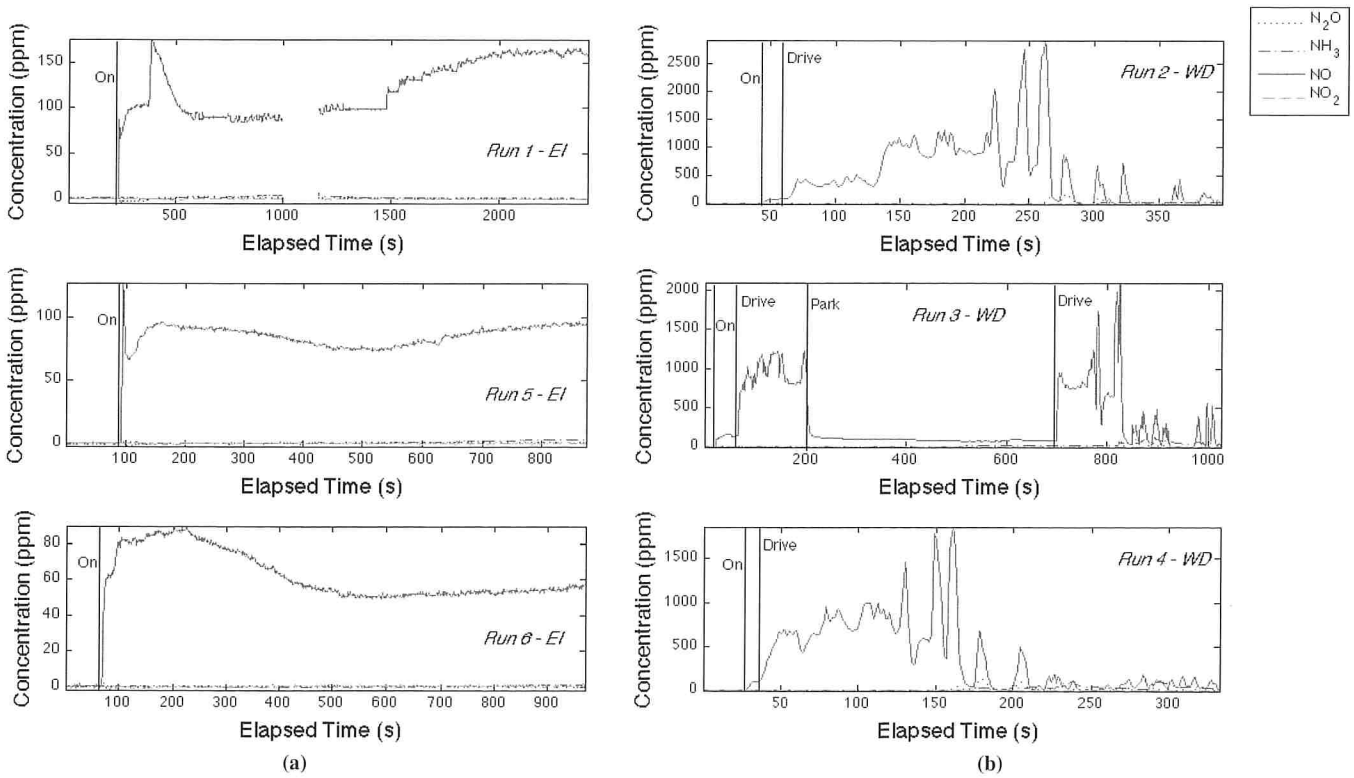

FIGURE 3 Nitrogen species concentrations over the course of (*a*) extended idle and (*b*) warm-up driving cold starts.

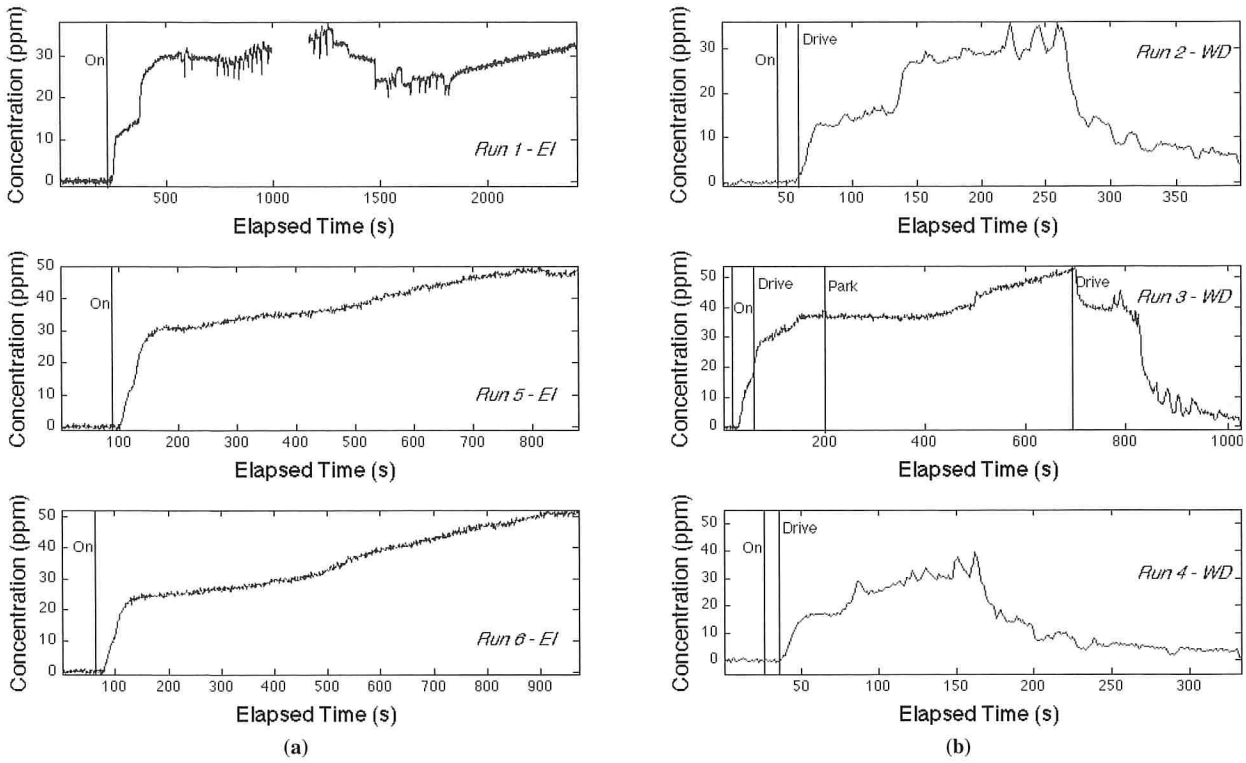

FIGURE 4 Formaldehyde emission concentration trends over cold-start sampling: (*a*) extended idle and (*b*) warm-up driving.

stop-and-go driving resulted in baseline formaldehyde concentrations within approximately 200 s. The MSAT compound 1,3-butadiene behaved similarly to formaldehyde in that it reached peak emissions either through gradual increase over extended idle or by reaching a plateau at high concentrations during the course of stop-and-go driving. Unlike formaldehyde, the decrease from peak 1,3-butadiene emissions was nearly instantaneous, at the apparent point of catalyst optimization, differing drastically from the optimization point as determined from CO/CO_2 relationships.

Unlike the MSAT products of combustion, constituents of gasoline emissions (toluene and *m*-xylene) reached their maximum emissions point nearly instantaneously. For toluene (Figure 5) and *m*-xylene (data not shown), the maximum peak emissions were recorded within 5 s of engine ignition, similar to the initial start-up behavior exhibited by CO. Extended idle conditions resulted in stabilized toluene concentration plateaus at levels less than the initial peak concentration (Figure 5, left panel). The concentration plateaus increased slightly after about 400 s of extended idle for Run 5-EI and Run 6-EI. Switching the vehicle to driving conditions again resulted in decreasing concentrations for these MSATs over time, best illustrated by the trends from Runs 2-WD and 4-WD in Figure 5. *m*-Xylene time series trends were similar to those for toluene, just at a lower concentration. It is important to note that the idling period that occurred after the vehicle was put into gear in Run 3-WD of Figure 5 (indicated by the time between the park partition and the second drive partition) resulted in a gradual increase to a plateau concentration of about 150 ppm. Thus, while the vehicle was in park for Run 3-WD, the trend of emission concentrations reproduced the extended idle trend in Run 5-WD and 6-WD (Figure 5, left panels). Once the vehicle was switched into gear again, the emissions pattern changed to the warm-up driving trend presented for Run 2-WD and Run 4-WD (Figure 5, right panels).

The four MSAT species investigated showed two distinct time trends. Toluene and *m*-xylene, expected components of gasoline, reach peak emission concentrations immediately, corresponding to excess unburned fuel at engine ignition. Formaldehyde and 1,3-butadiene, products of the combustion process recognized by the oxygen-containing structure and the structure with two double bonds, respectively, reached peak emission concentrations gradually over the warm-up and extended idle sampling scenarios.

The MSAT emissions quantified for the study were produced at concentrations well above the detection limits for the instrument. Toluene peak emissions reached the upper calibration concentration limit of 932 ppm, previously reported in Table 2, during the first sampling event. Formaldehyde peak emissions were in the upper range of the quantitation limits, but did not exceed the upper limit. Hot-stabilized emissions were well below peak emissions for these four compounds, the closest being formaldehyde with hot-stabilized emissions ranging 1.5 to 2 times below the peak emissions from the six sampling events.

Ambient Temperature Effects on Cold-Start Emissions

It is well documented that temperature influences cold-start emissions and this relationship is generally attributed to the requirement of establishing enriched air-to-fuel conditions at colder ambient temperatures to achieve engine ignition. Species from each category of emissions ("criteria" pollutants, HC*, greenhouse gases, and MSATs) were plotted to show the general relationship of temperature to peak concentration (Figure 6). Over the six runs, an inverse relationship of peak gas concentrations as a function of cold-start mean temperature was established for many of the compounds, with the exception of

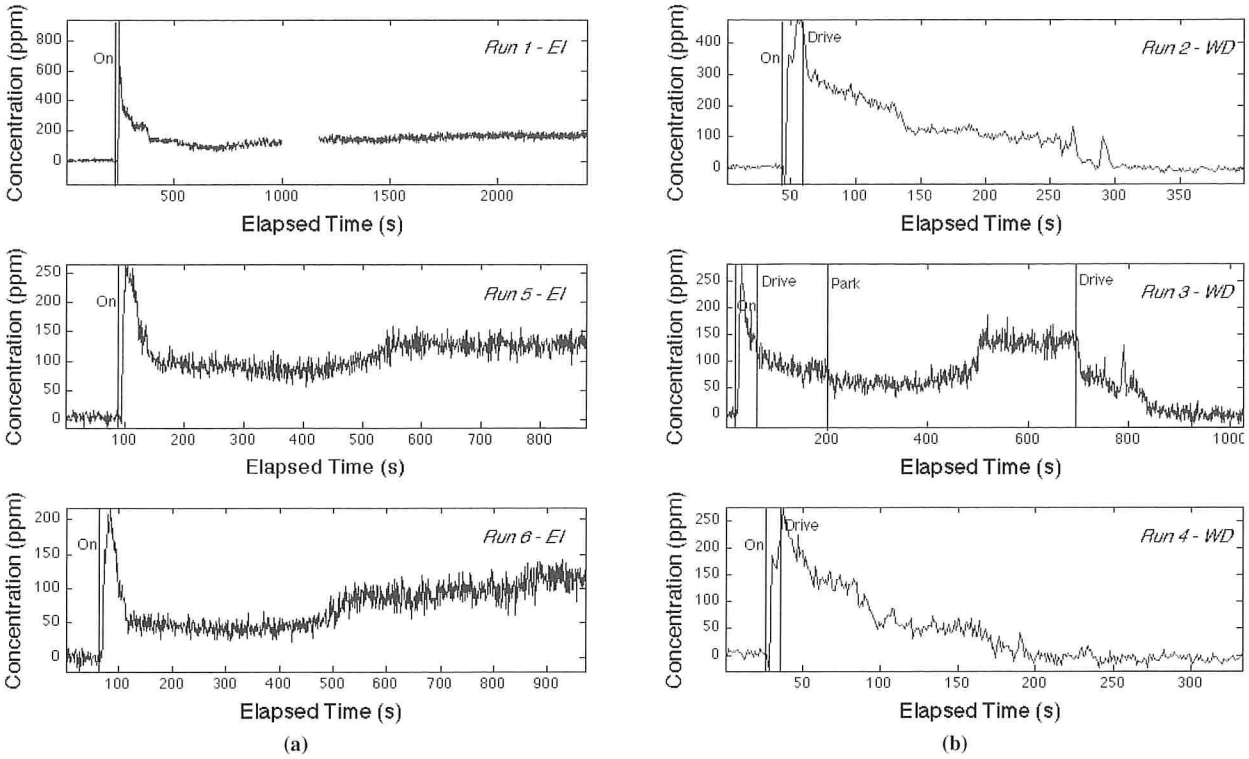

FIGURE 5 Toluene cold-start emissions trends: (*a*) extended idle and (*b*) warm-up driving.

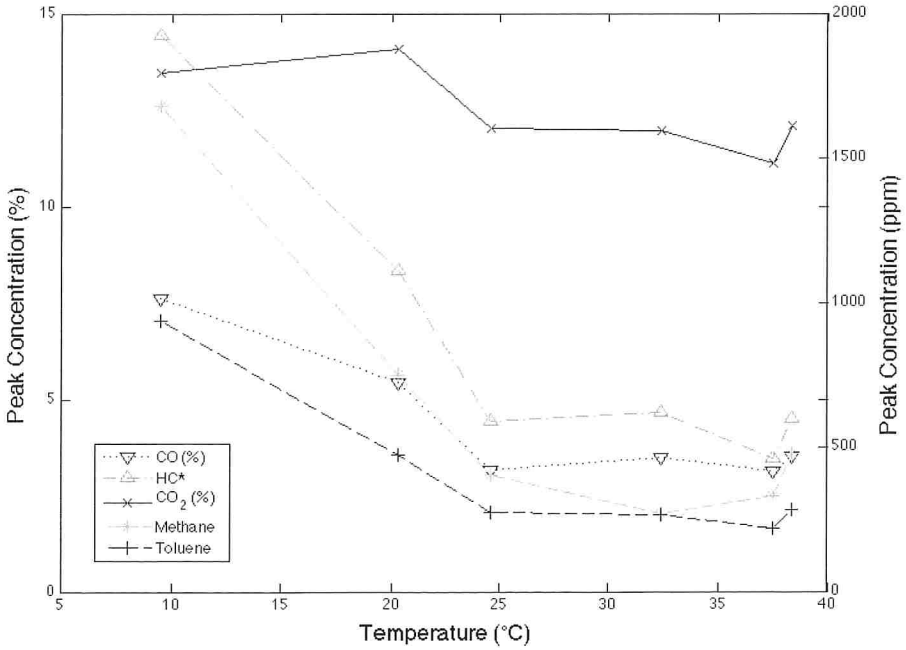

FIGURE 6 Peak emissions at cold start as a function of average ambient air temperature for six sampling events.

CO_2 (Figure 6). Only at the hottest average temperature experienced in the sampling (38.4°C, Run 3-WD) did that trend change for the compounds examined.

CONCLUSIONS

The gas-phase emissions during cold start of the 1999 Toyota Sienna minivan indicate that optimal function of the emission control devices can not be based solely on conversion of single criteria pollutants (i.e., CO) to less harmful by-products of combustion (i.e., CO_2), because the time frame associated with individual pollutant conversion varies by species. For some criteria pollutants, such as nitric oxide, warm-up driving operation produced elevated emissions induced by loading the engine. Carbon monoxide, another criteria pollutant, was emitted at high concentrations during enriched engine ignition conditions, but was mitigated relatively quickly as the catalyst achieved optimum operating conditions. Additionally, driver behavior after initial engine cold start was found to have a significant effect on gas-phase emissions, including the air toxics examined in this study. The air toxics were found to persist in high concentrations with extended idle conditions, as compared to the lower concentrations associated with warm-up driving. The magnitude of the concentration changes between these driving behaviors varied between compounds.

Overall, conversion of carbon monoxide to carbon dioxide emissions was examined to define the cold start and time to optimal oxidation of the pollutant. This time frame, however, could not be used as an indicator for optimal emission control device operation (and the end of cold-start emissions behavior), because it did not necessarily correspond to the pattern observed for other components of exhaust that were apparently affected differently by the catalyst. The behavior trend of CO and CO_2, under 9.5°C to 38.4°C ambient temperature test conditions, took approximately 90 s, on average, to convert the pollutant almost entirely to the greenhouse gas, indicated by the sharp decrease in CO and increase in CO_2. The characteristic CO and CO_2 trends were demonstrated regardless of the driving cycle or idle condition following the cold start of the engine. This might be expected because catalytic converters were first designed to control CO emissions.

The MSAT species, in contrast, were more sensitive to the driving versus idle condition. With extended idle, formaldehyde and 1,3-butadiene continued to increase during the entire sampling periods, ranging from 900 to 3,000 s. Toluene and *m*-xylene reached peak emissions within seconds of engine ignition for all sampling events, but after stabilized, lower concentrations were established, they also increased as extended idle continued. For warm-up driving, 1,3-butadiene and formaldehyde reached peak emissions during the course of driving, but all of the MSATs examined decreased significantly within 100 to 200 s of driving. The preliminary results of this study suggest that recent efforts to reduce vehicle idling behavior may have implications beyond the known fuel and emissions savings. Reduction in idling time could mitigate the elevated concentrations achieved in this study for extended idle conditions, as compared to the warm-up driving scenarios. With particular consideration of the health effects associated with MSAT emissions, these results suggest that periods of extended idling after cold starts prolong potential exposure at elevated concentrations of these toxic species. Furthermore, the MSAT data indicate that minimizing idle times will have significant air quality and human health benefits. Limiting idle to the approximate time it takes for the initial peak of fuel constituents, as little as a minute, could prevent further exposure to the air toxics.

Ambient temperature affected CO, HC*, methane, and toluene peak emissions significantly, illustrating decreasing peak concentrations for compounds from each previously defined emission category (criteria, hydrocarbons, greenhouse gases, and MSATs) as temperature increased over the range from 9.5°C to 38.4°C. Only at the highest temperature were these species not subject to the inverse trend. CO_2 did not respond to temperature changes over the course of the sampling events to the same extent as the other compounds investigated, but instead stabilized at approximately the same range of concentrations from 11% to 14%. The advantage of TOTEMS is that the sampling phases were performed in real-world scenarios, testing the temperature trend in actual vehicle application. Future work with TOTEMS will further investigate the relationship of real-world seasonal temperature influences on vehicle emissions.

Overall understanding of MSAT trends helps to inform models to better predict these toxic emissions for purposes of environmental air quality and human health and exposure. Peak MSAT emissions during cold-start events were found to respond to temperature similarly to HC*, CO, and methane, making these species possible predictors of MSAT emissions under various temperatures, for modeling purposes. In addition, the increasing concentration behavior of MSATs under extended idle conditions, unlike the decreasing emissions observed for immediate driving, may be an area to investigate in terms of human health and exposure to these toxic emissions.

ACKNOWLEDGMENTS

This project was funded by the U.S. Department of Transportation through the UTC program at the University of Vermont Transportation Research Center.

REFERENCES

1. *Environmental Fact Sheet: Air Toxics from Motor Vehicles.* Office of Transportation and Air Quality, U.S. Environmental Protection Agency, Ann Arbor, Mich., 1994.
2. Barth, M. J., J. Collins, G. Scora, N. Davis, and J. Norbeck. Measuring and Modeling Emissions from Extremely Low Emitting Vehicles. In *Transportation Research Record: Journal of the Transportation Research Board, No. 1987,* Transportation Research Board of the National Academies, Washington, D.C., 2006, pp. 21–31.
3. Collins, J. F., P. Shepherd, T. D. Durbin, J. Lents, J. Norbeck, and M. Barth. Measurements of In-Use Emissions from Modern Vehicles Using an On-Board Measurement System. *Environmental Science & Technology,* Vol. 41, No. 18, 2007, pp. 6554–6561.
4. Gierczak, C. A., T. Korniski, J. W. Butler, and T. J. Wallington. *Laboratory Evaluation of the SEMTECH-G Portable Emissions Measurement System (PEMS) for Gasoline Fueled Vehicles.* Paper 2006-01-1081. SAE International, 2006.
5. Jetter, J. J., S. Maeshiro, S. Hatcho, and R. E. Klebba. *Development of an On-Board Analyzer for Use on Advanced Low-Emission Vehicles.* Paper 2000-01-1140. SAE International, 2000.
6. Li, H. *Investigation of Cold Start Emissions for Modern SI Cars Under Real World Urban Driving Conditions.* Paper 2008-01-1648. SAE International, 2008.
7. Li, H., G. Andrews, D. Sawidis, B. Daham, K. Ropkins, M. Bell, and J. Tate. *Comparisons of the Exhaust Emissions for Different Generations of SI Cars Under Real-World Urban Driving Conditions.* Paper 2008-01-0754. SAE International, 2008.
8. Nam, E., A. Mitcham, and C. Ensfield. *Dynamometer and On-Board Emissions Testing of the Honda Insight and Toyota Prius.* Paper 2005-01-0681. SAE International, 2005.
9. Truex, T. J., T. Hayashi, J. Collins, J. J. Jetter, B. Knight, and N. Kishi. *Measurement of Ambient Roadway and Vehicle Exhaust Emissions—An Assessment of Instrument Capability and Initial On-Road Test Results*

with an Advanced Low Emission Vehicle. Paper 2000-01-1142, SAE International, 2000.
10. Robinson, M. K., K. M. Sentoff, and B. A. Holmén. Particle Number and Size Distribution Emissions During Light-Duty Vehicle Cold Start: Data from the Total Onboard Tailpipe Emissions Measurement System. In *Transportation Research Record: Journal of the Transportation Research Board, No. 2158,* Transportation Research Board of the National Academies, Washington, D.C., 2010, pp. 86–94.
11. Jimenez-Palacios, J. Understanding and Quantifying Motor Vehicle Emissions with Vehicle Specific Power and TILDAS Remote Sensing. In *Mechanical Engineering,* Massachusetts Institute of Technology, Cambridge, 1999, p. 361.
12. Andrews, G. E., H. Li, J. A. Wylie, G. Zhu, M. Bell, and J. Tate. *Influence of Ambient Temperature on Cold-Start Emissions for a Euro 1SI Car Using In-Vehicle Emissions Measurement in an Urban Traffic Jam Test Cycle.* Paper 2005-01-1617. SAE International, 2005.
13. Bielaczyc, P., and J. Merkisz. *Exhaust Emission from Passenger Cars During Engine Cold Start and Warm-up.* Paper 970740. SAE International, 1997.
14. Bielaczyc, P., and J. Merkisz. *Cold Start Emissions Investigation at Different Ambient Temperature Conditions.* Paper 980401. SAE International, 1998.
15. Ludykar, D., R. Westerholm, and J. Almen. Cold Start Emissions at +22, –7 and –20°C Ambient Temperatures from a Three-Way Catalyst TWC/Car: Regulated and Unregulated Exhaust Components. *Science of the Total Environment,* Vol. 235, 1999, pp. 65–69.
16. Weilenmann, M., J. Favez, and R. Alvarez. Cold-Start Emissions of Modern Passenger Cars at Different Low Ambient Temperatures and Their Evolution Over Vehicle Legislation Categories. *Atmospheric Environment,* Vol. 43, 2009, pp. 2419–2429.
17. Holmén, B. A., K. M. Sentoff, M. K. Robinson, and P. Montane. University of Vermont Total Onboard Tailpipe Emission Measurement System Instrumentation Package for Real-World Monitoring of Conventional and Hybrid Light-Duty Vehicles. Presented at 89th Annual Meeting of the Transportation Research Board, Washington, D.C., 2010.
18. Holmén, B. A., M. K. Robinson, K. M. Sentoff, P. D. Montane, and K. Hathaway. *The On-Board Tailpipe Emissions Measurement System (TOTEMS): A Report to the University of Vermont Transportation Research Center.* University of Vermont Transportation Research Center, Burlington, 2009.
19. *Gas Analyzer Quick Start Guide. Applus+ AutoLogic Inc. Manual.* AutoLogic, Sussex, Wisc., 2007.

The Transportation and Air Quality Control Committee peer-reviewed this paper.

Estimating In-Vehicle Concentration of and Exposure to Fine Particulate Matter

Near-Roadway Ambient Air Quality and Variability in Vehicle Operation

Xiaozhen Liu, H. Christopher Frey, and Ye Cao

Fine particulate matter ($PM_{2.5}$) exposure is associated with short-term and chronic respiratory effects. It is necessary to investigate human exposure to $PM_{2.5}$ to support the assessment of the association between exposure and adverse health effects. The methodology used in the current version of Stochastic Exposure and Dose Simulation Model for Particulate Matter for in-vehicle $PM_{2.5}$ concentration is reviewed. An alternative approach for estimating in-vehicle $PM_{2.5}$ concentration, based on the use of a dispersion model to estimate near-road $PM_{2.5}$ concentration and a mass balance model to estimate in-vehicle concentration, has been specified and applied. The objectives of this paper are to (*a*) demonstrate the application of the alternative approach to various scenarios, (*b*) analyze the sensitivity of the modeling results to the key inputs, and (*c*) evaluate this approach. Typical inputs for the alternative approach are reviewed. Sensitivities of these inputs to the modeling results and estimated human exposure have been analyzed. The in-vehicle $PM_{2.5}$ concentration was estimated to vary by more than a factor of two, depending on factors such as the cabin air exchange rate and filter efficiency of the ventilation system. Recommendations are made for field data that would be useful to better characterize variability in factors that affect in-vehicle $PM_{2.5}$ concentration.

Fine particulate matter ($PM_{2.5}$) includes particles that are 2.5 μm or less in aerodynamic diameter. Exposure to $PM_{2.5}$ is associated with short-term and chronic respiratory effects (*1*). Therefore, there is a need to quantify exposure to $PM_{2.5}$ to support assessment of its association with adverse health effects.

In 2007, 90% of U.S. commuters drove to work (*2*). Thus, the in-vehicle microenvironment is a potentially significant contributor to human exposure to pollutants, especially for commuters. A microenvironment is a location within which air pollutant concentrations are relatively uniform or well characterized. In-vehicle $PM_{2.5}$ concentration is high compared with those of other microenvironments, such as houses (*3*).

The Stochastic Exposure and Dose Simulation Model for Particulate Matter (SHEDS-PM) is a scenario-based human exposure model developed by the U.S. Environmental Protection Agency (USEPA). It simulates individual and population exposure to $PM_{2.5}$ (*4*). Eight microenvironments are accounted for in SHEDS-PM, including outdoors, residence, office, school, store, restaurant, bar, and in-vehicle. For each microenvironment, the penetration of ambient $PM_{2.5}$ is estimated based on a mass balance, linear regression, or scaling factor. For selected microenvironments (such as residence, restaurant, and bar), indoor sources of $PM_{2.5}$ emissions are estimated. The proportion of time that each simulated person spends in each microenvironment is based on sampling diary data from the Consolidated Human Activity Database (CHAD). The characteristics of housing that affect indoor air quality are based on census tract data from the 2000 U.S. Census. Details on SHEDS-PM are available elsewhere (*4, 5*). SHEDS-PM estimates in-vehicle exposure based on an average ratio of in-vehicle versus ambient $PM_{2.5}$ concentrations, with the latter estimated based on a fixed site monitor (FSM). FSMs typically represent areawide concentrations, but not localized concentrations on the roadway. The latter are influenced by vehicle emissions.

Liu et al. (*6*) reviewed the SHEDS in-vehicle $PM_{2.5}$ algorithm and inputs and developed an alternative approach of estimating in-vehicle $PM_{2.5}$ concentration. The alternative approach estimates $PM_{2.5}$ concentration near the roadway and uses a mass balance model to predict in-vehicle $PM_{2.5}$ concentration. The objectives of this paper are to (*a*) demonstrate the application of the alternative approach to various scenarios, (*b*) analyze the sensitivity of the modeling results to the key inputs, and (*c*) evaluate this approach.

METHODOLOGY

In SHEDS-PM, inhalation exposure to $PM_{2.5}$ is estimated on the basis of the amount of time spent in each microenvironment and the microenvironmental concentrations experienced by every individual. SHEDS simulates individuals in a selected population for a specified geographic area and time period. Individual activity patterns are sampled from CHAD diary data. Housing type is sampled from U.S. Census data at the census tract level. Air quality data may be input from FSMs, air quality model results, or arbitrary user-specified inputs. SHEDS-PM simulates commuting by vehicles to work, as well as noncommuting vehicle activity (*4*).

For the in-vehicle microenvironment, SHEDS simulates cars, trucks, buses, trains, and all other. The in-vehicle $PM_{2.5}$ concentration is estimated as a linear function of ambient $PM_{2.5}$ concentration:

$$C_{iv,vt} = k_{vt} C_{amb} + b_{vt} + \epsilon_{vt} \quad (1)$$

Department of Civil, Construction, and Environmental Engineering, North Carolina State University, Campus Box 7908, Raleigh, NC 27695-7908. Corresponding author: H. C. Frey, frey@ncsu.edu.

Transportation Research Record: Journal of the Transportation Research Board, No. 2158, Transportation Research Board of the National Academies, Washington, D.C., 2010, pp. 105–112.
DOI: 10.3141/2158-13

where

$C_{iv,vt}$ = in-vehicle $PM_{2.5}$ concentration for vehicle type vt ($\mu g/m^3$);
k_{vt} = in-vehicle/ambient ratio $PM_{2.5}$ concentration for vehicle type vt, constant;
C_{amb} = ambient $PM_{2.5}$ concentration ($\mu g/m^3$);
b_{vt} = in-vehicle nonambient $PM_{2.5}$ concentration for vehicle type vt ($\mu g/m^3$);
vt = vehicle types: car, bus, truck, train, and other vehicles; and
ϵ = error term for residual variability in in-vehicle $PM_{2.5}$ concentration, where $\epsilon \sim N(0, \sigma_\epsilon)$ and σ_ϵ is the standard deviation ($\mu g/m^3$).

The ratio of in-vehicle to ambient $PM_{2.5}$ concentrations, k_{vt}, for vehicle type vt is determined by comparing in-vehicle measurement data with ambient data. The background in-vehicle concentration b_{vt} is nonzero only when there are in-vehicle sources of $PM_{2.5}$, such as smoking (*7*).

Liu et al. (*6*) reviewed the in-vehicle algorithms and inputs for SHEDS-PM and performed case studies. The case studies indicated that the ratio of in-vehicle to ambient concentration is subject to substantial variability, ranging from 0.71 to 14.3 (*7–9*). Updates to in-vehicle microenvironmental inputs for SHEDS-PM were recommended and an alternative approach that integrates a dispersion model and a mass balance model to address the variability of in-vehicle $PM_{2.5}$ exposure was developed.

In this alternative approach, the $PM_{2.5}$ concentration surrounding the vehicle (C_{sv}) is predicted by superimposing the incremental component of ambient concentration on a roadway (C_{icr}) that is attributable to local emissions from vehicles operating on the roadway to an areawide concentration from a FSM or a gridded air quality model (C_{amb}). The incremental concentration is estimated by California Line Source Dispersion Model, Version 4 (CALINE4). CALINE4 predicts near-road incremental concentration, based on vehicle emissions, roadway characteristics, and meteorological data (*10*). Yura et al. (*11*) evaluated the performance of CALINE4 in predicting near-road $PM_{2.5}$ concentrations and found it produced results similar to measured data for areas close to the emission source and near to the ground in suburban areas. However, for urban areas, CALINE4 did not provide good predictions, which may be due to street canyon effects. There is not an existing modeling tool that is capable of estimating on-road $PM_{2.5}$ concentration accurately. Hence, near-road concentration is used as a surrogate for on-road concentration.

For air quality inside the vehicle, a mass balance is derived based on the schematic of the vehicle cabin and heating, ventilating, and air conditioning (HVAC) system of Figure 1. The model is based on these assumptions: (*a*) particles inside the vehicle cabin are well mixed; (*b*) particles enter the vehicle cabin via advection or infiltration from outside and by advection from the HVAC system; (*c*) in the HVAC system, air passes through a filter with filter efficiency η; (*d*) particles are removed from the vehicle cabin by advection or exfiltration to the outside, advection to the HVAC system in the case of air recirculation, and deposition to interior surfaces; (*e*) the deposition rate is independent of time and direction; (*f*) the filter removal efficiency for the HVAC system is constant; and (*g*) the HVAC system can accept air either from the vehicle cabin or from the outdoors.

The mass balance for the case of the HVAC system using outside air is

$$\frac{dC_{iv}}{dt} = \lambda_{in}C_{sv} - (\lambda_{in} + \lambda_{hvac})C_{iv} + \lambda_{hvac}C_{sv}(1-\eta) - C_{iv}\beta \quad (2)$$

where

C_{iv} = concentration in the vehicle, $\mu g/m^3$;
C_{sv} = concentration surrounding the vehicle exterior, $\mu g/m^3$;
λ_{in} = air exchange rate due to infiltration, L/h;
λ_{hvac} = air exchange rate for the HVAC system, L/h;
η = filter removal efficiency, fraction; and
β = deposition rate, L/h.

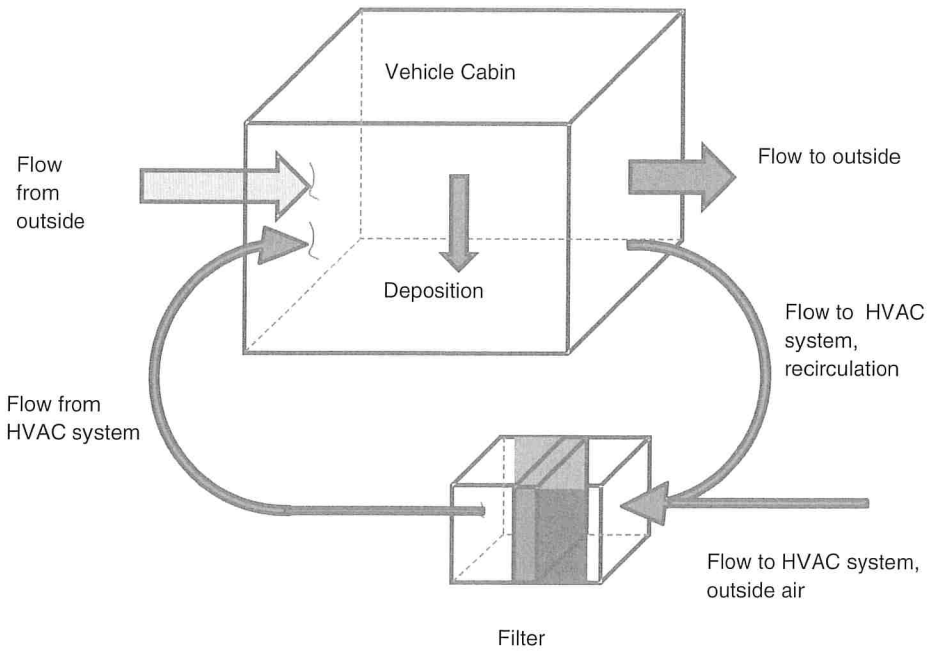

FIGURE 1 Schematic of air flow through the vehicle cabin and the heating, ventilating, and air conditioning system.

The terms in the equation represent advection of outside air into the vehicle, advection of cabin air to the outside, advection of outside air via the HVAC system filter, and deposition inside the cabin. In the case for recirculation of cabin air via the HVAC system, the mass balance is

$$\frac{dC_{iv}}{dt} = \lambda_{in}\left(C_{sv} - C_{iv}\right) - \lambda_{hvac}C_{iv}\eta - C_{iv}\beta \quad (3)$$

The terms for this mass balance include the net advection for outside air into the cabin versus cabin air to the outside, the net effect of cabin air that recirculates through the HVAC filter, and deposition inside the cabin.

The models in Equations 2 and 3 are solved numerically. The results from these models are used to specify the ratio of the in-cabin concentration, C_{iv}, to the concentration surrounding the vehicle, C_{sv}, or the areawide ambient concentration, C_{amb}. Hence, the slope k_{vt} in Equation 1 can be inferred and entered into SHEDS-PM to represent the in-vehicle air quality model. The intercept b_{vt} can be set to zero. In order to demonstrate the application of the alternative approach, the near-road incremental $PM_{2.5}$ concentration estimation model and the in-vehicle air quality model are applied for various scenarios. The model inputs are varied to analyze the sensitivity of the modeling results and estimated exposure to selected inputs.

Near-Road Incremental $PM_{2.5}$ Concentration

The inputs to CALINE4 include receptor positions, road geometry, and road activity. As a surrogate of on-road incremental $PM_{2.5}$ concentration, the receptor is set as close to the edge of the roadway as possible. Existing studies on near-road $PM_{2.5}$ concentration estimated by CALINE4 indicate that the closest valid distance is 3.4 m (*10*). Liu et al. (*6*) have identified the following key input variables for CALINE4: road geometry, traffic volume, emission factor, wind speed, and stability class. The values for these inputs are reviewed and the sensitivity of near-road incremental $PM_{2.5}$ concentration to these inputs is quantified.

In-Vehicle Air Quality Model

The in-vehicle air quality model has the following key inputs: $PM_{2.5}$ concentration surrounding the vehicle (C_{sv}), air exchange rates for the cabin and the HVAC system, filter efficiency, and deposition rate. The exterior concentration is sensitive to the roadway scenario and depends on vehicle speed, emission rate, traffic volume, and number of lanes. To illustrate these latter sources of variability, two scenarios are defined based on arterial and highway roadways.

Sensitivity of Exposure

Human exposure to $PM_{2.5}$ is estimated using SHEDS-PM, based on a case study for Wake County, North Carolina. The sensitivity of in-vehicle exposure and total exposure to the key inputs of the near roadway and in-vehicle air quality models are analyzed.

RESULTS

This section reviews the key inputs for the alternative approach and quantifies the sensitivity of $PM_{2.5}$ concentration and exposure to these inputs.

Near-Road Incremental $PM_{2.5}$ Concentration

The range of values for key inputs is summarized in Table 1. The sensitivity of near-road incremental $PM_{2.5}$ concentration to these inputs is estimated by altering these inputs over nominal ranges.

CALINE4 is able to model straight or curved roads, intersections, parking lots, and other roadway geometry (*9*). However, the human activity data used in SHEDS do not contain information regarding the time people spend on roadways of different geometries. Thus for simplicity, only straight roads are considered here. Road geometry is defined by start and end points of road links, road heights, lane and road width, and mixing zone width. The latter includes 3 m of additional width on both sides of the road. Estimated near-road concentration was found not to be sensitive to road length when varied over a range of 150 m to 10 km.

Chen et al. (*10*) reported an average traffic volume of 1,919 vehicles per lane per hour on a six-lane highway in Sacramento, California, and validated CALINE4 predictions of $PM_{2.5}$ concentrations near this road. The traffic volumes for different road types are estimated based on the number of lanes, average vehicle speed, and distance separating two vehicles in the same lane:

$$\mathrm{TV} = \frac{v}{v \times t_0 + l} \times 3{,}600 \text{ s/h} \quad (4)$$

where

TV = estimated traffic volume per lane, vehicles/hour;
v = average vehicle speed, m/s;
t_0 = average time interval between cars in the same lane, s; and
l = vehicle length, m.

For a time interval of 2 s and a vehicle length of 15 m, the estimated traffic volumes are approximately 1,600 vehicles per hour per lane for a 4-s following time over a range of speeds from 50 to 100 km/h.

Kristensson et al. (*12*) measured $PM_{2.5}$ emission factors in grams emitted per vehicle kilometer traveled (g/VKT) in a Swedish tunnel that included both gasoline and diesel light-duty vehicle traffic and found that they increase with vehicle speed. These real-world emission factors include all sources of $PM_{2.5}$, such as exhaust, brake wear, tire wear, and resuspension of particles deposited on the road. For vehicles at speeds from 45 to 70 km/h, 70 to 75 km/h, and 75 to 90 km/h, the average link-based emission factor was 0.033, 0.041, and 0.100 g/VKT, respectively. The overall average was 0.067 g/VKT, which is similar to 0.062 g/VKT as modeled by Chen et al. (*10*) in a U.S. validation study of CALINE4. Furthermore, the emission factors from the tunnel study are comparable to those obtained from the MOBILE6 emission factor model. For example, the $PM_{2.5}$ emission factor simulated by MOBILE6 using example data provided by USEPA is 0.033 g/VKT on average for all vehicle types, including

TABLE 1 Range of Values for Key Inputs for CALINE4

CALINE4 Input	Value	Unit
Traffic volume	1,600–6,800[a]	veh/h
Emission factor	0.033–0.100	g/VKT
Wind speed	1.0–5.4	m/s
Stability class	A, B, C, D, E, F, G	—

[a]Varies by road type and number of lanes. See Table 2 for more detail.

TABLE 2 Characteristics of Road Types

Road Type	No. of Lanes	Width per Lane[a] (m)	Total Width of Road (m)	Total Width of Mixing Zone[b] (m)	Emission Factor (g/VKT)	Average Vehicle Speed (mph)	Distance Between Vehicles (ft)	Traffic Volume Used in CALINE4[c] (veh/h)
Local I	2	3.15	6.3	12.3	0.033	30	279	1,617
Local II	3	3.15	9.5	15.5	0.033	30	279	2,425
Local III	4	3.15	12.6	18.6	0.033	30	279	3,233
Arterial	4	3.45	13.8	19.8	0.041	45	411	3,347
Highway I	4	3.6	14.4	20.4	0.100	60	543	3,407
Highway II	6	3.6	21.6	27.6	0.100	60	543	5,110
Highway III	8	3.6	28.8	34.8	0.100	60	543	6,813

[a]According to AASHTO (*14*), local roads must have lane widths between 2.7 and 3.6 m, arterial roads must have lane widths between 3.3 and 3.6 m, and highways must have lane widths no less than 3.6 m. The average values of the possible ranges of lane width are used in the estimation of total width of the road. The latter is the product of the number of lanes and width per lane.
[b]Calculated by adding 3 m on each side to the total width of the road.
[c]Time interval between vehicles in the same lane is 4 s.

exhaust, brake wear, and tire wear emissions. Such a result is similar in magnitude to that from the tunnel study measurements.

Wind speed affects air pollutant dispersion. Wind speed data in 2007 at six stations in North Carolina were examined to account for variability in the typical wind speeds in the study area. On a monthly basis, the average minimum and maximum monthly wind speeds were 2.3 and 5.4 m/s, respectively. On an annual basis, these were 3.3 and 4.9 m/s, respectively. The capacity of CALINE4 to estimate carbon monoxide (CO) concentrations under low wind speed conditions was verified at wind speeds of approximately 1.0 to 1.5 m/s (*13*). However, no comparable $PM_{2.5}$ validation studies have been conducted. It is assumed that the low wind speed performance of CALINE4 is suitable for estimation of $PM_{2.5}$ concentration. Thus 1.0 m/s is selected as the lower bound of the possible wind speeds.

To quantify variability in concentrations attributable to roadway geometry and vehicle operations, three categories including seven types of roadways were identified and compared. The categories are local, arterial, and highway. Table 2 lists these road types and their characteristics including geometry, traffic volume, and emission factor.

For each road type, CALINE4 is applied for various wind speeds and stability class. Atmospheric stability class ranges from very unstable (A) to very stable (G), and each stability class is associated with particular ranges of meteorological conditions such as wind speed. Not all stability classes can be used in combination with a particular wind speed. Low wind speeds can be associated with any stability class. However, the higher wind speeds considered can only be associated with stability classes B through E. For each wind speed, two bounding stability class are considered.

CALINE4 runs were conducted on a Windows XP quad-processor computer and had a run time of a few seconds. Table 3 shows the CALINE4 outputs. Among the road types, Highway III has the highest estimated near-road incremental $PM_{2.5}$ concentration (35.0 $\mu g/m^3$), whereas Local I has the lowest concentration (0.8 $\mu g/m^3$). As expected, the incremental concentrations decrease when wind speed increases. For example, for the Local I roadway, concentration decreases by 75% when wind speed increases from 1.0 to 5.4 m/s and by 68% for Highway III. More stable conditions lead to higher concentrations. For example, for a wind speed of 1.0 m/s and Highway III, the $PM_{2.5}$ concentration for stability class G is 16% times greater than for stability class A. Overall, concentrations varied by as much as an order of magnitude when comparing road types, a factor of three to four when comparing wind speeds, and only by 4% to 25% when comparing stability class.

TABLE 3 Near-Road $PM_{2.5}$ Increment ($\mu g/m^3$) Estimated Using CALINE4 for Road Type and Wind Speed Scenarios

	Wind Speed (m/s)									
	1.0		2.3		3.3		4.9		5.4	
	Stability Class									
Road Type	A	G	A	G	A	G	B	E	B	E
Local I	3.2	3.6	1.7	1.8	1.2	1.5	0.9	1.1	0.8	0.9
Local II	4.7	5.3	2.6	2.9	1.8	2.1	1.4	1.5	1.2	1.4
Local III	5.9	6.6	3.2	3.8	2.6	2.7	1.7	2.0	1.5	1.8
Arterial	7.7	8.7	4.2	5.0	3.2	3.6	2.3	2.6	2.1	2.4
Highway I	18.6	21.5	10.7	12.2	8.0	8.9	5.7	6.5	5.3	5.9
Highway II	25.4	28.8	15.0	17.0	11.6	13.1	8.0	9.6	7.8	8.9
Highway III	30.3	35.0	18.5	21.0	14.3	16.5	10.8	12.3	9.8	11.3

In-Vehicle Air Quality Model

Ott et al. (*15*) measured the air exchange rates (ACH) for four vehicles with variations in vehicle speed, window opening, and ventilation. ACH is the average volumetric air flow rate divided by the interior volume. The lowest mean ACH was 0.92/h, which was observed for a 2005 Toyota Corolla when the vehicle was stopped with the window closed and the fan off. The highest mean ACH of 78.6/h was observed for a 2005 Ford Taurus sedan at a speed of 20 mph with one window fully open and the ventilation fan turned off.

The U.S. National Human Activity Pattern Survey (*16*) indicates that people spent an average of 5.5% of the day in vehicles. Employed people commute twice per day, and each commute event has a duration of approximately 40 min. It is assumed that people spend approximately 1.5 h per day in a vehicle.

Rodes et al. (*17*) monitored both in-vehicle and on-road $PM_{2.5}$ concentration surrounding the vehicle for traveling events lasting 2 h. When the vehicle was at high speed and the ventilation was high, the ACH was higher than 20.7/h. When all windows were closed and ventilation was set to low for the same vehicle, the air exchange rate ranged from 1.8/h when the vehicle was stopped to 5.6/h when the vehicle was moving at a speed of 35 mph. Hence, these air exchange rates are assumed to be representative of the HVAC system.

During the summer, the typical scenarios of vehicle operation are (*a*) windows closed and ventilation on and (*b*) windows open and ventilation off. Two ACH values corresponding to the two scenarios are selected, respectively: (*a*) 31.3/h and (*b*) 71/h (*13*). Variability and uncertainty in filter efficiency is addressed by considering bounding and intermediate values of 0, 0.25, 0.50, 0.75, and 1.00. The deposition rate was varied from 0 to 1/h to assess its effect on the estimated in-vehicle concentration. Examples of the results of sensitivity analysis of the in-vehicle concentration model are shown in Figure 2, based on the assumption of a nominal $C_{sv} = 10\ \mu g/m^3$, $\lambda_{in} = 30.3$ and 71/h, $\eta = 0.5$, and $\beta = 1/h$.

For a vehicle cabin air exchange rate of 30.3/h and an HVAC system air exchange rate of 5.6/h, the dominant means of advection is exchange of outside air via windows. Hence, the filter processes only a small portion of the cabin air. Therefore, even if the filter efficiency were 100%, the reduction in in-cabin concentration compared to that outside the vehicle would only be 18%. As the cabin air exchange rate increases to 71/h, the in-vehicle concentration would be only 9% less than that of the outdoors even with 100% filter efficiency. At these high rates of advection of outside air via windows, there is little difference in whether the HVAC system intakes outside or recirculated air.

In contrast, if the cabin air exchange rate was relatively low, such as 5/h, and if the HVAC system air exchange rate was comparable at 5.6/h, then at 50% filter efficiency the in-vehicle concentration would be reduced compared to outside air by 33% using fresh air into the HVAC system and by 43% using recirculated air. As filter efficiency approaches 100%, the cabin concentration would approach only 43% of the outside value for either HVAC intake source. If the deposition rate were 0/h instead of 1.0/h, the cabin concentration would be 47% of the outside value. Hence, the results are not very sensitive to deposition rate.

For cases of high advection of outside air via windows, the ratio of in-cabin to outdoor concentration is approximately 0.82 to 0.99, depending on the filter efficiency. When the windows are closed and the HVAC system is in recirculation model, the ratio would be more likely to be in the range of 0.5 to 0.8.

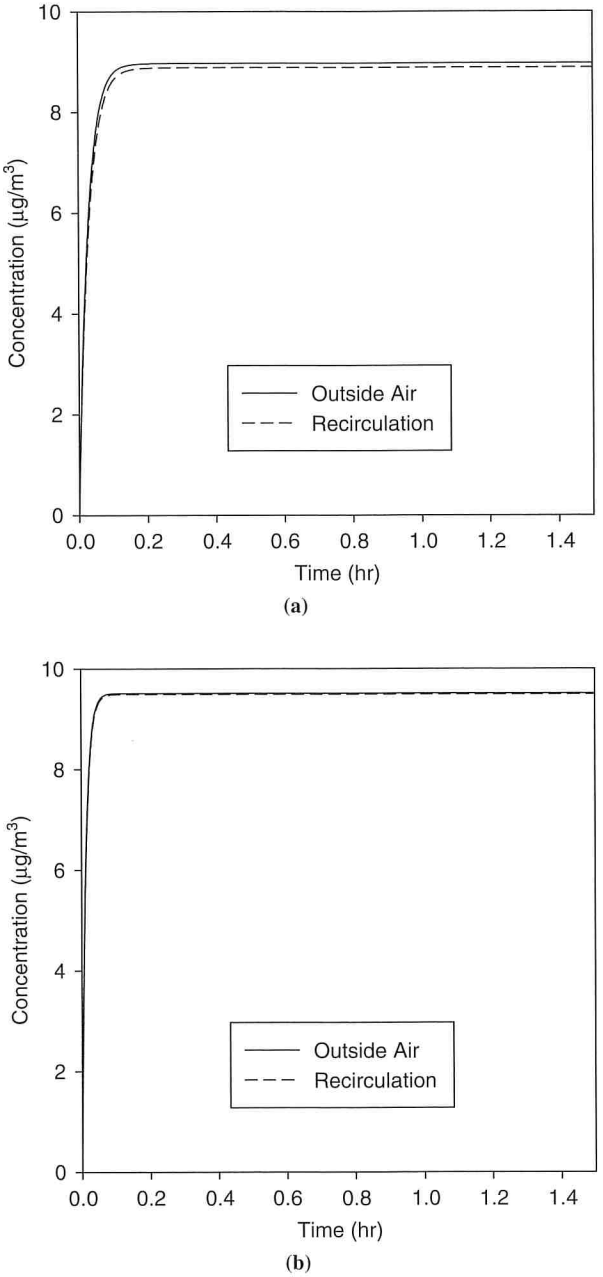

FIGURE 2 Example results for estimated in-vehicle $PM_{2.5}$ concentration as a function of time for HVAC system operation with outside and recirculated air for selected vehicle cabin air exchange rates, filter efficiency of 0.5, and deposition rate of 1.0/h: (*a*) λ_{in} = 30.3/h and (*b*) λ_{in} = 71/h.

Sensitivity of Exposure

The sensitivity analysis is based on a case study for Wake County, North Carolina. Wake County contains 105 census tracts and had a 2000 population of 630,000 people. A random sample of 1% of these individuals was simulated. People of all ages and genders were included and commuting was considered. $PM_{2.5}$ concentration data for the case study are based on hourly data from July 1, 2002 to July 30, 2002 from the output of the Congestion Mitigation and Air Quality Improvement Program model. The average $PM_{2.5}$ concentration

TABLE 4 Key Inputs for North Carolina Case Study

Micro-Environment	Calculation Scheme	Parameter	Distribution Type[c]	Distribution Values	Reference
All outdoor	Scaling factor[a]	Factor	Fixed	1.0	
Home	Mass balance	Penetration	Normal	Mean = 0.91, sd = 0.1	Meng et al., 2005 (*18*)
		Deposition	Normal	Mean = 0.79, sd = 0.31	
		Air exchange rate	Lognormal	Season 3 (summer)[d]: geo. mean = 0.555, geo. std. = 1.844	Murray and Burmaster, 1995 (*19*)
Office	Linear regression[b]	Slope	Fixed	0.18	Burke et al., 2001 (*5*)
		Intercept	Fixed	3.6	
		Residuals	Normal	Mean = 0, sd = 2.9	
School	Linear regression	Slope	Fixed	0.6	Burke et al., 2001 (*5*)
		Intercept	Fixed	6.8	
		Residuals	Normal	Mean = 0, sd = 5.4	
Store	Linear regression	Slope	Fixed	0.75	Burke et al., 2001 (*5*)
		Intercept	Fixed	9.0	
		Residuals	Normal	Mean = 0, sd = 2.1	
Restaurant	Linear regression	Slope	Fixed	1.0	Burke et al., 2001 (*5*)
		Intercept	Fixed	9.8	
		Residuals	Normal	Mean = 0, sd = 10	
Bar	Linear regression	Slope	Fixed	1.0	Burke et al., 2001 (*5*)
		Intercept	Fixed	9.8	
		Residuals	Normal	Mean = 0, sd = 10	
All other indoor	Linear regression	Slope	Fixed	0.85	Burke et al., 2001 (*5*)
		Intercept	Fixed	8.4	
		Residuals	Normal	Mean = 0, sd = 4	

[a]Scaling factor equation: $C_{micro} = aC_{amb}$, where: C_{micro} = microenvironmental PM concentration; C_{amb} = ambient PM concentration; a = factor.
[b]Linear regression equation: $C_{micro} = kC_{amb} + b + \epsilon$, where: k = slope; b = intercept; ϵ = residuals, which is used to calculate variability. The intercepts account for cooking or other emissions. Smoking is handled separately in SHEDS-PM.
[c]Fixed refers to constant value; normal refers to normal distribution; lognormal refers to lognormal distribution.
[d]The modeling period is from July 1 to July 30, thus only Season 3 (summer) has been used.

during this time period was estimated to be 12.7 μg/m³. All the key input assumptions for each microenvironment are listed in Table 4 except for the in-vehicle microenvironment.

Table 5 lists the inputs to the in-vehicle air quality model, the corresponding value of k_{vt}, the in-vehicle concentration, the in-vehicle exposure (assuming a total of 1.5 h of commuting per day, averaged over 24 h), corresponding total exposure for three values of the cabin air exchange rate, and the percentage of total exposure that occurs in vehicle.

The results indicate that in-vehicle exposure for a typical commuting scenario can represent approximately 10% to 20% of the daily average exposure for an individual, depending on the status of

TABLE 5 Example of Sensitivity of In-Vehicle Exposure to Vehicle Air Exchange Rate and HVAC Filter Efficiency for Highway Scenario with C_{icr} = 35.0 μm/m³

ACH (h⁻¹)	η	k_{vt}	In-Vehicle $PM_{2.5}$ Concentration C_{iv} (μg/m³)	Average 24-h In-vehicle $PM_{2.5}$ Exposure (μg/m³)	Average 24-h Total $PM_{2.5}$ Exposure (μg/m³)	Percentage of Total Exposure that Occurs In-Vehicle
5.0	0.00	0.83	39.7	2.5	13.8	18.1
5.0	0.25	0.68	32.2	2.0	13.3	15.1
5.0	0.50	0.57	27.1	1.7	13.0	13.0
5.0	0.75	0.49	23.4	1.5	12.8	11.5
5.0	1.00	0.43	20.6	1.3	12.6	10.2
30.3	0.00	0.97	46.2	2.9	14.2	20.3
30.3	0.25	0.93	44.2	2.8	14.1	19.6
30.3	0.50	0.89	42.4	2.6	13.9	19.0
30.3	0.75	0.86	40.7	2.5	13.8	18.4
30.3	1.00	0.82	39.2	2.4	13.7	17.8
71.0	0.00	0.99	47.0	2.9	14.2	20.6
71.0	0.25	0.97	46.1	2.9	14.2	20.3
71.0	0.50	0.95	45.3	2.8	14.1	20.0
71.0	0.75	0.93	44.4	2.8	14.1	19.7
71.0	1.00	0.91	43.6	2.7	14.0	19.4

NOTE: Assumptions: area wide concentration is 12.7 μg/m³, incremental near roadway concentration is 35.0 μg/m³, C_{sv} = 47.7 μg/m³, deposition rate is 1.0 μ/h, HVAC air exchange rate is 5.6 μ/h.

windows and HVAC system capabilities. The lowest contribution of in-vehicle exposure is associated with relatively little air exchange via windows, use of recirculated air, and a high filter efficiency. The highest contributions are associated with a high exchange rate with outside air and no filtering by the HVAC system. The in-vehicle concentrations during in-vehicle exposures are estimated to range from 21 to 47 $\mu g/m^3$, with 24-h averages ranging from 1.3 to 2.9 $\mu g/m^3$.

Riediker et al. (*7*) measured in-vehicle $PM_{2.5}$ concentrations for selected vehicles in Wake County, North Carolina, in 2001 and observed a mean of 24 $\mu g/m^3$ with a range from 4 $\mu g/m^3$ to 54 $\mu g/m^3$. The range of estimated in-vehicle concentrations in Table 5 is within the range of observed concentrations measured by Riediker et al. and thus is considered to be reasonable.

DISCUSSION OF DATA NEEDS

Although the near-road $PM_{2.5}$ concentration CALINE4 has been validated for CO and $PM_{2.5}$ (*8, 10, 13*), whether it is appropriate to use it as a surrogate for $PM_{2.5}$ concentration immediately surrounding a vehicle operating on the road has not been validated. Some studies indicate that self-pollution may occur for the in-vehicle microenvironment (*20, 21*). Self-pollution refers to infiltration into the cabin of the same vehicle's tailpipe emissions. Therefore, three sets of $PM_{2.5}$ concentration data may need to be collected simultaneously in future research to further develop the modeling approach: near-road, surrounding the vehicle, and self-emitted.

The near-road $PM_{2.5}$ concentration can be sampled by portable instruments located in a vehicle. Air can be drawn in by a pump through a size selective inlet. Airborne particles can be collected on a filter. By weighing the filter before and after sampling, the particle mass of the sample can be determined. Tiitta et al. (*22*) and Kaur et al. (*23*) measured near-road $PM_{2.5}$ concentrations with this method. $PM_{2.5}$ concentrations surrounding the vehicle can be sampled by the same instruments used to measure in-vehicle $PM_{2.5}$ concentrations. More simultaneous measurements of in-vehicle and surrounding-vehicle concentrations are needed in order to validate and further develop the mass balance modeling approach.

To further apply the mass balance model for in-vehicle concentration, data are needed for a variety of vehicles in order to characterize in-cabin and HVAC air exchange rates, taking into account inter-vehicle variability and variation in driver preference for operating conditions. The overall ACH for a running vehicle can be determined by the following procedure: (*a*) fill a Tedlar sampling bag with tracer gas for which the quantity is known, (*b*) release all the gas in the bag, and (*c*) measure the concentration decay in the vehicle as a function of time (*15*). The filter removal efficiency can be measured by comparing PM concentrations that enter the HVAC system to those that exit the HVAC system.

CONCLUSIONS

There is growing recognition of the importance of the contribution of in-vehicle exposures to $PM_{2.5}$ as a component of total daily average exposure. However, to date there are few field studies that quantify in-vehicle $PM_{2.5}$ concentration, and existing exposure models such as SHEDS-PM use highly simplified modeling techniques that are not able to account for key sources of variability. In particular, the use of a linear regression in which in-vehicle concentration is estimated based on a distant FSM explains very little variability in the in-vehicle concentration. The in-vehicle concentrations are influenced by emissions on the roadway, whereas an FSM might be located sufficiently far from the roadway that it is not a good indicator of on-road air quality. Thus, the preferred method for estimating in-vehicle concentration is to estimate the ambient concentration surrounding the vehicle, from which the concentration inside the vehicle can be estimated. However, there is not yet an accepted modeling approach for estimating on-road concentration. The most relevant surrogate to on-road concentration that can be reliably estimated with existing tools, such as CALINE4, is near-road concentration.

The near-road concentration is most sensitive to roadway type and wind speed and less sensitive to stability class. The near-road concentration estimated for highways is a factor of 6 greater than that for local roads and a factor of 3.5 greater than that for arterials, over a wide range of wind speeds and stability classes. Furthermore, near-roadway air quality varied by more than an order of magnitude among all of the combinations of road and atmospheric characteristics considered.

If the ambient concentration surrounding a vehicle is known, then a reasonable estimate can be made of the in-vehicle concentration using a mass balance model. The key factor to which in-vehicle concentration is sensitive, aside from the outdoor concentration, is the air exchange rate. For low ACH, filter efficiency is also an important factor. For occupants who wish to minimize average in-vehicle concentration, the preferred operating scenario is to keep windows closed and use the HVAC system in recirculation mode, as long as there are no in-vehicle emission sources. In-vehicle concentration in the on-road fleet is likely to be highly variable because of differences in driver choices regarding operation of windows and HVAC system, as well as intervehicle variability in cabin volume.

There are key data needs that would enable improved estimates of in-vehicle $PM_{2.5}$ concentrations. These include ability to estimate on-road rather than near-road ambient concentration, accounting for vehicle self-pollution in situations where it may be important, accounting for in-vehicle emissions sources such as cigarette smoking, validating model predictions of in-vehicle concentration based on simultaneous measurements of in-vehicle and outside-vehicle air quality, and characterization of the frequency distribution of factors such as interior volume, ACH, and filter efficiency.

The estimated results from the coupled near-road air quality and in-vehicle mass balance models as demonstrated here are comparable to those obtained from in-vehicle measurements. Thus, the methodology presented here is a promising basis for refinement of population-based exposure simulation models in order to better account for the in-vehicle contribution to total exposure.

ACKNOWLEDGMENTS

This work has been supported by National Institutes of Health and by the U.S. Environmental Protection Agency. The authors thank Janet Burke, Steve Perry, and Vlad Isakov of the U.S. Environmental Protection Agency for their support and help.

REFERENCES

1. *Air Quality Criteria for Particulate Matter: Final Report.* Publication EPA 600/P-99/002aF-bF. U.S. Environmental Protection Agency, Washington, D.C., Oct. 2004.
2. Table 1-38: Principal Means of Transportation to Work. In *National Transportation Statistics,* prepared by Research and Innovative Technology

Administration, Bureau of Transportation Statistics, for the U.S. Department of Transportation, Washington, D.C., Dec. 2008. http://www.bts.gov/publications/national_transportation_statistics/html/table_01_38.html. Accessed March 12, 2009.
3. Adams, H. S., M. J. Nieuwenhuijsen, R. N. Colvile, M. A. S. McMullen, and P. Khandelwal. Fine Particle ($PM_{2.5}$) Personal Exposure Levels in Transport Microenvironments, London, UK. *Science of the Total Environment,* Vol. 279, No. 1–3, 2001, pp. 29–44.
4. Burke, J. M. *Sheds-PM Stochastic Human Exposure and Dose Simulation for Particulate Matter: User Guide EPA Sheds-PM 2.1.* EPA/600/R-05/065. U.S. Environmental Protection Agency, Washington, D.C., 2005, pp. 11–15.
5. Burke, J. M., M. J. Zufall, and H. Ozkaynak. A Population Exposure Model for Particulate Matter: Case Study Results for $PM_{2.5}$ in Philadelphia, PA. *Journal of Exposure Analysis and Environmental Epidemiology,* Vol. 11, No. 6, 2001, pp. 470–489.
6. Liu, X., H. C. Frey, Y. Cao, and B. Deshpande. Modeling of In-Vehicle $PM_{2.5}$ Exposure Using the Stochastic Human Exposure and Dose Simulation Model. Paper 2009-A-238-AWMA. *Proc., 102nd Annual Conference and Exhibition,* Air & Waste Management Association, Detroit, Mich., June 16–19, 2009.
7. Riediker, M., R. Williams, R. Devlin, T. Griggs, and P. Bromberg. Exposure to Particulate Matter, Volatile Organic Compounds, and Other Air Pollutants Inside Patrol Cars. *Environmental Science and Technology,* Vol. 37, No. 10, 2003, pp. 2084–2093.
8. Lai, C. H., S. H. Liou, T. S. Shih, P. J. Tsai, H. L. Chen, Y. C. Chang, T. J. Buckley, and P. J. Strickland. Exposure to Fine Particulate Matter ($PM_{2.5}$) Among Highway Toll Station Workers in Taipei: Direct and Indirect Exposure Assessment. *Environmental Health,* Vol. 59, No. 3, 2004, pp. 138–148.
9. Hatano, M., P. Benson, K. Pinkerman, G. Brown, P. Connally, R. Cramer, G. Edwards, J. Quittmeyer, and K. Robertson. *CALINE4—A Dispersion Model for Predicting Air Pollutant Concentrations Near Roadways.* FHWA/CA/TL-84/15, Office of Transportation Laboratory, California Department of Transportation, Sacramento, Nov. 1989.
10. Chen, H. C., S. Bai, D. Eisinger, D. Niemeier, and M. Claggett. *Modeling Uncertainties and Near-Road $PM_{2.5}$*: A Comparison of CALINE4, CAL3QHC and AERMO. Department of Civil and Environmental Engineering, University of California–Davis, 2008, pp. 23–37, 45–48.
11. Yura, E. A., T. Kear, and D. Niemeier. Using CALINE Dispersion to Assess Vehicular $PM_{2.5}$ Emissions. *Atmospheric Environment,* Vol. 41, No. 38, 2007, pp. 8747–8757.
12. Kristensson, A., C. Johansson, R. Westerholm, E. Swietlicki, L. Gidhagen, U. Wideqvist, and C. Vesely. Real-World Traffic Emission Factors of Gases and Particles Measured in a Road Tunnel in Stockholm, Sweden. *Atmospheric Environment,* Vol. 38, No. 5, 2004, pp. 657–673.
13. Broderick, B. M., U. Budd, B. D. Misstear, D. Ceburnis, and S. G. Jennings. Validation of CALINE4 Modelling for Carbon Monoxide Concentrations Under Free-Flowing and Congested Traffic Conditions in Ireland. *International Journal of Environmental Pollution,* Vol. 24, No. 1–4, 2005, pp. 104–113.
14. *A Policy on Geometric Design of Highways and Streets,* 5th ed. American Association of State Highway and Transportation Officials, Washington, D.C., 2004, pp. 26–35.
15. Ott, W., N. Klepeis, and P. Switzer. Air Change Rates of Motor Vehicles and In-Vehicle Pollutant Concentrations from Secondhand Smoke. *Journal of Exposure Analysis and Environmental Epidemiology,* Vol. 18, No. 3, 2007, pp. 312–325.
16. Klepeis, N. E., W. C. Nelson, W. R. Ott, J. P. Robinson, A. M. Tsang, P. Switzer, J. V. Behar, S. C. Hern, and W. H. Engelmann. The National Human Activity Pattern Survey (NHAPS): A Resource for Assessing Exposure to Environmental Pollutants. *Journal of Exposure Analysis and Environmental Epidemiology,* Vol. 11, No. 3, 2001, pp. 231–252.
17. Rodes, C., L. Sheldon, D. Whitaker, A. Clayton, K. Fitzgerald, J. Flanagan, F. Genova, S. Hering, and C. Frazier. *Measuring Concentrations of Selected Air Pollutants Inside California Vehicles: Final Report.* ARB 95-339. Prepared by Research Triangle Institute, Sierra Research and Aerosol Dynamics for California Environmental Agency & South Coast Air Quality Management District, Diamond Bar, Calif., 1989, p. 135.
18. Meng, Q. Y., B. J. Turpin, L. Korn, C. P. Weisel, M. Morandi, S. Colome, J. F. J. Zhang, T. Stock, D. Spektor, A. Winer, L. Zhang, J. H. Lee, R. Giovanetti, W. Cui, J. Kwon, S. Alimokhtari, D. Shendell, J. Jones, C. Farrar, and S. Maberti. Influence of Ambient (Outdoor) Sources on Residential Indoor and Personal $PM_{2.5}$ Concentrations: Analyses of RIOPA Data. *Journal of Exposure Analysis and Environmental Epidemiology,* Vol. 15, No. 1, 2005, pp. 17–28.
19. Murray, D. M., and D. E. Burmaster. Residential Air Exchange-Rates in the Unites States—Empirical and Estimated Parametric Distributions by Season and Climatic Region. *Risk Analysis,* Vol. 15, No. 4, 1995, pp. 459–465.
20. Behrentz, E., D. R. Fitz, D. V. Pankratz, L. D. Sabin, S. D. Colome, S. A. Fruin, and A. M. Winer. Measuring Self-Pollution in School Buses Using a Tracer Gas Technique. *Atmospheric Environment,* Vol. 38, No. 23, 2004, pp. 3735–3746.
21. Sabin, L. D., K. Kozawa, E. Behrentz, A. M. Winer, D. R. Fitz, D. V. Pankratz, S. D. Colome, and S. A. Fruin. Analysis of Real-Time Variables Affecting Children's Exposure to Diesel-Related Pollutants During School Bus Commutes in Los Angeles. *Atmospheric Environment,* Vol. 39, No. 29, 2005, pp. 5243–5254.
22. Tiitta, P., T. Raunemaa, J. Tissari, T. Yli-Tuomi, A. Leskinen, J. Kukkonen, J. Harkonen, and A. Karppinen. Measurements and Modelling of $PM_{2.5}$ Concentrations Near a Major Road in Kuopio, Finland. *Atmospheric Environment,* Vol. 36, No. 25, 2002, pp. 4057–4068.
23. Kaur, S., M. J. Nieuwenhuijsen, and R. N. Colvile. Personal Exposure of Street Canyon Intersection Users to $PM_{2.5}$, Ultrafine Particle Counts and Carbon Monoxide in Central London, UK. *Atmospheric Environment,* Vol. 39, No. 20, 2005, pp. 3629–3641.

This paper has not been subject to review by the National Institutes of Health or the U.S. Environmental Protection Agency. The authors are solely responsible for its content.

The Transportation and Air Quality Committee peer-reviewed this paper.

Ecology and Transportation

I-90 Snoqualmie Pass East Project's Design Engineering Challenges of Integrating Transportation Needs with Landscape-Level Connectivity and Transportation Corridor-Crossing Objectives in Washington State

Randy Giles, Scott Golbek, Amanda Sullivan, and Jerry Wood

The Washington State Department of Transportation's (WSDOT) I-90 Snoqualmie Pass East Project has presented WSDOT engineers with many unique design challenges when integrating the ecological needs of the area with the transportation objectives of the project. The project faces issues of capacity, deteriorating concrete pavement, unstable rock slopes, and road closures associated with avalanches; there is also a real need to improve ecological connectivity of the area. I-90 is a physical barrier to the north–south movement of fish and wildlife. Wildlife attempting to cross the Interstate present a safety concern to motorists, and the barrier that I-90 forms between upstream and downstream aquatic habitats affects fish passage and hydrologic processes. To identify areas where investments in ecological connectivity should be made, WSDOT worked with dozens of agencies that manage land resources in the project area to design bridges and culverts that improve wildlife and aquatic connections. Integrating ecological objectives presented many design engineering challenges because of the project area's unfavorable construction conditions. Trade-offs and compromises between WSDOT and land resource managers were needed to find suitable solutions to problems. Issues that required compromises included eliminating scour issues while maximizing restoration areas; improving ground conditions for foundations without impacts to wetlands, endangered species, and footprint; creating habitat connections while treating stormwater; and designing bridges for clearance and connecting habitat.

The Washington State Department of Transportation's (WSDOT) I-90 Snoqualmie Pass East Project (I-90 project) is a 15-mi highway improvement project that will ensure the continued availability of Interstate 90 as a primary statewide corridor. Through the I-90 project, WSDOT will improve the safety and reliability of this corridor by reducing avalanche risks to the traveling public, minimizing road closures required for avalanche control work, and reducing the risk of rock and debris falling onto the interstate from unstable slopes. WSDOT will also fix structural deficiencies and provide for the recent and predicted increases in traffic volume. Ecological connectivity is another important project component. WSDOT will work to reduce wildlife–vehicle collisions by reconnecting habitat across I-90 and improving mobility of aquatic species and wildlife.

Plans for the project include widening the existing four-lane interstate to six lanes; replacing deteriorated concrete pavement; straightening sharp roadway curves; stabilizing unstable rock slopes; building a new, more efficient snowshed (a concrete shed covering the roadway to provide permanent protection from avalanches and other falling debris to travelers passing through Snoqualmie Pass); and constructing wildlife crossing structures. The first 5 mi of the I-90 project from Hyak to Keechelus Dam received funding in 2005 from the Washington State Legislature through the Transportation Partnership Account—a 9.5-cent increase in the gas tax—in the amount of $595 million. The remaining 10 project miles from Keechelus Dam to Easton remain unfunded.

The I-90 project corridor is located high along a mountain pass in the Central Cascades. The area's extreme weather conditions and inherent geographical and geotechnical complexities have presented WSDOT I-90 project engineers with many challenges when designing this improvement project. Integrating ecological connectivity objectives with transportation objectives has also presented challenges. Conflicts in objectives regarding crossing structure designs often surfaced that required the I-90 project design team and partnering resource agencies to compromise and accept trade-offs in order to move the project forward. Finding the right designs to optimize benefits required a great deal of collaboration, technical investigation, and engineering review.

In this paper, several case studies depict how conflicts in design between WSDOT engineers and various resource agencies, interdisciplinary teams, and technical committees were managed to resolve issues and reach compromises with satisfactory outcomes. In order to understand how WSDOT and project stakeholders integrated transportation and ecological connectivity objectives into the I-90 project, it is first necessary to understand the environment in which WSDOT is working and the process for developing the project's purpose and need.

I-90 PROJECT CORRIDOR ATTRIBUTES

I-90 spans 300 mi in Washington State from the Port of Seattle to the Idaho state line, and then continues east across the United States to Boston, Massachusetts. I-90 is the major east–west transportation

Washington State Department of Transportation, 1710 South 24th Avenue, Suite 100, Yakima, WA 98902. Corresponding author: A. Sullivan, SullivA@consultant.wsdot.wa.gov.

Transportation Research Record: Journal of the Transportation Research Board, No. 2158, Transportation Research Board of the National Academies, Washington, D.C., 2010, pp. 113–121.
DOI: 10.3141/2158-14

corridor across Washington and is vital to the state's economy (Figure 1) (*1*).

The I-90 project improves a 15-mi portion of I-90, beginning on the eastern side of Snoqualmie Pass at milepost 55.1, just east of the Hyak Interchange, where the existing highway narrows from six lanes to four lanes. The project end point is at milepost 70.3 at the West Easton Interchange, where the terrain becomes flatter and the highway is straighter. This 15-mi stretch of I-90 is in Kittitas County, Washington, and is predominately located on federal land within the Okanogan–Wenatchee National Forest.

The project corridor is located along a high mountain pass in the Central Cascades. The general topography is one of mountainous peaks and valleys. For the first 6 mi of the project area, I-90 runs along a narrow corridor between the shores of Keechelus Lake, a deep-water agricultural reservoir, and steep mountain slopes (Figure 2). These steep mountain slopes contain volcanic bedrock at varying depths that are subject to deep fissures and stress cracks with weakened slip planes, which when combined with high annual precipitation and freeze–thaw conditions makes them susceptible to landslides, debris flow, and avalanches.

I-90 is built primarily within an easement on national forest land. The large areas of protected state, federal, and conservation lands north and south of I-90 support a broad range of habitats and a diverse array of plants and wildlife. Since the late 1990s, the area has been managed according to the Snoqualmie Pass Adaptive Management Area Plan. This plan requires protection of old-growth habitat, removal of portions of existing Forest Service roads, and management of recreation to facilitate species movement. In recent years, there have been substantial private and public land conservation efforts to protect old-growth forest, provide larger contiguous blocks of forested habitat, and facilitate habitat connectivity across the I-90 corridor through the acquisition of private land. The Cascades Conservation Partnership, the Mountains-to-Sound Greenway Trust, the U.S. Fish and Wildlife Service (USFWS), and the U.S. Forest Service (USFS) have invested more than $100 million in these efforts during the past 5 years. These land purchases, along with the I-90 land exchange, have added 75,000 acres (approximately 117 mi^2) of land to the national forest system adjacent to and within the I-90 project area (*2*).

Even with conservation efforts, I-90's presence limits wildlife movement and forms a physical barrier between upstream and downstream aquatic environments. Existing culverts and narrow bridges limit aquatic species movement, and, in many cases, the highway embankment has filled in habitat that once made up channels, floodplains, and associated wetlands (*1*). Adequate connections between habitats and hydrologic features on either side of I-90 are necessary for the continued health of the project area's diverse ecosystems.

The last major road construction on I-90 Snoqualmie Pass began in the 1950s when President Dwight D. Eisenhower signed the Federal-Aid Highway Act of 1956, which started the construction of interstate highways; construction was completed in the 1970s. Since the 1970s, the state's transportation needs for I-90 over Snoqualmie Pass have changed and the existing roadway has deteriorated.

Today, daily traffic on Snoqualmie Pass averages about 27,000 vehicles, typically 22,400 passenger vehicles and 4,600 freight vehicles.

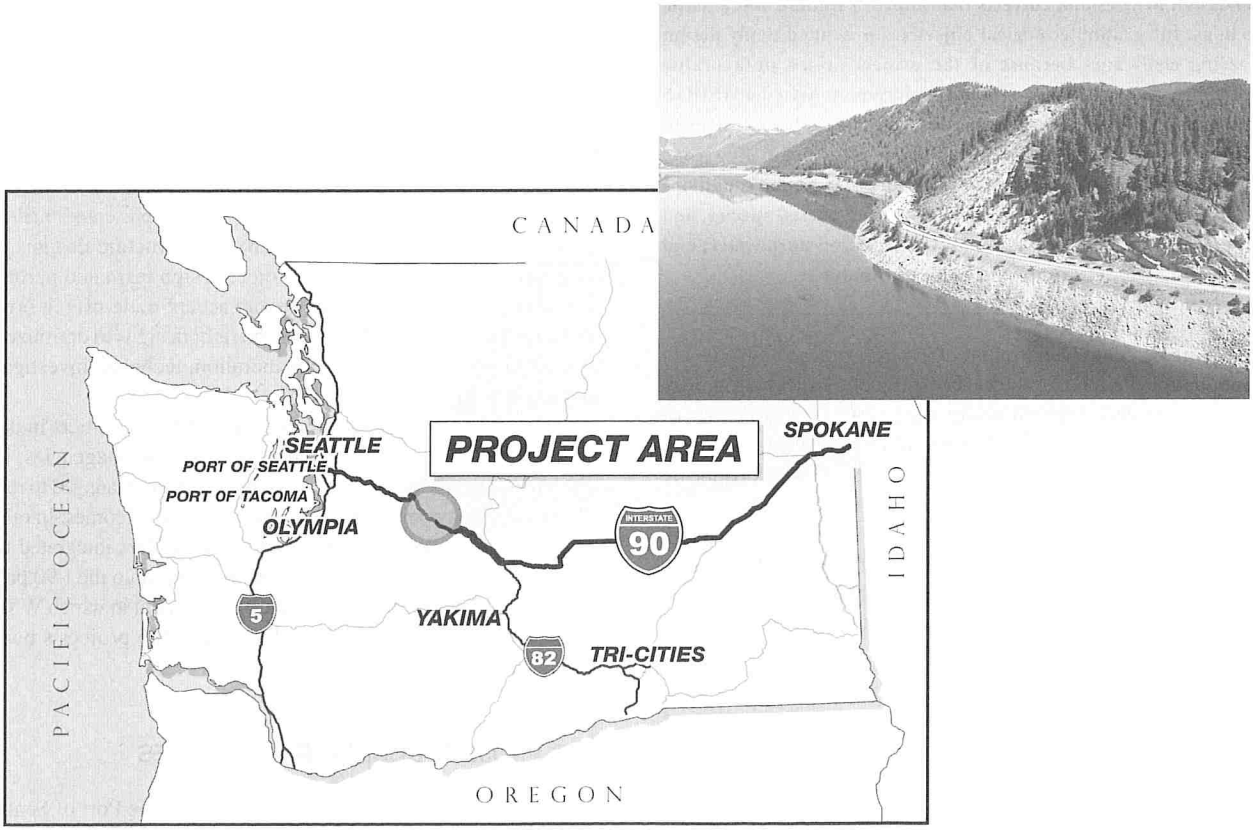

FIGURE 1 Washington State map showing Interstate 90, the I-90 project location, and typical topography.

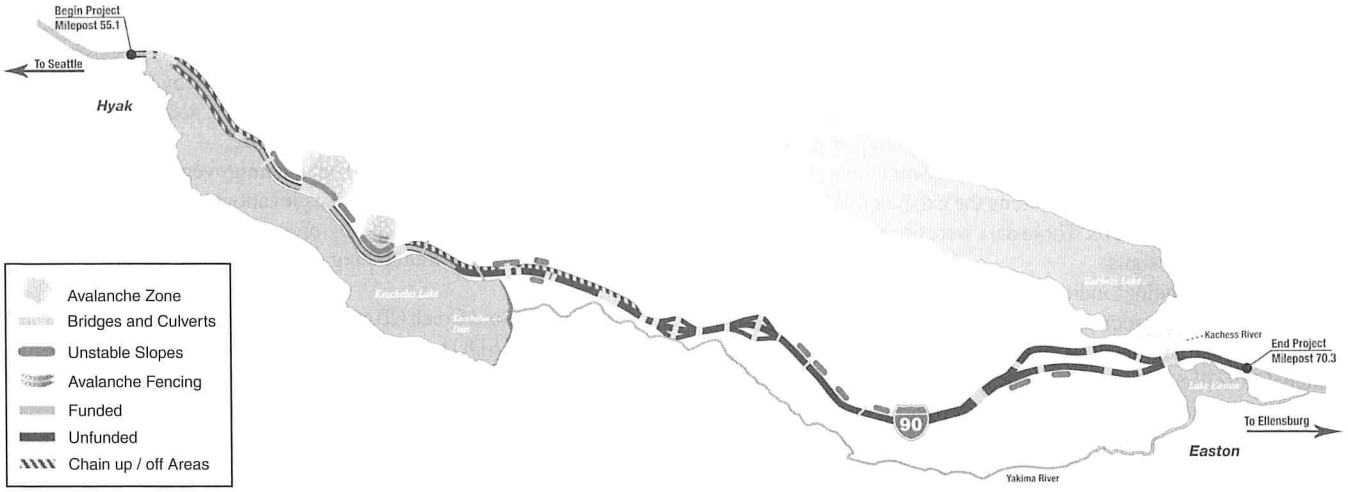

FIGURE 2 Map showing identified CEAs and the bridges and culverts (in yellow) that will be placed at each CEA to improve connectivity.

Traffic volumes can rise to more than 59,000 vehicles on weekends and holidays. According to WSDOT traffic studies, travel across Snoqualmie Pass is growing at an annual rate of 2.1%, with 51,000 vehicles projected to use I-90 daily by 2028.

IDENTIFYING PROJECT PURPOSE AND NEED

Seeing a need for additional highway capacity and safety improvements, WSDOT began the public scoping process for the I-90 project in 1999. By 2000, an interdisciplinary team (IDT) was formed, consisting of representatives from WSDOT, FHWA, USFS, Environmental Protection Agency (EPA), USFWS, and Washington Department of Fish and Wildlife (WDFW); advisory agencies included Washington State Parks, U.S. Army Corps of Engineers, and Washington Department of Ecology (Ecology). The IDT was formed to begin preliminary engineering and environmental analysis of the project area. Additional teams were formed, including a Mitigation Development Team consisting of biologists and hydrologists from WSDOT, USFS, USFWS, and WDFW, and a Wetlands Mitigation Technical Committee consisting of a geographic information system specialist, biologist, and environmental planner, to conduct further environmental analyses and provide design recommendations.

After 5 years of corridor analysis, WSDOT published the I-90 Snoqualmie Pass East Project Draft Environmental Impact Statement (draft EIS) for public review and comment in 2005. The draft EIS highlighted six build alternatives that could potentially meet the project's identified purpose and need for

- Reducing the risks of avalanche to the traveling public and eliminating road closures required for avalanche control work,
- Reducing the risk of rock and debris falling onto the roadway from unstable slopes,
- Fixing roadway structural deficiencies by replacing damaged pavement,
- Providing for the growth-related increases in traffic volume, and
- Connecting habitat across I-90 for fish and wildlife (*3*).

Over the next 2 years, WSDOT continued using existing partnerships and formed new teams, including a Stormwater Technical Committee and Wildlife Monitoring Technical Committee to help advance technical investigations and identify a preferred design alternative for the I-90 project. These collaborative efforts culminated with the release of the Final EIS in August 2008 that identified WSDOT's preferred design alternative for the I-90 project. FHWA issued its Record of Decision concurring with WSDOT's preferred alternative in October 2008, which paved the way to complete final design and for construction to begin.

DEVELOPING I-90 PROJECT DESIGN CONCEPTS

After identifying the I-90 project preferred alternative, project engineers began working with the IDT, mitigation team, and wetlands committee to develop conceptual design plans for ecological connectivity structures. The mitigation team presented design engineers with scientific information and site-specific technical report data that determined the existing ecological conditions within the project area. These data identified 14 north–south ecological linkage areas, or connectivity emphasis areas (CEAs), within the project area that provided the highest benefit-to-cost ratio and long-term solutions to the issue of ecological connectivity (Figure 2).

Each CEA provided an opportunity to improve connectivity for a unique assemblage of species. CEAs ranged in complexity from single stream crossings to multiple stream crossings with associated wetlands and areas of diffused surface flow to upland areas that were important travel corridors for wildlife (*2*). The mitigation team found that crossing structures would be more effective for some species if they contained habitat, rather than simply being physical connections between habitats on opposite sides of the highway. For instance, lower-mobility animals would feel more secure crossing a structure if it contained cover. Different animals show different preferences for crossing structures, whether the structures are small, medium, or large (*2*).

After analyzing all of the mitigation team's recommendations, WSDOT engineers and the mitigation team collaborated to develop conceptual designs for the highway alignment, drainage plans, staging and construction requirements, traffic control strategies, and initial bridge plans at each CEA. The design team also continued to develop designs independently.

While working with the mitigation team and technical committee, WSDOT and consultant engineers were also gathering geotechnical data from extensive drilling operations on the mountain slopes, in the lakebed of Keechelus Lake, and along the existing roadway to determine geological conditions. These data were essential to progressing conceptual CEA designs.

Geotechnical findings indicated that certain portions of the project area contained stable rock and favorable sediment, while other areas contained soft frangible rock and liquefiable soil conditions. Since liquefiable soil conditions result in global instability of structure foundations, WSDOT engineers had to rethink how to construct certain CEA concepts (bridges and culverts). Engineers worked to improve conditions and meet seismic regulations while still aligning with mitigation team and wetlands committee recommendations. In addition to seismic issues, WSDOT engineers had to reformat other CEA designs to address other unforeseen issues pertaining to erosion, stormwater treatment, clearance, and constructability. These design changes had to be made in a way that minimized footprint impacts, prevented wetland impacts, considered endangered species in the area, and preserved archeological, cultural, and recreational resources.

In the following sections, case studies explain how WSDOT I-90 project engineers modified original design concepts to resolve conflicts between ecological connectivity recommendations and objectives and the unforeseen seismic, erosion, stormwater treatment, clearance, constructability, and other resource issues.

IMPROVING GROUND CONDITIONS AT GOLD CREEK CEA WITHOUT IMPACTS TO WETLANDS, ENDANGERED SPECIES, AND FOOTPRINT

An important CEA identified by the mitigation team is located near the Gold Creek Valley. The Gold Creek CEA is located between Milepost 55.2 and Milepost 55.8, near the starting point of the I-90 project. Gold Creek crosses I-90 under 138- and 126-foot bridges and empties into Keechelus Lake at the northwest tip of the lake. This CEA connects old growth stands in mountain hemlock–subalpine fir forests and provides important hydrologic functions for Gold Creek. Gold Creek represents a critical area for linking the Alpine Lakes Wilderness to the Norse Peak Wilderness, which, in turn, links to other wilderness areas and national parks throughout the Washington Cascade Mountains (*2*).

To be successful at meeting objectives, WSDOT and the mitigation team determined that a high level of connectivity for the high- and low-mobility species associated with the mountain hemlock–subalpine fir forests, riparian habitats, wetlands, and floodplains must be provided year-round. Other objectives for this CEA include the following:

- Providing a high level of connectivity across the reservoir bed for approximately 9 to 10 months of the year. (The Keechelus Lake reservoir inundates the lakebed at high pool during late spring.)
- Significantly reducing wildlife–vehicle accidents in this high road-kill zone for deer and elk. This will require wildlife fencing around the crossing structures.
- Restoring natural channel migration processes and reducing floodplain confinement, particularly upstream of I-90 where floodplains and associated wetlands are not inundated by Keechelus Lake, and restoring capacity to convey flood flows, sediment, and debris through the Gold Creek crossing structure.
- Providing fish passage and habitat improvements for threatened bull trout for the full range of lake elevations.
- Improving water quality by properly treating stormwater and highway runoff, and minimizing deicer chemical use.

The initial Gold Creek CEA concept recommended by the IDT and accepted by WSDOT was to replace the existing 138- and 126-foot bridges with a 1,200-foot eastbound bridge and a 1,000-foot westbound bridge (*2*). This would provide a connection through the highway for approximately 9 to 10 months a year. Additional clearance for winter snowpack was also recommended.

After identifying objectives and conceptual Gold Creek CEA bridge designs, WSDOT conducted geotechnical drilling at the Gold Creek area. Geotechnical findings indicated areas of liquefiable soil conditions at the Gold Creek CEA site. Liquefiable soils (typically saturated sand) are a concern because during an earthquake, the soil looses shear strength and can flow like a liquid. This results in global foundation stability issues with bridge designs. To construct the bridges and meet seismic code requirements, WSDOT engineers would have to stabilize ground conditions.

Engineers originally proposed to improve liquefiable soils with a technique known as bottom-fed vibro-replacement stone columns. The stone columns were to range in diameter from 2.5 ft to 3.5 ft and would be constructed on a grid pattern designed to suit the load, soil, and performance types. Column holes were to be bored at varying design depths of approximately 50 ft deep in places, then dense, angular crushed or shot rock backfill would be introduced in discrete lifts from the ground surface. Repenetration of each lift would compact the stone in the surrounding soil. Once complete, the replacement stone columns would have effectively reduced foundation settlement, mitigated liquefaction potential, improved shear resistance, and increased bearing capacity.

The ecological impacts of the vibro-replacement ground stabilization technique, however, raised red flags among partnering resource agencies. Partners were concerned that construction of the stone columns would temporarily and permanently impact wetlands and expand the footprint of the roadway prism. This technique would require a pattern of stone columns roughly 50 ft beyond the toe of the highway embankment, necessitating construction within adjacent wetlands.

Understanding the importance of addressing resource agency concerns, WSDOT design engineers developed a list of plausible alternatives for improving the soil conditions at Gold Creek. WSDOT presented these alternatives to its partners and together they determined an acceptable method of improving ground conditions that met both transportation and ecological connectivity objectives.

The new, agreed-upon method of improving the liquefiable soils is compaction grouting. A very viscous (low-mobility) aggregate grout will be pumped in stages, starting up to 50 ft deep in places and working toward the ground surface. The grout will form a column of bulbs, which densifies and displaces the surrounding soils. WSDOT will construct the grout columns on a grid pattern designed to suit load, soil, and seismic performance. Once complete, the grout columns

will reduce foundation settlement, mitigate liquefaction potential, improve shear resistance, and increase bearing capacity. This technique uses a much smaller pattern (20 ft by 30 ft in total), localizes impacts to directly beneath the embankment fill area next to the bridge abutment, and allows minimization of the highway footprint.

ELIMINATING SCOUR ISSUES AT GOLD CREEK BRIDGES WHILE MAXIMIZING THE RESTORATION AREA

The Gold Creek CEA serves as a wildlife crossing structure, restores natural channel migration processes, and reduces floodplain confinement. Because of high spring flows within the creek, WSDOT engineers had to plan for scour in their bridge designs. Original bridge designs called for optimizing costs by keeping the foundations shallow—above ground water level—and using "launching toe" revetments consisting of large rip-rap to protect the foundation embankments (Figure 3).

The height and width of the planned revetments, however, resulted in a conflict with CEA objectives. Partnering resource agencies were concerned that revetments would reduce clearance and openness, limit the amount of revegetation that could occur, and reduce the amount of available wetland credit for the restoration area under the bridges.

WSDOT design engineers and the resource agencies collaborated on finding a new design that would satisfy CEA objectives and scour mitigation costs. The resulting compromise in design called for lowering the armament to just below ground level, thereby enabling revegetation and openness of the area. Bridge foundations will be accompanied by large rocks inserted underground, near the scour level at the toe of the bridge (Figure 3).

CREATING A HABITAT CONNECTION AT GOLD CREEK CEA–UPPER KEECHELUS LAKE, TREATING STORMWATER AND REDUCING WETLAND IMPACTS

The I-90 project corridor passes through the Wenatchee National Forest and runs adjacent to the northeastern shore of Keechelus Lake for the first 6 mi, then parallels the Yakima River for the remaining 9 mi. The project crosses five tributaries to Keechelus Lake and nine significant tributaries to the Yakima River, including the Kachess River. The project also crosses or is adjacent to numerous wetlands (*4*). Therefore, incorporating stormwater management systems into I-90 project is essential for minimizing contamination of terrestrial and aquatic habitats. Stormwater treatment facilities also present WSDOT with the opportunity to repair water quality problems caused by the existing highway. For example, in certain creeks located within the project area, water quality has been affected due in part to sediment (traction sand from both I-90 and the adjacent WSDOT maintenance facility sandpile) and the presence of metals (lead and arsenic) in stormwater runoff.

The selection, design, and mitigation process for this stormwater system is complex. Portions of the project are located on steep slopes (rock cliffs) where construction of stormwater best management practices (BMPs) would be very difficult and require extensive

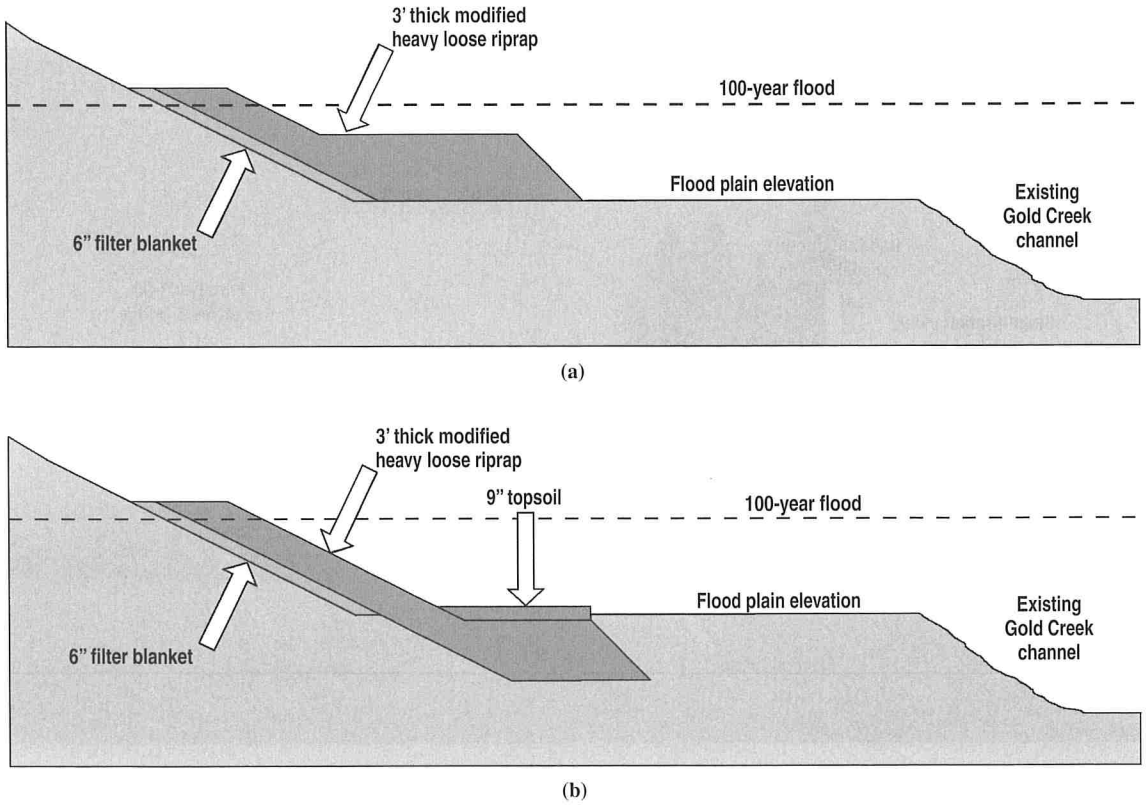

FIGURE 3 Original and modified designs for the Gold Creek Bridge foundations: (*a*) Option A and (*b*) preferred option.

structural support. Other typical freeway BMPs, such as infiltration swales and ditches, are infeasible because portions of the project are located in narrow corridors where cliffs are on one side of the freeway and a lake or river is on the other side, with no room for a median. And while not exactly a physical constraint, snow management and snow hydrology play a large role in how space is utilized and what BMPs are most suitable, with open areas in the median or adjacent to the freeway likely doubling as both snow storage areas as well as stormwater BMP locations (*4*).

To help identify issues and find the best solutions to solve stormwater treatment challenges, WSDOT created a multiagency Stormwater Technical Committee to review stormwater technical and permitting issues, evaluate mitigation approaches developed by WSDOT, and recommend appropriate, effective, and efficient mitigation methods to the design team. Committee members included WSDOT and consultants, USFS, and EPA staff who have permitting approval roles or are partner agencies with a strong interest in helping solve stormwater problems.

WSDOT and the stormwater committee conducted several in-depth studies and determined that a stormwater treatment and snow storage facility was needed near the Gold Creek CEA. The identified preferred location for the facility was at the WSDOT maintenance facility, just west of the Gold Creek CEA, where additional upland habitat was being created to enhance the effectiveness of a planned undercrossing. WSDOT engineers believed they could further enhance the Gold Creek CEA's effectiveness by reducing visibility and noise of the stormwater treatment facility and reducing noise from the maintenance facility by building a separation between the two areas.

Plans originally called for using a wide grassy swale to treat stormwater from the maintenance facility and building of a tall berm at the upland below the undercrossing to reduce light and noise. Engineers also planned for snow storage within the grassy swale.

As designs progressed, however, resource agencies expressed concerns over the footprint of the Keechelus Lake bench design and its impact on the wetland. But because so many transportation facility design objectives and ecological objectives needed to be met at this one location, all parties had to compromise on design. To reach compromises, several organized meetings were held among engineers, technical committees, and resource agencies. In the end, WSDOT compromised for less snow storage space and a more compact stormwater BMP with higher maintenance requirements. The resource agencies compromised by allowing minor wetland and footprint impacts through a shorter, vegetated berm and reduced upland area versus the previous taller bench design. WSDOT will add vegetation (tall trees) to the shorter and smaller berm design to make up the reduced structure height (Figure 4).

Further challenges arose when designing other stormwater treatment facilities for the I-90 project. Since the project corridor is constrained for most treatment options, media filter drains (MFDs) were selected and approved by Ecology as the most viable treatment option for use along the corridor. MFDs are linear flow-through stormwater treatment BMPs that can be placed along a highway shoulder for the treatment of sheet flow runoff generated from the highway pavement. MFDs remove suspended solids, phosphorus, and metals from highway runoff through physical straining, ion exchange, carbonate precipitation, and biofiltration.

MFDs as approved by Ecology, however, are not in line with USFS invasive species guidelines since they do not allow for vegetated plantings. Although WSDOT has engaged in a pilot program to test growing vegetation on MFDs elsewhere in the state, the pilot program is still underway and vegetated MFDs are still consid-

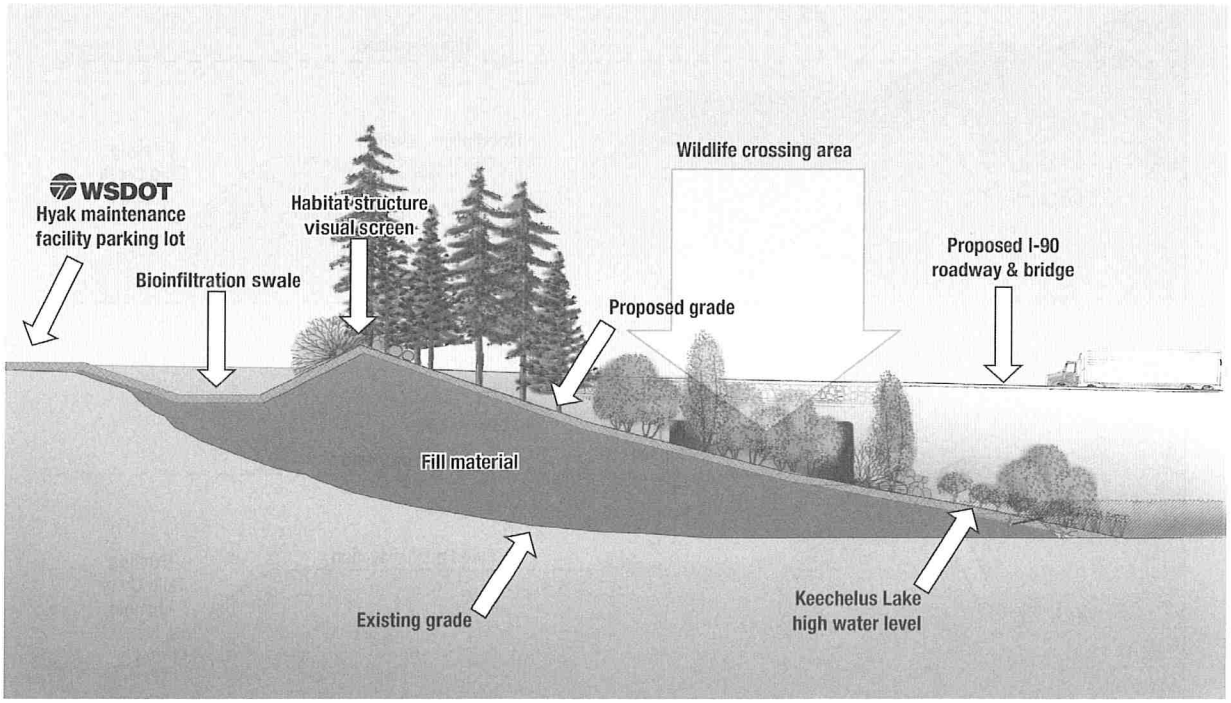

FIGURE 4 Near-shore habitat: conceptual plans for lowering the berm and vegetating it with tall trees to reduce noise and visibility of the stormwater treatment facility.

ered experimental. WSDOT sought and obtained approval for use of a vegetated MFD on Snoqualmie Pass in order to meet USFS objectives.

ELIMINATING SCOUR ISSUES AT WOLFE CREEK CEA WHILE ENHANCING WILDLIFE AND AQUATIC MOBILITY

The Wolfe Creek CEA is located between milepost 57.1 and milepost 57.3. The forest habitat adjacent to this CEA is the Western Hemlock Series, grading into the Pacific Silver Fir Series at higher elevations. The creek has a very steep gradient and provides limited fish habitat, although Pacific giant salamanders and tailed frogs are relatively common (*2*).

Currently, Wolfe Creek passes under I-90 in a 6-ft box culvert and empties into the east side of Keechelus Lake. The Mitigation Team recommended that WSDOT construct a 25-ft by 8-ft bottomless culvert westbound and a 20-ft by 10-ft bottomless culvert eastbound to meet the connectivity needs of wildlife and aquatic organisms, while passing flood flows and debris. This conceptual culvert would need to meet WDFW stream requirements for fish-bearing streams.

As engineering designs progressed at this CEA, hydrologic analysis identified scour issues from the high-velocity, steep gradient stream that could undermine the culverts' foundations and walls. WSDOT engineers considered using larger foundations for the bottomless culvert design, but the larger, deeper foundations were costlier and generated additional construction impacts to the creek banks and wetlands. Engineers also explored bridge options, versus a culvert, but foundation and cost issues proved formidable challenges.

Design engineers, working with WDFW, developed an alternative that included a four-sided box culvert with a stream-simulated bottom. The stream-simulated bottom, a standard WSDOT practice, was designed deep enough to hold 4 ft of stream simulation material and maintain the 8 ft of clearance needed to meet mitigation team recommendations. WSDOT presented this design option to resource agencies, and after thorough review, the agencies agreed that the four-sided box culvert design would provide a high level of protection for the roadway against scour and still meet the connectivity objectives of restoring capacity for flood and debris flow, providing fish passage for the full range of lake elevations and providing aquatic organism connectivity.

DESIGNING ROCKY RUN BRIDGES FOR CLEARANCE AND CONNECTING HABITAT

The Rocky Run Creek CEA is located between milepost 56.7 and milepost 56.9, with the creek originating above 4,800 ft elevation at Lake Lillian. The forest habitat adjacent to this CEA is the Western Hemlock Series, grading into the Pacific Silver Fir Series at higher elevations. The creek flows into the east side of Keechelus Lake and has a fairly steep gradient, although several fish species use this system.

The existing I-90 crossing over Rocky Run Creek is a 40-ft-long bridge eastbound and two 6-ft pipe culverts westbound. The Mitigation Team recommended that WSDOT improve connectivity in this area by building twin 120-ft bridges to meet the needs of wildlife and aquatic organisms, while passing flood flows and debris (*2*).

The challenge for WSDOT engineers was to design the mitigation team—recommended bridges to optimize clearance beneath the bridges for openness of habitat while keeping the footprint of the highway small to avoid impacts to Keechelus Lake. WSDOT engineers wanted to achieve clearance of at least 16 ft for each Rocky Run bridge to account for snow pack. Varying topography and road profiles between the separated eastbound and westbound lanes at Rocky Run Creek, however, would not allow engineers to achieve the clearance needed without further elevating the road profile and increasing the highway footprint. Elevating the profile, however, would not meet design standards for design speeds and also presented safety considerations. To elevate the road profile, engineers would have to create a large crest in the road, creating visibility issues and impacting other resources by enlarging the footprint.

WSDOT engineers decided to go back to the drawing board for the Rocky Run Creek bridge designs. Engineers first determined that the new I-90 road profile at Rocky Run Creek needed to be built at the same elevation for both eastbound and westbound lanes across the separated highway to minimize footprint. Engineers also determined that the only way to keep the consistent elevation levels across the bridges, while adding habitat benches under the bridges for connectivity purposes, was to compromise bridge clearance on the westbound structure. The resulting design called for a westbound bridge with reduced clearance and an eastbound bridge with greater clearance (Figure 5). The eastbound bridge was also lengthened to accommodate longer fill slopes and keep some habitat along the creek.

WSDOT engineers successfully overcame design challenges at Rocky Run Creek with new designs that achieved the connectivity objectives of providing moderate-level connectivity for high- and low-mobility species associated with the mountain hemlock–subalpine fir species assemblage zone, restoring capacity for flood and debris flow at the crossing structure, and providing fish passage for the full range of lake elevations.

After the best profile for the highway to meet clearance and footprint objectives at Rocky Run Creek was identified, archeological and cultural conflicts arose with a USFS service road. By elevating the highway profile to create clearance at the creek bridges, the USFS service road adjacent to I-90 would become lower than the adjacent interstate, resulting in possible embankment encroachment. WSDOT proposed to raise the profile of the USFS service road to remedy the problem, but this would require WSDOT to disturb an adjacent property containing old growth trees and a structure eligible for the National Historic Register and State Historic Preservation Office resources.

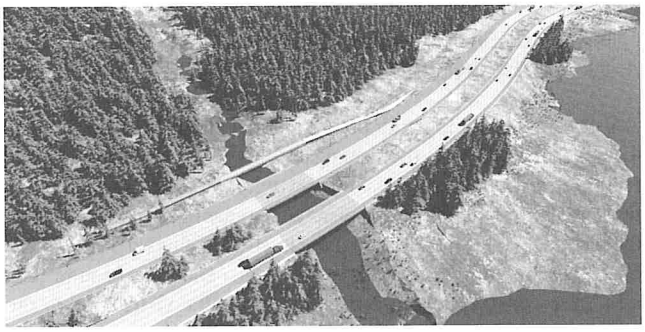

FIGURE 5 Rocky Run bridges: design visualization for Rocky Run CEA.

Because not many compromises were available to reduce the primary and secondary impacts of the situation, WSDOT engineers accepted that designing around this issue would require additional cost. WSDOT moved forward with plans to raise the profile of the USFS service road and reduce impacts to the historic property by adding a small system of precast concrete barrier to retain the existing slope. WSDOT also rerouted planned drainage systems in the area to lessen the impact near the historic site.

CONSTRUCTABILITY AND FLOODPLAIN ISSUES OF RESORT CREEK CEA

The Resort Creek CEA is located between milepost 59.3 and milepost 59.7. The forest habitat adjacent to this CEA is the Western Hemlock Series, grading into Pacific Silver Fir Series at higher elevations. Currently, Resort Creek flows under I-90 in a 6-ft pipe culvert that is a barrier to fish passage and drains into Keechelus Lake (2).

The mitigation team recommended that WSDOT install a series of bottomless culverts throughout the active channel-migration zone of Resort Creek. At least one of these culverts would have a minimum width of 30 ft and a minimum vertical clearance of 12 ft; the combined widths would span about 100 ft. These culverts would extend under both eastbound and westbound lanes, resulting in culvert lengths of about 150 ft. The series of culverts would allow the creek channel to shift location across the alluvial fan in response to sediment deposition and debris blockage. Culverts would be sized to meet WDFW stream simulation requirements for fish passage.

As WSDOT engineers advanced this design, uncertainty emerged about Resort Creek actually meandering across the alluvial fan. Additionally, the costs to install a temporary shoring system in order to construct the bottomless culverts and maintain traffic through the construction zone were exorbitant. WSDOT engineers reformulated designs by replacing the culverts with a 180-ft-long bridge that not only provided a large opening across the floodplain for natural creek function, but also created a better wildlife crossing structure for aquatic and terrestrial species.

WSDOT engineers presented this modified design to the IDT and Mitigation Team. The agencies agreed that this option achieved connectivity objectives (reducing wildlife–vehicle collisions, restoring capacity for flood and debris flow, providing fish passage, and restoring habitat and aquatic connectivity and channel migration) while meeting the additional objective of providing connectivity for large and small species.

MOVING DESIGN PLANS FORWARD AND PREPARING FOR CONSTRUCTION

After years of working with project partners and resource agencies to find viable solutions to competing objectives between transportation facility design and ecological connectivity, WSDOT engineers are finalizing the remaining design plans and preparing for construction of the second and third construction contracts. The funded 5-mi portion of the I-90 project from Hyak to Keechelus Dam has been broken into three construction contracts. Design and construction of the first construction contract (Phase 1A) are complete. Construction of Phase 1A began in July 2009 and was completed in November 2009. WSDOT built a long-term detour bridge at Gold Creek for use in the second construction contract of the project and mitigated for future lake storage impacts to Keechelus Lake—an irrigation reservoir—by excavating approximately 260,000 yd^3 of material from the lakebed. WSDOT has committed to a no-net-loss agreement with U.S. Bureau of Reclamation to not affect lake storage capacity during construction of the I-90 project.

WSDOT completed designs and permits for the second construction contract (Phase 1B) in fall 2009, with a November 2, 2009 contract advertisement date. This contract calls for replacing the deteriorated concrete pavement of the existing four lanes, adding a new lane in each direction, rebuilding bridges and culverts, stabilizing rock slopes, and extending chain up and off areas along the first 3 mi of the project. WSDOT expects to begin construction of Phase 1B in spring 2010.

Engineering designs and permitting actions are still underway for the third construction contract (Phase 1C) that will cover the remaining 2 project miles. Phase 1C calls for replacing deteriorated concrete pavement, adding a new lane in each direction, replacing the existing snowshed, addressing unstable slopes, and building new bridges. Phase 1C is expected to advertise to contractors in fall 2010, with construction scheduled to begin in spring 2011. All I-90 Hyak to Keechelus Dam Project improvements are scheduled for completion in 2015.

To move the remaining Phase 1 design plans forward, engineers are finishing geotechnical drilling on the rock cliffs and lakebed along the I-90 project corridor. Drilling core samples will help identify structural needs for the snowshed and the potentially unstable slopes along the corridor that will require stabilization measures as the rock cuts are excavated. WSDOT will stabilize slopes with grouted steel bars that are designed in accordance with the structural geology and height of each rock cut. WSDOT and a consultant team of geologists are also conducting geophysical studies using downhole surveys for bedrock mapping to identify terrain conditions and design the highway realignment.

Other work includes completing the structural designs for the remaining three CEAs, roadway drainage, and the new snowshed, which also includes mechanical system designs for illumination, ventilation, backup electrical generation, and intelligent transportation systems. Engineers are also finalizing construction schedules and other logistics for traffic control and staging.

Preconstruction wildlife monitoring activities continue to move forward as well. As part of the I-90 project wildlife monitoring plan, WSDOT and its partners are evaluating the locations and rate of wildlife–vehicle collisions; assessing the use and effectiveness of wildlife crossing structures, both existing and planned; characterizing the locations and rate of at-grade highway crossings by wildlife; estimating species occurrence and distribution in the project area; assessing the effectiveness of fencing; and appraising the effectiveness of jump-outs (5). Methods being used to meet preconstruction objectives include assessing wildlife use of existing culverts and underpasses via remote cameras, documenting crossing rates via snow tracking, evaluating the distribution of various target species via both noninvasive survey methods and live capture, and documenting wildlife–vehicle collisions. In addition, specific projects to monitor low-mobility species such as fish, amphibians, and pikas have been initiated.

Wildlife monitoring efforts will continue during and after construction of the I-90 project. The engineering team is working to ensure successful postconstruction monitoring efforts by integrating communication systems into the infrastructure of the highway. Engineers plan to install fiber optic communication cables at each CEA that will instantly transmit wildlife usage data, including images, to WSDOT for more efficient collection of information. Engineers

would also like to make the live feeds available for public viewing on the WSDOT website.

The engineering team continues to test various prototypes of wildlife exclusionary fencing to find a design that will withstand winter weather conditions and maintenance operations and redirect wildlife away from the interstate and to crossing structures. Several prototypes have been tested over the last two winter seasons; engineers are hopeful to finalize fencing plans this year.

CONTINUING COLLABORATION TO RESOLVE FUTURE ISSUES

Open and honest communication and the desire to establish and engage in partnerships early on are what inevitably allowed WSDOT to develop consensus for a long-term vision for the I-90 corridor. By sharing ideas and being adaptive in designs and receptive to compromises, WSDOT and its partners have designed a project that will not only improve the safety and reliability of a vital cross-state corridor, but will also promote the continued health of the delicate ecosystems of the Central Cascades for generations to come.

WSDOT will continue to collaborate with project partners, stakeholders, and resource agencies to overcome challenges as they arise during construction and in future designs. While the remaining 10 project miles from Keechelus Dam to Easton remain unfunded at this time, WSDOT, along with its project partners, stand ready to deliver.

REFERENCES

1. *I-90 Snoqualmie Pass East Project Final Environmental Impact Statement.* FHWA-WA-EIS-05-01-F. Washington State Department of Transportation, Aug. 2008, pp. 1-1, 1-8.
2. *Interstate 90 Snoqualmie Pass East Mitigation Development Team Recommendation Package.* Washington State Department of Transportation, July 2006, pp. ES-7, ES-8, ES-15-17, 1-4.
3. *I-90 Snoqualmie Pass East Project Draft Environmental Impact Statement.* FHWA-WA-EIS-05-01-D. Washington State Department of Transportation, June 2005, p. ES-1.
4. *Stormwater Treatment and BMP Report.* Washington State Department of Transportation and Otak, Inc., Aug. 2007, p. 1-2.
5. *I-90 Wildlife Monitoring Plan.* Washington State Department of Transportation and Western Transportation Institute, Feb. 2008, p. ix.

The Ecology and Transportation Committee peer-reviewed this paper.

California–Denmark Study on Acoustic Aging of Road Pavements

Hans Bendtsen, Erin Kohler, Qing Lu, and Bruce Rymer

Knowledge of acoustic aging of road pavements is needed by road administrators when developing policies and strategies for noise abatement. It is important to know how noise-reducing pavements, as well as pavements without such acoustic properties, perform over time. Methods such as the American traffic noise model method or the Nordic NORD2000 method use acoustic aging for accuracy in predicting noise. Noise performance models for road pavements are necessary if noise is to be integrated as an active parameter in pavement management systems. This paper contributes to ongoing international development in the field of acoustic aging by performing a comprehensive analysis of results from four Californian and Danish long-time noise measurement studies on asphalt pavements. There is not much information on which changes in the surface structure cause an increase in noise in the period between when the bitumen film is worn off and when the pavement begins to deteriorate with distresses such as raveling, cracking, and so forth. This study analyzes and compares trends in the development of noise over time. The development of the noise spectra is also analyzed. The increase of noise has normally been analyzed in relation to the age of pavements. The traffic load and an artificial indicator, defined as the change of noise predicted as a combination of actual physical age and traffic load, are investigated.

The purpose of this paper is to contribute to the ongoing international development in the field of acoustic aging of tire–pavement interactions by performing a comprehensive analysis of some Californian and Danish results from long-time noise measurement studies. The focus is on asphalt concrete pavements on highways. The paper is based on extracts of the results from the report "Acoustic Aging of Asphalt Pavements: A Californian/Danish Comparison" (*1*) with detailed documentation.

An international literature survey has been conducted by Bendtsen et al. (*1*). Noise level generally increases as pavement ages. For porous pavement (built-in air void content of more than 15%), it is a known phenomenon that air voids tend to clog in some facilities and that this increases the noise generated from air pumping. But for other dense and open-graded (but not really porous) pavement types, there is not much information on which changes in the surface structure cause this increase in noise in the period between when the bitumen film is worn off and when the pavement begins to deteriorate with distresses such as raveling, cracking, and so forth.

The most common measurement methods used today for detailed analyses of road traffic noise are the wayside statistical pass-by method (SPB) (*2*), the "close to source" methods such as the onboard sound intensity method (*3*), and the close proximity method (*4*). This project (*1*) focuses on the trend in noise levels measured in the same way—the relative changes of noise over the years—and not on the actual noise levels. Therefore, it is not crucial if noise results have been measured by different methods. These factors might influence the actual noise levels and can complicate direct comparison, but when only trends are compared, these differences are not important.

Two well-documented long-time noise measurement series from California and two from Denmark have been analyzed in this project (*1*). The results have already been documented in detail in separate national reports. The objective of the current report is to perform a comparison study of the trends for acoustic aging found in these four projects. In 2009 the University of California Pavement Research Center (UCPRC) finalized the third-year report on annual onboard sound intensity noise measurements on 65 to 76 pavement sections of different ages and mix types in California. Some results from this project are also included. The two Californian measurement series and the UCPRC study have all been carried out for the California Department of Transportation (Caltrans) and the two Danish measurement series have been carried out for the Danish Road Directorate. The following five measurement series are included:

1. Open-graded asphalt concrete (OGAC) on I-80 near Davis, California (10 years), one pavement type (*5*);
2. Five test sections with dense- and open-graded pavements on LA-138 in the Mojave Desert, California (5 years) (*6*);
3. Sixty-five to 76 pavements in the UCPRC/Caltrans monitoring project (3 years and pavements in different age groups and of different mix types) (*7*);
4. Three single-layer porous asphalt concrete (PAC), one dense-graded asphalt concrete (DGAC), and one OGAC pavements at Viskinge, Denmark (8 years) (*8*); and
5. Five thin OGAC and one DGAC pavements at M10 (Solrød) near Copenhagen, Denmark (5 years) (*9*).

The pavements included in this project were grouped in the following four main types:

1. DGAC;
2. OGAC, including open-graded rubberized pavements (RAC-O);
3. PAC; and
4. Thin asphalt layers (thin open) including different types of stone mastics asphalt pavements and an open-graded pavement, optimized for noise reduction.

H. Bendtsen, Danish Road Institute–Danish Road Directorate, Guldalderen 12, 2640 Hedehusene, Denmark. E. Kohler, Dynatest Consulting Inc., 165 South Chestnut Street, Ventura, CA 93001. Q. Lu, University of California Pavement Research Center, Davis and Berkeley, 1353 South 46th Street, Building 452, Richmond, CA 94804. B. Rymer, California Department of Transportation, Division of Environmental Analysis, 1120 North Street, Room 4301 MS27, Sacramento, CA 94274-0001. Corresponding author: H. Bendtsen, hbe@vd.dk.

Transportation Research Record: Journal of the Transportation Research Board, No. 2158, Transportation Research Board of the National Academies, Washington, D.C., 2010, pp. 122–128.
DOI: 10.3141/2158-15

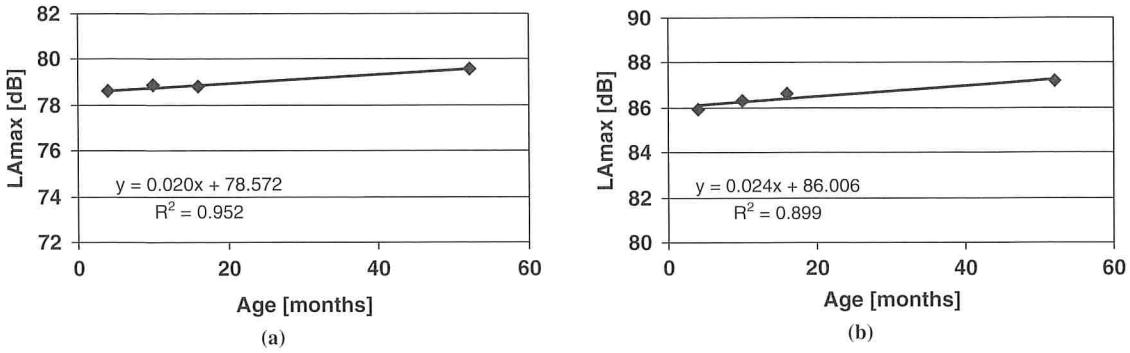

FIGURE 1 Maximum SPB noise level for (*a*) passenger cars [reference speed 96 km/h (60 mph)] and (*b*) multiaxle vehicles [reference speed 88 km/h (55 mph)] for the DGAC pavement (*1*, *6*).

RESULTS FROM A CALIFORNIAN TEST SECTION

This section presents some selected SPB results from the one of the Californian test sections carried out by Volpe Center for Acoustics. All the detailed results can be seen in Bendtsen et al. (*1*). Figures 1 and 2 show the results, including the frequency spectra from SPB noise measurements on a DGAC pavement.

Figure 1 shows the development of noise for the DGAC pavement at the LA-138 test section. The noise increase fits well with a linear regression with residual standard errors of 0.1 and 0.2 dB (see Table 1). The yearly increase was 0.24 dB for passenger cars and 0.29 dB for multiaxle vehicles. As shown in Figure 2, the increases take place in the whole range of the frequency spectrum.

Table 1 gives an overview of the noise trends for the four LA-138 pavements. For passenger cars, the dense-graded OGAC30 pavement has the lowest increases of 0.20 dB/year. For the other three more open-graded pavements, the increases vary between 0.24 and 0.40 dB/year. The increases for multiaxle vehicles are generally less than for passenger cars, with the DGAC pavement as an exception.

RESULTS FROM A DANISH TEST SECTION

This section presents some selected results from the one of the Danish test sections. All the detailed results can be seen in Bendtsen et al. (*1*). SPB noise measurements have been conducted over a period of 8 to 9 years (*8*). The results are reported as L_{AE} values and not L_{Amax}, which is now common for SPB measurements. There is a linear correlation between L_{AE} and L_{Amax} for SPB traffic noise measurements (*10*). One of the three porous pavements at the Viskinge test site is called PAC8 Type A. The development of noise can be seen in Figure 3. The yearly increase was 0.87 dB for passenger cars and 0.37 dB for multiaxle vehicles.

But in the 1st year a decrease of noise of 0.3 dB for passenger cars and 0.7 dB for multiaxle vehicles was observed. The frequency spectra for passenger cars in Figure 4 indicate what might be happening. This spectrum is significantly different from the spectra of the dense DGAC pavement. The noise decreased by 2 dB in the frequency range 800 to 1,000 Hz, which is important for the total A-weighted noise level. A new open porous pavement absorbs noise reflected on the pavement at frequencies typically below 1,000 Hz (engine noise) depending on the thickness of the porous layer. It seems like this absorption effect was improved over the 1st year. However, at the same time, the noise over 1,250 Hz increased, indicating an increase in the noise from air pumping. This might be caused by postcompaction of the pavement.

From the 1st to the 2nd year, the noise increased by 2 to 3 dB at frequencies above 1,000 Hz, indicating an increase in air pumping noise reflecting that the open pores of the pavement were beginning to clog. The noise also increased at 800 to 1,000 Hz, indicating that the noise absorption effect was reduced significantly. This is also an indication of clogging. In Year 7, heavy raveling was observed on this pavement. In this year there was a significant increase of around 2 to 3 dB of low-frequency noise below 1,600 Hz. This reflects that the pavement has become rougher because of the raveling. The trends

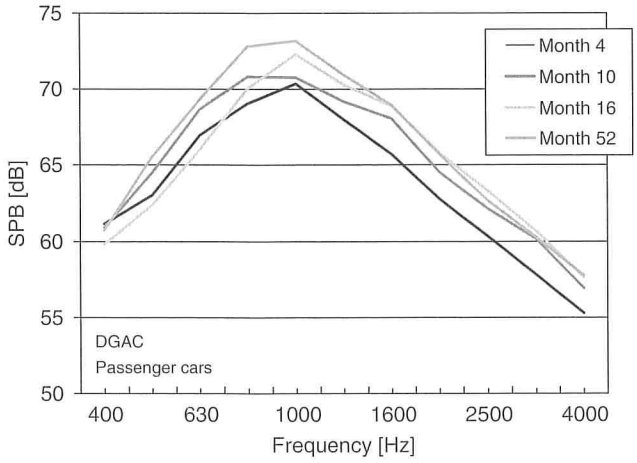

FIGURE 2 SPB noise spectra for passenger cars for DGAC pavement [reference speed 96 km/h (60 mph)] (*1*, *6*).

TABLE 1 Average Noise Increase per Year for Passenger Cars and Multiaxle Vehicles and Residual Standard Error for Four Test Pavements on LA-138 (*1*)

Pavement	Passenger Cars	Residual Standard Error Passenger	Multiaxle Vehicles	Residual Standard Error Multiaxle
DGAC	0.24 dB/year	0.1 dB	0.29 dB/year	0.2 dB
OGAC75	0.31 dB/year	0.3 dB	0.10 dB/year	0.2 dB
OGAC30	0.20 dB/year	0.2 dB	0.12 dB/year	0.2 dB
RAC-O	0.40 dB/year	0.3 dB	0.36 dB/year	0.2 dB

NOTE: Reference speed = 96 km/h (60 mph) for passenger cars and 88 km/h (55 mph) for multiaxle vehicles.

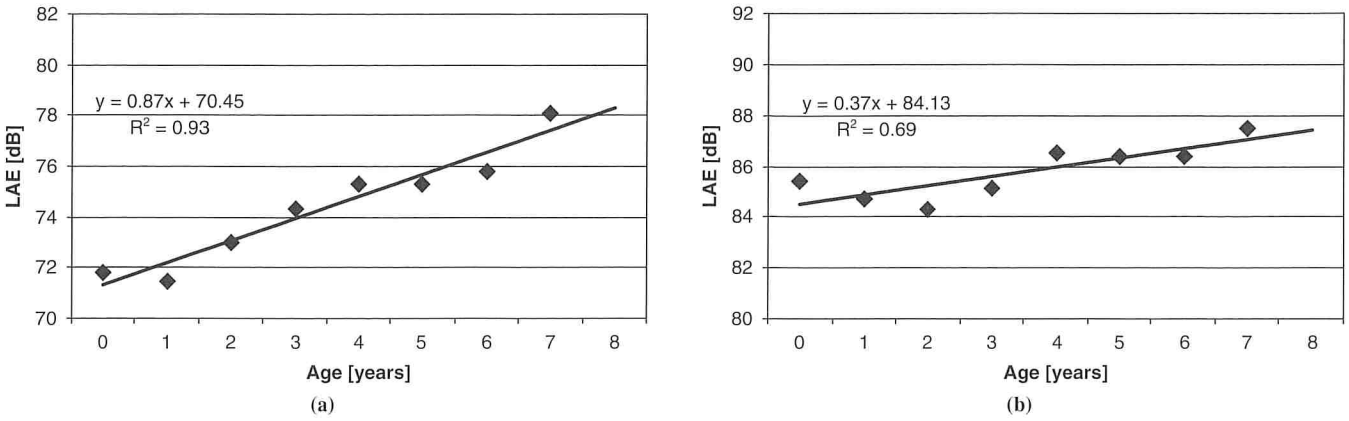

FIGURE 3 Noise level: (*a*) L_{AE} SPB noise level for passenger cars and (*b*) maximum SPB noise level for multiaxle vehicles for PAC8 Type A pavement [reference speed 80 km/h (50 mph)] (*1*, *8*).

of spectra for multiaxle vehicles are generally the same as for passenger cars. The noise increases around 2 dB in the frequencies below 1,600 Hz from Year 6 to Year 7 when raveling occurs.

Table 2 gives an overview of the noise trends on the five Viskinge pavements. For passenger cars, the dense-graded DGAC12 pavement had the lowest increases of 0.40 dB/year, followed by the open-graded OGAC12 pavement with 0.51 dB/year. For the three porous pavements, the increases were around twice as high with 0.81 and 0.87 dB/year. The increases for multiaxle vehicles were generally around 50% of the increase for passenger cars, with the PAC8 Type B pavement as an exception; here the trend for multiaxle vehicles was only a fourth of the trend for passenger cars.

The intention of the Viskinge experiment was to perform a "fast" life-cycle testing of porous pavements. For this reason the five pavements were deliberately built to break down faster than would normally be the case. Modifiers were not added to the bitumen. New Dutch results show that porous pavements built for long structural lifetime (with modified bitumen) can be constructed so they have a lifetime of around 11 years (*11*). The acoustic performance of the five pavements is "stretched" to a lifetime of 11 years by multiplying the yearly increases by 7/11. Table 3 shows the expected noise increases of new durable porous pavements with modified bitumen. The dense- and the open-graded asphalt concrete now for passenger cars gets a noise increase of 0.25 and 0.32 dB/year, respectively, and the porous pavements an increase of 0.52 to 0.55 dB/year. This stretching of the noise increases makes it possible to compare the results with the results from the other test sections included in this project (*1*) and will be used in the following analyses.

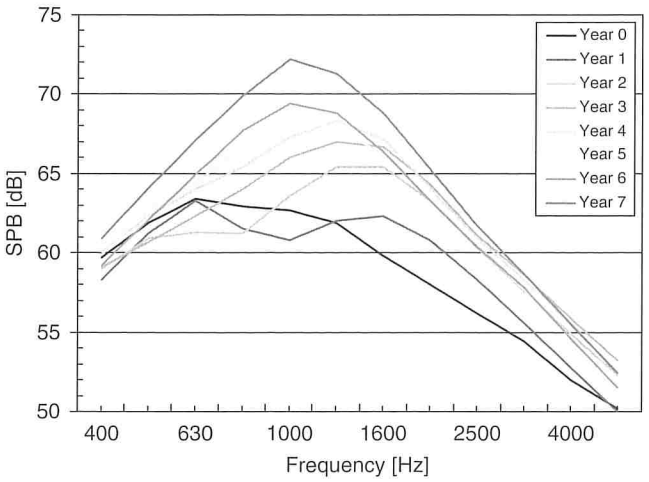

FIGURE 4 The SPB spectra for passenger cars at different ages for PAC8 Type A pavement [reference speed 80 km/h (50 mph)] (*1*, *8*).

ANALYSES

Different parameters have been used to describe the increase of noise. The increase of noise is often expressed as decibels per year. Two main factors are considered to affect the changes on the noise properties of a pavement. One relates to the physical and chemical changes in the materials caused by the weather elements, and the other has to do with the wear and tear caused by traffic. It can be argued that the combined effects of both the physical age of a pavement and the wear and tear from traffic are determining the increase of noise. The age reflects an accumulated effect of changing weather conditions such as sun radiation, rain, ice freeze and thaw, and so forth. In order to try to define an indicator that combines these two very different factors (age and traffic load), two artificial indicators called "mixed indicator" ($\Delta L_{Mix50/50}$ and $\Delta L_{Mix25/75}$) have been

TABLE 2 Average Noise Increase per Year for Passenger Cars and Multiaxle Vehicles and Residual Standard Error for Five Test Pavements as Measured at Viskinge (*1*)

Pavement	Passenger Cars	Residual Standard Error Passenger	Multiaxle Vehicles	Residual Standard Error Multiaxle
DGAC12	0.40 dB/year	0.3 dB	0.21 dB/year	0.5 dB
OGAC12	0.51 dB/year	0.3 dB	0.27 dB/year	0.2 dB
PAC8 Type A	0.87 dB/year	0.6 dB	0.37 dB/year	0.6 dB
PAC8 Type B	0.81 dB/year	0.8 dB	0.20 dB/year	0.9 dB
PAC12	0.83 dB/year	1.1 dB	0.44 dB/year	0.8 dB

NOTE: Reference speed 80 km/h (50 mph).

TABLE 3 Predicted Average Noise Increase per Year for Passenger Cars and Multiaxle Vehicles for Five Pavements Like the Viskinge Test Sections but Constructed for Long Structural Lifetime with Modified Bitumen, Assuming a Lifetime of 11 Years (*1*)

Pavement	Passenger Cars	Multiaxle Vehicles
DGAC12	0.25 dB/year	0.13 dB/year
OGAC12	0.32 dB/year	0.17 dB/year
PAC8 Type A	0.55 dB/year	0.24 dB/year
PAC8 Type B	0.52 dB/year	0.13 dB/year
PAC12	0.53 dB/year	0.28 dB/year

NOTE: Reference speed 80 km/h (50 mph).

defined (*1*). The noise increase has been analyzed for five different indicators:

1. ΔL_{age}. The change in noise per year (actual physical age of the pavement in decibels);
2. ΔL_{ADT}. The change in noise per 1 million vehicles (all types) passing per lane;
3. ΔL_{hvy}. The change in noise per 0.1 million heavy vehicles passing per lane;
4. $\Delta L_{mix50/50}$. An artificial indicator of the change in noise predicted as a combination of actual physical age and traffic load, where the age counts for 50% and the traffic load counts for 50%, called "mixed indicator 50/50"; and
5. $\Delta L_{mix25/75}$. An artificial indicator of the change in noise predicted as a combination of actual physical age and traffic load, where the age counts for 25% and the traffic load counts for 75%, called "mixed indicator 25/75."

The results for three of these indicators are shown in Figures 5 to 7.

Figure 5 shows an overview of the trends for noise increase per year for all the pavements included in the four test sites plus the California investigation. For passenger cars, the two Danish test roads (Viskinge and M10) generally have significantly higher yearly noise increases than the two Californian test roads (I-80 and LA-138). For multiaxle vehicles, the noise increases are not much different. Figure 6 shows the noise increase per 1 million vehicles (all types of vehicles) passing the test pavement. The noise increase per 1 million vehicles (ΔL_{ADT}) is calculated as follows:

$$\Delta L_{ADT} = \frac{\left(\Delta L_{age} \times 10^6\right)}{\left(ADT \times 365/N\right)} \quad (1)$$

where ADT equals the average daily traffic and N equals the number of lanes.

When traffic volume is taken into consideration instead of age, the ranking of the test sites changes significantly. The M10 sections with a high traffic load now have very low trends for noise increase, significantly lower than the LA-138 and Viskinge test sites.

It is believed by the authors that the porous pavements at Viskinge should have a higher noise increase than the thin open pavements at the M10 test site because of the tendency of these porous pavements to clog. This tendency to clog, is not seen on the open, but not porous, thin layers. Therefore, it was decided to try out a model where the

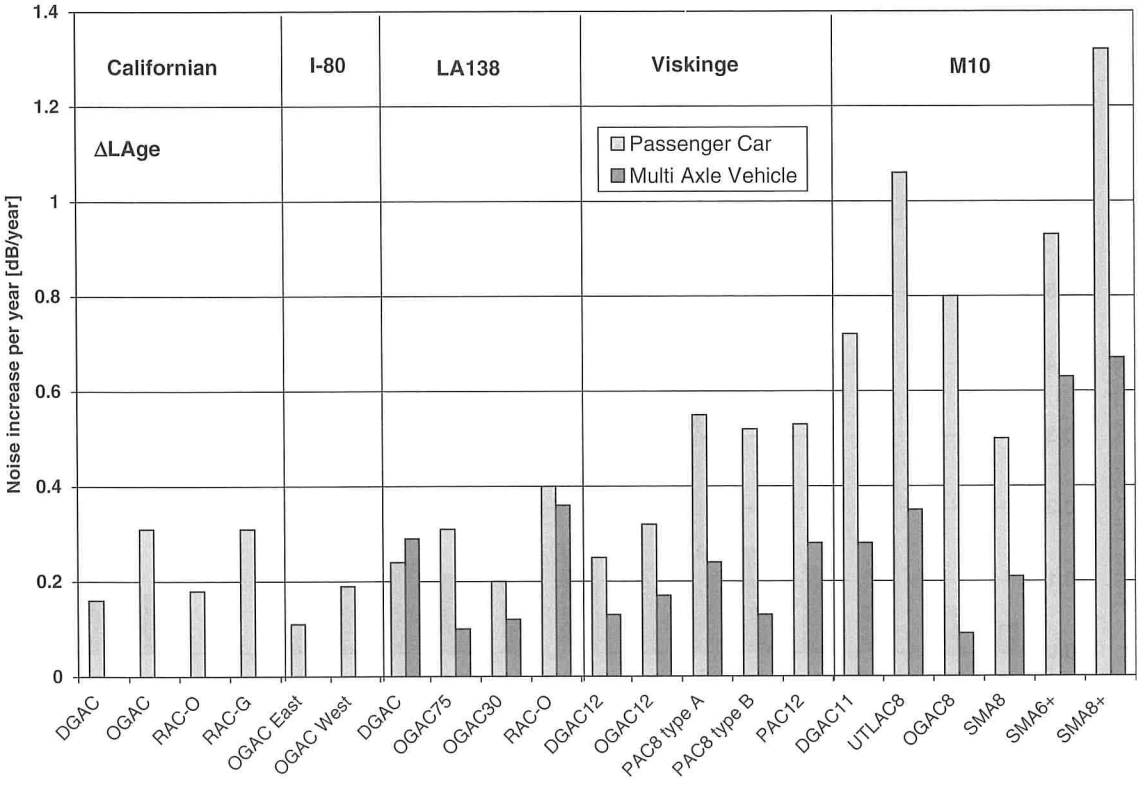

FIGURE 5 ΔL_{Age} noise increase per year of physical pavement age for all pavements in all four test sections for passenger cars and multiaxle vehicles (*1*).

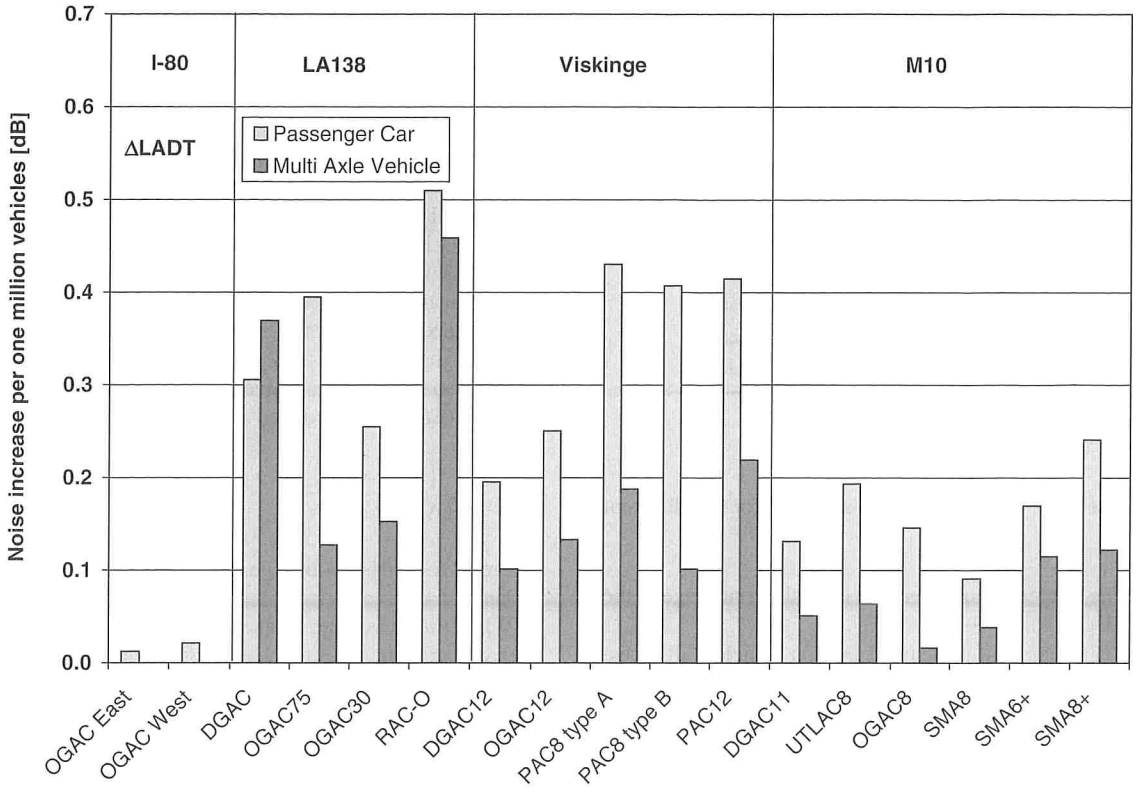

FIGURE 6 ΔL_{ADT} noise increase per 1 million vehicles passing actual lane for all pavements in all four test sections for passenger cars and multiaxle vehicles (*1*).

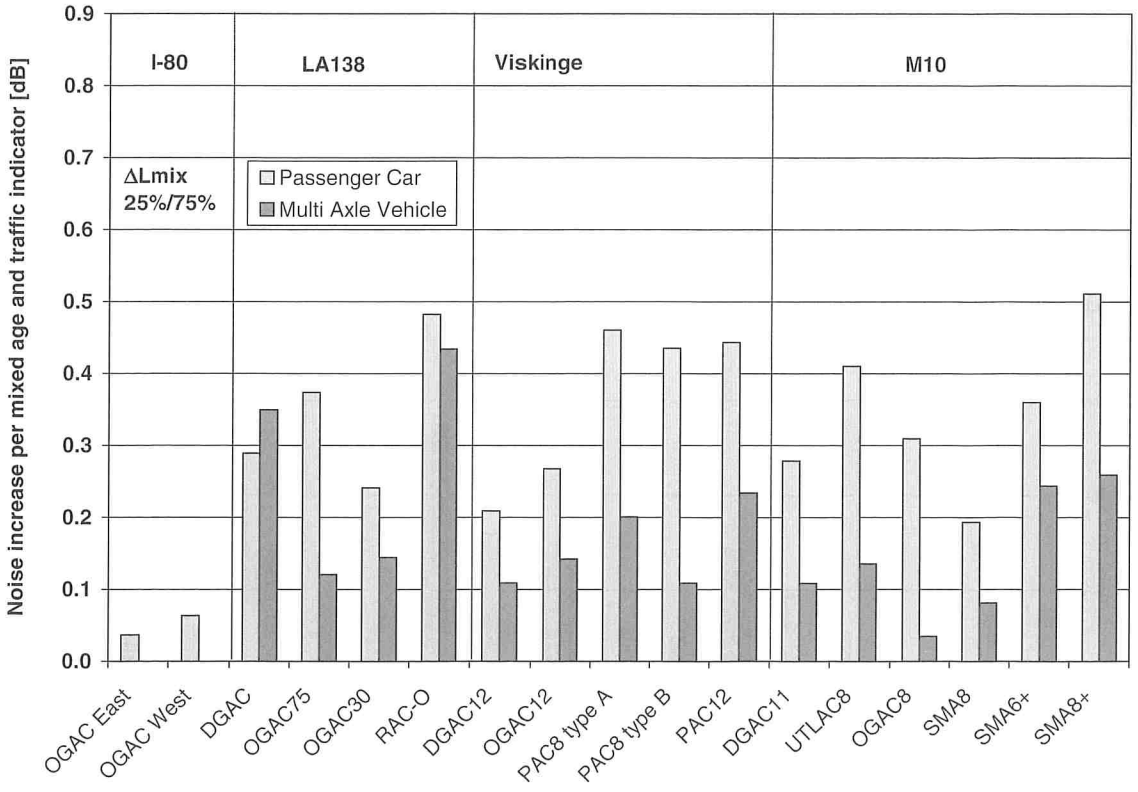

FIGURE 7 $\Delta L_{Mix25/75}$ noise increase per mixed indicator for change of noise predicted as combination of physical age and traffic load where age counts for 25% and traffic load counts for 75% (*1*).

TABLE 4 Average Noise Increase for Passenger Cars for Four Pavement Groups Expressed as Three Indicators: ΔL_{Age}, ΔL_{ADT}, and $\Delta L_{Mix25/75}$ (1)

Pavement Type	ΔL_{Age} [dB/year]	ΔL_{ADT} [dB/1 mil vehicles]	$\Delta L_{Mix25/75}$ [dB/mix]
All average	0.58	0.28	0.32
DGAC	0.40	0.21	0.26
OGAC	0.41	0.26	0.30
Thin open	0.84	0.24	0.39
PAC	0.53	0.42	0.45

NOTE: mil = million.

physical age counts for just 25%, and the traffic volume for 75%, of the noise increase. The $\Delta L_{Mix25/75}$ indicator is calculated as follows:

$$\Delta L_{mix25/75} = \Delta L_{age} \times 0.25 + \Delta L_{ADT} \times 0.75 \quad (2)$$

Figure 7 shows the mixed indicator $\Delta L_{mix25/75}$ for all 17 pavements. With $\Delta L_{mix25/75}$, the ranking of the LA-138, Viskinge, and M10 test sections is changed. The porous pavements at Viskinge now generally have a higher noise increase than the thin layers at M10.

In Tables 4 and 5 the average results for each pavement group are predicted and compared. The average noise increase per year for passenger cars (ΔL_{age}) is 0.58 dB. The DGAC pavements have the lowest increase, 0.40 dB/year, followed by OGAC with 0.41 dB/year. The two pavement types with the highest increases are the PAC and the thin open pavements, with 0.53 and 0.84 dB/year, respectively.

When the traffic volume (ΔL_{ADT}) instead of ΔL_{age} is used as an indicator for noise increase, the ranking of the pavement types changes significantly. The average $\Delta L_{mix25/75}$ for passenger cars is 0.32 dB. The $\Delta L_{mix25/75}$ indicator ranks the four pavement types in the following way. DGAC has the lowest increase of 0.26 dB, followed by OGAC with 0.30 dB and thin open pavements with an increase of 0.39 dB. The porous pavements have the highest increase of 0.45 dB using the $\Delta L_{mix25/75}$ indicator.

CONCLUSIONS AND RECOMMENDATIONS

The following conclusions and recommendations for highways are indicated:

- The noise level on asphalt pavements normally increases with time.
- The increases occur continuously and before significant pavement deterioration with raveling and cracking begins.

TABLE 5 Average Noise Increase for Multiaxle Heavy Vehicles for Four Pavement Groups Expressed as Three Indicators: ΔL_{Age}, ΔL_{ADT}, and $\Delta L_{Mix25/75}$ (1)

Pavement Type	ΔL_{Age} [dB/year]	ΔL_{ADT} [dB/1 mil vehicles]	$\Delta L_{Mix25/75}$ [dB/mix]
All average	0.27	0.15	0.18
DGAC	0.23	0.17	0.19
OGAC	0.12	0.11	0.11
Thin open	0.44	0.16	0.23
PAC	0.22	0.17	0.18

- There are exceptions where the noise is reduced over the first year of porous pavement lifetime.
- A linear regression gives a good fit. This was also seen in the European SILENCE study (*11*).
- The yearly noise increase is generally around two times higher for passenger cars than for heavy vehicles.
- There is a need for further research to determine which changes in the pavement surface structure cause the noise increase. Detailed analyses of pavement structure and noise spectra might be beneficial.
- More long-time measurement series are needed.
- It is important to follow existing experimental road pavement test sections.

Spectral analyses have been performed (*1*). The following very general tendencies are observed for the four pavement types:

- For DGAC, the higher-frequency air pumping noise increases in the first years, indicating that the pavement surface becomes denser (after compaction). After some years there is also an increase in the lower frequencies below 1,600 Hz, indicating that the pavement surface becomes rougher with an increase in the tire vibration noise.
- For OGAC, the tendencies for the different pavements included in the investigation are not very clear. For some of the pavements, there is a tendency that the higher-frequency air pumping noise increases in the first years, indicating that the pavement surface becomes denser (after compaction), and after some years there is also an increase in the lower frequencies below 1,600 Hz, indicating that the pavement surface becomes rougher with an increase in the tire vibration noise. But for some of the pavement, the increase at the lower frequencies happened before the increase at the higher frequencies.
- For the thin open pavements, the noise increases at the same time both at the lower and at the higher frequencies. This indicates that the pavement surface becomes rougher with an increase in the tire vibration noise and that the pavement surface becomes denser, causing increased higher-frequency air pumping noise.
- For PAC, the engine noise absorption effect at frequencies between 400 and 1,000 Hz is significantly reduced in the first 2 years. In the second year, clogging begins, and this increases the higher-frequency noise over 1,000 Hz because of increased generation of air pumping noise. As the porous pavements age, there is an increase in the low-frequency noise (under 1,600 Hz), indicating increased tire vibration noise caused by a rougher pavement surface structure.
- When heavy raveling occurs, tire vibration-generated low-frequency noise less than 1,600 Hz increases for all pavement types.

ACKNOWLEDGMENTS

This paper is based on a project carried out under the framework of the research technical agreement titled "Supplementary Studies for the Caltrans Quieter Pavement Research Program" between Caltrans and UCPRC as a part of the task set out in *Policy Documents: Guidelines for Caltrans Policy*. The Danish Road Institute/Road Directorate (DRI-DK) was subcontracted by UCPRC to work along with Dynatest on the project. The authors thank everyone involved in the long-time noise measurement series included in this project. Without their substantial work, it would not have been possible to accomplish this study.

REFERENCES

1. Bendtsen, H., Q. Lu, and E. Kohler. *Acoustic Aging of Asphalt Pavements: A Californian/Danish Comparison.* Report 171. Road Directorate/Danish Road Institute, 2009. http://www.roadinstitute.dk.
2. International Organization for Standardization. *Acoustics—Measurement of the Influence of Road Surfaces on Traffic Noise. Part 1: Statistical Pass-by Method.* ISO 11819-1: 1997, 1997.
3. Illingworth & Rodkin, Inc. *Further Development of the Sound Intensity Method of Measuring Tire Noise Performance of In Situ Pavements.* Report prepared for California Department of Transportation, Sacramento, Jan. 4, 2006. http://www.i80.dot.ca.gov/hq/env/noise/pub/2_Probe_SI_Report_04Jan06.pdf.
4. International Organization for Standardization. *Acoustics—Measurement of the Influence of Road Surfaces on Traffic Noise. Part 2: The Close-Proximity Method.* ISO/CD 11819-2: 2000, 2000.
5. Illingworth & Rodkin, Inc. *I-80 Davis OGAC Pavement Noise Study. Traffic Noise Levels Associated with Aging Open Graded Asphalt Concrete Overlay.* Report prepared for California Department of Transportation, Division of Environmental Analysis, Dec. 15, 2008.
6. *Caltrans Thin Lift Study: Effects of Asphalt Pavements on Wayside Noise.* U.S. Department of Transportation, Volpe National Transportation Systems Center, Environmental Measurement and Modeling for California Department of Transportation, Division of Environmental Analysis, Feb. 2009.
7. Lu, Q., E. Kohler, and J. Harvey. *Investigation of Noise and Durability Performance Trends for Asphaltic Pavement Surface Types: Three-Year Results.* Report prepared for California Department of Transportation, Division of Research and Innovation, Office of Roadway Research, 2009.
8. Bendtsen, H. Drainage Asphalt and Noise Reduction Over a Long Period. *Proc., Euronoise Conference,* Vol. 1, Munich, Germany, 1998.
9. Bendtsen, H., and E. Nielsen. *DRI-DWW Thin Layer Project: Final Report.* DRI Report 159, Danish Road Directorate/Road Institute, 2008. http://www.roadinstitute.dk.
10. Andersen, B. *Noise Emission from Vehicles on the Road Network* (in Danish with summary in English). Danish Transport Research Institute (DTU Transport), Rapport 2, 2003. http://www.transport.dtu.
11. Kragh, J. *Ageing of Porous Pavements: Acoustical Effects.* Technical Note 56, Danish Road Institute/Road Directorate, 2007. http://www.roadinstitute.dk.

The Transportation-Related Noise and Vibration Committee peer-reviewed this paper.

Acoustic Radiation from Pavement Joint Grooves Between Concrete Slabs

Paul R. Donavan

Sound generation and radiation from grooves in the joints between concrete slabs were modeled using relationships previously established for tire groove resonances and groove air pumping. Resonant behavior was clearly established from both in-lab and on-road onboard sound pressure level data. The strength of the noise source was found to be proportional to 20 times the logarithm of the groove cross-sectional area. This relationship, along with the accounting of residual texture background noise, was found to replicate that measured in laboratory testing. The model was then calibrated with the laboratory results and extended in speed range with a theoretical calculation of the sound radiation from the end of the joint groove. The predicted level produced by an isolated joint of specified dimension was then used to model the average sound intensity level for a pavement with a user-specified distance between joints, vehicle speed, and pavement texture-generated noise level. For smaller groove cross-sectional areas (~0.25 in.^{2}), the contribution of joint grooves was on the order of 1 dB for quieter pavement textures. For larger cross-sectional areas, such as a groove width of ½ in. and depth of 1 in., the contribution increased to almost 3 dB.

Impulsive noise associated with the passage of the tires over the joints in portland cement concrete (PCC) pavement has been reported by researchers and in recent literature (*1*). Examples of the impulses are shown in Figure 1 for two different PCC highway surfaces in California, an older longitudinally textured pavement (I-80) and new longitudinally broomed textured pavement (Mojave SR-58). In this figure, the impulses, beginning at about 0.004 s, are clearly higher than the residual sound pressure occurring after 0.010 s due to the pavement texture only. Depending somewhat on the pavement, the impulse persists for about 0.005 s and, particularly for the I-80 example, the time histories display "ringing" or oscillatory resonant behavior that decays with time. The ringing occurs with about the same repetition rate (0.001 s) for both cases, at least through the first three oscillations. Also, in both cases, the initial pressure rise is slightly less in absolute amplitude than the second peak as well as the negative peak in the impulse. Another indication of a resonant phenomenon is the observation that the period of oscillation is not affected by vehicle speed, as shown in Figure 2 for the broom texture surface.

The American Concrete Paving Association recently sponsored research at Purdue University to study the generation of noise by PCC joints (*2*). This work utilized the tire–pavement test apparatus (TPTA) to measure the effect of different joint parameters in carefully controlled laboratory conditions. The effects of joint width and joint depth were evaluated along with the effect of pavement slab offset. A typical time trace for passage over a joint is provided in Figure 3 for a case in which no slab offset is present and the groove is ⅜ in. (9.5 mm) wide and 1 in. (25.4 mm) deep for a test speed of 30 mph (48 km/h). A comparison of this trace to that in Figure 1 reveals several similarities. As in the previous case, the trace of Figure 3 indicates an oscillatory behavior with approximately the same repetition rate of 0.001 s. The TPTA case also decays with time and the initial positive pressure rise is slightly less than the negative peak or second positive peak. The higher levels associated with the event, however, last about twice as long as they do for the 60 mph (97 km/h) case of Figure 1, about 0.01 s at 30 mph versus 0.005 s at 60 mph. Given a tire footprint length of about 5.3 in. (135 mm), these times correspond approximately to the time duration that the tire is actually covering the joint.

In this paper, a model of sound generation caused by the passage of a tire over a PCC joint is developed and some the indicated trends are presented. In doing this, the results from the Purdue University study are used to validate the theoretical trends documented and to calibrate the model for noise prediction. This work also draws on research work that was completed at the General Motors Research Laboratories in the late 1970s and early 1980s that considered sound generation and radiation from grooves in tires (*3, 4*).

MODEL DEVELOPMENT

The physics of the model is illustrated in Figure 4. Simply stated, the tire rolls over the joint squeezing air out of the channel and forms an "organ pipe" open at two ends. The sound radiation is produced by the initial pumping of air out of the groove and is maintained by organ pipe resonances that persist until the tire lifts off of the joint. The corresponding mechanisms for grooves in tires operating on uniform pavement have been documented for both longitudinal (circumferential) (*4*) and lateral (*3*) grooves. Model development involves three steps: accounting for the groove resonances, determining the source strength of air displacement, and calibrating the model.

Groove Resonance

With regard to sound radiation and resonate behavior, the circumferentially ribbed tire (Figure 5) is directly analogous to the PCC joint problem (*4*). In both cases, the organ pipes formed are open on

Illingworth & Rodkin, Inc., 505 Petaluma Boulevard South, Petaluma, CA 94952. pdonavan@illingworthrodkin.com.

Transportation Research Record: Journal of the Transportation Research Board, No. 2158, Transportation Research Board of the National Academies, Washington, D.C., 2010, pp. 129–137.
DOI: 10.3141/2158-16

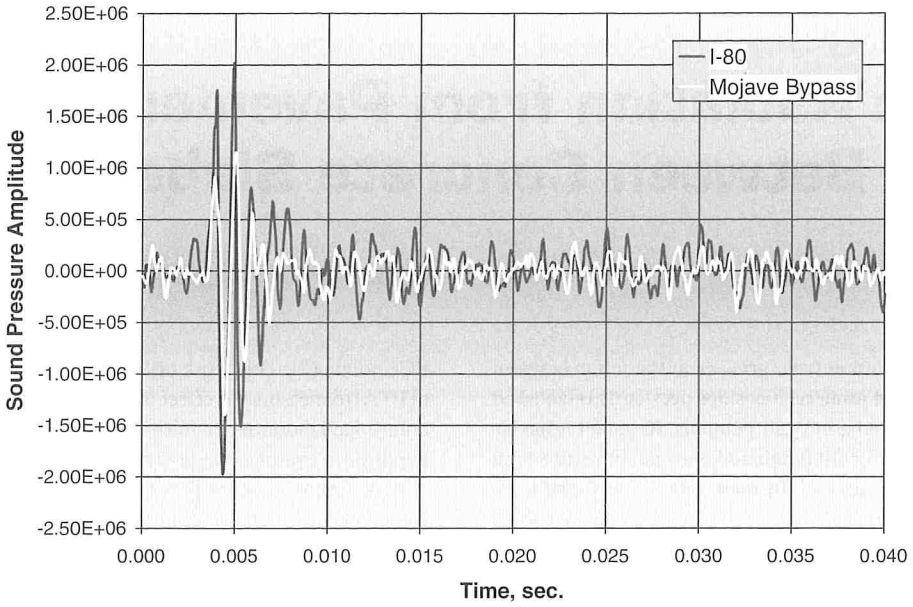

FIGURE 1 Joint slap for two different California PCC pavements: sound pressure versus time.

both ends. When the cross-sectional dimensions of the pipe are small compared to an acoustic wavelength, the resonances or standing waves in the pipes occur at specific frequencies defined by

$$f_n = \frac{(n * c)}{(2 * L)} \qquad n = 1, 2, 3, \ldots \tag{1}$$

where

f_n = frequency of the nth mode,
L = length of the organ pipe, and
c = speed of sound.

For an ideal pipe, the sound pressure at the ends of the pipe is zero and, for the first mode, a maximum in pressure occurs in the middle of the pipe. For higher modes, pressure alternates from being at a maximum at the center pipe to being zero at the center. In the ideal case, the acoustic particle velocity is exactly 90° out of phase with the pressure producing maximum levels at the exits to the pipe. In real cases, such as for tire–pavement noise, the terminations of the pipe are not ideal and not well defined. For the case of circumferential straight ribs, an effective pipe length is given by

$$L_{\text{eff}} \approx L + 2 * \left(0.6 * \left[\left(\frac{s}{\pi} \right)^{1/2} \right] \right) \tag{2}$$

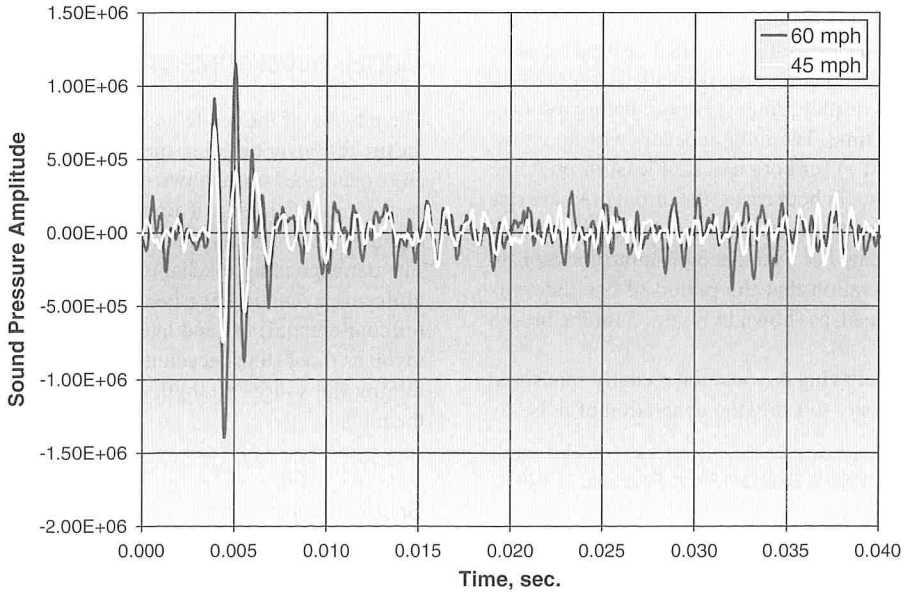

FIGURE 2 Joint slap for Mojave Bypass pavement at 60 and 45 mph.

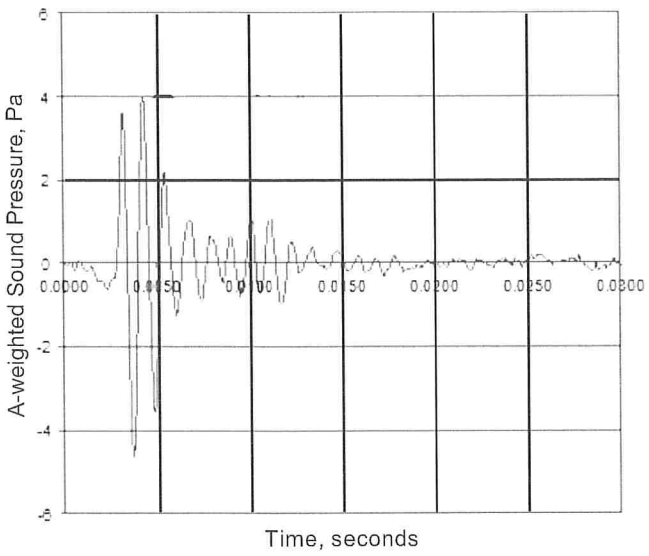

FIGURE 3 Joint slap recorded on the Purdue TPTA at 30 mph (2).

where L_{eff} is the effective pipe length and s is the cross-sectional area of the pipe. This effective pipe length has been found to provide reasonable agreement with experimental results and the behavior has been shown to vanish when the grooves are filled with lightweight foam (Figure 6) (4). For the two tires used in the Purdue study (P205/70R15 Uniroyal Tiger Paw and Goodyear Aquatred 3), the width of the contact patch is approximately 5.5 in. and 6.1 in. (140 and 155 mm), respectively. For the Aquatred, this leads to an effective length of 0.166 m. As a result, the frequencies of the first four modes are f_1 = 1,039 Hz, f_2 = 2,078 Hz, f_3 = 3,117 Hz, and f_4 = 4,156 Hz. It will be noted from the expression for f_n that when the cross-sectional area of the pipe (or groove) is small compared with the length L, as in this case, the resonant frequency is determined only by the width of the tire contact patch. As a result, only small differences in the resonant frequencies would occur for changes in the width and depth of the groove. This implies that for a given tire, the resonant frequencies would be essentially the same independent of the joint geometry. This is partially confirmed by the time traces of Figures 1 and 3, which correspond to joint widths of approximately ⅛, ⅜, and ½ in. for the I-80, Purdue, and Mojave joints, respectively.

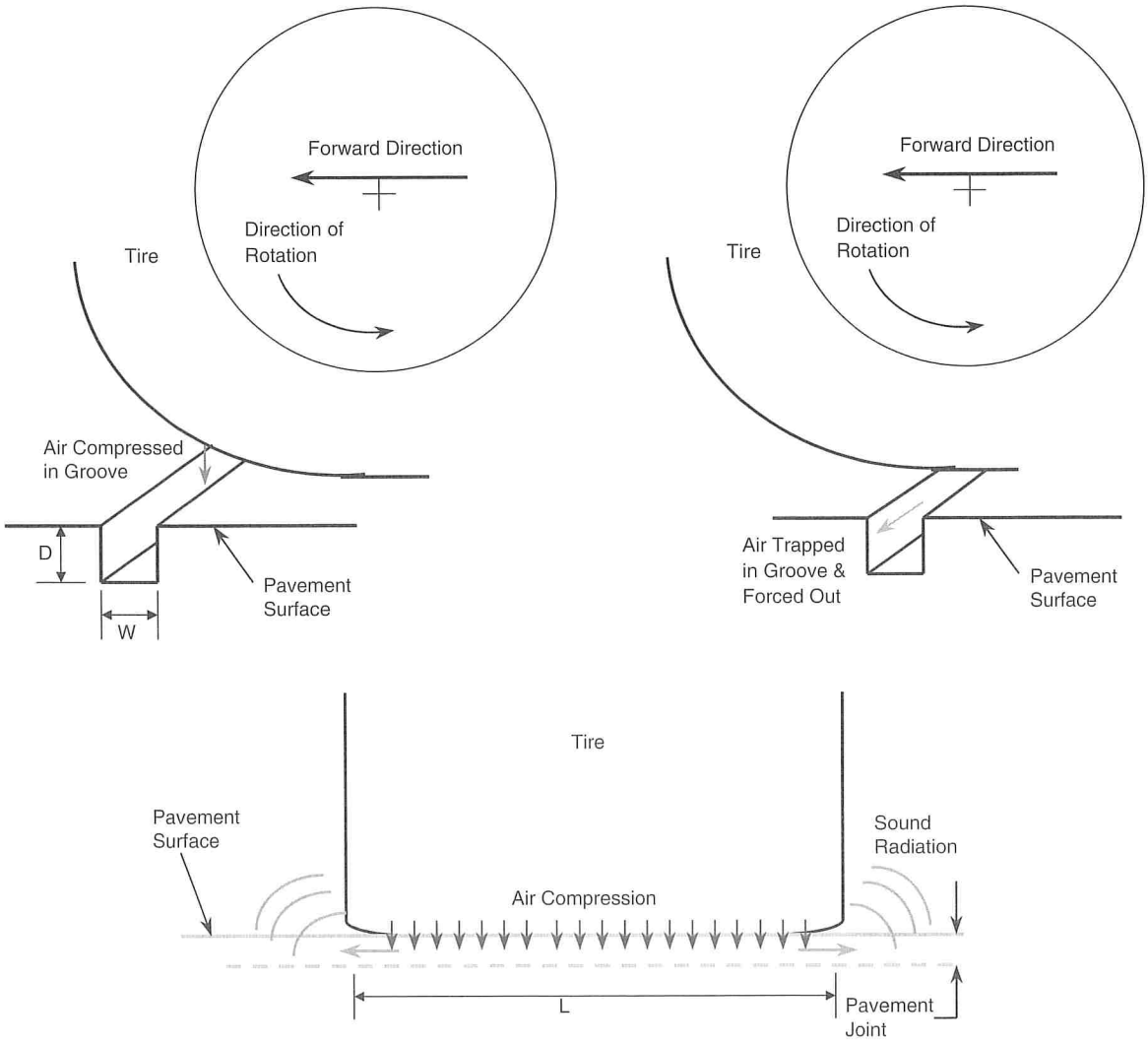

FIGURE 4 Illustration of envelopment of pavement groove, related geometry, and noise mechanism from side and through cross section.

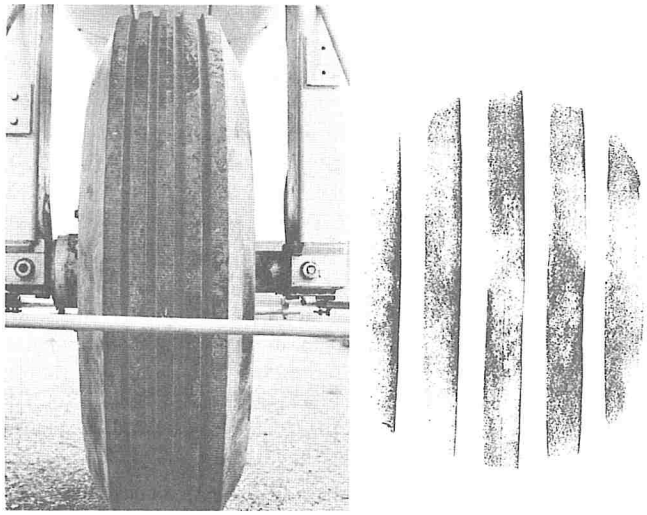

FIGURE 5 Photograph and contact patch of straight-ribbed HCR truck tire (*4*).

In the Purdue investigations, it was also noted that the shape of the frequency spectra did not shift with joint dimension or tire passage velocity (*5*).

A comparison of the sound generation and radiation between circumferential rib tire and transverse joint in the PCC pavement shows that some differences do exist in the source of the excitation of the "organ pipes." For the rib tire, the relative flow through the tube due to the rolling tire does not produce acoustic excitation because the process is continuous. For this tire, the excitation is supplied by vibration of the tire tread forming three of the sidewalls of the tube. This vibration is induced by pavement roughness and, to a lesser degree, by shear stresses produced in the rolling tire (*6*). For the pavement joint, the initial excitation is created by abrupt volume change as the tire seals against the pavement groove. This excitation process is analogous to that produced by a transverse groove in a tire, typically called tread pattern "air pumping" (*3*).

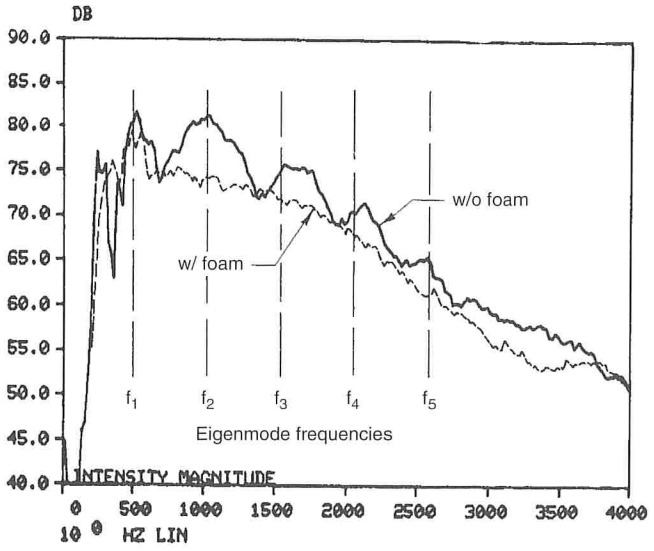

FIGURE 6 Influence of groove resonance for straight-ribbed tire sound intensity level with and without foam in ribs.

Although the excitation mechanism is similar between the transverse joint and the transverse tread element, the resonance characteristic is different because the tread element pipe is closed on one end and open on the other. This has the effect of eliminating the even number modes from Equation 1. The boundary condition is that at the closed end of the tube the acoustic velocity must be zero and pressure must be at a maximum. When this condition is applied to the pressure mode shapes for tread groove, only the first and third modes meet this requirement for closed tube equal in length to $L/2$ (i.e., maximum pressure at center of length L). When source strength is analyzed by forcing air out of the groove, the source strength of the closed-end tube of length $L/2$ is identical to that of the open tube of length L because of symmetry.

Source Strength Analysis

The driving force for the source strength of both the tire and pavement groove is the change in volume as the air is expelled from the groove. This change in volume results in air motion at the open end of the tube, which in turn results in an acoustic pressure pulse. The pressure at some distance r alongside the tire can be expressed as (*3*)

$$p(r,t)=\left(\frac{1}{r\pi}\right)*\rho*D*W*\left(\frac{dv_L}{dt}\right) \tag{3}$$

where

ρ = density of air,
D and W = depth and width as defined in Figure 4, and
v_L = acoustic velocity at the end of the tube.

For the groove, the variables of importance are the groove dimensions D and W and the rate of change of the velocity at the end of the tube. For fixed dv_L/dt, the pressure is directly proportional to the cross-sectional area of the groove. By using this expression, the relative effect of the increasing groove width and depth can readily be determined as

$$\text{SPL} \propto 20*\text{Log}\left[p(r,t)\right] \propto 20*\text{Log}(D*W) \tag{4}$$

where SPL is the relative sound pressure level. With this relationship, relative SPL as a function of either groove width or depth can be plotted for different values of each. With this simple expression and the addition of a background noise corresponding to that of the TPTA, the results from the Purdue study were approximately matched. In the TPTA results, the increase in level for a ¼-in.-wide, 1-in.-deep groove to a 1-in.-wide groove was on average 8.4 dB with a standard deviation of 1.5 dB (*2*). The modeled result using Equation 4 with the TPTA texture background noise of 91 dB(A) was 8.9 dB.

The other feature of Equation 3 is the dependence on the air velocity time derivative at the exit of the groove. This velocity is directly related to the rate of change of air volume in the groove. This rate of change is also a function of how rapidly the tire envelops the groove. The transfer function that relates volume change to v_L is also dependent on frequency corresponding to the modes of the groove. To examine this transfer function, the instantaneous air volume ($q[t]$) in the initial open groove is considered. The rate of change of this quantity then has a relationship to the rate of change of the air particle velocity at the open end of the tube. This relationship can be expressed in the frequency domain through the Fourier transform, $Q(\omega)=\Im[q(t)]$, where ω is the angular frequency, $\omega=2\pi f$.

Similarly, the particle velocity at L is given as $V_L(\omega) = \Im[v_L(t)]$. These two quantities are related to each other through a complex transfer function, $T_1(\omega)$:

$$V_L(\omega) = T_1(\omega) * Q(\omega) \tag{5}$$

It can be shown that the expression for $T_1(\omega)$ is given by

$$T_1(\omega) = c^2 * \left(\frac{2}{L}\right) * \sum_j \frac{1}{\left(\omega_j^2 - \omega^2\right)} + i\omega * \left(2\delta_j * \omega_j\right)$$

$$j = 1, 2, 3, \ldots \text{ to } \infty \tag{6}$$

(2) with ω_j given by Equation 1, i indicating an imaginary number ($I = \sqrt{} - 1$) and

$$\delta_j = \left(\frac{R}{2} * \rho * \omega_j\right) \tag{7}$$

where R is the flow resistance taken as 366 Ns/m^4 for air in the tube. With the effective tube length defined by the tire contact patch width, the magnitude of the transfer function $T_1(\omega)$ is provided in Figure 7. From this figure, it is shown that the modal structure cited in regard to Equations 1 and 2 is retained.

The sound pressure at r alongside the tire as defined by Equation 3 can also be expressed as its Fourier transform, $P(r, \omega)$. This sound pressure is then related to the air velocity at the end of the tube by

$$P(r, \omega) = V_L(\omega) * T_2(\omega) = T_1(\omega) * Q(\omega) * T_2(\omega) \tag{8}$$

where the transfer function between the acoustic velocity and pressure is given by

$$T_2(\omega) = i\omega * \rho * D * W * \left(\frac{1}{\pi r}\right) * e^{-ir*\omega/2} \tag{9}$$

The magnitude of this transfer function is also plotted in Figure 7 and is seen to increase monotonically with frequency.

With $T_1(\omega)$ and $T_2(\omega)$ defined, the sound pressure can be solved if $Q(\omega)$ is known. Following the case of the transverse groove, the shape of the volume change pulse for the groove in the pavement application is taken to be of the form

$$q(t) = \left(\frac{\Delta V}{V}\right) * \frac{1}{2} * \left[1 - \cos\left(2 * \pi * \frac{t}{T}\right)\right] \qquad \text{for } T \geq t \geq 0$$

$$q(t) = 0 \qquad \text{for all other } t \tag{10}$$

where

V = volume of the groove,
ΔV = change in volume, and
T = duration of the volume change.

The shape of this function is plotted in Figure 8 starting at time $t = 0$. The full duration of this plot shows the amount of time (0.005 s) that the tire contact patch remains over the groove at 60 mph for the Aquatred tire. For comparison, the volume velocity corresponding to 30 mph is also shown in Figure 8. In this case, the maximum amplitude is reduced by half so the total volume displacement remains equal between the two speeds. The Fourier transform of Equation 10 was taken and values of T equal to 0.00047, 0.00071 and 0.00095 s were used to calculate $Q(\omega)$ for 60, 45, and 30 mph, respectively, corresponding to a ½-in. groove width. The magnitude of the results of these calculations is shown in Figure 9. These results show that for the slower speed, the volume velocity varies more with frequency (i.e., not as "flat"), up to several thousand Hertz, as would be expected for the longer event duration. The magnitude of $P(\omega)$ can now be calculated using the already determined transfer functions, $T_1(\omega)$ and $T_2(\omega)$, and is shown in Figure 10 for the speeds of 60, 45, and 30 mph. In these plots, it is apparent how the slower tire speeds reduce the levels at frequencies above

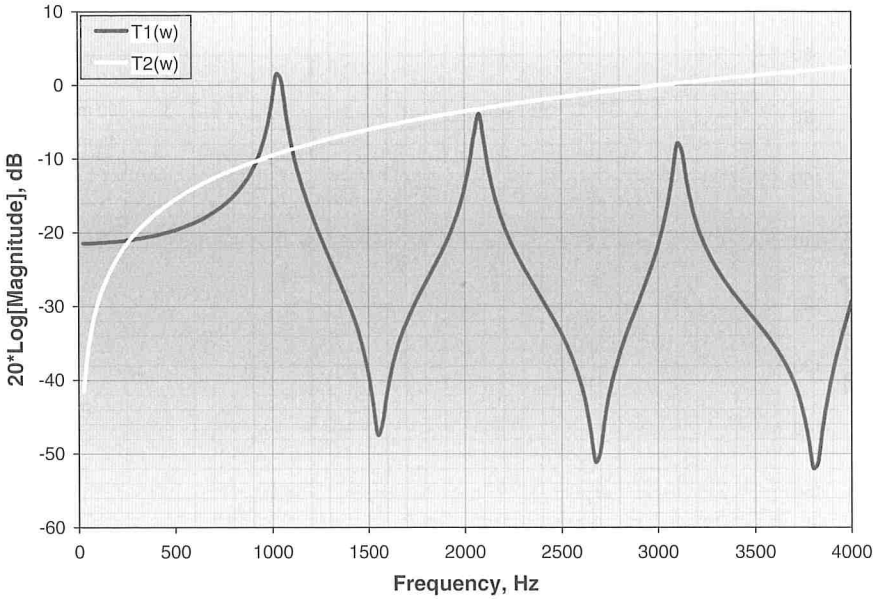

FIGURE 7 Magnitude of transfer functions between volume change and air velocity at opening of groove, $T_1(\omega)$, and transfer function between air velocity and sound pressure, $T_2(\omega)$.

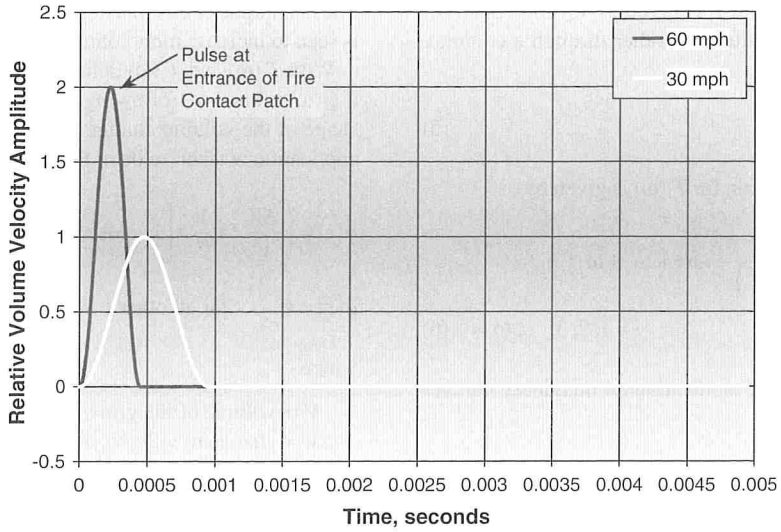

FIGURE 8 Assumed shape of volume velocity pulse as groove is enveloped at 60 and 30 mph.

1,500 Hz. At the resonant peak of the first mode (~1,000 Hz), a reduction of about 4 dB can be seen between the speeds of 60 and 30 mph. These plots also reinforce the earlier observation that, at least for the lower tube mode, the frequency peak of the radiated sound is independent of vehicle speed.

Level Calibration

The results of Figure 10 are relative because the absolute magnitude of $q(t)$ is not known. However, using the results of the Purdue research, the model can be calibrated if the sound produced by a slap is isolated for one or more groove geometries. In the Purdue work, the sound pressure levels for a variety of the joint geometries are reported as measured over a 0.08-s window (see Figure 3). This window includes energy from both the groove response and the residual level of the TPTA surface texture. To isolate the groove response, this residual level needs to be removed and energy remaining in the pulse quantified. The Purdue data were reported at speeds of 10, 15, 20, 25, and 30 mph for groove depths of 1 in., ½ in., and ⅛ in. and groove widths of 1 in., ¾ in., 7/16 in., and ¼ in. These results were curve-fit as a function of groove width at each speed and the zero width intercept was used as residual level. The residual as a function of speed was then subtracted on an energy basis from the results with the various groove cases to extract the isolated groove response for each of the geometries. Due to the low groove response levels at the ⅛-in. depth relative to the residual texture noise, only the cases for the 1-in. and ½-in. depth were used.

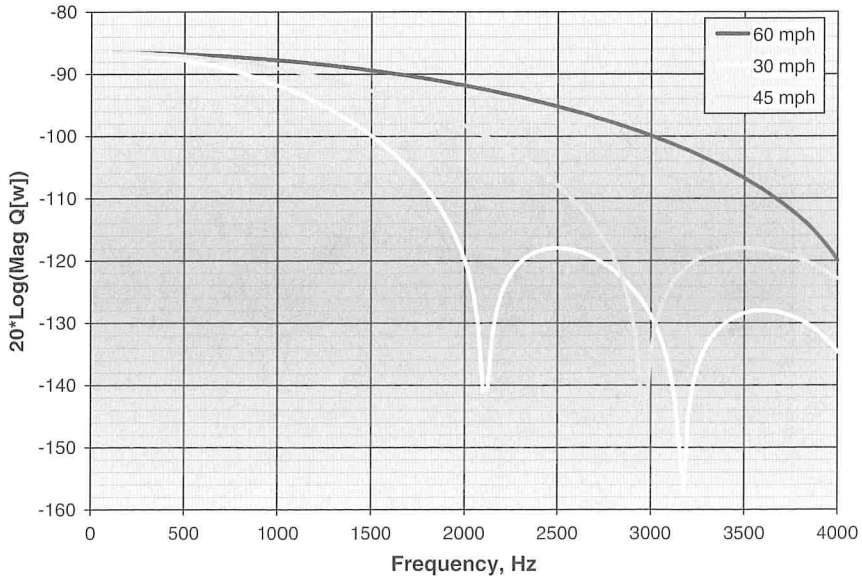

FIGURE 9 Calculated relative magnitude of groove volume velocity pulse as function of frequency for assumed pulse shape at 60, 45, and 30 mph.

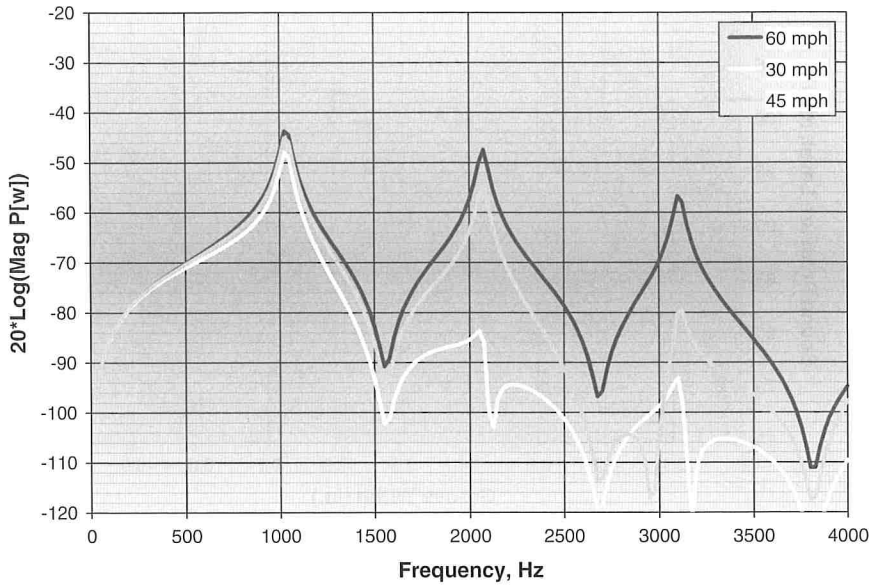

FIGURE 10 Calculated relative magnitude of the acoustic pressure at open end of pavement groove as function of frequency 60, 45, and 30 mph.

These data were then fit to those predicted by the model for the appropriate geometry for a speed of 30 mph corresponding to the same speed calculated in Figure 10.

The results of Figure 10 were used to extend the calibration to higher speeds. The differences between the speeds in narrow band levels were summed into one-third octave bands and applied to a Mojave burlap drag spectrum. The difference in overall A-weighting was determined and found to be 4.9 dB going from 30 to 60 mph and 1.9 dB going from 45 to 60 mph. As a final step in isolating the pulse, the duration of the groove response relative to the 0.08-s time window needs to be taken into account. The differences cited above reflect equal energy summed over the 0.08-s period (see Figure 8). To determine the root mean square level of the pulse, the energy must be divided by the duration of the pulse. In going from 30 to 60 mph, the energy of the pulse (the sum of the p^2 values) is the same. However, the time period of the summation is half as long at 60 mph than at 30 mph. This results in a ratio of the inverse time periods of 0.010/0.005, which amounts to a 3-dB correction relative to the analysis period of 0.08 s. For 45 mph relative to 30 mph, this amounts to 1.2 dB. Including this correction and the earlier adjustment arising from Figure 10, the total difference between 30 and 60 mph is 7.9 dB, and 4.8 dB for 30 to 45 mph. Fitting these results to a logarithmic function with speed, it is found that the relationship of groove response with tire operating speed of S is $26.5*\text{Log}_{10}(S)$. Given this relationship and that of Equation 4, the sound level of the groove response can be calculated at any speed and groove geometry by using the calibrated level of 99.2 dB(A) at a speed of 30 mph for a 1-in.-wide and 1-in.-deep reference groove.

MODEL DESCRIPTION AND RESULTS

With the model calibrated in the manner discussed above, the sound pressure level produced at a chosen speed can be calculated for varying groove geometries. The results of such calculations are shown in Figure 11 for a tire operating speed of 60 mph. As expected from Equation 4, this shows the trend that as the groove dimensions increase, the sound level also increases.

To apply this model to an actual pavement and calculate the overall time average level, two further parameters are needed. First is the repetition rate of the slaps, which can be determined by the joint spacing and the tire operating speed. The repetition rate in slaps per second is then multiplied by the energy of one pulse and the length of the reference time window, 0.08 s, to obtain the average level contribution of the joint grooves. Second is the residual texture noise level of the pavement. The noise level of the pavement is typically measured using the onboard sound intensity (OBSI) in the United States. For use with these data, the sound intensity level of the groove response is taken to be equal to the sound pressure level in this case as the model corresponds to a compact noise source and free-field propagation. The overall level for a pavement is energy sum of the groove contribution and the texture-generated noise level. An example of this is given in Figure 12 for a case where the joint spacing is 13 ft, the vehicle speed is 60 mph, and the residual pavement texture OBSI level is 99.0 dB(A), corresponding to a typical, quieter burlap drag or ground PCC textured pavement. In this case, the joint groove adds about 1 dB to the overall level when the groove cross-sectional area reaches 0.25 in.^{2}, or for a groove dimension of ½ in. deep by ½ in. wide. The model can also be used in the reverse calculation. If the overall OBSI is known along with the joint parameters, the residual texture level could be calculated.

The results shown in Figure 12 can be used to give some direction in efforts to reduce the contribution of PCC joint slap to overall levels. If groove width is limited to ⅛ in., even for relatively low noise texture, the contribution of the joint groove to overall level will be negligible for depths up to at least 1 in. If filled with sealer to within ⅛ in. of the pavement surface, the contribution of joint grooves can also be made negligible. As an example, for a 1-in.-deep by ½-in.-wide groove filled to within ⅛ in. of the pavement surface, the overall level would be reduced by about 2½ dB given the assumed texture level of 99.0 dB(A). It should be noted that for higher texture levels, the contribution of the joint grooves will diminish somewhat. For

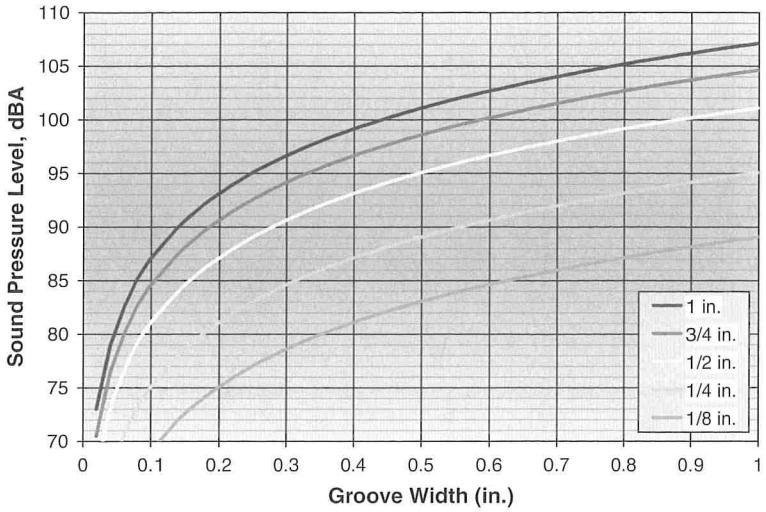

FIGURE 11 Sound pressure levels calculated for joint grooves of varying dimension at 30 mph using calibrated model.

example, if the conditions of Figure 12 are compared to pavement with a residual of 103 dB(A) and a joint groove ½ in. deep by ½ in. wide is used, the contribution of the joint to the overall level would decrease to 0.4 dB for noisier texture from 0.9 dB for the quieter texture.

In considering the results of this model, it should be realized that the source levels do not include the effect of any offset or "faulting" of the concrete slabs. According to the research work done at Purdue, this effect can be quite significant (*2*). At 30 mph, it was reported that the level offset alone produced increases in sound pressure level of about 1 dB per 0.025 in. of step height. Because of this effect of slab offset, field validation of the groove effects model is problematic unless it is verified that offsets do not exist. However, the results of the model are consistent with those obtained on the Mojave Bypass for the contribution of joint slap for longitudinally tined, burlap drag, broomed texture surfaces (*7*). In that research, the contribution of joints was determined by trigging a 0.08-s analysis window such that the joint was included and then excluded. The difference in these levels produced isolated level of the joints. These derived joint levels were found not to be dependent on the pavement texture as would be predicted by the model.

CONCLUSIONS

Grooves between PCC pavement slabs can contribute to the total measured noise level, particularly when the noise levels generated by the pavement texture are relatively low. The radiation of sound from the grooves demonstrates the same resonant behavior as that associated with longitudinal, circumferential grooves in tires and transversely oriented grooves in the tire tread patterns. Drawing upon

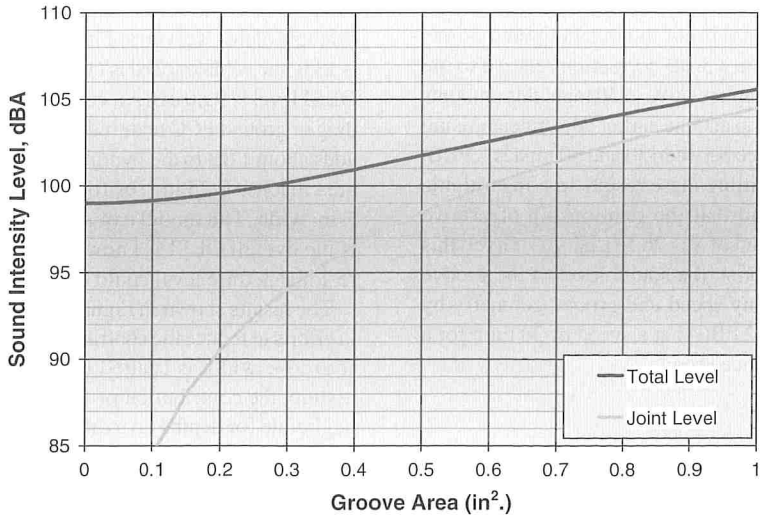

FIGURE 12 Model results of overall pavement OBSI level for joints spaced 13 ft apart, vehicle speed of 60 mph, and pavement texture OBSI level of 99.0 dB(A).

these cases, the sound radiation from the transverse grooves present between concrete slabs can be modeled and compared to laboratory and road data. The source strength of the groove radiation is proportional to 20 times the logarithm of the cross-sectional area. By considering residual noise introduced by the pavement texture, laboratory trends are readily duplicated. Once calibrated for the level produced by single, isolated groove response, the model results can be applied in situations representative of actual highway pavement for determining the contribution of joint grooves to overall pavement noise level. This contribution can be made negligible by minimizing the cross-section area of the groove.

ACKNOWLEDGMENTS

The development of this model was funded by the American Concrete Pavement Association through the efforts of Larry Scofield of that organization. Use and interpretation of the TPTA results were facilitated by Robert Bernhard and Will Thornton, both formerly with Purdue University. The measurements conducted on the Mojave PCC research sites were made through the support of the California Department of Transportation (Caltrans) and Bruce Rymer.

REFERENCES

1. Donavan, P. Noise Evaluation of Various Pavement Texture on New Portland Cement Concrete. *Noise Control Engineering Journal,* Vol. 57, No. 2, 2009, pp. 62–76.
2. Dare, T., T. Wulf, W. Thornton, and R. Bernhard. *The Effect of Joints in Portland Cement Concrete Pavement.* Report SQDH 2008-1 and HL 2008-7. Purdue University Institute for Safe, Quiet, and Durable Highways, West Lafayette, Ind., 2008.
3. Wilken, I. *A Theoretical Prediction of the Noise Generated by the Compression of a Tire Cross Groove.* Research Report FD-89. General Motors Research Laboratory, Warren, Mich., 1976.
4. Donavan, P. *The Role of Acoustic Tube Resonance in the Radiation of Sound from Circumferentially Ribbed Truck Tires.* Research Publication GMR-3846. General Motors Research Laboratory, Warren, Mich., 1981.
5. Bernhard, R., and W. Thornton. Preliminary Results Using the Tire/Pavement Test Apparatus. *Proc., Inter-Noise 2003,* Seogwipo, Korea, 2003.
6. Donavan, P. *Quantification of Noise Mechanisms for a Straight-Ribbed, HCR Bias-Ply Truck Tire.* Research Report EM-547. General Motors Research Laboratory, Warren, Mich., 1982.
7. Donavan, P. Influence of PCC Surface Texture and Joint Slap on Tire/Pavement Noise Generation. *Proc., NoiseCon 2004,* Baltimore, Md., 2004.

The Transportation-Related Noise and Vibration Committee peer-reviewed this paper.

Quantitative Assessment of Environmental and Economic Benefits of Recycled Materials in Highway Construction

Jin Cheol Lee, Tuncer B. Edil, James M. Tinjum, and Craig H. Benson

The benefits of using recycled materials in highway pavements was assessed quantitatively by conducting life-cycle analysis and life-cycle cost analysis on pavements consisting of conventional and recycled materials for a highway construction project in Wisconsin. Results of the analysis indicate that using recycled materials in the base and subbase layers of a pavement can result in reductions in global warming potential (20%), energy consumption (16%), water consumption (11%), and hazardous waste generation (11%) while also extending the service life of the pavement. In addition, using recycled materials in the base and subbase layers can result in a life-cycle cost savings of 21%. The savings are even greater if landfill avoidance costs are considered for the recycled materials incorporated in the pavement. Extrapolation of the benefits to conditions nationwide indicates that modest changes in pavement design to incorporate recycled materials can contribute substantially to the emission reductions required to stabilize greenhouse gas emissions at current levels.

New construction and rehabilitation of the roadway system in the United States occurs continuously to meet the nation's transportation needs. These activities consume large amounts of natural materials and energy, produce wastes, and generate greenhouse gas emissions (*1*, *2*). Thus any regional or national sustainability plan in the United States must account for roadway construction and rehabilitation.

A sustainable approach to material consumption begins with design and planning that reuses and incorporates suitable by-products that would otherwise be disposed. Ideally, products can be designed so that recycling and reuse occur at all stages of the life-cycle, resulting in limited waste generation. For road construction, Gambatese and Rajendran (*1*) and Kibert (*3*) show that reuse and recycling can significantly contribute to more sustainable road construction practices. However, lack of comparative analysis methods, examples, and protocols for actual construction projects hinders the ability to quantify tangible environmental and economic benefits that can be achieved through reuse and recycling in pavement design and construction.

Carpenter et al. (*4*) illustrate how a life-cycle assessment (LCA) approach can be used to quantify the environmental impacts of using recycled materials in lieu of conventional construction materials and remark on the economic benefit that can be accrued using recycled materials in roadway construction. However, their analysis does not include rehabilitation activities, which are some of the most energy-intensive phases in the roadway life cycle. They also do not quantify the economic benefits from using recycled materials. In the context of sustainability, direct comparisons of the life-cycle cost using recycled materials instead of conventional materials are important.

In this study, comparative environmental and economic life-cycle analyses were conducted to quantify the environmental and economic benefits that could be accrued by using recycled materials when constructing a 4.7-km-long section of the Burlington Bypass in southeastern Wisconsin. Rehabilitation activities were explicitly included in the life-cycle analysis using the international roughness index (IRI) as a metric to define when rehabilitation would be required, as suggested by FHWA (*5*). The benefits illustrated in this quantitative analysis are expected to encourage wider adoption of recycled materials in roadway construction and rehabilitation.

EVALUATION OF THE BURLINGTON BYPASS

A comparative life-cycle analysis was conducted for construction of a section of Wisconsin State Highway 36/83 near Burlington, Wisconsin (the Burlington Bypass), assuming that the pavement would be constructed with conventional or recycled materials. The Burlington Bypass consists of 17.7 km of highway that routes traffic on WIS-11 and WIS-36/83 around the City of Burlington, Wisconsin. The bypass is intended to improve safety, reduce delays, and to provide an efficient travel pattern that reduces truck traffic in the downtown area of the city of Burlington (*6*). The western portion of the bypass is being constructed between spring 2008 and fall 2010. A 4.7-km-long section of the western portion of the bypass was analyzed in this study.

A flowchart for the evaluation procedure is shown in Figure 1. The steps include creating pavement designs using conventional and recycled materials, predicting the service life of each design, identifying rehabilitation strategies, and conducting LCA and life-cycle cost analysis (LCCA). LCCA is a financial-based decision-making

J. C. Lee, Recycled Materials Resource Center and Department of Civil and Environmental Engineering, 2231 Engineering Hall; T. B. Edil, Recycled Materials Resource Center and Department of Civil and Environmental Engineering, 2226 Engineering Hall; J. M. Tinjum, Engineering Professional Development and Department of Civil and Environmental Engineering, 2214 Engineering Hall; and C. H. Benson, Recycled Materials Resource Center, Geological Engineering, 2218 Engineering Hall, University of Wisconsin–Madison, 1415 Engineering Drive, Madison, WI 53706-1691. Corresponding author: T. B. Edil, edil@engr.wisc.edu.

Transportation Research Record: Journal of the Transportation Research Board, No. 2158, Transportation Research Board of the National Academies, Washington, D.C., 2010, pp. 138–142.
DOI: 10.3141/2158-17

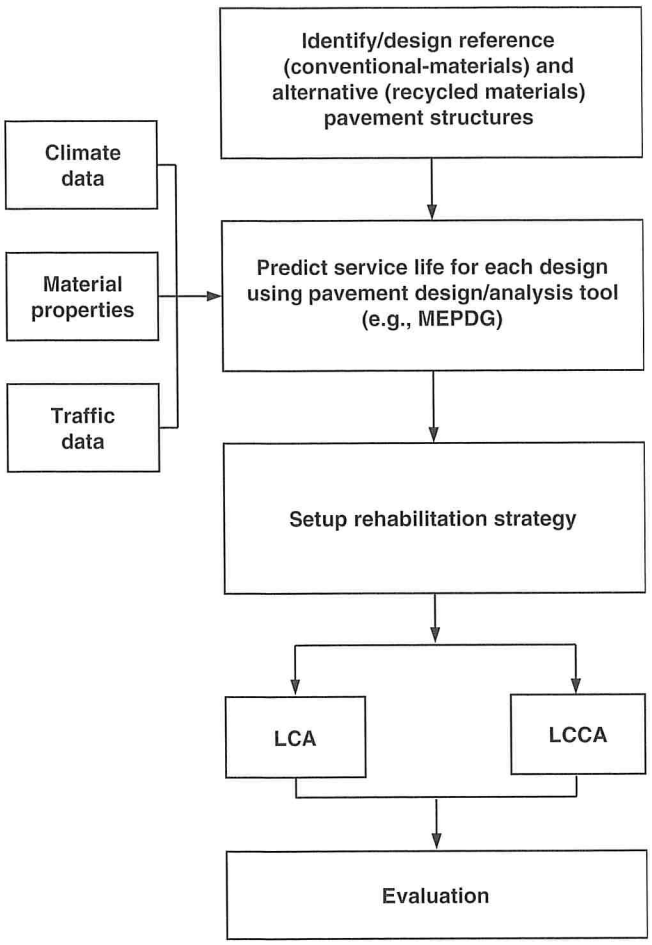

FIGURE 1 Flowchart for comparative life-cycle analysis of conventional and alternative pavement designs.

tool for long-term assessment of construction projects that can be used to systematically determine costs attributable to each alternative course of action over a life-cycle period and to make economic comparisons between competing designs (*7, 8*).

Environmental analysis of the conventional and alternative pavements was conducted with LCA. Four environmental variables were considered in the assessment: energy consumption, greenhouse gas emissions, water consumption, and generation of hazardous wastes, as defined by the U.S. Resource Conservation and Recovery Act (RCRA).

The two potential pavement designs considered in the analysis are shown in Figure 2, a conventional pavement design proposed by the Wisconsin Department of Transportation (WisDOT) and an alternative pavement design employing recycled pavement material stabilized with fly ash as the base course and foundry sand as the subbase. Recycled materials can also be used in hot-mix asphalt (HMA) and in other elements in the right-of-way (e.g., pipes, guide rails, barriers, etc.); in this study, however, recycled materials were only used in the base and subbase layers of the pavement.

The same layer thicknesses were used in the conventional and alternative designs and the structural capacity of both pavements was determined using the same procedure. However, the recycled materials have different engineering properties than the conventional materials, which resulted in differences in the calculated service life. Design parameters for the recycled materials were obtained from recommendations made by Geo Engineering Consulting (*9*), which are based on research findings reported by Li et al. (*10*) and Tanyu et al. (*11, 12*).

The pavements were assumed to be serviceable until the IRI reached 2.7 m/km, as recommended by FHWA (*5*). Once this IRI was reached, the pavement was assumed to require rehabilitation. The IRI was predicted using the *Mechanistic–Empirical Pavement Design Guide* (MEPDG) *Version 1.0* (*13*). MEPDG primarily uses three key variables in the analysis: (a) traffic data, (b) climate conditions, and (c) material properties.

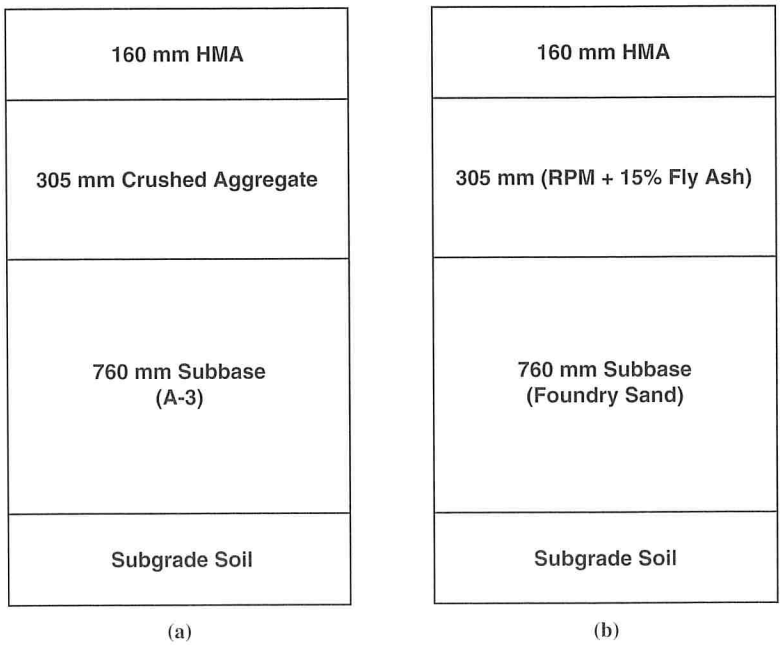

FIGURE 2 Schematic of two pavement designs: (*a*) reference (conventional) materials and (*b*) alternative (recycled) material.

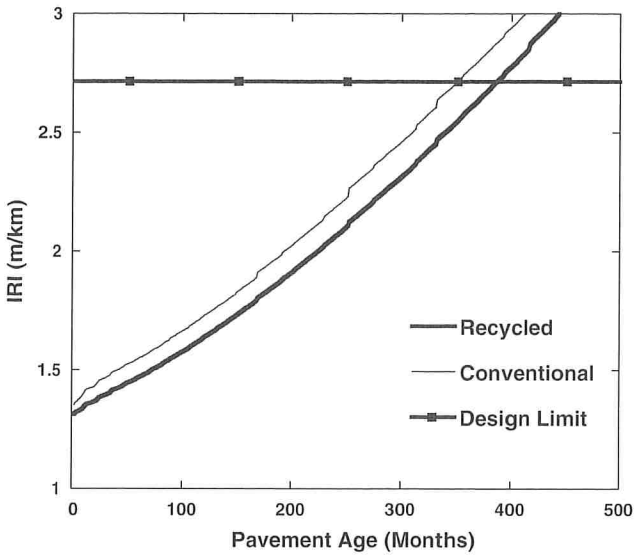

FIGURE 3 IRI as a function of pavement age for pavements constructed with conventional and recycled materials as predicted using MEPDG.

Predictions of the IRI for the conventional and recycled designs are shown in Figure 3. The conventional and recycled material designs reach their terminal serviceability at 29 and 32 years, respectively. The service life for the pavement using recycled materials is 3 years longer because of the superior properties of the recycled materials relative to the conventional materials.

LIFE-CYCLE ASSESSMENT

The LCA was conducted using the spreadsheet program PaLATE Version 2.0 (*14*). PaLATE was used because it includes information on a variety of recycled materials, including the fly ash and foundry sand used in the base and subbase in this study. PaLATE employs reference factors to calculate environmental impacts for a project. For example, PaLATE uses CO_2 emission factors for construction equipment from U.S. Environmental Protection Agency inventory data (*15*) to compute emissions from construction for a project. Total effects are computed as the product of unit reference factors and the quantity of an activity or material in the project.

PaLATE employs economic input–output (EIO) LCA, which permits an assessment of environmental impacts of the entire supply chain associated with conventional and recycled construction materials. EIO-LCA uses economic input–output data (e.g., data from the U.S. Department of Commerce) as well as resource input data and environmental output data to analyze both the direct impact and supply chain effects (*16*). More details of the LCA approach used in PaLATE can be found in *Pavement Life-Cycle Assessment Tool for Environmental and Economic Effects* (*14*).

The LCA was conducted for a 50-year period, which is the standard practice employed by WisDOT. This analysis included one rehabilitation of the pavement at 29 or 32 years, as noted previously. Energy use and global warming potential (reported in carbon dioxide equivalents, CO_2e) reported by PaLATE were used for comparing the environmental attributes of the pavements constructed with conventional and recycled materials. Generation of RCRA hazardous waste and water consumption during construction was also considered in the environmental assessment.

The LCCA was conducted using the spreadsheet program RealCost Version 2.5 (*17*). As with the LCA, the LCCA was conducted for a 50-year period. Agency costs and work zone user costs were included in the LCCA. The user costs include delay costs (cost of delay time spent in work zones) and crash costs associated with construction and rehabilitation.

RESULTS AND ANALYSIS

Results of the LCA are shown in Table 1 for material production, transportation, and construction (placement of the materials in the roadway). The column labeled "difference" corresponds to the total percent change in the environmental metric by using recycled materials in lieu of conventional materials. For both cases, the HMA component dominated the energy and water usage, CO_2 emissions, and hazardous waste generated. Thus the overall benefits of using recycled materials in the base and subbase course are modest. Using recycled materials in the HMA (or an alternative asphalt construction process) and in other elements of the right-of-way (e.g., pipes, guide rails, barriers, signage) in the alternative design would further enhance the environmental benefits. However, as illustrated subsequently, using recycled materials only in the base and subbase layers results in significant environmental and economic benefits.

Greenhouse Gas Emissions

The quantities in Table 1 indicate that a 20% reduction in global warming potential (CO_2e) can be achieved in this case study using

TABLE 1 LCA Predictions for Pavements Using Conventional and Recycled Materials

	Conventional Materials			Recycled Materials			
Environmental Metric	Material Production	Transportation	Construction	Material Production	Transportation	Construction	Difference (%)
CO_2 (Mg)	3,630	323	111	3,028	163	54	−20
Energy (GJ)	66,680	4,318	1,476	58,023	2,187	723	−16
RCRA hazardous waste (Mg)	629	31	9	611	16	4	−6
Water (L)	17,185	735	144	15,637	372	70	−11

NOTE: GJ = gigajoules = 0.001 terajoules (TJ); Mg = megagrams.

recycled materials. Most of the reduction in CO_2e (74%) is from reduced emissions during material production. Heavy equipment operation is the main source of CO_2e emissions during material production. Most recycled materials are available as a by-product from another operation (e.g., fly ash is a by-product of electric power production) and therefore do not require mining, crushing, and so forth. Consequently, production of recycled materials requires less usage of heavy equipment relative to conventional materials, which results in a reduction in CO_2e emissions.

To stabilize greenhouse gas emissions at current levels, the construction industry worldwide must reduce emissions by 22.7 billion Mg-CO_2e over the next 50 years (*18*). Highway construction accounts for 6.8% of total construction (*19*). Accordingly, the highway construction industry must reduce emissions by 1.54 billion Mg-CO_2e over 50 years. The LCA for this case study indicates that a reduction of 819 Mg-CO_2e could be achieved using recycled materials in the 4.7-km portion of the Burlington Bypass considered in this study, or 174 Mg-CO_2e/km. The United States alone is projected to construct 6 million kilometers of roadway over the next 40 years (*4*). Based on this construction rate and the emissions reductions computed in this study, using recycled materials in roadway construction could achieve an emissions reduction of 1.30 billion Mg-CO_2e over 50 years using the relatively modest changes in pavement design illustrated in this example. Thus, with other modest changes to pavement designs, reducing emissions by 1.54 billion Mg-CO_2e over 50 years in roadway construction appears practical.

Energy Savings

The quantities in Table 1 indicate that approximately 13% of the total energy savings obtained using recycled materials is associated with material production. These energy savings are analogous to the reductions in emissions associated with material production and are associated with the heavy equipment used to mine and process conventional construction materials. Use of recycled pavement materials in situ also reduces the energy associated with transportation (e.g., transport to a landfill for disposal and transport of new materials to the construction site).

The total energy savings (16%) using recycled materials for the 4.7-km section is 11.5 terajoules (TJ), or 2.4 TJ/km, which corresponds to the annual energy consumed by 115 average households in the United States (based on 2005 energy use statistics) (*20*). Similar application of recycled materials on a nationwide basis [assuming 150,000 km of construction annually, based on Carpenter et al. (*4*)] corresponds to an energy savings of 360,000 TJ in the United States annually, which is equal to the energy consumed by 3,600,000 average homes (e.g., a city the size of New York or Los Angeles). Thus substantial energy savings can be accrued on a nationwide basis using recycled materials in roadway construction.

Other Environmental Impacts

Using recycled materials in the pavement design also reduced the amount of hazardous waste produced and the amount of water consumed. The reduction in hazardous wastes results in lower management costs (*21*). The reduction in water use is substantial. The use of recycled materials results in a savings of 1,985 L of water (11% or 422 L/km) for the 4.7-km section considered in the analysis. Similar application of recycled materials on a nationwide basis [assuming 150,000 km of construction annually, based on Carpenter et al. (*4*)] could potentially result in an annual reduction of 1.2 million megagrams of hazardous waste and a savings of 63 million liters of water nationwide.

TABLE 2 Life-Cycle Costs for Pavement Designs Using Conventional and Recycled Materials

Category	Reference	Alternative	Saving
Agency cost ($)	9,044,570	7,107,230	1,937,340 (21%)
User cost ($)	10,570	8,380	2,190 (21%)
Total ($)	9,055,140	7,115,610	1,939,530 (21%)

Life-Cycle Cost

The life-cycle costs and the cost savings using recycled materials are summarized in Table 2. These cost savings include avoidance of landfill disposal of the recycled materials based on an average landfill tipping fee of $40/Mg (Wisconsin Department of Natural Resources, *22*). As shown in Table 2, total life-cycle costs can be reduced 21% by using recycled materials in lieu of conventional materials.

CONCLUSION

The potential benefits of using recycled materials and industrial by-products instead of conventional materials in a highway construction project in Wisconsin have been described. LCA and LCCA were used to evaluate environmental and economic benefits. The analyses indicate that using recycled materials in the base and subbase layers of a highway pavement can result in reductions in global warming potential (20%), energy consumption (16%), water consumption (11%), and hazardous waste generation (6%). Overall, use of recycled materials in the base and subbase has a potential life-cycle cost savings of 21% while providing a longer service life.

When extrapolated to a nationwide scale, using recycled materials in roadway construction has the potential to provide the reductions in greenhouse gas emissions needed to maintain emissions by the highway construction industry at current levels. In addition, energy savings commensurate with the annual energy consumption of households in a U.S. city comparable in size to New York or Los Angeles can be achieved by using recycled materials in roadway construction on a nationwide basis.

ACKNOWLEDGMENTS

The Wisconsin Department of Transportation and Charles Coulter (Lafarge Corporation) provided information for this study. Gary Whited of the Wisconsin Construction and Materials Support Center assisted in the study.

REFERENCES

1. Gambatese, J. A., and S. Rajendran. Sustainable Roadway Construction: Energy Consumption and Material Waste Generation of Roadways. *Proc., Construction Research Congress 2005*, San Diego, Calif., 2005.

2. *Primer on Transportation and Climate Change.* AASHTO, 2008.
3. Kibert, C. J. Policy Instruments for a Sustainable Built Environment. *Journal of Land Use and Environmental Law,* Vol. 17, 2002, pp. 379–394.
4. Carpenter, A. C., K. H. Gardner, J. Fopiano, C. H. Benson, and T. B. Edil. Life Cycle Based Risk Assessment of Recycled Materials in Roadway Construction. *Waste Management,* Vol. 27, 2007, pp. 1458–1464.
5. *Life-Cycle Cost Analysis in Pavement Design.* Pavement Division Interim Technical Bulletin FHWA-SA-98-079, FHWA, U.S. Department of Transportation, 1998.
6. *Burlington Bypass Project.* Wisconsin Department of Transportation. http://www.dot.wisconsin.gov/projects/d2/burl/index.htm. Accessed April 7, 2009.
7. Bull, J. W. *Life Cycle Costing for Construction.* Taylor & Francis, London, 1993.
8. Kirk, S. J., and A. Dell'isola. *Life Cycle Costing for Design Professionals.* McGraw-Hill, New York, 1995.
9. Geo Engineering Consulting. *Implementation Recommendations of Equivalency of Alternative Working Platforms and Their Pavement Design Strength Contribution.* Wisconsin Highway Research Program Report 0092-06-08. Wisconsin Department of Transportation, 2009.
10. Li, L., C. H. Benson, T. B. Edil, and B. Hatipoglu. Sustainable Construction Case History: Fly Ash Stabilization of Recycled Asphalt Pavement Material. *Geotechnical and Geological Engineering,* Vol. 26, No. 2, 2008, pp. 177–188.
11. Tanyu, B. F., C. H. Benson, T. B. Edil, and W.-H. Kim. Equivalency of Crushed Rock and Three Industrial By-Products Used for Working Platforms During Pavement Construction. In *Transportation Research Record: Journal of the Transportation Research Board, No. 1874,* Transportation Research Board of the National Academies, Washington, D.C., 2004, pp. 59–69.
12. Tanyu, B. F., W.-H. Kim, T. B. Edil, and C. H. Benson. Development of Methodology to Include Structural Contribution of Alternative Working Platforms in Pavement Structure. In *Transportation Research Record: Journal of the Transportation Research Board, No. 1936,* Transportation Research Board of the National Academies, Washington, D.C., 2005, pp. 70–77.
13. *Mechanistic–Empirical Design of New and Rehabilitated Pavement Structures Version 1.00.* NCHRP. http://www.trb.org/mepdg/software.html. Accessed Feb. 16, 2009.
14. *Pavement Life-Cycle Assessment Tool for Environmental and Economic Effects Version 2.0.* Recycled Materials Resource Center. http://www.rmrc.unh.edu/Resources/CD/PaLATE/PaLATE.htm. Accessed Feb. 16, 2009.
15. *Gasoline and Diesel Industrial Engines-Emission Factor Documentation for AP-42 Section 3.3.* U.S. Environmental Protection Agency, Oct. 1996. http://www.epa.gov/ttn/chief/ap42/ch03/final/c03s03.pdf. Accessed Oct. 21, 2009.
16. Horvath, A. Construction Materials and Environment. *Annual Review of Environment and Resources,* Vol. 28, 2003, pp. 559–586.
17. *RealCost Version 2.5.* FHWA. http://www.fhwa.dot.gov/infrastructure/asstmgmt/lccasoft.cfm. Accessed Feb. 16, 2009.
18. Socolow, R. H., and S. W. Pacala. A Plan to Keep Carbon in Check. *Scientific American,* Sept. 2006, pp. 50–57.
19. *Industry General Summary 2002: 2002 Economic Census Construction Subject Series.* U.S. Census Bureau, U.S. Department of Commerce, 2005.
20. *2005 Residential Energy Consumption Survey-Detailed Tables.* Energy Information Administration. http://www.eia.doe.gov/emeu/recs/recs2005/c&e/detailed_tables2005c&e.html. Accessed July 9, 2009.
21. *RCRA Hazardous Waste Delisting: The First 20 Years.* U.S. Environmental Protection Agency. http://www.epa.gov/waste/hazard/wastetypes/wasteid/delist/report.pdf. Accessed Oct. 21, 2009.
22. *Posted Gate Landfill Tip Charges in Upper Midwest States, 2006 and 2008.* http://www.dnr.state.wi.us/org/aw/wm/solid/landfill/outofstate.htm. Accessed Oct. 22, 2009.

The Waste Management and Resource Efficiency in Transportation Committee peer-reviewed this paper.

Environmental and Sustainability Impact Assessment of Infrastructure in the United Kingdom

Richard Willetts, Jim Burdon, Jacqui Glass, and Matthew Frost

Sustainability, now embedded within the legislation and development policy of the United Kingdom, is beginning also to be implemented within the design and construction process. Methods to assess the sustainability of construction projects have been in development since the early 1990s, but to date the majority have focused on the building sector, with little consideration for the detailed assessment of civil engineering projects. In addition, the tools developed have rarely considered sustainability in its widest sense, instead concentrating on the more quantifiable aspects of the environment, ecology, and building material use. The U.K. civil engineering industry has attempted to fill this gap with the development of the Civil Engineering and Environmental Quality Assessment and Award Scheme (CEEQUAL). The use of CEEQUAL is voluntary, but it is seen as a benchmark for assessing the environmental and social impact of infrastructure. Background to sustainability assessment for projects in the United Kingdom and the development of CEEQUAL and areas for improvement are presented. The paper then presents the results of a backanalysis for three infrastructure projects, with CEEQUAL to assess the design teams' compliance with and comprehension of sustainability issues within their projects. Although infrastructure design teams are likely to engage with sustainability issues in assessment areas in which they have previous experience (such as environmental impact and biodiversity), more education is required to encourage increased awareness in the relatively new areas of design assessment, including minimizing carbon footprint, material specifications, and material use and reuse.

Sustainability is generally considered to involve the protection of the environment and resources while ensuring economic equity and social inclusion for all. Sustainable development has been on the political horizon for 20 years, but only in the past decade has it begun to be enshrined within policy and legislation.

The United Kingdom (U.K.) government has made commitments to the ambitions of sustainability since 1994 (*1*) when it produced its first U.K. strategy for sustainable development. This has since been reviewed and updated and also led to a sector-specific strategy for the U.K. construction industry in 2008 (*2*).

R. Willetts, Jacobs Engineering and Loughborough University, and J. Burdon, Jacobs Engineering, Wheatcroft House, Landmere Lane, Nottingham, NG12 4DG, United Kingdom. J. Glass and M. Frost, Department of Civil and Building Engineering, Loughborough University, Loughborough, Leicestershire LE11 3TU, United Kingdom. Corresponding author: M. Frost, m.w.frost@lboro.ac.uk.

Transportation Research Record: Journal of the Transportation Research Board, No. 2158, Transportation Research Board of the National Academies, Washington, D.C., 2010, pp. 143–150.
DOI: 10.3141/2158-18

The construction industry is one of the largest sectors in the United Kingdom providing work for 2.1 million people, generating nearly 10% of gross domestic product. Through its construction, operation, and maintenance, the built environment contributes nearly 50% of all U.K. carbon emissions and 33% of landfill waste and consumes 13% of raw materials and 50% of water (*3, 4*). These figures illustrate why the sector needs to be a leader in embracing sustainability to minimize its detrimental impact on the planet and mitigate the negative impacts on future generations.

Although much progress has been made in moving sustainability forward in some areas (namely, building design, waste, and procurement), there is still much room for improvement. Civil engineering and the delivery of transportation infrastructure is one of the areas where little direct attention has been focused. It is essential that engineers be aware of the principles behind sustainable development and the ways in which they can help in its delivery to guarantee a more secure future for all.

To allow engineers to be able to play their vital role in the delivery of sustainable development, it is essential that robust methods of assessment be developed and used to help better inform decision making at the appropriate opportunities (*5*). The growing regulatory and institutional emphasis on sustainability issues has led to the development of a variety of assessment methodologies that currently focus predominantly on the environmental aspects and consequent impacts of construction projects.

This paper provides a review of the sustainable infrastructure assessment methodologies available to the U.K. construction sector before presenting a methodology developed by the Institution of Civil Engineers (ICE), the U.K. government, and leading members of industry specifically for the civil engineering sector, the Civil Engineering and Environmental Quality Assessment and Award Scheme (CEEQUAL). Three case studies are carried out using the CEEQUAL methodology to identify current levels of environmental performance in the design of a series of small projects as part of development infrastructure schemes, before conclusions are drawn on the key areas requiring focus from engineers to help improve the design teams' performance on future projects.

SUSTAINABLE DEVELOPMENT OF INFRASTRUCTURE IN THE UNITED KINGDOM

Sustainability is a term that is used widely and interchangeably throughout all sectors and has any number of meanings to the individual or group depending on context and understanding (*6*). Its ambiguity becomes apparent when it is understood to have

anywhere from 200 to 500+ definitions (*7, 8*). There is, however, one widely adopted definition that is seen as the benchmark for what sustainability should mean—Brundtland's definition—according to which sustainability is a ". . . development that meets the needs of the present without compromising the ability of future generations to meet their own needs" (*9*). The Brundtland report (*9*) identified the importance of environmental protection and the social importance of providing for other citizens and future generations; these underlying principles have been developed and adapted in several notable models that have split the idea of sustainable development into three areas: environmental protection, social equity, and economic prosperity.

The United Kingdom's first strategy on sustainable development was issued in 1994 and set out the government's general principles, objectives, and approach to environmental issues (*1*). The U.K. strategy has been continually updated and the current version (*10*) sets out four priority areas:

- Sustainable consumption and production,
- Climate change and energy,
- Natural resource protection and environmental enhancement, and
- Sustainable communities.

These four priorities are set within five guiding principles: living within environmental limits; ensuring a strong, healthy, and just society; achieving a sustainable economy; promoting good governance; and using sound science responsibly.

Although the government has been investigating ways to address sustainable development since the early 1990s, it is only since 2000 that it has turned its attention to the construction industry (*11*). Construction is recognized as being of major importance to the successful delivery of the U.K. sustainable development agenda (*12*); it clearly affects the delivery of all four priority areas of the U.K. sustainable development strategy (*10*) and underpins many of the 68 headline indicators, such as CO_2 emissions, aggregate extraction, water resource use, waste created by construction and demolition, land use, productivity, and road freight. Maine (*13*) believes that the construction sector is unique because it can touch on the major elements of the sustainability agenda; it can influence both short-term (construction) and medium- and long-term (maintenance and use) goals. The main purpose of sustainable construction is to apply the principles of sustainable development, conserving present resources for the benefit of future generations, to the construction sector (*14*). This definition though, and many others, struggle to grapple with the scale and fuzzy boundaries of the sector, which can include material extraction, product manufacture, transportation, demolition, building services, as well as design and even urban planning (*11, 14*). In fact, the majority of definitions focus on environmental aspects, but fail to capture the more holistic nature of sustainability. In addition, there is the need to define not only the actual construction process, but also preconstruction (planning and urban design) and post-construction (maintenance, operation, and deconstruction), in a more cross-cutting way (*8, 11, 15*).

Legislation is now seen as the main driver for sustainability in the built environment in the United Kingdom (*16*). In 2008 the Department for Business, Enterprise and Regulatory Reform (BERR) released its "Strategy for Sustainable Construction," which aims "to provide a catalyst to achieve a step change in sustainability of the procurement, design, construction and operation of all built assets." The BERR strategy was developed within the context of four principles set out in *Securing the Future* (*10*) and *Rethinking Construction* (*17*), which is still seen as the U.K. construction industry's principal driver for change. The strategy also has a crossover with the *Egan Review* (*18*), which reviewed the skills needed for industry workers to meet the sustainable communities' agenda (*19*). The BERR strategy does not aim to act as new legislation but uses existing legislation and a combination of mandatory and voluntary targets to tackle the gaps in existing legislation to provide a more sustainable built environment and suggests future policy direction (*4*) through the following:

- Procurement. Integrated teams and supply chains to carry out 50% of projects by value by end of 2007 and complete review of public procurement strategy.
- Design–Building Research Establishment Environmental Assessment Method (BREEAM). Excellent standards for all new construction on government estate; greater industry adoption of design quality indicators.
- Innovation. Increase in industry undertaking innovative work and adopting European Union schemes.
- People agenda. Tougher targets for the reduction of health and safety incidents and increased staff training and retention.
- Better regulation and business support simplification.

In addition, four key areas are to be improved:

- Climate change. All new homes to be zero carbon by 2016, increased energy efficiency across the board.
- Water. Reduced consumption across the sector and consultation on adoption of sustainable urban drainage systems.
- Biodiversity. Aim to maintain and increase biodiversity.
- Waste and materials. Zero waste to landfill by 2020 and greater use of "green" materials.

Notable omissions from the BERR document are planning, energy, and infrastructure. The first two are excluded because they are being reviewed and legislated independently, and infrastructure is excluded because it is believed that the civil engineering sector is developing its own strategy sufficiently well (*4*). However, several industry bodies [e.g., Chartered Institute of Building (*20*), Construction Industry Council (*21*), and Quarry Products Association (*22*)] have voiced concern that the omission of civil engineering is far from desirable and will not lead to a holistic, inclusive solution. This concern is reinforced by Rydin et al. (*11*), who observe that the industry will try to fill the smallest possible definition of sustainable development, rather than aim to place itself at the center of creating a sustainable built environment.

The ICE strategy, *Sustainable Development Strategy and Action Plan for Civil Engineering* (*23*), revises an earlier strategy from 2002. This sets out four strategic aims for the ICE to pursue in its approach to sustainable development:

- Promote strong leadership within civil engineering,
- Embed the principles of sustainable development into everyday work activities and decision making,
- Build capacity for sustainable development in the industry and profession, and
- Create and influence a policy framework that demands more socially and environmentally responsible behavior.

The strategy also aims to promote the CEEQUAL and investigate measures for addressing climate change as well as identifying good practice for social aspects of corporate responsibility. It acknowledges that current methods of work and resource consumption are unsustainable and emphasizes generating stakeholder uptake of sustainability issues and the promotion of whole life costing and life cycle assessment. A formula for the calculation of the carbon footprint of U.K. infrastructure is to be developed along with guidance on building sustainable roads. The major push, however, is on developing people and skills to be able to further the sustainability agenda.

The government strategy for sustainable development and construction clearly emphasizes development of efficient, low-energy, "green" buildings and assessment techniques for energy and resource use; indoor environmental quality; and ecological loadings (*24, 25*). Resulting advances in sustainable construction can and will have some influence on the development of more sustainable infrastructure, but to date there has been far less attention paid to the "greening" of infrastructure (*26*).

Unlike buildings, infrastructure incurs less frequent running costs, so it can be harder to demonstrate the benefits of greater expenditure on constrained short-term budgets for long-term savings. Despite the possible deterioration of a piece of infrastructure and subsequent increased costs in its maintenance, plus the environmental and social impacts, little is done by infrastructure operators to seek innovative solutions in operation or in procuring new projects (*27*). Possible reasons for this include a perceived increase in potential costs, risks, and fear of the untested or untried (*27, 28*). The lack of attention to infrastructure is particularly problematic given that highways, drainage systems, and utilities supply all have a major impact on the priority areas for national sustainable development (*29–31*), for example, through the following:

- Consumption of large quantities of primary and secondary construction materials and generation of waste;
- Some of the most heavily consumed materials, concrete and asphalt, require large amounts of energy in their production and transportation leading to significant greenhouse gas emissions;
- Depletion of natural resources leading to environmental degradation along with loss of natural habitats and major impacts (visual, increased noise, increased emissions, loss of habitat, etc.); and
- Incorrectly specified infrastructure failing to support the behavioral changes required to deliver sustainable communities and transport.

For the infrastructure sector to realize its potential and drive change, a shift away from the traditional project objectives of cost, time, and quality—which are used as the current paradigm through which one views a project, defines the problem space, and develops solutions that are suitable to meet these needs—is required (*32, 33*). Various work has started to examine the wider issues that should be considered in infrastructure delivery, but much of this has been restricted to a narrow part of the sustainable development agenda. The main emphasis has been on environmental issues, focusing mainly on recycling and reuse of materials, waste reduction, and energy efficiency in infrastructure construction and maintenance. Given that such a wide range of issues should be encompassed within sustainable infrastructure, it is understandable that a significant body of research is developing related to tools and assessment methods that are said to aid project teams in managing and delivering sustainable infrastructure construction.

ENVIRONMENTAL ASSESSMENT METHODS

Fenner (*5*) states that to be able to engineer sustainability, it is vital that engineers have robust assessment methodologies available, while Hurley et al. (*34*) add that these methods are vital to aid engineers in decision making and the measurement of progress. Kaatz et al. (*25*) state that "sustainability assessment methods for building projects have a major role to play in introducing sustainability values and principles into mainstream construction," and the importance of measurement methods for sustainable construction is supported further in the literature (*25, 35–37*).

The Building Research Establishment (BRE) (*38*) and the SUE-MoT project (*39*) identified more than 600 tools related in some way to evaluating at least one of the "three pillars" of sustainability, including distinct types of tools for urban planning, design, and rating systems, and life cycle analysis tools and infrastructure. While it was found that nearly all these tools did address environmental issues, few addressed the holistic nature of sustainability and this is noted elsewhere in the literature (*7, 25*). Kaatz et al. (*40*) suggest that this may be due to the difficulty in measuring the intangible benefits of social, cultural, and economic aspects of sustainability and his view is supported by Rydin et al. (*11*), who believe that the industry attempts to fit the smallest definition of the problem space as possible. Xing et al. (*41*) state that the current assessment methods are not holistic in their assessment and cannot therefore be described as sustainability assessment tools; while this may be the case, with their increasing adoption and requirement in public procurement in the United Kingdom, it is likely that they will continue to be used for the foreseeable future.

Although this may not be ideal, there are a number of benefits to be gained from the use of these environmental assessment methods (EAMs), including improved teamwork, multidisciplinary dialogue, and increased opportunities (*42*), as well as promoting environmentally conscious construction and assisting in the delivery of market and regulatory needs (*43*). Fenner and Ryce (*44*) add that these methods can drive change in the supply chain and manufacturing markets, define benchmarks for performance within the industry, and aid policy making.

However, EAMs are not without their critics (*36, 44*); they can lead to "point-hunting," which wastes resources to try and score points, they can not always be context specific, and they tend to address too narrow a section of the built environment, focusing on the project and not its wider implications. They also need regular updating to align with the latest ideas on what constitutes best practice and require accurate qualitative and quantitative inputs (often based on assumptions by the designer that can undermine the environmental benefits of the assessment method).

A selection of the tools most often used in U.K. construction at the project level (*36, 45, 46*) is presented below before a discussion of CEEQUAL, which is seen as the most suitable for assessing infrastructure.

Building Research Establishment Environmental Assessment Method

Building Research Establishment Environmental Method (BREEAM) was established in 1990 and is the definitive standard in the United Kingdom for environmental best practice of buildings and can be used for an increasing variety of developments, including commercial, industrial, leisure and laboratories, schools, retail, and, most recently, communities. It lacks social and economic detail but this will be

addressed in the future. The issues that it addresses include management, energy use, health and well-being, pollution, transport, land use, ecology, materials, and water. Credits are awarded against specific criteria, depending on performance in each category as judged by external qualified assessors. The total credits are then tallied to give a final score of pass (>25% points), good (>40% points), very good (>55% points), excellent (>70% points), and outstanding (>85% points). The scheme is reviewed regularly to keep it up to date with regulatory requirements and adjusted accordingly. It is now specified as a requirement for all publicly procured buildings.

Sustainable Project Appraisal Routine

The Sustainable Project Appraisal Routine is a design tool developed by the consultants at Arup that aims to inform decision making and aid delivery of sustainable developments. It is based on a radar diagram split into four quadrants assessing social, economic, environmental, and prudent use of resources. In an attempt to address sustainability holistically, no weighting is added to any of the 20 or more subthemes; these can be adjusted by the client and design team to suit the specific project requirements. Criteria are scored qualitatively from –3 to 3 and a web diagram is produced that provides a strong visual representation of how the project performs, with the most sustainable aspects being closer to the center.

South East England Development Agency Development Checklist

The South East England Development Agency Development Checklist was the first tool developed by a regional development agency, although nearly all have their own versions now, covering all of England. It can be used to demonstrate or review the sustainability credentials at the planning stage of a project and how the project meets the regional sustainability issues, such as land use, energy, water, and transportation.

Code for Sustainable Homes

The Code for Sustainable Homes aims to deliver zero carbon homes in the United Kingdom by 2016 by phased integration into the building regulations. Mandatory for all new homes, it scores buildings on topics including energy efficiency, water consumption, surface water runoff, waste, pollution, health and well-being, management, and ecology. It is based on the original EcoHomes methodology and, as such, awards a points score for performance, where Level 3 is currently mandatory, with Level 6 (zero carbon) being required by 2016. It is owned by the U.K. government but overseen by BRE, who train the licensed assessors to carry out the awards.

CEEQUAL TOOL

CEEQUAL is a voluntary scheme to recognize best practice in civil engineering regarding environmental sustainability. While there are many tools available to the construction professional, CEEQUAL (www.ceequal.com) is widely recognized as being the only definitive tool for the assessment of environmental impact due to infrastructure works (*3, 39, 47, 48*) and is the BREEAM equivalent for infrastructure. CEEQUAL began to be developed in 2000 by ICE with government funding and the support and involvement of 40 industrial partners representing clients, consultants, and contractors. In 2003 following extensive testing in industry, the scheme was launched with the first eight awards being given. Since then, the scheme has been revised several times to take into account changes in regulations and to update the scheme to reflect current thinking on best practice. The scheme plays a key role in the ICE Sustainable Development Strategy and Action Plan discussed earlier.

The scheme looks to promote best practice in the environmental and, more recently, social performance of civil engineering schemes by assessing and benchmarking performance to reward schemes that go beyond legal compliance. To date, in excess of £8 billion ($12 billion) (£1 = $1.50; April 10, 2010 exchange rate) of construction has been registered for assessment under the scheme, with close to 40 schemes receiving awards (*49*).

Similar to BREEAM, CEEQUAL is a credit-based assessment method with 12 sections. The 12 sections have had a weighting applied and are broken down as follows:

1. Project management, 10.9%;
2. Land use, 7.9%;
3. Landscape issues, 7.4%;
4. Ecology and biodiversity, 8.8%;
5. Historic environment, 6.7%;
6. Water resources and the water environment, 8.5%;
7. Energy and carbon, 9.5%;
8. Material use, 9.4%;
9. Waste management, 8.4%;
10. Transport, 8.1%;
11. Effects on neighbors, 7.0%; and
12. Relations with the local community and other stakeholders, 7.4%

The 12 sections contain a total of 208 questions, which total 2,000 points. Each question provides an overview of why the questions are being asked and what is considered suitable evidence to satisfy the requirements of receiving the credits. The scores for each credit are split out to represent the role of client, designer, and contractor, so that each member is scored according to their relative potential to influence the credit. The questions vary from simply scoring points for yes-or-no type questions that ask if certain investigations have been carried out to questions where the score varies depending on the level of achievement (e.g., the percentage of waste diverted from landfill). Some questions also have scores broken down into stages (e.g., if observations were made, were they assigned to someone and did that person take action?), so the level of implementation is again rewarded.

The awards that are available include the following:

1. Whole project award (WPA), applied for jointly by or on behalf of the client, designer, and principal contractor;
2. WPA with an interim client and design award;
3. Client and design award;
4. Design-only award;
5. Construction-only award; and
6. Design and Construction award.

Assessments are undertaken by a qualified assessor who has attended a training course run by CEEQUAL Ltd. and using the *CEEQUAL Manual*, which provides guidance on what the questions require and

what counts as suitable evidence. The assessor is most often a member of the project team and is responsible for determining which questions are of no relevance to the scheme (not all questions can be evaluated and guidance is given in the scheme manual on which questions can be removed), collating evidence, and scoring the scheme's performance. The assessor also works with the scheme verifier who is appointed by CEEQUAL Ltd. when the scheme is registered. The verifier is external to the project and the companies involved and provides an independent review; the verifier's approval is also required for questions to be removed as well as for checking evidence suitability and relevance. The scores are recorded using a spreadsheet that, when completed to the assessor's and verifier's satisfaction, is sent to CEEQUAL Ltd. for approval. Awards are given as pass (over 25%), good (over 40%), very good (over 60%), and excellent (over 75%); these percentages are based on total points scored after removal of questions not considered relevant to the project and represent how far past statutory compliance the project has gone.

Not much literature on the scheme has been published apart from brief overviews of the scheme's scope. The only review of the scheme in use is by Campbell-Lendrum and Feris (*50*), who tested the scheme on a railway embankment works and concluded that the scheme "provided benchmarks for targeting, driving and measuring improvements" and they felt that "the depth, breadth and balance of the issues covered by the assessment process make it appropriate to a wide range of other civil engineering projects." Although other tools are being developed, they will be broadly based on CEEQUAL (*48*) or similar approaches (*51*). The scheme has a number of recognized drawbacks, however, including not addressing the holistic nature of sustainability and placing emphasis on environmental best practice; it is also seen as being "shallow" in its coverage of community and economic issues and not addressing the scheme over its life cycle (*39*), although CEEQUAL has been revised recently to address some of these shortcomings.

CASE STUDIES

The aim of this research, therefore, was to assess how a design team was performing with regards to environmental performance (at the design stage), beyond that required for legal compliance, by backanalyzing a series of projects using the CEEQUAL methodology. In reviewing the literature it was apparent that CEEQUAL was the most appropriate assessment method for the nature of the works (described below) and the scope of assessment required. Although CEEQUAL was not designed as a design tool or for reviewing project performance in this manner, it was felt that an assessment would provide a good indication of progress and which areas required attention from the design team to improve their level of environmental performance for future schemes.

Three case studies were chosen that were felt to be representative of the project work most often undertaken within the design team. This design team represents one small performance unit of a large, international, multidisciplinary, design consultancy. The team specializes in the delivery of the infrastructure (drainage, utility supply, and highways) to support residential, industrial, and commercial developments for both private and public development organizations. The three case study projects had been completed at the time of assessment, so they had been approved and accepted by the relevant adopting authorities who would take ownership of the infrastructure, to be compliant with the current relevant regulations and specifications.

Although the assessments were undertaken by a qualified assessor, the case studies were not undertaken as true CEEQUAL assessments in that they were not registered with CEEQUAL Ltd. or subject to external verification. However, the CEEQUAL methodology was applied as rigorously as possible for the nature of the projects to achieve an accurate assessment result and to benchmark current design team performance. The assessment was undertaken using Version 4 of the manual (the most recent revision).

Case Study 1. Highways, drainage, and footpaths to support a new industrial park on a greenfield site for a public body in a rural location. The project aimed to act as an economic stimulus for the area.

Case Study 2. Highways, drainage, and footpaths to support a large new residential development on a brownfield regeneration site for a public development body. This project had strong aspirations regarding the social aspects of sustainability.

Case Study 3. Highways, drainage, and footpaths to support a new commercial development on an inner-city brownfield site for a private developer.

The schemes were assessed as closely as possible to a real assessment with questions being evaluated, evidence identified and reviewed, and scores awarded. The final scores were found to be as follows:

Case Study 1: 21.3%;
Case Study 2: 29.2%; and
Case Study 3: 10.5%.

This would mean that Case Study 2 would score a "pass" while the other two case studies would fail to score an award under the scheme. This is not surprising given than none of the projects set out with ambitions for environmental performance beyond regulatory compliance, which they all achieved. Figure 1 shows a more detailed breakdown of the scores across each section.

It is not surprising that the overall scores reflect a relatively poor performance for demonstrating "best practice" when this was never an ambition. One of the common themes in the literature is that if a project is to achieve minimal environmental impact, it is essential that it is identified as a clear ambition from the outset, with all parties involved being engaged. Another reason for poor scores is that the scheme works on the premise that no evidence means no points; this rationale was followed in the assessments, but it became clear that there were a number of areas, such as design rationale and decisions or recording quantities, that were not carried out as thoroughly as possible. If a project is to be carried out under the scheme, it is essential that the assessor clarifies what evidence is both relevant and suitable and ensures that data are thoroughly recorded.

It is clear that one of the main reasons that Case Study 2 received the highest score was its performance in the relations with the community and other stakeholders. This is not surprising since the development set out with high ambitions for social performance and so a greater number of workshops and community liaison activities were held compared to the other projects. The scheme also fared better on a number of other issues because it was constructed on a brownfield site, bringing the land back into use and dealing with potential contamination appropriately.

Case Study 3 scored the worst; this is influenced by the client being a private developer rather than a public body. Consequently, the client had less of an organizational commitment to sustainability and environmental protection with a clear emphasis on the traditional

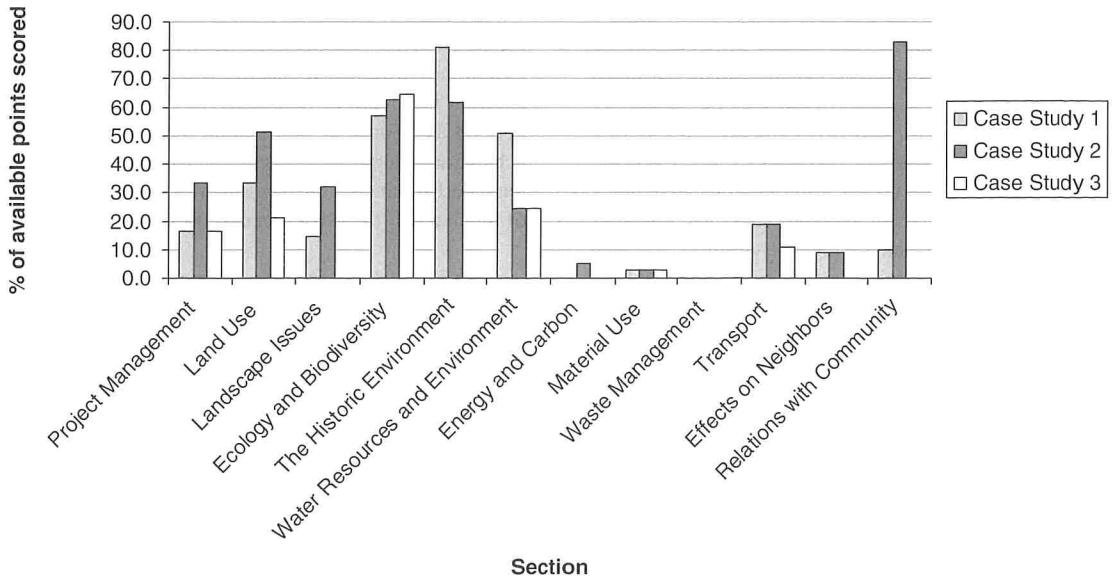

FIGURE 1 Case studies' CEEQUAL section scores.

development paradigm of cost, time, and quality as the key drivers for project delivery. It is evident from Figure 1 that the sections in which all three schemes failed to score or only achieved a minimal score are energy and carbon, material use, waste management, and effects on neighbors, whereas land use, ecology and biodiversity, and the historic environment generally gained better levels of achievement.

The main reason for the scores being slightly better in the three aforementioned topics is that the design team had a better understanding of and experience with these topics from dealing with planning and regulatory issues and working on larger schemes that have required greater focus on these issues. Furthermore, good use was made by the design team of expertise in these fields, especially ecology and biodiversity.

It is perhaps surprising that waste was one of the lowest scoring topics since it is one of the areas that has received the greatest level of industry attention in recent years and there is a large amount of guidance available, but the most obvious reason for this is the design team's belief that waste is predominantly an issue for the contractor. Although the importance of the contractor's role in waste minimization is reflected in CEEQUAL by the number of questions applying to the contractor only, there are still credits available for the designer, who has to incorporate the principles and set targets for waste minimization during the design phase. These opportunities were not exploited in the case study projects.

The area of energy and carbon is a fairly new concept to the general design of civil engineering works, but one that will be of growing importance in the coming years as targets are set to reduce national consumption and outputs. This section deals with issues such as life-cycle energy assessments, life-cycle carbon assessments, percentage reductions achieved in the design and completed works based on these assessments as well as energy and emissions in use, and whether opportunities have been explored to minimize these and incorporate renewable energy sources. Although the skills are available to carry out all these requirements in-house, it is clear that the design team will need to become more familiar with the general concepts and terminology so that they can recognize opportunities for incorporating these requirements as well as understanding at what point in the project the greatest opportunity to influence the design presents itself and provide the relevant information accordingly.

Again, poor scores in the nuisance to neighbors section were recorded for reasons similar to those in the waste section, with the design team believing that issues related to noise, vibration, air quality, and light spillage during the construction phase are the responsibility of the contractor. Therefore, the design team did not consider the potential to minimize these impacts through the design process, although they were taken into account during the design when considering the operation of the infrastructure.

One of the main concepts that has come out of the CEEQUAL assessment analysis is the potential that the designer has to minimize environmental impact through better specification in a wide variety of issues from waste to landfill and recycling targets, levels of responsibly sourced materials, and percentage of materials to be reused on site, to levels of coatings and treatments applied off site. CEEQUAL also allows the designer to require contractors to have green travel plans and to review past environmental performance of contractors and subcontractors before the invitation to bid stage.

The other issue that the assessments have raised is the importance of considering the project over its life cycle and the impacts that the project will have not just during the construction phases and on opening, but what impacts it will have on the environment over its entire life cycle and how consumption and impacts can be minimized over its entire operation.

CONCLUSIONS

The growing need for designers and all construction professionals to recognize the importance of sustainable development within civil engineering has been identified from a policy and regulatory standpoint within the U.K. construction industry. The need to recognize the importance of consideration of economic, environmental, and social issues has been discussed as well as the methods that are currently available to help engineers achieve this. It has become apparent that

there are a variety of tools available, but, at present, most do not fully assess sustainability, with the majority focusing on the environmental aspects and impacts (mainly related to buildings).

CEEQUAL has been identified as the tool most suitable for the U.K. context to assess the environmental impact of civil engineering schemes and a brief overview of its history and scope has been given. Three case studies have been assessed using CEEQUAL to help inform the design team of their current level of performance in this area, in addition to legal and regulatory compliance.

As expected, the schemes that set out with no environmental ambitions scored fairly poorly under the scheme, which aims to reward those that go beyond legal compliance and implement best practice. Issues with which the team is familiar (mainly through past experience), such as ecology and biodiversity, were integrated well into their designs, using appropriate expertise available to the designers in-house to maximize their success.

Poor scores in areas such as carbon and energy and material use, with which the team members were not so familiar, demonstrated a need to improve their level of understanding and education on these topics, so that they can better integrate the concepts and seek out the relevant expertise to minimize these impacts. The design team should also seek to influence the construction process through better specification and taking ownership of the impacts created in the construction process as well as during its operation at the earliest opportunity in a project. It is anticipated that as a follow-up to this work, a toolbox will be created to raise awareness of infrastructure design engineers' sustainable literacy with an emphasis now placed on delivering clear advice and guidance on how to assess and consider these impacts, with the first modules focusing on the areas highlighted in this research as being lacking.

Because it is not likely that a single individual will be familiar with all the issues that should be considered in order to deliver a completely "green" civil engineering scheme, the CEEQUAL scheme provides the engineer with an overview of the key topics and provides insight into who should be consulted and on what issues. Although CEEQUAL does not provide the complete solution to ensuring that designs will be sustainable (because it does not fully consider all aspects of economic and social issues), it provides a useful starting point to improving the environmental credentials of the design team. While there is the potential for such checklists to lead to a narrow focus on the part of the designer by not considering the wider context of the project, the scheme is not so overly proscriptive; instead it provides guidance on how to improve the environmental impact of the civil engineering projects.

ACKNOWLEDGMENTS

The study by the authors into sustainable infrastructure design and delivery received contributory funding from EPSRC through the Engineering Doctorate Scheme run from the Centre for Innovative and Collaborative Engineering at Loughborough University.

REFERENCES

1. United Kingdom. Department of the Environment. *Sustainable Development: The UK Strategy.* Report CM 2426, Jan. 1994.
2. United Kingdom. Department for Business, Enterprise and Regulatory Reform. *Strategy for Sustainable Construction,* 2008.
3. United Kingdom. Department of Trade and Industry. *Review of Sustainable Construction,* 2006.
4. United Kingdom. Department for Business, Enterprise and Regulatory Reform. *Draft Strategy for Sustainable Construction: A Consultation Paper,* 2007.
5. Fenner, R. A. Editorial: Can Sustainability Count? *Proceedings of the Institution of Civil Engineers: Engineering Sustainability,* Vol. 161, No. ES1, March 2008, pp. 1–2.
6. Adetunji, I. O. *Sustainable Construction.* Centre for Innovative Construction Engineering, Department of Civil and Building Engineering, Loughborough University, Loughborough, Leicestershire, United Kingdom, 2006.
7. Parkin, S., F. Sommer, and S. Uren. Sustainable Development: Understanding the Concept and Practical Challenge. *Proceedings of the Institution of Civil Engineers: Engineering Sustainability,* Vol. 156, No. 1, 2003, pp. 19–26.
8. Shah, S. S. *Sustainable Practice for the Facilities Manager.* Blackwell, Oxford, United Kingdom, 2007.
9. World Commission on Environment and Development and G. H. Brundtland. *Our Common Future.* Oxford University Press, Oxford, United Kingdom, 1987.
10. United Kingdom. Department for the Environment, Transport and the Regions. *Securing the Future: Delivering UK Sustainable Development Strategy,* 2005.
11. Rydin, Y., U. Amjad, S. Moore, M. Nye, and M. Whitaker. *Sustainable Construction and Planning: The Academic Report.* Centre for Environmental Policy and Governance, London School of Economics and Political Science, 2006.
12. United Kingdom. Department for the Environment, Transport and the Regions. *Building a Better Quality of Life: A Strategy for More Sustainable Construction,* 2000.
13. Maine, B. Construction, Law and the Environment: A Historical Review. *Proceedings of the Institution of Civil Engineers,* Vol. 160, No. 4, 2007, pp. 169–177.
14. Kibert, C. The Next Generation of Sustainable Construction. *Building Research and Information,* Vol. 35, No. 6, 2007, pp. 595–601.
15. Hill, R., and P. A. Bowen. Sustainable Construction: Principles and a Framework for Attainment. *Construction Management and Economics,* Vol. 15, No. 3, 1997, pp. 223–239.
16. *Guide L: Sustainability.* Chartered Institution of Building Services Engineers, London, 2007.
17. Egan, J. *Rethinking Construction: The Report of the Construction Task Force.* Department for the Environment, Transport and the Regions, London, 1998.
18. Egan, J. *The Egan Review: Skills for Sustainable Communities.* 2004. http://www.communities.gov.uk/publications/communities/eganreview. Accessed Feb. 7, 2008.
19. Great Britain. Office of the Deputy Prime Minister. *Sustainable Communities: Building for the Future,* 2003.
20. Chartered Institute of Building. *Response to the Draft Strategy for Sustainable Construction.* Last update 2007. http://www.ciob.org.uk. Accessed Jan. 2008.
21. Construction Industry Council. *Response to Draft Strategy for Sustainable Construction.* 2007. http://www.cic.org.uk/activities/consult.shtml. Accessed Feb. 8, 2008.
22. Quarry Products Association. *Response to the Draft Strategy for Sustainable Construction.* Last update 2007. http://www.qpa.org/con_other01.htm. Accessed Feb. 8, 2008.
23. *Sustainable Development Strategy and Action Plan for Civil Engineering.* Institution of Civil Engineers, London, 2007.
24. Cole, R. Building Environmental Assessment Methods: Redefining Intentions and Roles. *Building Research and Information,* Vol. 33, No. 5, 2005, p. 255.
25. Kaatz, E., D. Root, P. Bowen, and R. Hill. Advancing Key Outcomes of Sustainability Building Assessment. *Building Research and Information,* Vol. 34, No. 4, 2006, pp. 308–320.
26. Huang, R. Y., and C. H. Yeh. Development of an Assessment Framework for Green Highway Construction. *Journal of the Chinese Institute of Engineers,* Vol. 31, No. 4, 2008, pp. 573–585.
27. Hartshorn, J., M. Maher, J. Crooks, R. Stahi, and Z. Bond. Creative Destruction: Building Toward Sustainability. *Canadian Journal of Civil Engineering,* Vol. 32, 2005, p. 170.
28. Roberts, C., and S. Sims. Cashing in on the Green Machine: Are Developers Missing Out? Working Paper in Real Estate and Construction. *International Journal of Housing Markets and Analysis,* Vol. 1, No. 4, 2007, pp. 362–378.
29. Chandler, J., J. Reid, I. Schiavi, A. Hewitt, R. Griffiths, and E. Bendall. *Sustainable Choice of Materials for Highway Works: A Guide for Local*

Authority Highway Engineers. Department for the Environment, Transport and the Regions, London, 2008.
30. Meng-Li, L. Strategies and Ecological Engineering Considerations of Road Construction in Taiwan. *Journal of Ecotechnology,* Vol. 1, 2005, pp. 9–28.
31. Forman, R. T. T., and L. E. Alexander. Roads and Their Major Ecological Effects. *Annual Review of Ecology and Systematics,* Vol. 29, 1998, pp. 207–231.
32. Fenner, R., C. Ainger, H. Cruickshank, and P. Guthrie. Widening Engineering Horizons: Addressing the Complexity of Sustainable Development. *Proceedings of the Institution of Civil Engineers: Engineering Sustainability,* Vol. 159, No. 4, 2006, pp. 145–154.
33. Gambatese, J. A., and A. S. Rajendran. Sustainable Roadway Construction: Energy Consumption and Material Water Generation of Roadways. *Proc., Construction Research Congress: Broadening Perspectives,* ASCE, Reston, Va., 2005, pp. 102–108.
34. Hurley, L., R. Ashley, and S. Mounce. Addressing Practical Problems in Sustainability Assessment Frameworks. *Proceedings of the Institution of Civil Engineers: Engineering Sustainability,* Vol. 161, No. 1, 2008, pp. 23–30.
35. Cole, R. Changing Context for Environmental Knowledge. *Building Research and Information,* Vol. 32, No. 2, 2004, pp. 91–109.
36. Braithwaite, P. Improving Company Performance Through Sustainability Assessment. *Proceedings of the Institution of Civil Engineers: Engineering Sustainability,* Vol. 160, No. 2, 2007, pp. 95–103.
37. Ding, G. K. C. Sustainable Construction—The Role of Environmental Assessment Tools. *Journal of Environmental Management,* Vol. 86, No. 3, 2008, pp. 451–464.
38. *Assessment of Sustainability Tools.* Report 15961. Building Research Establishment, Glasgow, Scotland, 2004.
39. Levett-Therivel Sustainability Consultants. *Analysis of Sustainability/Social Tools.* SUE-MoT, Oxford, United Kingdom, 2004.
40. Kaatz, E., D. Root, and P. Bowen. Broadening Project Participation Through a Modified Building Sustainability Assessment. *Building Research and Information,* Vol. 33, No. 5, 2005, pp. 441–454.
41. Xing, Y., R. M. W. Horner, J. Bebbington, and M. A. El-Haram. A Framework Model for Assessing Sustainability Impacts of a Built Environment. *Accounting Forum,* Vol. 33, 2009, pp. 209–224.
42. Cole, R. Building Environmental Assessment Methods: Assessing Construction Practices. *Building Research and Information,* Vol. 18, No. 8, 2005, pp. 949–957.
43. Kaatz, E., G. Barker, R. Hill, and P. Bowen. A Comparative Evaluation of Building Environmental Assessment Methods: Suitability for the South African Context. *Proc., Sustainable Building Conference 2002,* Oslo, Norway, 2002.
44. Fenner, R. A., and T. Ryce. A Comparative Analysis of Building Rating Systems. Part 1: Evaluation. *Proceedings of the Institution of Civil Engineers: Engineering Sustainability,* Vol. 161, No. 1, 2008, pp. 55–63.
45. Jefferson, I., D. V. L. Hunt, C. A. Birchall, and C. D. F. Rogers. Sustainability Indicators for Environmental Geotechnics. *Proceedings of the Institution of Civil Engineers: Engineering Sustainability,* Vol. 160, No. 2, 2007, pp. 57–78.
46. Atkinson, C., A. Yates, and M. Wyatt. *Sustainability in the Built Environment: An Introduction to Its Definition and Measurement.* IHS BRE Press, Bracknell, United Kingdom, 2009.
47. *Practical Evaluation Tools for Urban Sustainability.* 2006. http://www.petus.eu.com/. Accessed Feb. 8, 2008.
48. *Proposed Plan for the Assessment of Knowledge and Practice for Sustainable Infrastructure.* 2005. http://www.persi.us/documents/PlanProposedNA.doc. Accessed Feb. 8, 2008.
49. *New Civil Engineer.* CEEQUAL Annual, 2009. http://www.ceequal.co.uk/pdf/ceequal_annual_09.pdf. Accessed Jan. 6, 2009.
50. Campbell-Lendrum, E., and J. Feris. Trialing CEEQUAL on a London Railway Embankment. *Proceedings of the Institution of Civil Engineers: Engineering Sustainability,* Vol. 161, No. 1, 2008, pp. 71–76.
51. Ghumra, S., M. Watkins, P. Phillips, J. Glass, M. Frost, and J. Anderson. Developing an LCA-Based Tool for Infrastructure Projects. *Proc., ARCOM Conference,* Nottingham, United Kingdom, Sept. 2009.

The views expressed in this paper are solely those of the authors and not those of Jacobs Engineering.

The Waste Management and Resource Efficiency in Transportation Committee peer-reviewed this paper.

TRANSPORTATION RESEARCH RECORD:
JOURNAL OF THE TRANSPORTATION RESEARCH BOARD

Peer Review Process

The ***Transportation Research Record: Journal of the Transportation Research Board*** publishes approximately 25% of the more than 3,000 papers that are peer reviewed each year. The mission of the Transportation Research Board (TRB) is to disseminate research results to the transportation community. The Record series contains applied and theoretical research results as well as papers on research implementation.

The TRB peer review process for the publication of papers allows a minimum of 30 days for initial review and 60 days for rereview, to ensure that only the highest-quality papers are published. At least three reviews must support a committee's recommendation for publication. The process also allows for scholarly discussion of any paper scheduled for publication, along with an author-prepared closure.

The basic elements of the rigorous peer review of papers submitted to TRB for publication are described below.

Paper Submittal: June 1–August 1

Papers may be submitted to TRB at any time. However, most authors use the TRB web-based electronic submission process available between June 1 and August 1, for publication in the following year's Record series.

Initial Review: August 15–November 15

TRB staff assigns each paper by technical content to a committee that administers the peer review. The committee chair assigns at least three knowledgeable reviewers to each paper. The initial review is completed by mid-September.

By October 1, committee chairs make a preliminary recommendation, placing each paper in one of the following categories:

1. Publish as submitted or with minor revisions,
2. Publish pending author changes and rereview, or
3. Reject for publication.

By late October, TRB communicates the results of the initial review to the corresponding author indicated on the paper submission form. Corresponding authors communicate the information to coauthors. Authors of papers in Category 2 (above) must submit a revised version addressing all reviewer comments and must include a cover letter explaining how the concerns have been addressed.

Rereview: November 20–January 25

The committee chair reviews revised papers in Category 1 (above) to ensure that the changes are made and sends the Category 2 revised papers to the initial reviewers for rereview. After rereview, the chairs make the final recommendation on papers in Categories 1 and 2. If the paper has been revised to the committee's satisfaction, the chair will recommend publication. The chair communicates the results of the rereview to the authors.

Discussions and Closures: February 1–May 15

Discussions may be submitted for papers that will be published. TRB policy is to publish the paper, the discussion, and the author's closure in the same Record.

Many papers considered for publication in the *Transportation Research Record* are also considered for presentation at TRB meetings. Individuals interested in submitting a discussion of any paper presented at a TRB meeting must notify TRB no later than February 1. If the paper has been recommended for publication in the *Transportation Research Record*, the discussion must be submitted to TRB no later than April 15. A copy of this communication is sent to the author and the committee chair.

The committee chair reviews the discussion for appropriateness and asks the author to prepare a closure to be submitted to TRB by May 15. The committee chair reviews the closure for appropriateness. After the committee chair approves both discussion and closure, the paper, the discussion, and the closure are included for publication together in the same Record.

Final Manuscript Submittal: March 15

In early February, TRB requests a final manuscript for publication—to be submitted by March 15—or informs the author that the paper has not been accepted for publication. All accepted papers are published by December 31.

Paper Awards: April to January

The TRB Executive Committee has authorized annual awards sponsored by Groups in the Technical Activities Division for outstanding published papers:

- Charley V. Wootan Award (Policy and Organization Group);
- Pyke Johnson Award (Planning and Environment Group);
- K. B. Woods Award (Design and Construction Group);
- Patricia F. Waller Award (Safety and System Users Group);
- D. Grant Mickle Award (Operations and Preservation Group); and
- John C. Vance Award (Legal Resources Group).

Other Groups also may nominate published papers for any of the awards above. In addition, each Group may present a Fred Burggraf Award to authors 35 years of age or younger.

Peer reviewers are asked to identify papers worthy of award consideration. Each Group reviews all papers nominated for awards and makes a recommendation to TRB by September 1. TRB notifies winners of the awards, which are presented at the following TRB Annual Meeting.

Transportation Research Board
www.TRB.org

TRANSPORTATION RESEARCH BOARD
500 Fifth Street, NW
Washington, DC 20001

ADDRESS SERVICE REQUESTED

THE NATIONAL ACADEMIES™
Advisers to the Nation on Science, Engineering, and Medicine

The nation turns to the National Academies—National Academy of Sciences, National Academy of Engineering, Institute of Medicine, and National Research Council—for independent, objective advice on issues that affect people's lives worldwide.
www.national-academies.org

ISBN 978-0-309-14284-7
90000
9 780309 142847